PS97

16 February – 8 April 2016
Punta Arenas – Punta Arenas

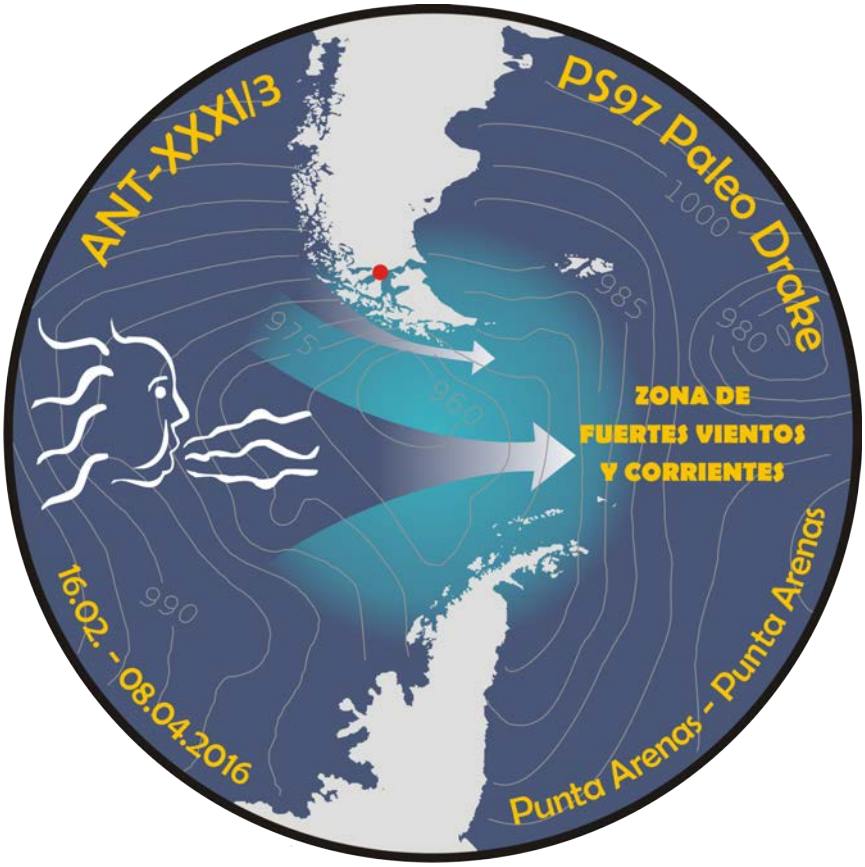

Chief Scientist
Frank Lamy

Coordinator
Rainer Knust

CONTENTS

APPENDIX

1. ÜBERBLICK UND FAHRTVERLAUF

Frank Lamy AWI

Zusammenfassung

Die Drake Passage (DP) ist die wichtigste geographische Engstelle für den Antarktischen Zirkumpolarstrom und spielt eine herausragende Rolle für die heutige Ozeanzirkulation und das globale Klima. Trotz ihrer Wichtigkeit für unser heutiges und wahrscheinlich auch zukünftiges Klima, ist bisher wenig über klimatische und ozeanographische Veränderungen auf längerfristigen, geologischen Zeitskalen bekannt. Das wichtigste wissenschaftliche Ziel der geologischen Arbeiten in der Drake Passage und vor dem angrenzenden Südamerika ist deshalb unser Wissen über die paläozeanographische Rolle der Drake Passage bei globalen Klimaänderungen im Quartär auf orbitalen und sub-orbitalen Zeitskalen zu verbessern.

Schwerpunkt der *Polarstern* Expedition PS97 waren marin-geologische Arbeiten auf zwei Nord-Süd Profilen über die westliche und zentrale Drake Passage. Die dabei gewonnenen Oberflächenproben und Sedimentkerne in der offenen Drake Passage sind die ersten Tiefseesedimente, die seit den geologischen Beprobungen mit dem amerikanischen Forschungsschiff *El Tanin* in den 1960er Jahren gewonnen werden konnten. Ein weiteres Hauptarbeitsgebiet der geologischen Arbeiten waren der argentinisch/chilenische Kontinentalhang der Scotia Sea und der südchilenische pazifische Kontinentalhang zwischen Kap Hoorn und der Magellan Straße. Im Bereich der Antarktischen Halbinsel wurden Oberflächenproben und Sedimentkerne im Bereich der Bransfield Straße genommen. Die wichtigsten Ergebnisse der geologischen Arbeiten während PS97 sind:

- Während aller Transitstrecken (genehmigt außerhalb der 3-Meilen Zone vor Argentinien und Chile) und Stationssuchfahrten in den Arbeitsgebieten wurden Hydrosweep- und PARASOUND-Daten aufgezeichnet (insgesamt ca. 5900 nm). Diese Daten bildeten die wichtigste Grundlage, um geeignete Sedimentkern-Lokationen zu indentifizieren. Die PARASOUND-Daten dokumentieren eine nur sehr lokal vorhandene Sedimentbedeckung im Bereich des argentinisch/chilenische Kontinentalhanges der Scotia Sea und der Polarfrontzone im Bereich der westlichen Drake Passage.
- Oberflächensedimente konnten mit dem Multicorer an 53 Stationen und mit dem Großkastengreifer an 11 Stationen, insgesamt sehr erfolgreich gewonnen werden. 41 Schwereloteinsätze, davon 33 erfolgreich, erbrachten ca. 160 m Sedimentkerne. 32 Kolbenloteinsätze, davon 30 erfolgreich, erbrachten ca. 300 m Sedimentkerne. Der längste Kern war 22,73 m lang.
- Das wichtigste geologische Ergebnis ist die Gewinnung von Sedimentkernen entlang eines N-Süd Profiles über die zentrale Drake Passage im Bereich der Shackleton Störungsszone. Dieses Transekt beginnt südlich der Polarfront und erstreckt sich bis in die zentrale Polarfrontzone. Erste sedimentphysikalische Messungen und stratigraphische Einstufungen an Bord deuten auf überwiegend zeitlich hochauflösende Sedimentabfolgen hin, die einen kompletten Glazial-Interglazial Zyklus abdecken.
- Vor Chile konnten wir Sedimentkerne über ein Tiefenprofil zwischen ca. 600 und 4000 m Wassertiefe gewinnen, um Änderungen der Wassermassenstruktur im nördlichen Antarktischen Zirkumpolarstrom vor dem Eintritt in die Drake Passage zu rekonstruieren.
- Die geophysikalischen und geologische Vorerkundung von potentiellen *International Ocean Discovery Program* (IODP) Kernlokationen am chilenischen Kontinentalhang im Bereich einer Sedimentdrift mit höchster zeitlicher Auflösung (Sedimentmächtigkeit bis zu 900 m) war sehr erfolgreich. Ein zweites geophysikalisches Kreuzprofil wurde an einer Lokation ca. 50 nm westlich des Chile Grabens mit Sedimentmächtigkeiten von ca. 500 m durchgeführt. Auch diese Lokation ist sehr vielversprechend.

- Im Bereich der Antarktischen Halbinsel (Südshetland Inseln und Bransfield Straße) konnten zahlreiche lange Sedimentkerne gewonnen werden. Diese beinhalten zeitlich höchstauflösende holozäne Sedimentabfolgen, die u.a. zur Bestimmung von Schmelzwasser-Einträgen und der Weiterentwicklung von Meereisrekonstruktionen mit Biomarkern dienen sollen.

Ergänzt wurden die marin-geologischen Arbeiten durch paläoklimatische Landarbeiten. Ziel dieser Arbeiten waren die nur mit dem Helikopter vom Schiff aus erreichbaren äußersten chilenischen Inseln (*Isla Noir* und *Isla Cabo de Hornos*). Trotz widriger Wetterbedingungen, konnten auf beiden Inseln Sedimentkerne aus Seen gewonnen werden.

Ein weiterer Schwerpunkt der Expedition PS97 waren ozeanographischen Arbeiten, um den bisher wenig bekannten Cape Horn Strom und die westliche Drake Passage besser abzubilden. Dabei ging es insbesondere um Strömungsmessungen. Darüber hinaus wurden aber auch umfangreiche Wasserproben und Planktonfänge für die Verbesserung, Kalibrierung und Validierung mehrerer Mikrofossil-basierter Proxymethoden gewonnen. Insgesamt wurden 69 CTD/Rosette Stationen durchgeführt.

Umfangreiche Wasserbeprobungen und Laboruntersuchungen an Bord von *Polarstern* wurden von der biologischen Arbeitsgruppe durchgeführt. Ein Schwerpunkt liegt hierbei auf der Untersuchung, wie die Limitierung von Spurenmetallen und deren Recycling funktioniert und wie sich der globale Klimawandel auf die Mikroalgengesellschaften in der Drake Passage und der Westantarktischen Halbinsel auswirken wird. Zu diesem Zweck wurde an drei biologischen Hauptstationen über etwa einen Tag eine aus Teflon bestehende Membranpumpe und ein Schlauch aus Polyethylen zur Probenahme verwendet. Damit wurde das spurenmetallarme Meerwasser aus 25 m Tiefe direkt in einen Reinraumcontainer gepumpt und anschließend für umfangreiche Experimente genutzt.

Die paläoklimatischen Landarbeiten wurden durch weitere geologische und geodätische Arbeiten im Bereich des chilenischen Kontinentalrandes und der nördlichen Antarktischen Halbinsel ergänzt. Neben glazial-geologischen Fragestellungen, steht hierbei auch die Erforschung der tektonischen Entwicklung des Scotia Meer Region im Fokus. Dabei wurden an verschiedenen Lokationen Gesteinsproben für die thermochronologische Datierung gewonnen. Die geodätische Arbeitsgruppe erforschte über die Ausbringung von geodätischen Messstationen rezente Krustenbewegungen im Bereich der Antarktischen Halbinsel und des chilenischen Kontinentalrandes.

Fahrtverlauf

Die *Polarstern*-Expedition PS97 begann am 20.02.16 um 01:30 Uhr mit dem Auslaufen in Cabo Negro bei Punta Arenas, nach Beendigung der Bunker-Arbeiten. Aufgrund von logistischen und witterungsbedingten Verzögerungen konnten wir somit erst 4 Tage verspätet auslaufen. An Bord befanden sich 44 Besatzungsmitglieder sowie 52 Wissenschaftler/innen, Meteorologen, Techniker und Hubschrauberpersonal. Die wissenschaftlichen Teilnehmer aus 6 Arbeitsgruppen unterschiedlicher geologischer, ozeanographischer, geodätischer, und biologischer Disziplinen, darunter 13 Frauen, waren international bunt gemischt. So haben wir Kolleginnen und Kollegen aus Argentinien, Chile, Deutschland, Frankreich, Niederlande, Peru, Schweiz und Spanien an Bord. Eine Chilenin und zwei argentinische Wissenschaftler erfüllen dabei Aufgaben als offizielle Beobachter ihrer Heimatländer, da wir in beiden Ländern in küstennahen Gewässern innerhalb der 12 Meilenzone gearbeitet haben.

Gleich zu Beginn gab es neben dem Zeitverlust zusätzlich noch Änderungen in der Fahrtroute. Aufgrund der für die nächsten Tage vorhergesagten Wellenhöhen von bis zu 8,5 m im Südost-Pazifik vor Südchile, mussten wir unser Programm komplett umstellen und über

die Magellanstrasse in den Südwest-Atlantik ausweichen. Dort wurde zwar ebenfalls Sturm vorausgesagt, allerdings bot das südliche Südamerika bei den vorherrschenden Wind- und Wellenrichtungen aus Nordwest etwas Schutz. Wir kamen deshalb auf „nur“ maximal 4-5 Meter Wellenhöhe und erreichten am 21.02.16 unser erstes Arbeitsgebiet am argentinischen Kontinentalhang. Etwas westlich der Banco Namuncurá (Burdwood Bank) wurde an 2 Lokationen bei 460 m und 1310 m eine CTD mit Strömungsmesser (L-ADCP) eingesetzt, sowie die Wassersäule mit der Rosette beprobt. Im Anschluss begann die geologische Stationssuche mit PARASOUND und HDROSWEEP. Dabei zeigte sich, dass feinkörnige Sedimente in diesem Bereich des argentinischen Kontinentalhangs fast nicht vorhanden sind. Zwei Versuche Sedimente mit dem Multicorer und ein Versuch mit dem Schwerelot im tieferen Bereich des Hanges bei ca. 2500 m (PS97/005) blieben weitgehend erfolglos. Außer einigen Resten von Tiefwasserkorallen und grobem Sand konnten wir leider kein Sediment gewinnen. Aufgrund des wieder zunehmenden Windes (10-11 Beaufort) musste die weitere Stationssuche leider abgebrochen werden und wir suchten Schutz südlich der Isla de los Estados. Dort wurde am 22.02.16 ein Kastengreifer gefahren. Anschließend dampften wir westwärts im Schutz von Feuerland, um schließlich südlich den chilenischen Kontinentalhang zu erreichen.

Am 23.02.16 gelang es uns schließlich die ersten mächtigeren Sedimentabfolgen in einer Wassertiefe von 600 bis 750 m zu lokalisieren. Im Bereich einer „Sedimentdrift“ konnten wir drei ca. 6,5 bis 9 Meter lange Sedimentkerne gewinnen (PS97/009-011). Parallel zu den marin-geologischen Arbeiten begannen wir mit den Landarbeiten. Ein dreiköpfiges Team wurde mit dem Helikopter auf die Kap Horn Insel geflogen. Die weit vor dem chilenischen Festland gelegenen Inseln sind schwer zugänglich und die Seen sind nur mit dem Helikopter erreichbar. Leider konnte der Helikopter bei tiefer Wolkendecke nicht in der Nähe des Sees landen und ein Transport der Ausrüstung zu Fuß wäre zu zeitaufwendig gewesen. Deshalb musste dieser erste Versuch eine Seebohrung leider abgebrochen werden. Trotzdem konnten wir parallel eine geodätische Messstation auf der Insel installieren.

Am 24.02.16 passierten wir früh morgens Kap Hoorn und fuhren über den chilenischen Schelf in den südlichsten Teil unseres Arbeitsgebietes am pazifischen Kontinentalhang von Chile. Trotz im PARASOUND ersichtlicher Sedimentbedeckung konnten dort zunächst nur zwei kurz Schwerlotkerne (PS97/014-015) gewonnen und ein Multicorer erfolgreich eingesetzt werden. Bei guten Wetter- und Seeverhältnissen begannen wir bei ca. 55°30´S ein CTD-LADCP Transekt vom Schelf in Richtung des offenen Pazifiks (PS97/016-019). Dieses Profil wurde im mittleren Teil unterbrochen und wir bewegten uns nach Nordwesten bis ca. 54°20´S. In diesem Gebiet wurden mehrere Multicorer und Sedimentkerne mit nach Westen zunehmenden Kerngewinnen von bis zu 6 Meter Länge (PS97/026) erbohrt. Parallel zu den marinen Arbeiten am chilenischen Kontinentalhang, konnte das Landprogramm aufgrund von verhältnismäßig günstigen Wetterbedingungen erfolgreich fortgesetzt werden. Auf der „Isla Noir“ konnte ein vierköpfiges Team mehrere Sedimentkerne in einem See gewinnen. Am 27.02.16 konnten wurde das Team zurückgeholt und gleichzeitig kommnten auch noch weitere Helikoptereinsätze zur Gesteinsprobennahme im Bereich Bahia Cook – Isla Londonderry durchgeführt.

Am 28.02.16 setzten wir das begonnene CTD-LADCP Profil über den Cape Horn Strom in den offenen Südost-Pazifik fort (PS97/029-033). Dort begann unsere erste Überfahrt über die Drake Passage (westlicher Teil). Über die Subantarktische Front (SAF) und die Polarfront (PF) hinweg setzten wir das ozeanographische Profil fort. Mächtige Sedimente nördlich der SAF wurden aufgrund der zeitlichen Fixierung der biologischen Station südlich der PF erst auf der Rückfahrt beprobt. Südlich der PF wurde ein erster Testlauf für die Membranpumpe zur Wassergewinnung für die biologischen Projekte durchgeführt. Aufgrund von zu starkem Wind und Wellenverhältnissen, musste dieser aber abgebrochen werden (PS97/041). Nach einer weiteren CTD-LADCP Station konnten die ca. 24-stündigen biologischen Wasserpumparbeiten am 02.03. und 03.03.2016 dann bei ruhigem Wetter erfolgreich

durchgeführt werden. Im Anschluss haben wir am Phoenix Rücken in geringen Wassertiefen von 1200 bis 2300 mit dem Multicorer Oberflächensedimente beprobt. Erst bei ca. 61°S gelang es uns dann aber einen Schwerlotkern von ca. 2 m Länge zu gewinnen (PS97/046). Nach Süden hin wurde die Sedimentbedeckung nun immer mächtiger. So konnten wir längere Kolbenlote fahren und Kerngewinne von bis zu 13,65 m erzielen (PS97/049). Im Bereich der Hero Störungszone wurde die Sedimentbedeckung erneut gering mächtiger. Hier konnten nur kurze Schwerelote bis an den Nordrand des Südshetland-Grabens gewonnen werden (PS97/051-52).

Am 06.03.16 wurde die südlichste CTD-LADCP Station des Transektes über die westliche Drake Passage südlich des Grabens am Kontinentalhang der Antarktischen Halbinsel abgeschlossen. Vorbei an Smith Island dampften wir weiter nach Südosten in Richtung Graham Land auf der antarktischen Halbinsel. Vor Trinity Island liegend, wurde der Versuch unternommen mit dem Helikopter geodätische Messstationen auf der Antarktischen Halbinsel auszubringen. Aufgrund von tiefhängender Bewölkung musste dieser Versuch aber leider aufgegeben werden. Auf dem Weg wurden mehrere Schwerelotkerne mit bis zu 12,27 m Länge gewonnen (PS97/056). Zusätzlich gewannen wir an mehreren Stationen Oberflächensedimente mit dem Multicorer. Vom 07.03. – 09.03.2016 hielten wir uns im Bereich der Bransfield Strasse südlich der Südshetland-Inseln auf. Dort wurde eine intensive HYDROSWEEP/PARASOUND Vermessung, sowie Sedimentbeprobungen mit Schwere-, Kolbenlot, und Großkastengreifer durchgeführt. In den weichen Sedimenten dieser Region wurden durchweg lange Sedimentkerne mit mehrmals >10 m Länge gewonnen (z.B. PS97/071). Parallel wurden mehrere Hubschraubereinsätze zur Beprobung von Gesteinen und Schwebfrach in Schmelzwasserzuflüssen, Ausbringung eines weiteren geodätischen Messpunktes bei der chilenischen Antarktis-Station Arturo Prat, und ein Besuch der argentinischen Station Carlini durchgeführt. Während der Zeit im Bereich der antarktischen Halbinsel herrschten insgesamt gute Wetter- und Seeverhältnisse vor.

Am 10.03.16 setzten wir unsere Fahrt in Richtung Elephant Island fort. Dort wurden in der westlichen Bransfield-Strasse, im Bereich eines >2000 m Beckens zwei lange Sedimentkerne von bis zu 15,86 m Länge gewinnen (PS97/072). Am 11.3.16 wurden wir durch einen Sturm gezwungen vor Gibbs Island abzuwettern. Die im Bereich Elephant Island und der vorgelagerten Gibbs Island geplanten Hubschrauberflüge für die geodätischen und land-geologischen Arbeitsgruppen konnten zu diesem Zeitpunkt nicht durchgeführt werden und wurden am 12.03.16 nachgeholt. Anschließend wurden am Kontinentalhang vor Elephant Island ein Multicorer und Schwereloteinsatz gefahren, letzter ohne Sedimentgewinn. Am 13.03.16 wurden ca. 35 nm nördlich von Elephant Island Wasserpumparbeiten für die zweite biologische Station (PS97/076) durchgeführt. An selber Stelle wurde auch eine CTD-LADCP mit Wasserbeprobung auf Tiefe gefahren. In der direkten Umgebung wurden anschließend eine Sedimentdrift mit 2 Schwereloten beprobt und ein Kerngewinn von bis zu 13 m erzielt (PS97/077-078).

Am 14.03.16 begann unsere zweite Überquerung der Drake Passage an ihrer engsten Stelle entlang der Shackleton Störungszone, die sich von Elephant Island nach Nordwesten bis an die Südspitze des südamerikanischen Schelfes vor Kap Hoorn erstreckt. Wir querten die Shackleton Störungszone nach Westen und konnten dort an und nördlich der Südlichen Antarktischen Zirkumpolarstrom Front (SACCF) zwei bis zu acht Meter lange Sedimentkerne gewinnen (PS97/79-80). Nach erneuter Querung auf die Nordost-Seite des untermeerischen Gebirgszuges am 15.03.16, konnten wir über die PF hinweg ein detailliertes Profil mit sechs Sedimentkernen, die zwischen 6 und 14 m lang sind, gewinnen (PS97/083 bis PS97/089). Nach einem kurzen Zurückdampfen auf die eintägige dritte biologische Station (PS97/087), ging es am 19.03. nordwestwärts in Richtung der Subantarktischen Front. Nach Station PS97/089 verschwand die Sedimentbedeckung erneut, abgesehen von einem kleinen Sedimentbecken bei Station PS97/090.

Obwohl das Wetter und die Seebedingungen bei unserer zweiten Überquerung der Drake Passage außergewöhnlich gut waren, verschlechterten sich die mittelfristigen Wettervorhersagen nun stetig. Wir wussten von unserer ersten Überfahrt über die westliche Drake Passage, dass es dort nördlich der Subantarktischen Front durchgehende Sedimentbedeckung gibt. Vor zwei Wochen konnten wir zeit- und wetterbedingt in diesem Gebiet leider keine Sedimentkerne gewinnen. Deshalb entschieden wir uns kurzfristig dazu, diese schon bekannten Kernlokationen anzufahren und dort ein relativ engständiges Profil von Sedimentkernen zu gewinnen (PS97/92-94). Trotz Windstärke 7-8 Beaufort konnten wir hier am 20.03.16 an Station PS97/093 ein 20 m langes Kolbenlot einsetzen und mit 16,5 m Kerngewinn die zu diesem Zeitpunkt Rekordlänge auf PS97 erzielen.

Nachdem Abschluss der geologischen Arbeiten im subantarktischen Südost-Pazifik direkt südlich des Chile Tiefseegrabens, dampften wir mit voller Kraft westwärts zurück an die Kap Hoorn Insel, die wir am 21.03.16 morgens erreichten. Dort hatten wir in der zweiten Expeditionswoche auf der Insel eine geodätische Messstation eingerichtet, die nun mit dem Helikopter wieder erfolgreich eingeholt werden konnte. Gleichzeitig hatten wir im Februar einen See vom Helikopter aus vorerkundet, konnten aber aufgrund der Wetterverhältnisse damals nicht landen. Diesmal sah es besser aus. So entschieden wir kurzfristig eine dreiköpfige Landgruppe mit Seebohrausrüstung für zwei Tage auf der Kap Hoorn Insel auszusetzen. Trotz widriger Wetterbedingungen, besonders am 22.03.16, konnte die Gruppe erfolgreich einen ca. 4 m langen Sedimentkern aus dem See gewinnen. Gleichzeitig führten wir am 22.3.16 und 23.03.16 mit *Polarstern* Profilfahrten am östlich von Kap Hoorn gelegenen Kontinentalhang durch. Wie bereits in der zweiten Expeditionswoche weiter nördlich war die Lokalisierung von Kernlokationen mit ausreichender Sedimentbedeckung erneut schwierig, da sich hier der Bereich mit den stärksten Bodenströmungen am Nordrand der Drake Passage befindet und deshalb nur sandige Restsedimente finden lassen. Trotz einiger verbogener Kernrohre, konnten wir an drei Stationen Oberflächenproben und bis zu 8 m lange Schwerelot-Kerne gewinnen (PS97/095-097). Am 23.03.16 um 08:00 Uhr unterbrachen wir die Arbeiten am Kontinentalhang kurz, um die Landgruppe wieder an Bord zu holen. Leider musste diese Aktion bei sich rasch verschlechternden Flugbedingungen nach dem ersten Helikopter-Einsatz abgebrochen werden und die komplette Bohrausrüstung zunächst zurückgelassen werden. Am 23.03.16 beendeten wir die geologischen Arbeiten in der Scotia Sea und fuhren um die Spitze des südamerikanischen Schelfes herum in den Südost-Pazifik. Dort begannen wir am 24.03.16 ein detailliertes ozeanographisches Profil mit CTD-LADCP und Kranzwasserschöpfer. Dieses Profil (PS97/098-108) bildet das südlichste von insgesamt vier Profilen über den bisher kaum untersuchten Kap Hoorn Strom. Leider konnten einige Schelfstationen aufgrund der sich am 25.03.16 rasch verschlechternden Wetter- und Seebedingungen nicht mehr durchgeführt werden. Dafür tat sich am 25.03.16 morgens unerwartet ein Wetterfenster für Helikopterflüge auf und es konnte die gesamte Seebohrausrüstung, die wir zuvor auf der Kap Hoorn Insel zurücklassen mussten, geborgen werden.

Nach dem Abbruch des CTD Profils durchquerten wir am 26.03.16 rauhe See mit Windstärken, die teilweise Beaufort 10 erreichten. Bei langsamer Fahrt gegen Wind und Welle erreichten wir abends die etwas geschützten Gewässer der Bahia Cook am Eingang der chilenischen Fjorde. Hier warteten wir einige Stunden den Höhepunkt eines erneuten Sturmes ab. Nach dem Herausfahren aus der Bahia Cook nahmen Wind und Wellen erneut rasch zu. Obwohl einige Gegenstände von Tischen flogen und das ein oder andere Glas zu Bruch ging, ist zum Glück nichts Schlimmes passiert. Bei leicht abnehmenden Winden erreichten wir am 27.03.16 eine Kernstation, die wir bereits auf dem Hinweg beprobt hatten (PS97/020). Wir wollten nun mit unserem zweiten Kolbenlot mit kleinerem Durchmesser versuchen doch noch einen längeren Kern an dieser für einen Tiefbohrvorschlag für das „International Ocean Discovery Program (IODP)“ anvisierten Station zu gewinnen. Auch wenn wir uns mehr erhofft hatten, konnten wir immerhin 3 Meter Sediment gewinnen (PS97/109). Eine zweite potenzielle IODP Station etwa 40 Seemeilen nordwestlich brachte

leider nur 36 cm Sediment (PS97/110). Im weiteren Verlauf des Ostersonntags (27.03.16) verschärfte sich die Wetterlage erneut. Am Mittag und Nachmittag wurden Wellenhöhen von teilweise über 8 m erreicht, die sich aber schnell wieder abbauten, so dass wir am späten Abend eine weitere Kernstation (PS97/111) mit fast 10 m Kerngewinn abarbeiten konnten.

Nach Beendigung der Station PS97/111, nahmen wir in der Nacht Kurs nach Westen, in den offenen Südost-Pazifik hinaus. Kurz nach der Überquerung des Chile Grabens mit mächtigen Turbiditablagerungen, wurde der Sedimentcharakter schnell anders. Etwa 50 Seemeilen westlich des Chile Grabens auf einem Plateau in knapp 3900 m Wassertiefe zeigte das PARASOUND wohlgeschichtete Sedimentabfolgen mit einer Eindringung der Schallwellen von bis zu 100 m. Ein 20 m Kolbenlot (PS97/112) erbrachte eine fast 15 m langen Sedimentkern. Später erreichten wir an derselben Station mit einem 25 m Lot den Rekordkerngewinn von 22,37 m. Aufgrund der PARASOUND Daten und der Kerngewinne, entschieden wir kurzfristig, das erste Mal auf dieser Expedition Seismik zu fahren, da diese Kernlokation großes Potential für einen IODP Bohrvorschlag hat. Trotz einiger Probleme mit der Ausrüstung, sind die seismischen Profile bei guten Wetter- und Seebedingungen am 29.03.16 erfolgreich abgeschlossen worden. Erste Auswertungen zeigen etwa 500-600 m Sedimentmächtigkeit in diesem Gebiet an. Anschließend ging unsere Fahrt am 30.03.16 zurück in Richtung Kontinentalhang. Wir begannen schon vor der Überquerung des Tiefseegrabens mit einem weiteren ozeanographischen Profil mit CTD und LADCP Strömungsmessungen. Dieses dritte CTD Profil über den Cape Horn Strom soll die Variabilität dieses klimatisch und ozeanographisch wichtigen und bisher wenig erforschten Meeresstromes besser abbilden. Das Profil begann in mehr als 4000 m Wassertiefe und bestand aus 12 Stationen über den Kontinentalhang hinauf auf den chilenischen Schelf bei etwa 120 m Wassertiefe (PS97/115-127). Unterbrochen durch eine Kernstation in etwa 2500 m Wassertiefe (PS97/122) mit einem für den Kontinentalhang sehr guten Kerngewinn von mehr als 10 m, wurden die ozeanographischen Arbeiten am 31.03. abgeschlossen.

Im weiteren Verlauf nahm der Wind wieder zu und wir nutzten die Zeit zur Suche von Sedimentkern-Stationen mit HYDROSWEEP und PARASOUND. So arbeiteten wir uns im Zickzack-Kurs, um möglichst weite Bereiche des Kontinentalhanges abzufahren, nach Norden fort. In der Nacht zum 01.04.16 konnten zwei Sedimentstationen lokalisiert werden und erfolgreich mit Multicorer, Kolbenlot und Schwerelot beprobt werden (PS97/128-129). Dabei wurde der Tiefenbereich von ca. 1800 m bis 3000 m abgedeckt. Am 02.04.16 erreichten wir schließlich unser letztes Arbeitsgebiet am Kontinentalhang vor dem pazifischen Eingang der Magellanstraße. In diesem Gebiet wurden bereits 2007 auf einer Expedition mit dem französischen Forschungsschiff Marion Dufresne Sedimentkerne gezogen. Damals konnte auf Marion Dufresne mit 6 t Gewicht ein 30 m langer Kolbenlot-Kern aus ca. 1000 m Wassertiefe gewonnen werden (MD07-3128). Auf PS97 waren wir an dieser Station (PS97/137) mit ca. 8 m Kernlänge bei knapp 2 t Gewicht weniger erfolgreich. Allerdings konnten wir in der Umgebung erstmalig noch weitere Sedimentkerne gewinnen und vergleichsweise flache Wassertiefen von 850 m (PS97/138) und 600 m (PS97/139) beproben. In der Umgebung der Marion Dufresne Kernstation haben wir eine detaillierte Profilfahrt mit HYDROSWEEP und PARASOUND durchgeführt, um die Sedimentbedeckung und Tiefenstruktur genauer zu kartieren. Dabei zeigten sich eine hohe Sedimenteindringung im Tiefenbereich um ca. 1000 m. Wir vermuten, dass es sich hierbei um eine „Sedimentdrift“ handelt, in der es durch relativ geringere Strömungsgeschwindigkeiten bevorzugt zur Sedimentation kommt. Derartige Sedimentabfolgen sind für die Paläoozeanographie besonders interessant, da dort oftmals hohe Ablagerungsraten auftreten, die eine hohe zeitliche Auflösung der späteren Rekonstruktionen erlauben. Da der FS Marion Dufresne Kern von dieser „Sedimentdrift“ bereits sehr gute Paläoklimazeitreihen geliefert hat, entschlossen wir uns das zweite Mal auf PS97 dazu ein seismisches Kreuzprofil zu fahren. Ein Tag mit relativ guten Wind- und Seeverhältnissen erlaubte unseren Geophysikern mit Hilfe der Mannschaft und anderer Wissenschaftler erneut den Geophysik-Streamer

auszubringen. Die ersten Auswertungen der seismischen Profile sind sehr vielversprechend und lassen auf ein 700-900 m mächtiges Sedimentprisma schließen.

Im Anschluss an die Seismik begannen wir mit dem nördlichsten ozeanographischen Profil über den Cape Horn Strom vor Chile. Bei stark zunehmendem Wind mussten diese Arbeiten in der Mitte des Profils abgebrochen werden. Wellenhöhen von 7 m aus Nord bis Nordwest, das heißt von der Seite, machten unsere Flucht in den Schutz der Magellanstraße sehr ungemütlich. Zum Glück erreichten wir am 04.04.16 abends sichere Gewässer. Für die Zeit unseres Abwetterns am 05.04.16 schätzte unser Meteorologe außerhalb des Schutzes der Magellanstraße Windstärke 12 und einer mittleren Wellenhöhe von 10 m. Am Abend des 05.04.16 beruhigte sich die Lage langsam, so dass wir um 22 Uhr erneut nach Westen herausfuhren, um das begonnene ozeanographische Profil zu beenden. Dieses konnte am 06.04.16 um 16 Uhr beendet werden. Unsere 151. und letzte Station PS97/151 war damit abgeschlossen. Am 07.04.16 unternahmen wir den Versuch eines Hubschraubereinsatzes für die Landgeologie, der aber aufgrund der Wetterverhältnisse leider abgesagt werden musste. Im Anschluss begann die *Polarstern* mit dem Transit durch die Magellanstraße nach Punta Arenas. Am 08.04.16 um 07:00 Uhr lagen wir auf Reede. Das Ausschiffen der Wissenschaftler begann um 10:00 Uhr. Damit war die *Polarstern*-Expedition PS97 zu Ende.

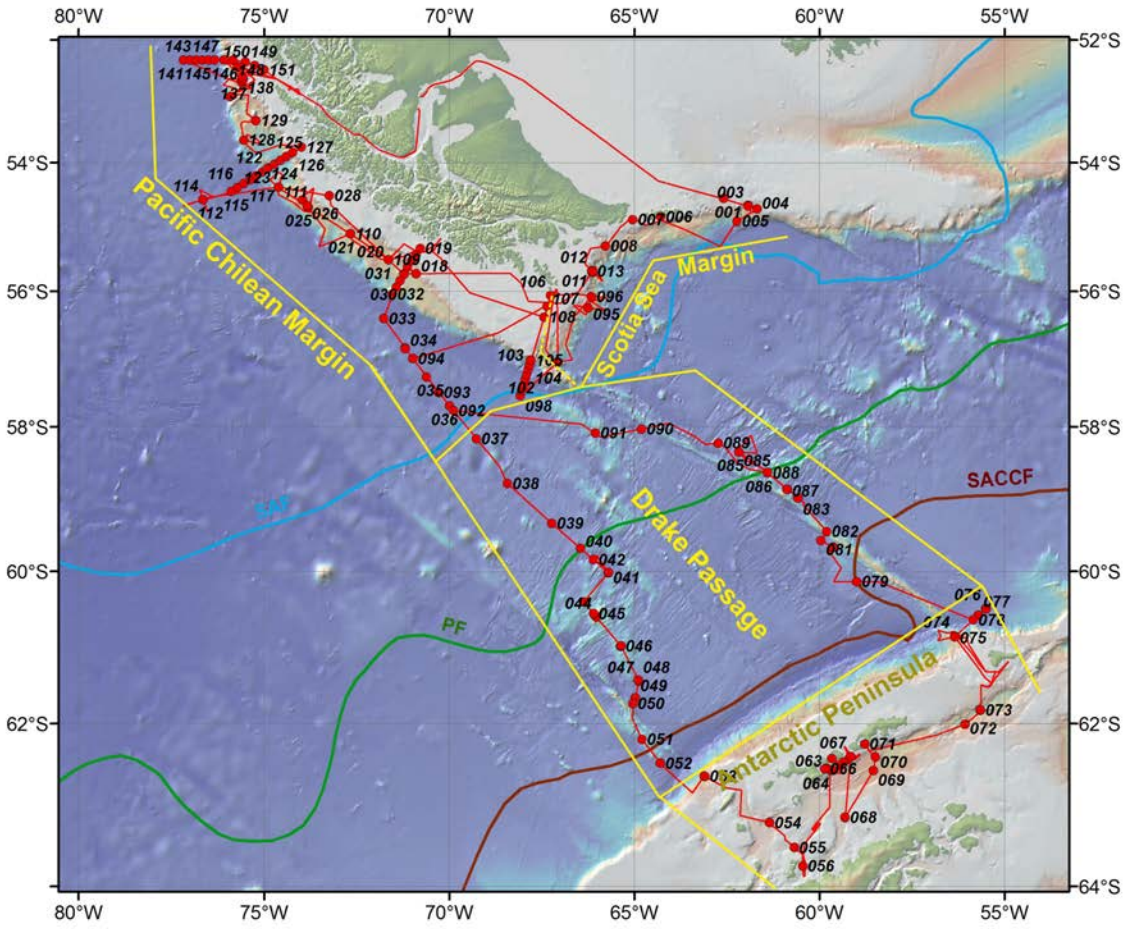

Abb. 1.1: Fahrtroute und Stationen des FS POLARSTERN während der Expedition PS97 von Punta Arenas entlang des südamerikanischen Kontinentalrandes, im Bereich der Drake Passage und des Nordrandes der Antarktischen Halbinsel. Die Zahlen auf der Karte beziehen sich auf die Stationsbezeichnungen (PS97/XXX). SAF= Subantarctic Front; PF= Polar Front; SACCF= South Antarctic Circumpolar Current Front.

Fig. 1.1: Cruise track and stations of RV POLARSTERN during expedition PS97 from Punta Arenas along the South American continental margin, the Drake Passage, and the northern rim of the Antarctic Peninsula. Numbers refer to stations (PS97/XXX). SAF= Subantarctic Front; PF= Polar Front; SACCF= South Antarctic Circumpolar Current Front.

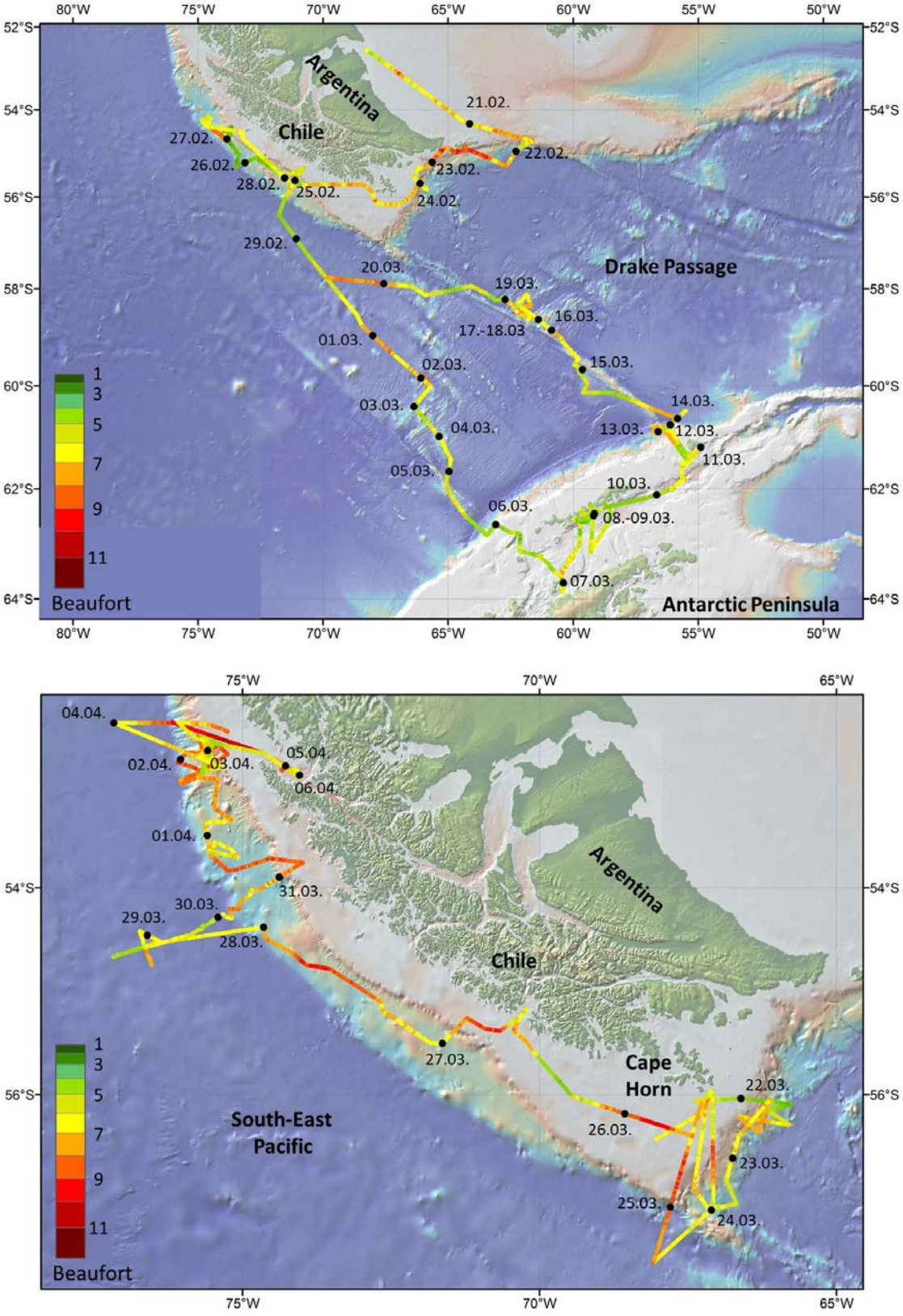

Abb. 1.2: Windstärke entlang der Fahrtroute der Polarstern Expedition PS97.

Fig. 1.2: Wind strength along the cruise track of Polarstern expedition PS97.

Summary

The *Polarstern* expedition PS97 “Paleoceanography of the Drake Passage (PaleoDrake)” started on February 16, 2016 in Punta Arenas (Chile) and ended on April 8, 2016 again in Punta Arenas. Onboard *Polarstern* were 44 crew members as well as 52 scientists, meteorologists, technical staff and helicopter pilots. The scientific members belonged to six working groups with research expertise in geology, oceanography, geodesy and biology. Scientific members came from Argentina, Chile, Germany, France, Netherlands, Peru, Switzerland and Spain. One Chilean and two Argentine scientists on board fulfilled the role of official expedition observers, nominated by their home countries.

The principal working area of cruise PS97 was the Drake Passage which forms the major geographical constriction for the flow of the Antarctic Circumpolar Current and plays an essential role in the modern ocean circulation patterns and global climate. Despite its importance for modern and likely also future climate, little is known about past climatic and oceanographic changes on longer, geological time-scales in this region. Therefore, the principle scientific goal of the marine geological work is to enhance understanding of the paleoceanographic role of the Drake Passage during Quaternary global climate variations at orbital and sub-orbital time-scales.

Polarstern Expedition PS97 focussed on marine geological investigations on two north-south transects across the western and central Drake Passage. The recovered surface sediment samples and sediment cores in the open Drake Passage are the first deep-sea sediments taken in this area since the geological work performed with the American research vessel Eltanin in the 1960ies. A second major geological working area was the Argentinian/Chilean continental slope in the Scotia Sea and the Pacific southern Chilean continental margin between Cape Horn and the Magellan Strait. In the area of the Antarctic Peninsula we recovered surface sediment samples and sediment cores in the Bransfield Strait. The major results of the geological work of PS97 include:

- We acquired Hydrosweep and PARASOUND data during all transits and coring site surveys (outside the approved 3-miles zone of Chile and Argentina), in total over a length of ca. 5900 nm. These data formed the most important background information for localizing suitable coring sites. The PARASOUND data document a very sparse sediment cover along the Argentinean/Chilean Scotia Sea margin and within the Polar Frontal Zone of the western Drake Passage.
- Surface sediments were recovered successfully at 53 stations with the Multicorer and at 11 stations with the Giant Box Corer. Fourty-one gravity corer deployments, of which 33 were successful, yielding ~160 m sediment cores. Thirty-two piston corer deployments, of which 30 were successful, yielded ca. 300 m sediment cores. The longest core had a length of 22.73 m.
- The most important geological achievement is the recovery of sediment cores along a north-south transect across the central Drake Passage in the area of the Shackleton Fracture Zone. This Transect starts south of the Polar Front and extends north into the central Polar Frontal Zone. First shipboard sediment-physical measurements and stratigraphic age determinations suggest that we mostly recovered high-resolution sediment records extending over one complete glacial-interglacial cycle.
- Off Chile we could recover sediment cores over a depth range from ca. 600 m to 4000 m, in order to reconstruct changes in the water mass structure within the northern Antarctic Circumpolar Current before entering the Drake Passage.
- The geophysical and geological survey for potential *International Ocean Discovery Program* (IODP) drilling locations at the Chilean continental slope at a sediment drift with high resolution sediment sequences with a total thickness of up to 900 m was very successful. A second geophysical cross profile was accomplished at a deep-sea

location about 50 nm west of the Chile Trench. The data suggest up to 500 m sediment thickness. This site is likewise very promising for IODP drilling.

- In the area of the Antarctic Peninsula, we recovered several long sediment cores from the Bransfield Strait. These cores contain high-resolution Holocene sediment records, which will be used for improving the reconstruction of melt water fluxes and biomarker-based sea-ice reconstructions in the Antarctic realm.

The marine geological work was supplemented by paleoclimatic land work. This work was carried out on the southern Chilean islands Isla Noir and Isla Cabo de Hornos, which are only accessible by Helicopter. In spite of bad weather conditions, we could recover sediment cores from lakes on both islands.

An additional focus of Expedition PS97 were oceanographic measurements in order to better document the poorly known Cape Horn Current and the western Drake Passage. A major achievement was the acquisition of current velocity measurements. In addition, we obtained a substantial set of water samples and plankton hauls. These will be used to improve the calibration and validation of a variety of microfossil-based proxy methods. In total we worked at 69 CTD/rosette stations.

Extensive water sampling and subsequent laboratory experiments onboard *Polarstern* were undertaken by the biological working group at 3 major biological stations within the Drake Passage. A major focus of the biological work is to understand how trace metal limitation and cycling operates and how global change will affect the Drake Passage and Antarctic Peninsula ecosystems. To achieve this, a teflon membrane pump connected to a polyethelene line was used to pump surface seawater from 25 m depth for ca. 24 hours directly into a trace metal clean van where the seawater could be sampled.

The paleoclimatic work on land was complemented by geological and geodetic investigations at the Chilean continental margin and the northern Antarctic Peninsula (South Shetland Islands). Besides glacial-geological questions, our work focused on the investigation of the long-term tectonic reconstruction of the Scotia Sea area. For this purpose, we collected rock samples for thermochronological analyses. The geodetic working group investigated recent crustal motion patterns at the Antarctic Peninsula and along the southern Chilean margin.

Itinerary

The *Polarstern* Expedition PS97 began on February 20th, 2016 at 1:30 am after we had finished fuelling at Cabo Negro close to Punta Arenas. We left with four days delay due to weather related logistical issues. Fourty-four crew and fifty-two scientists, meteorologists, technicians and helicopter staff were on board. The scientific team formed six working groups focussing on geological, oceanographic, geodetic and biological research. A wide mix of nationalities were on board, with scientists from Argentina, Chile, Germany, France, Netherlands, Peru, Switzerland and Spain. Our work was going to take place within the 12 nautical mile zone of Chile and Argentina, hence one Chilean and two Argentine scientists acted as official observers during our cruise.

In addition to our delayed departure we also had to change our planned route. The weather forecast for the southeast Pacific indicated wave heights of up to 8.5 meters at the Chilean coastal margin, hence we changed our programme and exited the Strait of Magellan through the south-west Atlantic. Though the forecasted storm also impacted this area, Tierra del Fuego provided some shelter from the dominating wind and waves coming in from north-westerly direction. We arrived at our first working area on the 21st of February 2016 at the Argentine continental margin with wave heights of “just” 4-5 meters. West of Banco Namuncurá (Burdwood Bank) two CTDs with current meters (L-ADCP) and water column rosettes were deployed at two locations (460 & 1310 meters). Immediately therefafter, we

started looking for our first geological station with PARASOUND and HYDROSWEEP. Our surveys showed that hardly any fine grained sediment deposits occur at the Argentine continental margin. Two multi-cores and one gravity core at ca. 2500 meters water depth (PS97/005) were largely unsuccessful. Apart from coral remains and coarse-grained sands we could not obtain any sediment. Due to the increasing winds (10-11 Bft) we had to interrupt further station work and sought shelter at Isla de los Estados, where we used a box corer on the 22nd of February 2016 (PS97/005). We then continued westward, in the lee of Tierra del Fuego to reach the southern Chilean continental margin.

On February 23, 2016 we finally managed to localize sediment deposits at 600750 meters water depth. From a sediment drift we obtained 6.5-9 meters of sediment cores (PS97/009-011). Parallel to the marine geological work we also started with the land work. A team of three was flown out to Isla de Hornos, located southwest of the Chilean mainland, with the aim of obtaining lacustrine sediment cores. However the low cloud cover hindered the helicopter from landing close to the lake site. Carrying all the equipment from the helicopter landing site was not possible, hence the coring work had to be abandoned. Never the less we meanwhile managed to install a geodetic station on the island.

On February 24,2016 we passed Cape Horn in the early morning heading toward our southern most working area off the Chilean continental margin. Though the PARASOUND indicated considerable sediment cover only two short gravity cores (PS97/014-15) and a multi-corer could be successfully retrieved from this site. During good weather and sea conditions we began the first of four CTD-LADCP transect from 55°30'S toward the open Pacific (PS97/016-019). Due to logistical reasons, the transect had to be interrupted half-way through as we then moved northwards to 54°20'S. We recovered several multicores and sediment cores with increasing sediment length toward west of up to 6 meters (PS97/026). Parallel to the marine geological work along the Chilean continental shelf, the land work could also be continued due to favorable weather condition. On Isla Noir a team of four could obtain several lacoustrine sediment cores. On February 27, 2016 the island team and equipment could be recovered successfully. In parallel, a second land team recovered geological samples from Bahia Cook/Isla Londonderry.

On the February 28, 2016 we continued the CTD-LADCP profile of the Cape Horn current over the open southeast Pacific (PS97/029-033). Here our first traverse of the western Drake Passage commenced. We covered the Subantarctic and Polar Fronts (SAF & PF; Fig. 1.1) with the oceanographic profile. Major sediment deposits were identified north of the SAF. However due to the biological stations' timing constraints, these were sampled on the return leg. South of the PF a test run of the biological membrane pump was undertaken. Due to strong winds and high waves the work had to be interrupted (PS97/041). Following another CTD-LADCP station the biological water pump was run for 24 hours between on March 2 and 3, 2016. After this we sampled surface sediment with the multi-corer at the Phoenix Ridge in water depths of 1200-2300 meters. At roughly 61°S we managed to recover two-meter gravity core (PS97/046). South of here the sediment cover was gradually increasing, so we employed our piston-corer with sediment recovery of up to 13.65 meters (PS97/049). In the Hero Fracture Zone sediment cover decreased again. From here until the northern margin of the south Shetland Trench, we used the gravity corer to obtain sediment (PS97/051-52).

On March 6, 2016 we finished the first CTD-LADCP transect across the Drake Passage, terminating in front of the Antarctic Peninsula continental margin. We passed Smith Island in southeasterly direction to get closer to Graham Land, Antarctic Peninsula. Approaching Trinity Island the geodetic team headed toward the Antarctic Peninsula via helicopter to install two geodetic measuring sites. Unfortunately, the attempts had to be abandoned due to clouds building up along the coastal areas that would have hindered sight by the helicopter

pilots. During our path toward the Antarctic Peninsula we obtained several gravity cores with sediment recovery of up to 12.27 meters (PS97/056). In addition we obtained several multi corer surface samples. Between March 7 and 9, 2016 we were working in the Bransfield Strait south of the South Shetland Islands. Here we conducted extensive hydrosweep and PARASOUND surveys and obtained several gravity, piston and box corer samples. This region is characterized by soft sediment, hence several long sediment cores of >10 meters in length could be recovered (e.g. PS97/071). Parallel to the marine geological work, several helicopter flights took place: thermochronological and cosmogenic rock sampling, glacier meltwater sampling for suspended sediment load determination, geodetic instrument installation at the Chilean Station Arturo Prat and a visit to the Argentine station Carlini. Throughout our time around the Antarctic Peninsula the weather and sea conditions were better than expected.

On the 10th of March 2016 we continued towards Elephant Island. Here, in the western Bransfield Strait in a 2000-meter deep basin two sediment cores of up to 15.86 meters were recovered. On the 11th of March 2016 we were forced to seek shelter in front of Gibbs Island due to an impending storm. The planned land work on Gibbs and Elephant Island for the geodetic and geological work had to be postponed for a day due to the deteriorating weather conditions, they were conducted on March, 12 2016. Following the land work a multi- and gravity corer were run along the continental margin of Elephant Island, with no sediment recovery from the latter. On the March 13, 2016, ca. 35 nautical miles north of Elephant Island the second biological station was completed (PS97/076). At the same site a deep CTD-LADCP with water sampling was conducted whilst in the immediate vicinity two gravity cores with a sediment recovery of up to 13 meters were obtained (PS97/077-078).

On the 14th of March 2016 we embarked on our second travers of the Drake Passage. Specifically the transect was aimed at covering the narrowest section of the Drake Passage, along the Shackelton fracture zone, which stretches from Elephant Island toward north west up to the southern margin of the South American shelf, just south of Cape Horn. Along the western margin of the Shackelton Fracture Zone we obtained sediment cores at and north of the South Antarctic Circumpolar Front (SACCF, Fig. 1.1) with recoveries of 2-8 meters (PS97/079-080). Following migration toward the north-east side of the submarine mountain range, we managed to obtain a detailed sediment profile across the PF with a total of six cores of 6-14 meters in length (PS97/083-089). A brief U-turn was undertaken for the third biological station (PS97/087), after which we continued north, towards the SAF. After station PS97/089 sediment cover close to disappeared apart from a small pocket at PS97/090.

Though the weather and sea conditions had been relatively pleasant during our second Drake Passage transect, the forecast for the following days were not looking good. We therefore had to decide whether to continue our original trajectory towards Cape Horn or to move back to our first transect. Two weeks prior, during our first Drake Passage transect, we identified significant sediment cover north of the SAF. Unfortunately time constraints and poor weather hindered sampling at this time. We therefore decided to return to our first transect route to obtain a close network of sediment cores (PS97/092-094). We managed to deploy a 20 meter long piston corer and recovered 16.5 meters of sediment on March 20, 2016 (PS97/093). At this point during the expedition, this constituted our maximum sediment recovery.

After finalizing our marine geological work in the sub-Antarctic south-east Pacific just south of the Chile trench we continued toward Cape Horn island. We reached the island in the morning hours of March 21, 2016. During the second week of our expedition we had established a geodetic measuring station here, which we managed to successfully recover with the helicopters. In a second attempt with more promising weather a land group of three recovered on the island during two days a long core from a lake. Parallel to the land work *Polarstern* conducted hydro-acoustic profile work east of Cape Horn along the continental

margin between March 22 and 23, 2016. Similarly to our experience from the second week, localization of coring sites with substantial sediment cover was proving difficult. This part of the Drake Passage has one of the strongest bottom currents with residual sandy sediments. Though several bent cores were retrieved, we managed to obtain surface sediment at three locations and one long gravity core of 8 meters here (PS97/095-097). On March 23, 2016 at 8 am we halted our work along the continental margin to bring the land group back on board. Due to rapidly deteriorating weather only one helicopter flight was possible. Hence the land group made it back, but the coring equipment had to be left on Cape Horn. On the March 23, 2016 we finished our marine geological work in the Scotia Sea and commenced our work in the south-east Pacific. On March 24, 2016 we started a detailed oceanographic profile with the CTD-LADCP. This profile (PS97/098-108) forms the southern most of four profiles aimed at examining the Cape Horn current. Unfortunately some of the planned stations along the profile could not be completed due to once again deteriorating weather conditions. Nonetheless a brief window of good weather on March 25, 2016 allowed for recovering the abandoned coring equipment on Isla Hornos.

After prematurely halting the CTD profile work we passed rough seas on the 26th of March 2016 with wind speeds of up to 10 Bft. With reduced vessel speed against wind and waves we arrived at Bahia Cook in the Chilean fjords. Another storm was in the forecast, and we sought shelter here for several hours. Exiting Bahia Cook wind and waves once more increased in speed and height. Though several items fell from the tables and the one or other glass broke, nothing major was damaged. With slightly decreasing winds we reached a previously visited and sampled coring site on the 27th of March 2016 (PS97/020). We wanted to use our second piston corer with smaller diameter to obtain an even longer sediment record from this site. In particular we wanted a second core, as this site forms part of a deep ocean-drilling proposal for IODP. Though we were expecting more, we obtained a 3-meter long sediment core (PS97/109). Another potential location for an IODP site 40 nm northwestwards only saw a recovery of 36 cm (PS97/110). The weather in the afternoon of Easter Sunday was becoming more serious with wave heights of up to 8 meters. Luckily things calmed down toward the evening where we managed to obtain another 10-meter long sediment core (PS97/111).

After finishing our station work at PS97/111 we headed westward entering the open south-east Pacific. Shortly after passing the Chile trench with massive turbidite deposits the sediment character changed significantly. About 50 nm west of the Chile trench on a plateau in 3900 meters water depth the PARASOUND showed nicely layered sediment with a penetration depth of up to 100 meters. A 20-meter long piston corer (PS97/112) had a recovery of close to 15 meters of sediment at this site. Later that day we ran another 25-meter long piston corer with our record recovery of 22.37 meters of sediment. Based on the PARASOUND and our sediment recovery we decided to establish a seismic profile, as this site has great potential for an IODP drilling location. Though we had some initial problems with our seismic equipment, the profiles were successfully completed on March 29, 2016. Initial data analysis indicates sediment cover of 500-600 meters. On the March 30, 2016 we headed back towards the Chilean continental margin and started with another CTD-LADCP oceanographic profile shortly after passing the Chilean trench. The third CTD profile is also aimed at understanding the oceanographic characteristics of the little studied Cape Horn Current. The profile started at a water depth of 4000 meters and consisted of 12 stations up until the Chile shelf where water depths were ca. 120 meters (PS97/115-127). Shortly interrupted by another coring site with a sediment recovery of over 10 meters (PS97/122) the oceanographic transect work was completed on the March 31, 2016.

Winds were increasing in speeds again; hence, we used the time to identify suitable sediment coring sites with HYDROSWEEP and PARASOUND surveys. For this purpose, we crossed the Chilean continental slope several times in northerly direction . In the night of the 1st of April we had located two coring sites where multi, piston and gravity corers were

deployed (PS97/128-129)at water depths of 1800-3000 meters. On the April 2, 2016 we reached our last working area at the entrance of the Magellan Strait on the Pacific side. In the same area, an expedition by the French research vessel Marion Dufresne in 2007, had recovered a 30-meter long sediment core at 1000-meter water depth using 6 tons of weights (MD07-3128). We were less successful and recovered 8 meters of sediment using 2 tons of weight (PS97/137). That said, we managed to obtain cores from proximal sites in relatively shallow water depths of 850 and 600 meters (PS97/138-139). We also ran detailed HYDROSWEEP and PARASOUND surveys at and surrounding the Marion Dufresne core site to map the sediment cover and structure. At ca. 1000 meters a sediment drift was identified likely located here due to low current velocities and preferential sediment deposition. These types of sediment deposits are particularly interesting for paleoceanographic work. Typically high sedimentation rates at these sites allow for paleoclimatic reconstructions with high temporal resolution. The Marion Dufresne core from this sediment drift has provided highly insightful paleoclimate time-series data, hence we decided to run our second seismic profile at this site. Relatively good wind and sea conditions allowed for a successful geophysical work. Preliminary analysis of the seismic profiles suggests a sediment succession of ca. 700-900 meters thickness.

After finishing the seismic work we moved northward to start the fourth oceanographic profile over the Cape Horn Current. As wind speeds were increasing this work had to be interrupted. Wave heights of up to 7 meters from north and north-westerly direction made for a rather uncomfortable retreat into the Strait of Magellan. Luckily we reached calmer waters in the evening of April 4, 2016. Whilst we were waiting for the storm to pass, our meteorologist forecast winds speeds of up to 12 Bft and wave heights of 10 meters outside of the sheltered areas. In the evening of April 5, 2016 the weather was slowly calming down so that we could once more head for the open Pacific to continue with the oceanographic profile. The CTD profile was completed on the 6th of April 2016 at 4 pm as our 151st and last station of the PS97 Expedition. On the 7th of April we attempted another helicopter flight for the land geologists, however the weather did not allow for it in the end. *Polarstern* started its transit through the Strait of Magellan to Punta Arenas and reached Punta Arenas on the April 8, 2016 at 7 am. The scientists were shuttled to the harbor starting 10 am the same day, which marked the end of the *Polarstern* Expedition PS97.

2. WEATHER CONDITIONS

Max Miller and Hartmut Sonnabend DWD

During the night to Saturday, February 20, 2016, 01:30 am, *Polarstern* left Punta Arenas for the expedition PS97. Rain, 10° C and fresh northerly winds were observed.

A small storm approached Cape Horn from the west. After leaving the Strait of Magellan, winds veered northwest to west and increased up to Bft 7 on Saturday afternoon (Feb. 20th). During the night to Sunday, winds peaked temporarily at Bft 8 and forced a sea state of 4 m. A new storm already developed west of Tierra del Fuego. Therefore, winds abated only for short times during the night to Monday (Feb. 22nd) but increased up to force 10 from northwest on Monday morning. We avoided rough seas by operating within the shelter of the Island *Isla de los Estados*.

During the following days troughs (westerly winds at Bft 8) and ridges (calming down) alternated while crossing the Drake Passage. Sea state did not exceed 5 m.

During the night to Sunday (Mar.06th) a low crossed Drake Passage. We got into its centre at only light and variable winds while sailing off the Antarctic Peninsula. On Sunday southwesterly winds increased clearly. However, between the South-Shetland-Islands and the Antarctic Peninsula we often were protected by the islands. Within the lee of Trinity Island we observed a Foehn effect: temperature rose and humidity decreased. Afterwards winds did not exceed Bft 6 and the islands prevented a significant sea state.

On Wednesday (Mar. 09th) a storm formed west of Tierra del Fuego and its centre reached the northern end of the Antarctic Peninsula during the night to Friday (Mar. 11th). On Friday morning, (we operated within the lee of Elephant Island) westerly winds peaked at force 10 for short times. After leaving the shelter of the island we still observed a sea state of 5 to 6 m.

On Saturday (Mar. 12th) a ridge enabled helicopter flights to Gibbs and Elephant Island at only moderate winds from southwest.

On Monday (Mar. 14th) a low formed over Bellingshausen Sea and got stationary. Therefore *Polarstern* steamed north within the Drake Passage at north-westerly winds Bft 6 to 7. On Thursday (Mar. 17th) the low finally moved towards the Weddell Sea via Antarctic Peninsula. Winds veered southwest and abated clearly.

On Saturday (Mar. 19th) a new storm arrived at Bellingshausen Sea, extended towards Drake Passage and moved slowly to Weddell Sea. Saturday afternoon northerly winds freshened rapidly up to force 8 and veered west in the evening. On Sunday stormy conditions continued at a sea state of 5 meters. Approaching Cape Horn on Monday (Mar. 21st) winds abated in connection with a weak ridge.

During the following days, a large low over Amundsen Sea established oneself. Several secondary lows moved along its east side and kept the stormy condition going on west of Drake Passage and along the Pacific coast of Tierra del Fuego. On Good Friday (Mar. 25th) while steaming from Cape Horn towards Bahia Cook we observed north-westerly winds 9 to 10 and a sea state of 8 m. Only on Easter Sunday (Mar. 27th) the large low moved away towards Antarctic Peninsula and on Easter Monday a ridge followed. Winds decreased temporarily to Bft 3.

Already during the night to Tuesday (Mar. 29th) a new low approached from the South Pacific and forced another stormy period until Saturday (Apr. 02nd) with only short breaks. Winds

from west to northwest peaked at Bft 9 for several times together with a sea state up to 7 m and winds did not fall below force 6. Only during the night to Sunday (Apr. 03rd) a weak ridge crossed our operation area.

But a new storm reached Amundsen Sea. It built a trough to the north, which moved slowly towards the coast of Tierra del Fuego and created the stormy highlight at the end of the cruise. During the night to Monday (Apr. 04th) winds from northwest to north increased up to Bft 8 and on Monday up to Bft 10. Until we reached the Strait of Magellan the sea state of 7 m has not been fully developed. On Tuesday we stayed within the protection of the Strait of Magellan to avoid forecasted wind force 12 outside. On Wednesday (Apr. 06th) final scientific work could be done off the coast at Bft 6 to 9 and a sea state of 5 to 6 m. On Wednesday evening while entering the Strait of Magellan again winds from northwest increased temporarily up to Bft 10 due to the funnel like entrance.

On Friday morning, April 08th 2016, *Polarstern* reached Punta Arenas at gusty westerly winds and some showers.

Figures 2.1 to 2.3 summarize the weather conditions during Polarstern Expedition PS97.

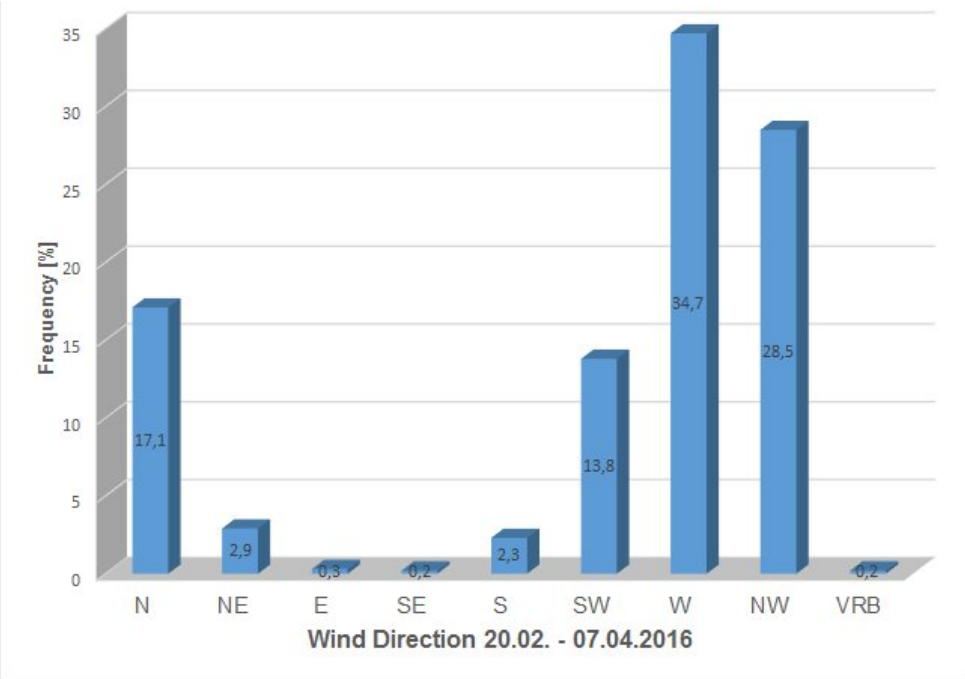

Fig. 2.1: Distribution of wind direction.

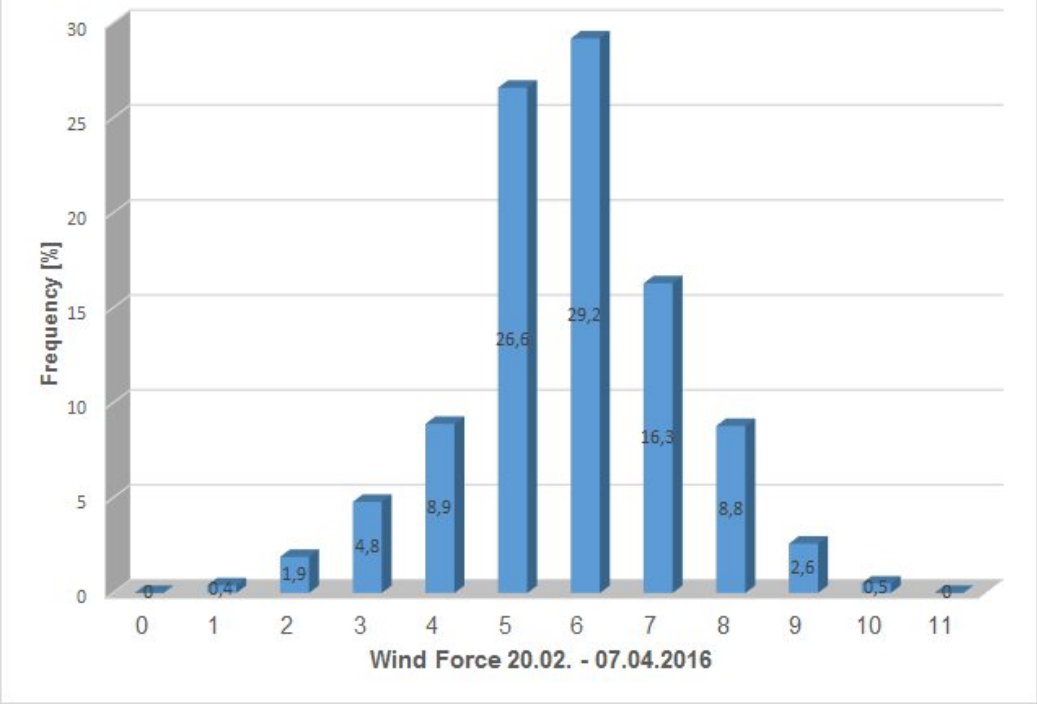

Fig. 2.2: Distribution of wind force.

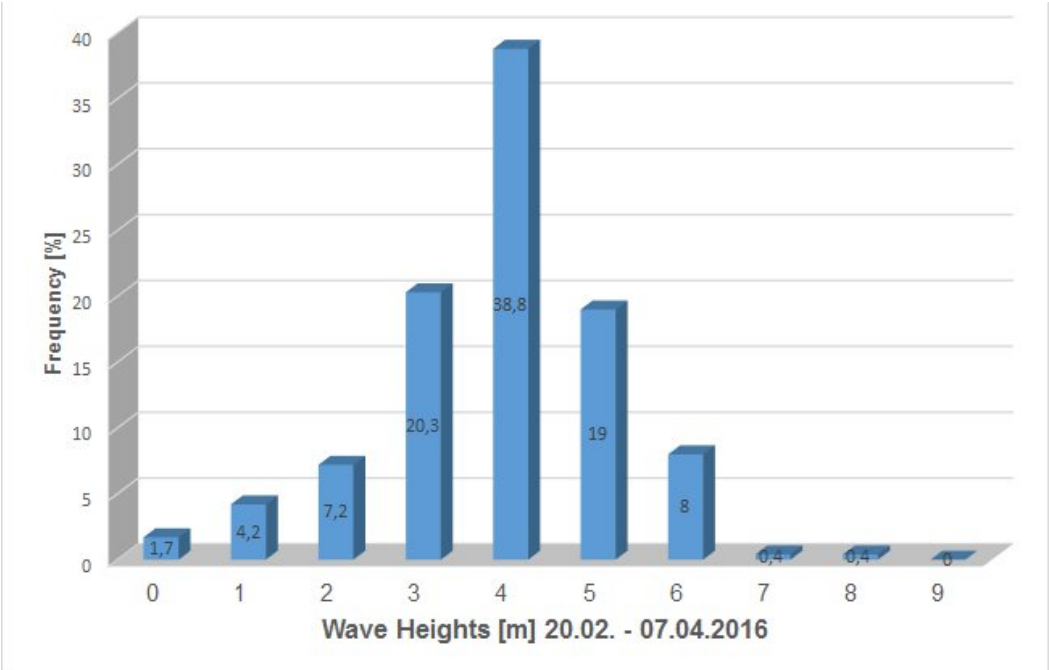

Fig. 2.3: Distribution of wave heights.

3. MARINE GEOLOGY AND PALEOCEANOGRAPHY

3. 1. Background of Marine Geology and Paleoceanography

Frank Lamy[1], Helge W. Arz[2], Christian Hass[1], Gerhard Kuhn[1], Rolf Kilian[3], Carina Lange[4], Juliane Müller[1], Dirk Nürnberg[5]
Not on board: Ralf Tiedemann[1], Andreas Mackensen[1], Gregor Knorr[1], Bernhard Diekmann[1], Boris Dorschel[1], Ulysses Ninnemann[6], Alina Polonia[7]

[1]AWI, [2]IOW,
[3]U Trier,
[4]UdeC/COPAS/IDEAL,
[5]GEOMAR,
[6]U Bergen
[7]CNR-ISMAR Bologna

Background and objectives

The Antarctic Circumpolar Current (ACC) is the world's largest current system. Through inducing pronounced upwelling and formation of new water masses, the ACC fundamentally affects the global meridional overturning circulation (Marshall and Speer, 2012), atmospheric CO_2 content (e.g. Toggweiler et al., 2006), and the stability of Antarctica´s ice sheets. The ACC physically and chemically homogenizes the circumpolar ocean while thermally isolating Antarctica by limiting poleward meridional heat transport. The bulk of the geostrophic transport in the ACC is associated with the Polar and Subantarctic Fronts (PF and SAF) whose positions are determined by the location of the maximum westerly wind stress and bottom topography (e.g., Orsi et al., 1995).

The flow of the ACC is constricted to its narrowest extent in the Drake Passage (DP). This so-called "cold water route" through the DP is one important pathway for the return of fresh and cold waters to the Atlantic, which strongly affects the strength of the Atlantic meridional overturning circulation, in concert with the "warm water route" inflow of warm and salty Indian Ocean water masses through the Agulhas Current system (Gordon, 1986; Beal et al., 2011). Modelling studies suggest that abrupt climate changes and the stability of the Atlantic meridional overturning circulation (Knorr and Lohmann, 2007) strongly depend on the interplay of the cold and warm water route, the latter of which transports relatively warm and salty water from the Indian ocean into the Atlantic (Knorr and Lohmann, 2007). Paleoceanographic reconstructions suggest that in many regions, the PF and SAF, which today delimit the bulk of the ACC transport, may have moved northward during the last glaciation. These inferences have been made from a number of sediment records in the Atlantic sector of the Southern Ocean (e.g., Asmus et al., 1999; Diekmann et al., 2000; Walter et al., 2000; Gersonde et al., 2003), whereas the few published studies from the Pacific Southern Ocean suggest a limited movement of the sea-ice margin and oceanic fronts during the last glacial maximum (LGM) (e.g., Gersonde et al., 2005). These results are in contrast to high resolution sediment records from cores along the southern Chilean margin that suggest a more substantial movement of the northern margin of the ACC (Lamy et al., 2004, 2007; Kaiser et al., 2005) and the SAF (Caniupán et al., 2011; Verleye et al., 2010). New sediment cores have been recently retrieved from the Pacific Southern Ocean during cruises with RV *Polarstern* (PS75) and RV Sonne (SO-213; SOPATRA). The sediment record from these cruises suggest that also in this sector regionally varying but generally more substantial northward shifts of the fronts occurred during glacials (Benz et al., in press). Yet little is known about the movement of these fronts relative to the DP, the region most likely to control changes in ACC transport, Antarctic Intermediate Water (AAIW) production, and interbasin mixing. AAIW, characterized by a salinity minimum and high oxygen content, occupies the 600-1100 m layer of the water column in the oceans of the Southern Hemisphere (Hanawa & Talley, 2001). It is generally agreed that this water mass is formed at the ocean's surface in the high latitudes of the Southern Ocean east and west of the Drake Passage (e.g., Piola & Georgi, 1982; England et al., 1993; Hanawa & Talley, 2001). The subduction and the spreading of this global water mass contributes to the ventilation of the permanent thermocline and of the Oxygen Minimum Zone (OMZ) along the Eastern South Pacific, the removal of atmospheric CO_2, and to the regulation of temperature anomalies.

Previous paleoceanographic work in the DP was strongly limited by few systematic sediment coring attempts in the recent past. Extensive coring in this region dates back to the 1960s when several expeditions were carried out with the American Navy Ship USNS *Eltanin* (e.g., Goodell, 1965). The marin-geological information from these cruises was an important base for the geological work during Expedition PS97 and served as guidance in some decision regarding coring sites..

Satellite tracked surface drifters reveal that today Subantarctic surface water of the ACC is transported northeastward across the Southeast Pacific from ~53°S/100°W towards the Chilean coast at ~40°S/75°W (Chaigneau and Pizarro, 2005). Here, surface waters bifurcate northward into the Humboldt Current System (HCS) and southward into the Cape Horn Current (CHC) flowing towards the DP (e.g., Strub et al., 1998). The northward deflection of ACC water into the HCS presently only comprises a small fraction of the total ACC flow. In contrast, the CHC and the underlying Southeast Pacific Slope Water provide a major fraction of the present DP throughflow reaching locally more than 50% of the total throughflow in the northern part of the Drake Pasage (Well et al., 2003). Grain-size and geochemical studies on a high-resolution sediment core (MD07/3128), located at the southern Chilean margin off the mouth of the Strait of Magellan, suggest important changes in the strength of the CHC over the past 60 kyr BP (Lamy et al., 2015). These changes can be interpreted in terms of strongly reduced contributions of northern ACC water to the DP throughflow during the last glacial in general, and particularly during millennial-scale cold phases as known from e.g. Antarctic ice-cores. At the same time, advection of northern ACC water into the HCS was likely enhanced (Lamy et al., 2015). This northward supply of cold waters into the HCS in the surface and below at intermediate water levels provides an important linkage between high and low latitudes affecting e.g. the tropical eastern Pacific (e.g., Rincon-Martinez et al., 2010) and beyond (Euler & Ninnemann, 2010). In contrast, preliminary studies from the Scotia Sea suggest constant flow speed through the DP between the Last Glacial maximum and the Holocene (McCave et al., 2014). The present Chilean margin results are so far only based on one single core. Therefore, more high resolution records on the CHC contribution to the DP throughflow including records of multiple glacial/interglacial cycles are required. High-resolution sediment archives are expected further southwest along the Chilean margin as indicated by seismic data (Polonia et al., 2007). The recovery of sediment cores from different water depths along the southern Chilean margin was a major goal of Expedition PS97.

The strength and position of the southern westerly wind belt (SWW) plays a crucial role for the DP throughflow and the ACC in general (e.g. Marshall and Speer, 2012). Furthermore, the wind belt is very important for global climate including the forcing of atmospheric CO_2 variations (Lamy et al., 2007; Anderson et al., 2009, Denton et al, 2010;). Proxy reconstructions of SWW changes during the last glacial in the Southeast Pacific sector suggested a northward shift or extension forced by shifts of sea surface temperature (SST), gradients and oceanic fronts (e.g., Lamy et al., 1999; Moreno et al., 1999; Lamy et al., 2007). These northward shifts are largely consistent with results from the South Atlantic sector (e.g., Stuut & Lamy, 2004; Barker et al., 2009;) and the Southwest Pacific/Indian Ocean region (e.g., De Deckker et al., 2012; Lorrey et al., 2012). However, all these studies have so far been based on records from the northern SWW margin and little is known from the present core of the westerlies, with even less understanding of the southern margin towards Antarctica, an area covered by this *Polarstern* expedition. Though a number of modelling studies have targeted changes in the position and strength of the SWW during the LGM, results are inconclusive (e.g., Rojas et al., 2009). Regarding the role of the DP some modelling studies suggest that the volume transport through the passage has been reduced during glacial stages and subsequently increased across the last glacial termination (Knorr et al., 2003; 2007) accompanied by a southward shift of the ACC and the associated fronts.

An additional major target of PS97 was to retrieve high-resolution Holocene sediment records from southernmost Patagonia and the Antarctic Peninsula region (Bransfield Strait), located north and south of the DP, respectively (Figure 3.1.1). Instrumental climate time-series from this region including the western Antarctic Peninsula (AP) only cover the past few decades (e.g., Gille et al, 2002; Schneider et al., 2003; Garreaud et al., 2007). These data suggest that rapid regional warming of air temperatures on the AP and adjacent islands observed over the last 50 years is exceptional. Ice core data from the AP suggest that this warming is unprecedented within the past 500 years (Vaughan et al. 2001). The long-term perspective from ice-cores, marine and terrestrial sediment archives is crucial for distinguishing natural and anthropogenic climate changes as the baseline for accurate future projections. This is particularly true for reconstructions of the SWW, which have intensified at its southern margin over the past 40 years and are expected to do so over the next centuries. This may provide a positive feedback on global warming through reducing the uptake of anthropogenic CO_2 or even promoting outgassing of old naturally stored CO_2 through upwelling (e.g., Russel et al., 2006). Global warming at an increasing pace ever since the end of the Little Ice Age (c. AD 1350-1900) causes significant change in the coastal marine environments of the West Antarctic Peninsula (WAP) and beyond. High-resolution sediment cores from Maxwell Bay (MB, King George Island, South Shetland Islands) provide crucial information on the impact of climate change as well as the means for the reconstruction of the climate fluctuations themselves (Hass et al., 2010; Monien et al., 2011). The vertical sediment flux in Maxwell Bay is controlled by summer melting processes that cause sediment-laden meltwater plumes to form in the tributary fjords. These leave a characteristic signature in the sediments downstream which can be used to distinguish summer and winter-dominated periods through the past two millennia. Considering that the WAP is located in today's warmest part of the AP, the records provide insights into the climate factors affecting the Antarctic Peninsula Ice Sheets and potentially also the whole West Antarctic Ice Sheet with possible consequences on a global scale (Bamber et al. 2007).

Paleo sea-ice reconstructions based on biomarkers are successfully performed in the Arctic realm (Müller et al., 2011). In the Southern Ocean, however, they remain a major challenge. So far, biomarker-based sea ice reconstructions in the Southern Ocean are mainly based on the identification of this C_{25}-HBI diene and related C_{25}-HBI trienes, which serve as indicators of phytoplankton productivity. The applicability of these compounds to qualitatively reconstruct past sea ice conditions has been demonstrated by a limited number of studies in the Scotia Sea (Collins et al., 2013) and along the AP (e.g. Barbara et al., 2013). Investigations into the potential use of these HBIs to also estimate past SSTs, however, are still pending. Organic geochemical bulk (TOC, CNS) and biomarker (HBIs, *n*-alkanes, sterols, alkenones etc.) analyses of surface sediments and longer sediment cores from the DP (i.e. along a transect from ice-free into ice-covered areas) that cover Holocene and Pleistocene time intervals will contribute to paleoenvironmental reconstructions in the Southern Ocean. Further, the biomarker data will be compared to microfossil data and sea ice estimates based on diatom assemblages. Analyses of long sediment cores basically target the assessment of past changes in sea ice, SST, and paleoproductivity conditions associated with climate shifts. In particular, in areas and time intervals, where diatom assemblages are affected by silica dissolution, biomarker-based sea ice reconstructions may provide important information on ice-ocean-atmosphere interactions and CO_2 ventilation changes associated with glacial-interglacial climate transitions.

The main scientific questions and objectives addressed by our coring program include:

1) How has the SWW varied with climate and impacted ACC transport through the DP? The northern part of the DP is presently located in the center of the westerlies. Available westerly wind strength records from adjacent southern Patagonia only cover the Holocene. Though these are discussed controversially, there is some evidence that winds increased during the early Holocene warm interval, whereas wind speeds were reduced in the northern part of the

SWW. The reverse pattern seems to apply for the relatively cold late Holocene. Do these patterns likewise extend to glacial/interglacial changes with thus reduced wind speeds and throughflow in the DP during colder glacials?

2.) How did the latitudinal positions of the PF and SAF as well as the winter and summer sea-ice margins in the DP change across the past glacial/interglacials and at millennial time-scales, e.g. during MIS 2-4? The location of the fronts is crucial for the ACC flow through the DP. Therefore, we performed several coring transects spanning the ACC frontal systems starting north at the Pacific entrance of the Magellan Strait, along the southernmost Chilean margin, and across the DP. The records are expected to provide constraints on the history of ACC transport and surface water gradients to infer frontal movements in the vicinity of DP

3.) What is the role of the Cape Horn Current in contributing to DP throughflow? Data from core MD07/3128 (Lamy et al., 2015), suggest strongly varying flow speeds of the CHC from the Holocene to the last glacial including the well-known Antarctic-type millennial-scale variations. Are these changes extending into the previous glacials and interglacials?

4) How has deep and intermediate water circulation changed over time in the DP region? The SE Pacific off southernmost Chile is presently the major formation area of AAIW. Depth transect across the continental margin covering deep (SE Pacific Slope Water; Circumpolar Deep Water), intermediate, and mode water levels are needed to reconstruct these circulation changes at glacial/interglacial and during millennial time-scales.

5) Is there a consistent pattern of short term climate and ocean variability during the Holocene and what is the amplitude and timing in the present center of the westerlies over southernmost South America and at the southernmost margin of the westerlies over the northernmost WAP? Can warm phases of the early Holocene and the past millennium (in particular the Medieval Warm Period) serve as analogues for future warmer conditions?

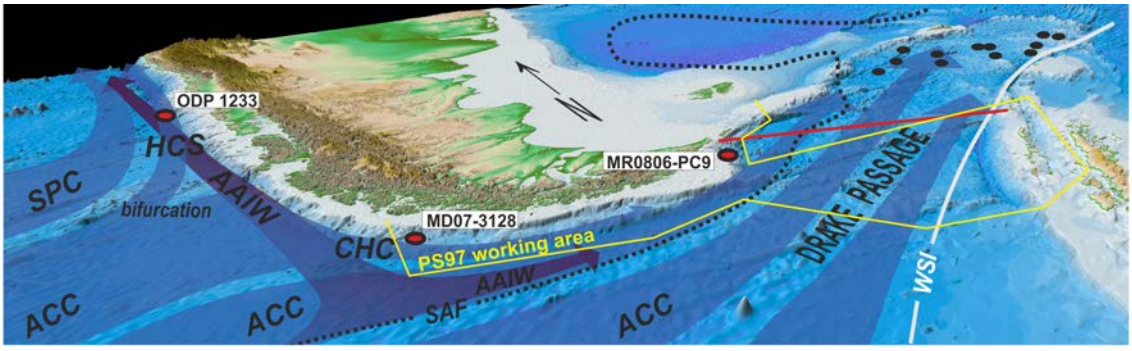

Fig. 3.1.1: Three dimensional view of the southern South Amerca, the DP and the northern Antarctic Peninsula with simplified oceanography and core locations of previously studied sediment cores in the region (red dots; ODP 1233 (e.g., Lamy et al., 2004), MD07/3128 (e.g. Caniupán et al., 2011), MR0806-PC9 (Shiroya et al., 2013, Lamy et al., 2015)); black dots indicate sediment cores studied by McCave et al. (2014). PS97 working area at the southern Chilean margin, the Scotia Sea margin and the Antarctic Peninsula is marked in yellow. Map modified from Lamy et al. (2015). ACC=Antarctic Circumpolar Current; AAIW=Antarctic Intermediate Water; CHC=Cape Horn Current; SAF=Subantarctic Front; SPC=South Pacific Current; WSI= winter sea-ice margin

Work at sea

Work at sea is described in the sub-chapters 3.2 (Surface Sediments), 3.3 (Sediment coring and core documentation) and 3.4 (Core logging and physical properties**).**

Preliminary Results

Preliminary results are summarized in 3.5 (Preliminary results of Marine Geology and Paleoceanography) for each of the four working areas.

Data management

All data will be uploaded to the PANGAEA database. Unrestricted access to the data will be granted after three years, pending analysis and publication.

This cruise report contains a detailed appendix including core photos (A.5), core descriptions (A.6), smear slide analyses (A.7), coarse fraction analyses (A.8), physical properties (A.9) and the PARASOUND records for each coring site (A.10).

3. 2. Surface sediment sampling

Carina Lange[1], Juliane Müller[2], Lorena Rebolledo[1], Hartmut Schulz[3]

[1]UdeC/COPAS/IDEAL, [2]AWI, [3]U Tübingen

Work at sea

Undisturbed surface sediments, reflecting the most recent sedimentary and environmental conditions in a given study area, provide an important means for the calibration of microfossil and geochemical proxies against observational data. This is important as new proxies evolve continuously, and testing their applicability and reliability, e.g. sea surface temperature or sea ice proxy, is a crucial step within paleoceanographic and paleoclimate research. The multicorer permits the recovery of up to 12 surface sediment samples and the uppermost 30 to 60 cm of sediment usually spanning the most recent geological history. The surface sediments recovered during *Polarstern* Expedition PS97 in the DP and adjacent southern South American continental shelf/slope areas and the Antarctic Peninsula constitute a highly valuable reference data set for the evaluation of how different proxies respond to and reflect the different oceanic domains and polar to subpolar frontal systems. Additionally, these near-surface samples are useful when the upper part of a gravity or piston core is disturbed or missing. By combining proxy records from both the Multicorer and the piston/gravity corer, a complete sequence and hence, stratigraphy can be established.

Surface and near-surface sediment sampling during RV *Polarstern* cruise PS97 was carried out at 64 stations by means of a Multicorer (MUC) and/or giant box grab (GBG) (Fig. 3.2.1).

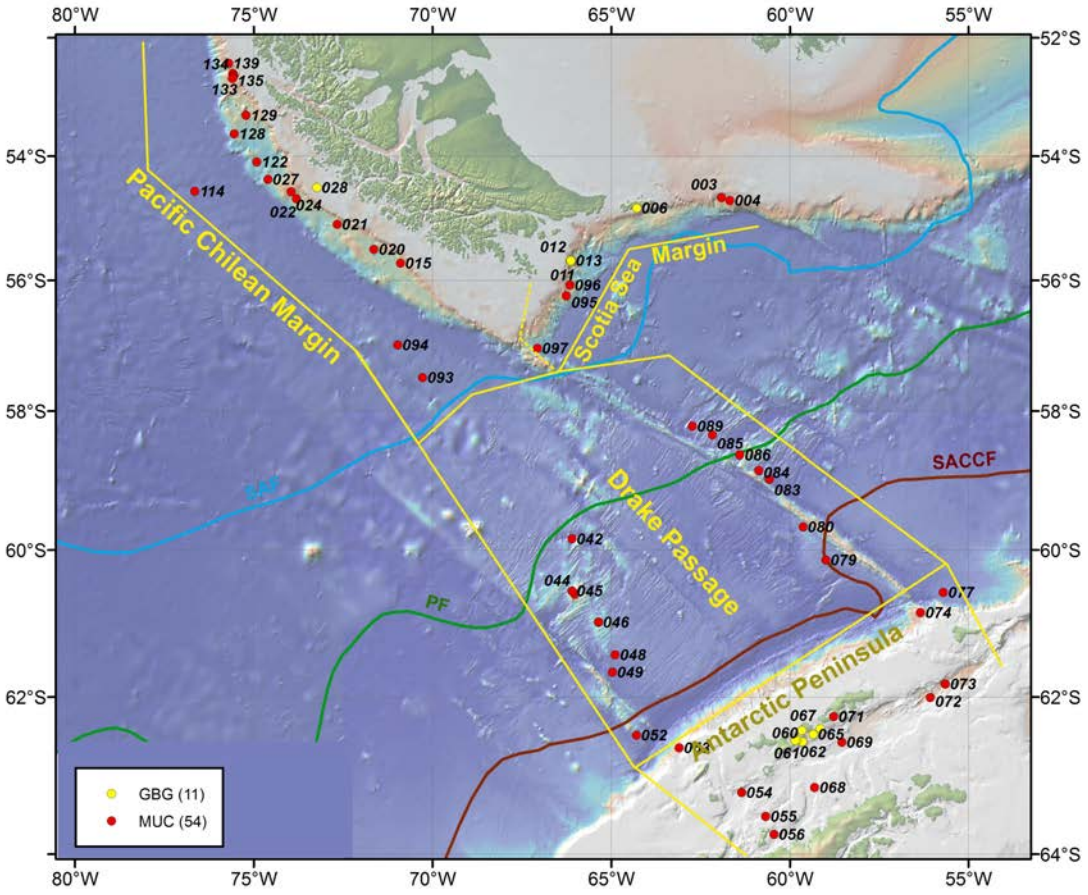

Fig. 3.2.1: General view of Multicorer and giant box grab stations in the four working areas of PS97.

The 12-tubes Multicorer (MUC67; manufactured by Fa. Wuttke, Henstedt-Ulzburg, Germany), with an inner tube diameter of 6 cm and a length of 60 cm, was deployed at 48 stations and usually recovered undisturbed surface sediments and overlying bottom water. The 8-tubes Multicorer (MUC100; manufactured by Fa. Wuttke, Henstedt-Ulzburg, Germany) with an inner tube diameter of 10 cm and a length of 60 cm was used at four stations. The recovery of sediments with the MUC100 was not successful at stations PS97/003-1, PS97/004-1, PS97/009-1, probably due to the high content of coarse sand at these locations. In contrast, over-penetration of both devices, MUC67 and MUC100, occurred at stations PS97/072 and PS97/073, and is likely related to the occurrence of very soft, biosiliceous sediments. Only MUC cores with an intact surface and a water layer on top of the sediment were sampled. Sediment-filled multicore tubes have been retrieved at 46 stations.

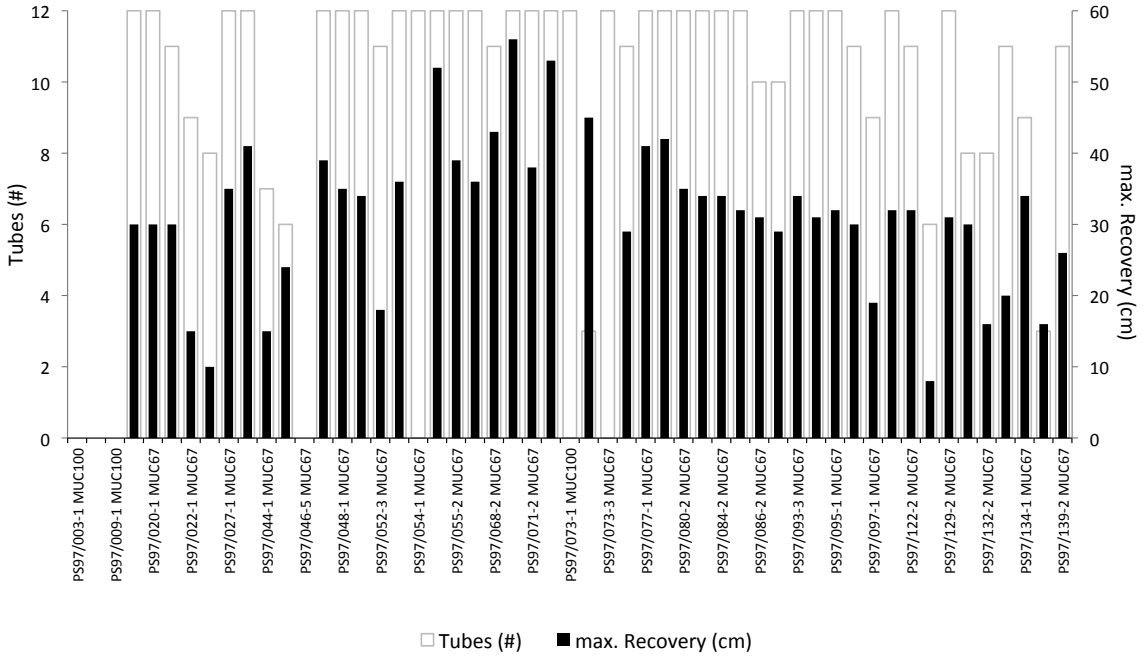

Fig. 3.2.2: Recovery of the 8-tubes (MUC100) and 12-tubes (MUC67) multicores at all PS97 stations.

All MUC tubes were sampled immediately after recovery to avoid e.g. photo-oxidation and degradation of biomarkers and pigments. For multidisciplinary investigations of the recovered sediments, the multicorer tubes were sampled according to the following scheme:

Tab. 3.2.1: Distribution of tubes for the different post-cruise investigations.

# Tubes	Working Group	Sampling	Storage
1	Sedimentology	1 cm slices in pre-weighed Whirlpack bags	4°C
2	Benthos	1 cm slices in Kautex bottles & Whirlpack bags	4°C
1	Organic Geochemistry	1 cm slices in glass vials covered with aluminum foil	-20°C
2	Plankton	1 cm slices in Whirlpack bags	4°C
1	Micropaleontology	1 cm slices in Whirlpack bags	4°C
1	Isotopes	1 cm slices in Whirlpack bags	4°C

2	Silicates	1 cm slices in Whirlpack bags	4°C
1	Pigments	1 cm slices in Whirlpack bags	-80°C
1	Archive	not sampled; sediment archived in plastic foil	-20°C

Multicorer tubes for benthic life incubation experiments were obtained at station PS97/133-1. The cores were subsampled with a so-called pushcorer and stored at 4°C. In general, at each station water samples for geochemical and isotope analyses were collected from the overlying water in the the cores designated for benthos (benthic foraminifers) sampling.

Samples for smear slides and onboard microscopic characterization of the sediment's fine and coarse fraction were taken from the MUC surface and from intervals of lithological change (Fig. 3.2.3). Smear slides were analyzed with a Leica Laborlux 11POL petrographic microscope (100 to 630X magnification), and the coarse fraction with a Leica S8APO binocular scope (10 to 80X magnification). Micropaleontological and sedimentological information obtained at each station is summarized in appendix A.7 and A.8. Further details on the coarse fraction analyses can be found in Chapter 3.3.

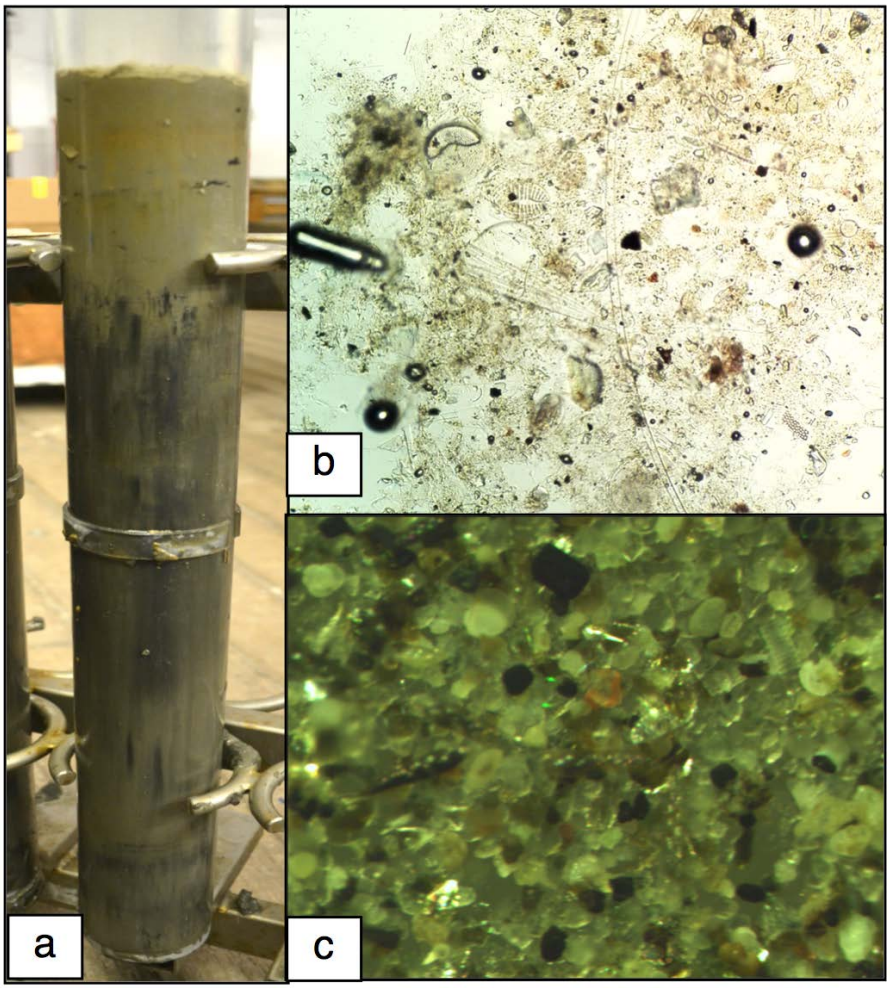

Fig. 3.2.3: MUC tube retrieved at station PS97/054-2 (a; J. Müller). Microscope images of the fine fraction from the surface layer (b; L. Rebolledo) and of the coarse fraction from the base of the MUC (c; H. Schulz) permit an immediate micropaleontological and sedimentological characterization.

The lithological classification followed the scheme suggested by Mazzullo et al. (1988). Pelagic particles are defined as bioclastic grains composed of the skeletal remains of calcareous and siliceous microfauna and microflora derived from foraminifers, nannofossils, diatoms, radiolarians, sponge spicules and silicoflagellates. The siliciclastic components consist of terrigenous minerals and rock fragments. Sediment names consist of a principal name related to the major biogenic component (calcareous and/or siliceous) and the degree of compaction. For siliciclastic sediments, the principal name describes the texture based on the Udden-Wentworth grain-size scale (Wentworth, 1922).

The giant box grab (GKG; volume of sample 50*50*60 cm (manufactured by Fa. Wuttke, Henstedt-Ulzburg, Germany) was successfully deployed at 8 stations. Surface sediments and usually two archive tubes (diameter 12 cm) were taken for organic geochemical, micropaleontological, pigment and sedimentological studies, while the remaining sediment has been sieved and sampled for thermochronological investigations (see chapter 4.3.).

3. 3. Sediment coring and core documentation

Marcelo Arevalo[1], Helge W. Arz[2], Peter Busch[3], Bruno Canella[4], Vania Carrera[5], Lutz Eberlein[2], Sophie Ehrhardt[6], Alessa Geiger[7], Christian Hass[1], Rolf Kilian[8], Gaston Kreps (Arg Observer), Gerhard Kuhn[1], Carina Lange[9], Lester Lembke-Jene[1], Norbert Lensch[1], Juliane Müller[1], Dirk Nürnberg[10], Sascha Plewe[2], Lorena Rebolledo[9], Thomas Ronge[1], Simon Schröder[1], Hartmut Schulz[11], Marc Wengler[1]

[1]AWI, [2]IOW,
[3]U Dresden,
[4]Arg. Observer,
[5]Chi. Observer,
[6]U Bremen,
[7]U Glasgow,
[8]U Trier,
[9]UdeC/COPAS/IDEAL,
[10]Geomar,
[11]U Tübingen

Work at sea

During PS97, 32 piston corers (PC) with a gear length between 10 and 25 m and 41 gravity corers (GC) with a gear length between 3 and 15 m were used to recover long sedimentary sequences (Table 3.3.1). Sixty-three deployments were successful and resulted in a total core recovery of 461.45 m. Additionally, 20.75 m were recovered by the pilot corer (TC) triggering the PC (Table 3.3.1; Fig. 3.3.1). The gear types and the length of the coring devices were chosen based on sediment acoustic profiles with the PARASOUND echo-sounding system considering acoustic patterns such as the strength of characteristic reflectors, their spacing, and the total sub-bottom penetration (Chapter 6.2). The sediment cores taken with piston and gravity corers were cut into 1 m long segments on board *RV Polarstern*. Before closing the core segments with plastic caps, smear slides were taken from each segment base in order to conduct biostratigraphic analyses. After the measurement of the physical properties using a GEOTEK multi-sensor core logger (MSCL) (Chapter 3.4) for un-split core segments, cores were selected for opening and sampling based on initial biostratigraphic and physical property analyses. After opening and splitting of the cores, the core sections were photographed (Appendix A.5). Sediment core description was performed on the archive half and sediment colors were determined using the “Munsell Soil Color Chart“.

Visual core description (Appendix A.6) was complemented by microscopic analysis of sediment smear slides and coarse fraction analyses (Appendix A.7 and A.8) from all major lithologies found in the individual cores. Smear slides were prepared and examined with a Leica Laborlux 11POL petrographic microscope (100 to 630X magnification). Where possible, maximum ages were determined from core catcher samples at the base of each core, and in some cases, samples within cores were examined to refine age determination. By combining magnetic susceptibility and Gamma-Ray-Attenuation (GRA)-density data with shipboard diatom biostratigraphic findings, preliminary age-models for some of the recovered

cores were established (Table 3.2.1, chapter 3.5). Shipboard diatom identification and dating follows the published work of Zielinski and Gersonde (2002) and Zielinski et al. (2002).

On-board sampling was carried out on the work half and samples for bulk parameter (water content, density, contents of $CaCO_3$, C_{org}, and biogenic silica) studies were taken. The bulk parameter samples (~6-10 cm^3 in volume each) were taken with syringes and stored in pre-weighed glasses. In total, ~250 core meters were opened and sampled. Core segments, which were not opened during the expedition, were stored in a reefer container at a temperature of 4° C for transport to Bremerhaven.

The lithological classification of the sediments followed the scheme suggested by Mazzullo et al. (1988). According to this classification, the hemipelagic to pelagic sediments are mainly of siliciclastic origin. Pure biogenic sediments are rare. The siliciclastic components consist of terrigenous mineral and rock fragments of the sand, silt, and clay size fractions. Sand- and gravel-sized material of glaciogenic origin (ice-rafted debris, IRD) is regionally enriched. For siliciclastic sediments, the principal name describes the texture (gravel, sand, mud (silt+clay)) based on the Udden-Wentworth grain-size scale (Wentworth, 1922). Biogenic sediments are composed of skeletal remains of marine calcareous and siliceous microfauna and microflora, e.g. foraminifers, coccoliths, diatoms, and radiolarians as well as minor amounts of sponge spicules and silicoflagellates. Moreover, we found rather unconsolidated calcareous and siliceous biogenic sediments (oozes). The principal name of biogenic and siliciclastic sediments is preceded by major modifiers and followed by minor modifiers that may refer to mixed biogenic, siliciclastic, and volcaniclastic components:
1. 25-50%: components in this range modify the principal name.
2. 10-24%: components in this range are added with the suffix “-bearing” (e.g., foraminifer-bearing).
3. 0-9%: components with these abundances are not named, unless they are of significant importance for the interpretation. In these cases we used (~5 % “with”; ~1 % “with traces of”).

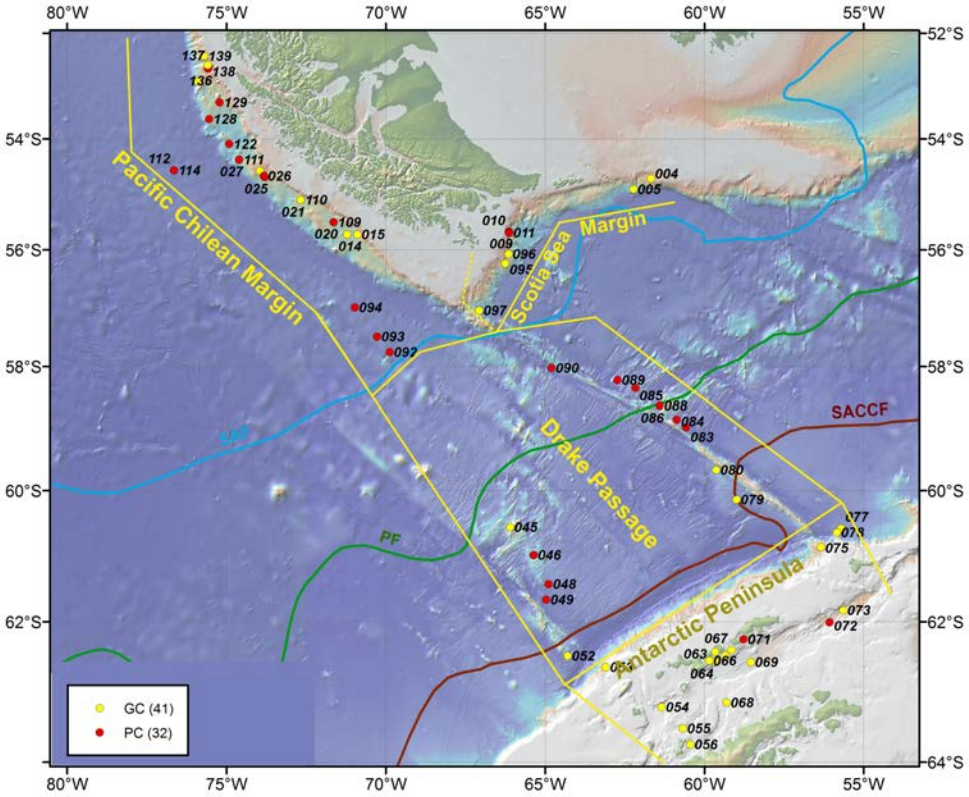

Fig. 3.3.1: Overview map with coring stations (piston cores (PC) and gravity cores (GC)) in the four working areas.

3.3.1: Piston corer (PC) and gravity corer (GC) deployments and recoveries listed by working areas. Physical properties were measured on nearly all cores onboard RV *Polarstern*. Selected cores were opened and described onboard RV *Polarstern*.

Station Number	Gear [m]	Latitude	Longitude	Water Depth (ANPHS) [m]	Core recovery [m]	TC recovery [m]	Preliminary Age	Opened/described	Physical properties
Scotia Sea Margin (SSM)									
PS97/004-2	GC 5 m	54° 43.58' S	61° 40.51' W	747.7	0		-		
PS97/005-1	GC 5 m	54° 55.33' S	62° 13.58' W	2439.8	0		-		
PS97/009-2	PC 20 m	55° 41.02' S	66° 8.65' W	555.5	9.04		MIS3	x	x
PS97/010-1	PC 10 m	55° 41.66' S	66° 7.55' W	661.2	6.91		MIS5	x	x
PS97/011-1	PC 10 m	55° 42.17' S	66° 8.19' W	626	6.53		MIS4	x	x
PS97/095-2	PC 15 m (small)	56° 14.69' S	66° 14.96' W	1644.7	8.04	0	?	x	x
PS97/095-3	PC 15 m (small)	56° 14.68' S	66° 14.96' W	1647	0		-		
PS97/096-2	GC 5 m	56° 4.56' S	66° 9.02' W	1612.6	0		-		
PS97/097-2	GC 10 m	57° 3.25' S	67° 4.09' W	2312	4.8		?	x	x
PS97/097-3	GC 10 m	57° 3.28' S	67° 4.10' W	2310.4	2.93		?		x
Pacific Chilean Margin (PCM)									
PS97/014-1	GC 5 m	55° 43.93' S	71° 12.94' W	2102.6	0.44		Holocene	x	
PS97/015-1	GC 5 m	55° 43.88' S	70° 53.54' W	1872.1	0.85		Holocene	x	x
PS97/020-2	GC 3 m	55° 30.79' S	71° 38.22' W	2070.4	0.46		Holocene		
PS97/021-2	GC 5 m	55° 6.93' S	72° 40.14' W	1839.2	0		-		
PS97/021-3	GC 5 m	55° 6.90' S	72° 40.15' W	1822.7	0		-		
PS97/022-2	GC 5 m	54° 42.03' S	73° 48.41' W	1615.9	2.76		MIS2	x	x
PS97/023-1	GC 5 m	54° 40.86' S	73° 49.94' W	1597.8	1.83		MIS2	x	x
PS97/024-1	GC 5 m	54° 35.28' S	73° 57.29' W	1278	1.6		?	x	x
PS97/025-1	PC 10 m	54° 42.03' S	73° 48.44' W	1620.4	5.43	0.52	20 kyrs	x	x
PS97/026-1	PC 10 m	54° 40.84' S	73° 49.98' W	1604.3	6.08		45 kyrs	x	x
PS97/027-2	GC 5 m	54° 23.09' S	74° 36.35' W	2341.8	2.01		MIS2	x	x
PS97/092-1	PC 15 m (small)	57° 45.78' S	69° 52.73' W	3823.7	7.89	1	MIS12	x	x
PS97/093-1	PC 15 m (small)	57° 29.94' S	70° 16.56' W	3781.4	11.16	0.82	~1000 kyrs		x
PS97/093-2	PC 20 m (small)	57° 29.95' S	70° 16.48' W	3782.2	16.45	0.99	~1300 kyrs	x	x
PS97/094-2	PC 20 m (small)	57° 0.16' S	70° 58.29' W	3996.1	9.09	0.79	?	x	x
PS97/109-1	PC 15 m	55° 30.79' S	71° 38.22' W	2084	3		MIS2-5 ?	x	x
PS97/110-1	GC 10 m	55° 6.94' S	72° 40.14' W	1840.3	0.31		Holocene		
PS97/111-1	PC 15 m (small)	54° 23.08' S	74° 36.39' W	2364	9.93	0.99	MIS6		x
PS97/112-1	PC 20 m (small)	54° 34.74' S	76° 38.94' W	3866.9	14.58	0.22	MIS7	x	x
PS97/114-2	PC 25 m (small)	54° 34.73' S	76° 38.82' W	3869.3	22.37	0.82	MIS11	x	x
PS97/122-1	PC 15 m (small)	54° 5.81' S	74° 54.90' W	2557.9	10.77	0.94	MIS2-4		x

Station Number	Gear [m]	Latitude	Longitude	Water Depth (ANPHS) [m]	Core recovery [m]	TC recovery [m]	Preliminary Age	Opened/described	Physical properties
PS97/128-1	PC 15	75° 32.73' W	53° 38.06' S	2313.4	10.69	0.95	MIS2-4		x
PS97/129-1	PC 15	75° 12.76' W	53° 19.29' S	1870.2	7.32	0.96	MIS2-4		
PS97/130-1	GC 5 m	52° 55.77' S	75° 54.25' W	3239.2	1		MIS2-4		
PS97/136-1	PC 15	52° 40.97' S	75° 34.87' W	1063.1	0	0	MIS2-4		
PS97/137-1	PC 15	52° 39.57' S	75° 33.89' W	1027.6	8.5	0	MIS2-4		x
PS97/138-1	GC 10 m	52° 36.98' S	75° 35.17' W	839.8	2.71		MIS2-4		x
PS97/139-1	GC 10 m	52° 26.56' S	75° 42.42' W	640	4.54		MIS2-4		x
Drake Passage (DP)									
PS97/045-2	GC 5 m	60° 34.25' S	66° 5.66' W	2293	0		-		
PS97/046-3	GC 5 m	60° 59.87' S	65° 21.64' W	2789	1.37		?	x	x
PS97/046-4	PC 10 m	60° 59.83' S	65° 21.37' W	2775.3	2.26	0.91	?	x	x
PS97/048-2	PC 10 m	61° 26.39' S	64° 53.22' W	3448.1	8.22	0.94	~180 kyrs	x	x
PS97/049-1	PC 20 m	61° 40.28' S	64° 57.76' W	3757.5	13.65	1	~190 kyrs	x	x
PS97/052-4	GC 5 m	62° 29.94' S	64° 17.62' W	2890.4	3.14		Last Glacial	x	x
PS97/079-2	GC 15 m	60° 8.54' S	58° 59.48' W	3541.3	8.28		~100 kyrs	x	x
PS97/080-1	GC 10 m	59° 40.48' S	59° 37.88' W	3105.9	1.24		-	x	x
PS97/083-2	PC 10 m	58° 59.66' S	60° 34.22' W	3762.3	6.08	0.91	~190 kyrs	x	x
PS97/084-1	PC 15 m	58° 52.14' S	60° 51.94' W	3557	10.94	0.9	~134 kyrs	x	x
PS97/085-1	PC 10 m	58° 21.27' S	62° 10.05' W	3086.5	7.76	0.89	~50 kyrs		x
PS97/085-3	PC 20 m	58° 21.27' S	62° 10.03' W	3090.8	14.43	0.89	~150 kyrs	x	x
PS97/086-1	PC 15 m	58° 38.65' S	61° 23.84' W	2968.8	0	0.78	-		x
PS97/088-1	PC 15 m (small)	58° 38.64' S	61° 23.82' W	2964.8	12.18	0.93	~390 kyrs	x	x
PS97/089-1	PC 15 m (small)	58° 13.60' S	62° 43.59' W	3437.2	10.02	0.9	~27 kyrs	x	x
PS97/090-1	PC 15 m (small)	58° 1.60' S	64° 47.83' W	4178.9	9.7	0.88	MIS9	x	x
Antarctic Peninsula (AP)									
PS97/053-2	GC 5 m	62° 39.77' S	63° 5.61' W	2016.1	2		Last Glacial	x	x
PS97/054-3	GC 15 m	63° 13.98' S	61° 20.61' W	1279.3	9.32		Holocene		x
PS97/055-1	GC 15 m	63° 32.09' S	60° 40.36' W	722.6	11.09		Holocene		x
PS97/056-2	GC 15 m	63° 45.45' S	60° 26.42' W	634.5	12.27		Holocene		x
PS97/059-1	GC 15 m	62° 26.24' S	59° 39.50' W	353.8	7.87		Holocene		x
PS97/062-2	GC 15 m	62° 34.19' S	59° 50.86' W	477.5	2.71		Holocene		x
PS97/063-1	GC 15 m	62° 33.58' S	59° 47.84' W	468.5	8.25		Holocene		x
PS97/064-1	GC 15 m	62° 35.00' S	59° 38.73' W	462.8	7.24		Holocene		x
PS97/065-1	GC 15 m	62° 29.22' S	59° 20.86' W	480.7	8.38		Holocene		x
PS97/066-1	GC 15 m	62° 34.16' S	59° 50.91' W	493	8.12		Holocene		x
PS97/067-1	GC 5 m	62° 25.01' S	59° 8.60' W	550.3	4		Holocene		x

Station Number	Gear [m]	Latitude	Longitude	Water Depth (ANPHS) [m]	Core recovery [m]	TC recovery [m]	Preliminary Age	Opened/described	Physical properties
PS97/068-1	GC 10 m	63° 10.08' S	59° 18.22' W	793	10.02		Holocene		x
PS97/069-2	GC 15 m	62° 35.37' S	58° 32.53' W	1635.4	5.2		Holocene		x
PS97/071-1	PC 20 m	62° 15.51' S	58° 46.32' W	442.4	15.86	0.94	Holocene		x
PS97/072-1	PC 20 m	62° 0.39' S	56° 3.86' W	1992.9	15.83	0.88	Holocene		x
PS97/073-4	GC 15 m	61° 49.73' S	55° 38.73' W	2624.1	8.75		Holocene		x
PS97/075-1	GC 15 m	60° 52.53' S	56° 20.48' W	1851.4	0		Holocene		
PS97/077-2	GC 13 m	60° 35.43' S	55° 42.21' W	3543	13.02		Holocene/ Last Glacial	x	x
PS97/078-1	GC 13 m	60° 39.15' S	55° 50.38' W	3666.4	2.23		Holocene/ Last Glacial	x	x
Total: 73	**32 PC 41 GC**				**PC: 300.71 GC: 160.74**	**20.75**			

Sand fraction description (coarse fraction analyses; size fradtion >63 µm)

The sediments were described based on their biogenic and mineralogenic compounds. We define samples with more than 50% mineralogenic content (volume-%) as sands with different grades of fine to coarse grain size or even to the size of gravel (>2mm particle diameter). Sand compositions with more than 50% of components of biogenic origin, can be classified as oozes, e.g. planktic foraminiferal ooze; diatom ooze; radiolarian ooze; pteropod ooze). However, to keep focus on the limited size-range we examined, we describe the mentioned biogenic sediment types as planktic foraminiferal sand, diatom sand, etc.. Accordingly, mineralogenic sands are termed following their main constituent as quartz sand, volcanic glass sand, sand of accessory minerals, etc.

For the sediment description, schemes and forms were adapted similar to those of smear slide analysis for a rapid and simple first characterization of the washed sand fraction under a binocular scope. Fourteen categories were recognized and the relative abundances were estimated to a sum of 100%. The upper five categories (Table 3.3.2) comprise the gross mineralogenic matter. It was difficult without polarized light to distinguish between quartz and feldspar (category 1), because both frequently appear as solid, colorless, transparent or milky-colored mineral fragments in a narrow size range. In contrast, rock fragments (2) can be easily determined by the observation of different adherent mineral phases, difference in reflectance, roundness or color. Additionally, sizes of rock particles are often very variable, reaching sizes of gravel in some cases and may be seen in the area as representatives of IRD (Ice-Rafted Detritus). (3) Mica constitutes the easily recognizable transparent to semi-transparent groups of phyllosilicates and are extremely flat particles with an irregular periphery, and shiny surfaces. Because of their relative softness (Mohs 2-3), there can be a wide size spectrum of that group within one sample. (4) Volcanic minerals and glass group together a wide range of transparent to non-transparent rock glasses and pumice. (5) Accessory minerals comprise all mineralogenic matter that formed after sediment deposition in the sediment or on the sediment surface, e.g. Fe- and Mn- Oxides and hydroxides, by (early) diagenesis.

Table 3.3.2: Categories used for the semi-quantitative description of the sand fraction (>63µm) during PS97.

PS97 Sand fraction analysis	
1	Quartz + Feldspar
2	Rock Fragments
3	Mica
4	Volcanic glass
5	Accessory minerals
1	Foraminifers
2	Diatoms
3	Radiolarians
4	Sponge spicules
5	Fish remains
6	Plant debris/organic
7	Ooids
8	Pellets
9	Bioclasts
	Sum (100%)

The nine categories for biogenic content in the coarse fraction constitute the content of three major microfossil groups (1) benthic and planktic foraminfers, (2) diatoms, (3) radiolarians, and the two macrofossil groups (4) sponge spicules and (5) fish remains. The microfossil groups may form a major fraction or may even dominante as a single category, whereas (4)

and (5) are only of minor importance in deep-sea sediments. The same holds for the categories (6) to (9). In almost all samples these groups did not exceed 5% individually. Given the same categories as for the smear slide analysis, a qualitative comparison is possible between both methods, smear slide and coarse fraction . The estimates represent semi-quantitative estimates of the washed residues. One to 5 cc of fresh sediment were taken with a spatula from either Multicores (MUC: 0-1cm or TOP; BASE), trigger cores (TC: TOP, BASE) or from long Gravity (GC: TOP, BASE) and Piston cores (PC: TOP, BASE). Samples were washed with the filtered ships´ tab water for 5 to 30 minutes through a standard screen sieve (Retsch 63 µm mesh size, 10 cm diameter). The residues were screened under a binocular with variable magnification between 10X and 80X, and photographed. However, because of the ships vibrations, magnifications >40X could not be fixed for photography and screening. It was often impossible to obtain fully representative pictures. All photographs were taken from the wet sample. Later the water was removed and the sample was dried in an oven at 40 - 45°C for 24h. The sands obtained were kept in small Eppendorf vials of 1,5 ccm. These sands are available for documentation and further analyses.

From each sample 1 to 8 pictures of 2.3MB size were made in short intervals using a digital camera system TUCSEN TSDT-TCA-3.0C attached to a laptop. Due to the permanent vibrating and shaking ship, the objects frequently were rolling aside or out of focus, and required high optical depth. Therefore areas of the pictures may be compromised.

A total of 614 pictures reflecting the selection of detailed pictures on the coarse fraction is available (1.44 GB). Magnification was in most cases 16X. By the above reasons, it was impossible to reveal all characteristics and described features in one picture. In many cases 2 - up to 10 pictures were taken. No scale bars are provided. However, the lower limit of grain size in a sample is defined as 63µm. Frequently, the photographs show different views of a sample, whereas the description represents averaged estimations, reflecting the bulk constituents.

Appendix A.8 includes a catalogue of 146 coarse fraction descriptions illustrating the washed sediment on board during the cruise.

Biostratigraphy and Biogeography

For the late Pleistocene, few biotratigraphic implications can be found using macrofossils or foraminiferal markers (BF benthic, PF planktic foraminifers). However, warm/cold indicators following glacial/interglacial climatic cyclicity of global climate show if the surface sediment may represent the present interglacial. As expected, we observed the most diverse planktic foraminiferal fauna in the warmer subantarctic waters in the northern sections of the Argentinian/Chile and South Chilean margins, and the DP transects, reflecting the present, Holocene boundary conditions. A qualitative zonation from warm to cold surface waters includes the following alignment.

“Warmest” to “Coldest” assemblages along an imaginary temperature scale comprise the species *Orbulina universa -Globigerinita glutinata –Globorotalia scitula - Globorotalia truncatulinoides -Globiorotalia inflata -Neogloboquadrina pachyderma* dextral (Npd) - *Globigerina bulloides- Neogloboquadrina pachyderma sinistral* (Nps). Following this scheme, we found the most diverse PF with the largest fractions of warm species in the core tops of multicores, trigger cores and long cores in the North, on the Pacific and Atlantic (Scotia Sea) sides south of the Magellan Strait. Towards the south, with decreasing water temperatures, Herb (1968) suggested that PF sediment faunas were becoming increasingly diluted by other biogenic and mineralogenic compounds, and more monospecific with the “coldest” species Nps as the only species occurring in polar waters. He suggested that the southern limit of

Nps occurrence was congruent with the average position of the Polar Frontal Zone (PFZ), that extends in the middle of DP from NE (57°S) to SW (61°S) (Fig. 3.3.2).

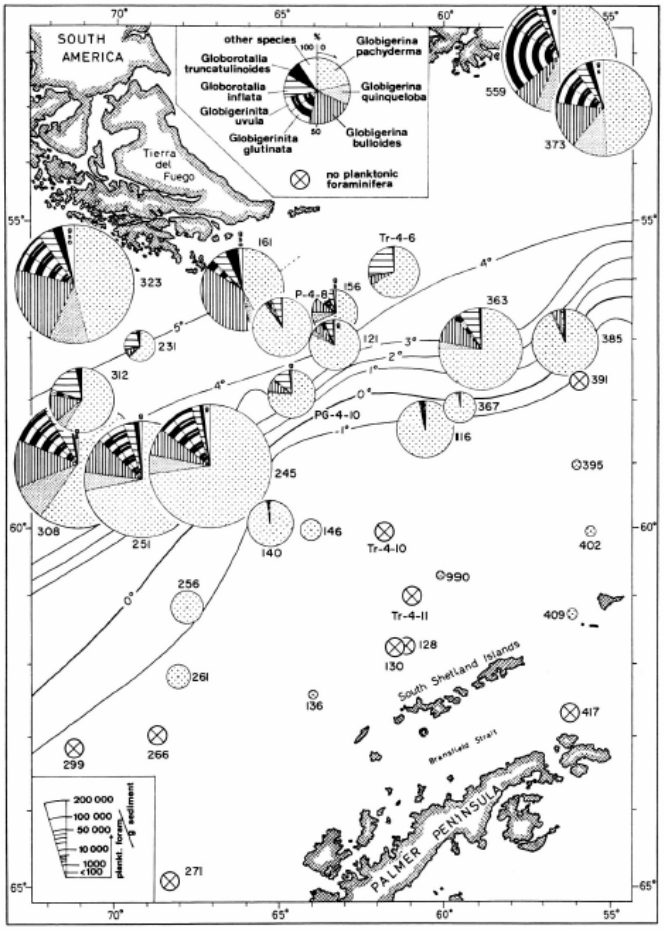

Fig. 3.3.2: Distribution of planktonic foraminifera in the DP. Foraminiferal numbers are indicated by the radius of the circles. Relative abundances of species are expressed by the angle of the respective sector of a circle. Isotherms show approximate surface/subsurface temperatures (June-October) of the mixed layer (Herb, 1968). Note the strong contrast between both, species and foraminiferal numbers, between the NW and the SE. The 1°-2° surface water isotherm indicates the Polar Frontal Zone (PFZ).

In contrast to Herb (1968), the samples of PS97 show that the widespread dominance of foraminiferal sands composed of Nps can be extended to the south of the PFZ. Pictures and estimates of core station PS97/046 (60° 59.87', S 65° 21.64' W, 2789 m water depth) and from PS97/052 (62° 29.94' S¸ 64° 17.62' W, 2890.4 m water depth) show that Nps is widespread and rather well preserved in the southern part in the DP (Fig. 3.3.3).

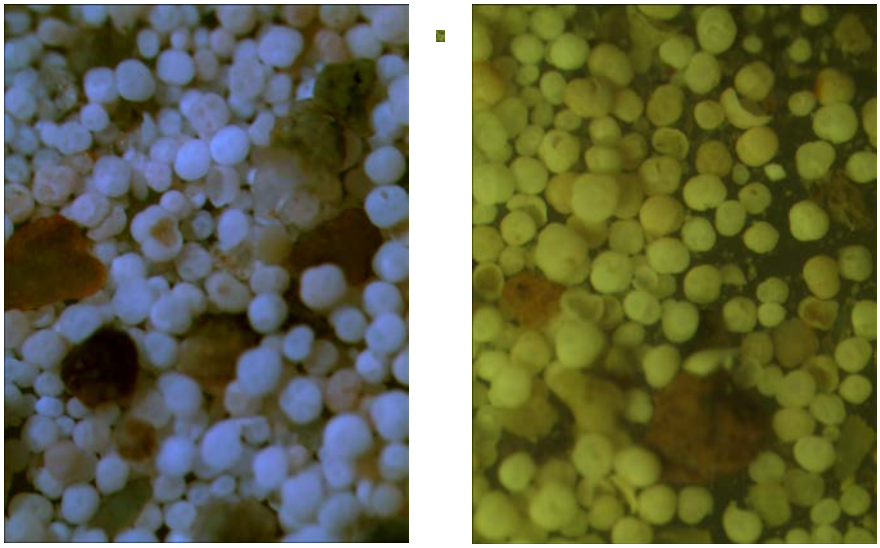

Fig. 3.3.3: Two sediment surface samples as examples for dense and planktic foraminiferal sands with high relative content of intact shells of Nps. Left: PS97-046-3 (TOP-63micron-20X; Photo Hartmut Schulz); right: PS97-052-3 (TOP-63micron-16X; Photo Hartmut Schulz).

Further, sand fraction analysis of the core catchers of the long cores retrieved at the same stations show distinctly less, but still rather well preserved Nps. However, without dense sampling to determine the fluctuating patterns of Nps, it is still uncertain what climatic stage is represented by these lowered abundances at a certain core level. Glacial sediment south of the PFZ might be extremely devoid or even free of PF. However, most samples in cores from the DP show at least a few specimens per sample volume of ca. 5-10 cc (Fig. 3.3.4) that may permit stable isotope dating or even faunal analyses, which are planned for the future.

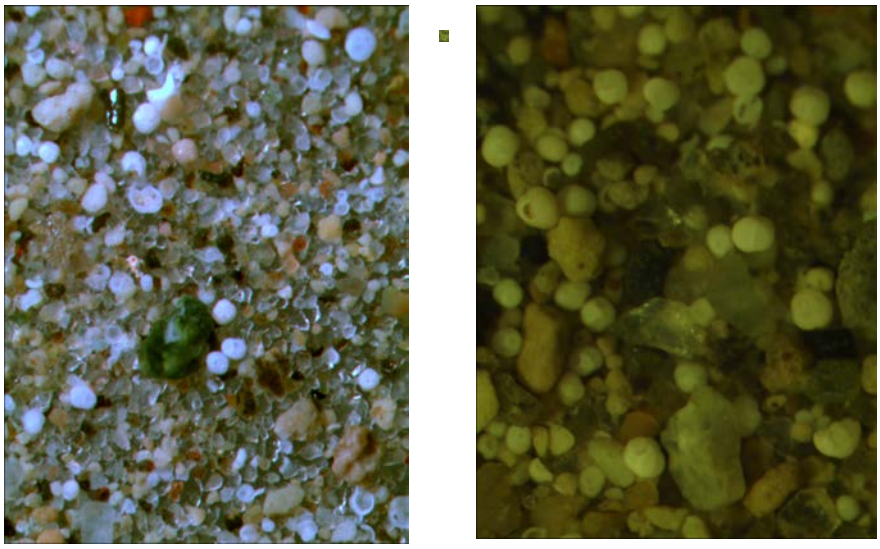

Fig. 3.3.4. Two sediment core catcher samples as examples for the relative change in Nps preservation and density with high contents in planktic foraminiferal sands. Left: PS97-046-3 (CC-63micron-16X; Photo Hartmut Schulz); right: PS97-052-4SL (CC-63micron-16X; Photo Hartmut Schulz).

3.4 Multi-sensor core logging and physical properties measurements

Gerhard Kuhn, Thomas Ronge, Marc Wengler AWI

Work at sea

Multi Sensor Core Logging (MSCL) was performed as a first non-destructive measurement on all obtained sediment cores. Additionally the measurements were used to compare and correlate cores taken in close position to each other or to established isotope or ice core records. Lithological changes and a certain cyclicity may be already seen within the logging data and provide information on the variability of terrigenous or biogenic (mostly biogenic opal, or carbonate) sediment components.

Furthermore, sound velocity and density measurements could be used to calculate synthetic seismograms, which can be compared to sub-bottom profiling data obtained with the ATLAS PARASOUND sediment echo sounder (Chapter 6.2) or with air-gun reflection seismics (Chapter 6.3) during the cruise. Subsequently, these results enable the calculation of key parameters e.g. the true sediment thickness and distribution around coring locations and for core-to-core correlations as well.

Parameters measured on whole round core sections are: the magnetic Susceptibility, sound velocity of the pressure wave (vP), and gamma ray attenuation density calibrated as wet bulk density (WBD).

To calculate sediment fluxes and mass accumulation rates of specific compounds the water content and the sediment density will be measured on individual samples taken from the cores that were opened during the cruise.

Physical properties of the sediments such as wet bulk density, p-wave velocity and magnetic susceptibility were detected on all collected sediment cores (Table 3.4.1) using a GEOTEK multi-sensor core logger (MSCL). In addition, core diameter and temperature were measured for data processing and the calculation of additional values like porosity and seismic impedance. The parameters listed in the logger settings of the MSCL software (version 6) and given in Table 3.4.1 were used for calibration that was conducted after the Geotek MSCL manual and after Gunn & Best (1998) and Best & Gunn (1999). The AWI MSCL device (MSCL#14) was used for continuous whole-core measurement at 1 cm resolution.

For example, density, velocity, and magnetic susceptibility measurements of core PS97/122-1 are shown in Fig. 3.4.1. The core was taken on the Chilean Margin and shows a clear pattern of cyclic variations in about 1 meter distances. However, some of these variations are artifacts, which result from a thickening of core sections by their respective end-caps. This artificial thickening might result in minima in the density data. Partly this could also come from core voids at the section breaks or inappropriate core handling. Sound velocities are about 1500 m/sec. Values below are due to incomplete sound transfer through the core either in sandy parts or in nearly all the cores from the Antarctic Peninsula that contained free methane gas especially in the lower sections. Core PS97/069-2 was measured down from 120 cm. All data are plotted in Appendix A.9.

All physical property data were corrected, and faulty values, e.g. at core section boundaries, were deleted partly. In order to obtain true volume corrected $\varkappa$ (Kappa) magnetic susceptibility in (10^{-6} SI-units) values the magnetic susceptibility sensor data were processed drift and volume corrected and multiplied by the correction factor (Table 3.4.1).

Back at AWI, the individual samples will be weighed, freeze-dried and milled. Water content, bulk-, grain-, wet-, and dry-bulk densities, and the porosity will be determined and corrected

for salt content. In addition to the physical properties the geochemical and mineralogical composition of these samples will be measured

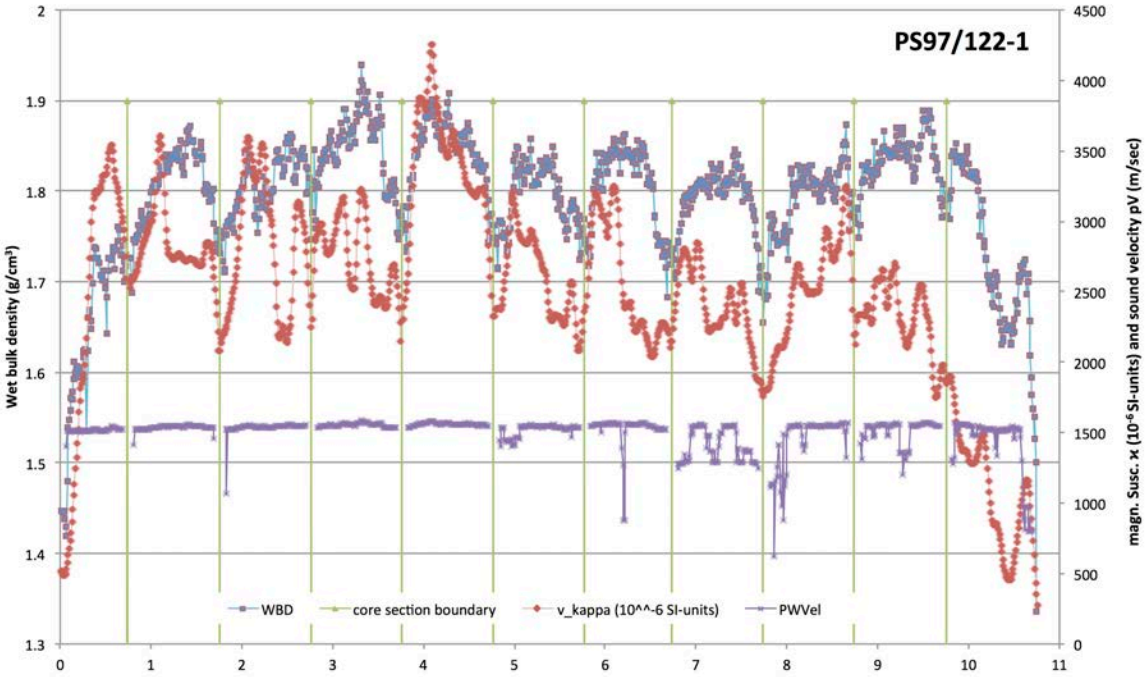

Fig. 3.4.1: Downcore changes in density (g/cm3), magnetic susceptibility (κ, 10-6 SI-units), and p-wave velocity of piston core PS97/122-1. Density as well as κ changes are clearly visible at core breaks.

To verify the MSCL measurements individual sediment samples were taken from all opened cores in a 10-cm spacing for physical property measurements (water content, sediment density) and further geochemical, sedimentological and mineralogical investigations.

Table 3.3.1: Sensors and parameter settings for measurements with the GEOTEK multi-sensor core logger during PS97.

P-wave velocity and core diameter plate-transducers diameter: 4 cm transmitter pulse frequency: 500 kHz pulse repetition rate: 1 kHz recorded pulse resolution: 50 ns gate: 900 µs delay: 10 µs P-wave travel time offset: 7.63 µs (PC90, 90 cm outer diameter, 2*2.7 mm liner thickness) P-wave travel time offset: 8.78 µs (PC125, 125 cm outer diam., 2*3.7 mm liner thickness) P-wave travel time offset: 7.17 µs (GC125, 125 cm outer diam., 2*2.5 mm liner thickness) temperature = 20 °C, salinity = 35 psu, not corrected for water depth and in situ temperature; calibrated with water core of known temperature and theoretical sound velocity
Temperature bimetal sensor, calibrated with Hg-thermometer
Density

gamma ray source: Cs-137; activity: 356 MBq; energy: 0.662 MeV aperture diameter: 5.0 mm (PC + Trigger Core TC and GC) gamma ray detector: Gammasearch2, Model SD302D, Ser. Nr. 3047, John Caunt Scientific Ltd.; count time 10 s Gamma ray attenuation measurement and density calculation with equation type $y=Ax^2+Bx+C$, (Coefficients A, B, and C determined with measurements on calibration cores PC90: A=0.0008, B=-0.0872, C=10.343 PC125: A=0.00001, B=-0.06249, C=10.13197 GC125: A=0.00053, B=-0.08693, C=10.38295
Fractional porosity Mineral grain density = 2.65, water density = 1.026
Magnetic susceptibility (MS) coil sensors: BARTINGTON MS-2C, Ser. Nr. 716, and Ser. Nr. 203 nominal inner coil diameter: (#716) 14 cm, and (#203) 10 cm coil diameter: 14.8 cm and 10.8 cm respectively (factors B, Den and LD were deactivated in the GEOTEK processing software). alternating field frequency: 565 Hz, count time 10 s, precision 0.1 * 10^{-5} (SI) magnetic field strength: ca. 80 A/m RMS Krel: 1.44 (PC, 8.46 cm core-ø); 1.73 (PC, 11.76 core-ø); 1.56 (GC, 12 cm core-ø) coil sensor MS volume (ϰ) correction factor for 10^{-6} (SI): 6.926 (PC90), 5.778 (PC125); 5.4378 (GC125)
Core thickness measurement Penny + Giles, Type HLP 190…, Ser #. 92730147, calibrated with distance pieces

3.5. Preliminary results of Marine Geology and Paleoceanography

Helge W. Arz[1], Christian Hass[2], Gerhard Kuhn[2], Frank Lamy[2], Carina Lange[3], Juliane Müller[2], Dirk Nürnberg[4]

[1]IOW, [2]AWI, [3]UdeC/COPAS/IDEAL, [4]GEOMAR

This chapter summarizes the preliminary results from sediment surface sampling and sediment coring. We also consider the sediment distribution based on our PARASOUND and HYDROSWEEP surveys (see also Chapter 6.2). Where possible, we provide first tentative age estimates based on biostratigraphic markers and the graphical correlation of magnetic susceptibility and density records of the individual cores to Antarctic ice-core temperature reference records (EDML (Epica Community Members, 2006); EPICA Dome C (Jouzel et al., 2007) and the Lisiecki & Raymo (2005) benthic isotope stack. At selected sites from the Chilean and Argentinean margin, we also correlated the physical properties data to independently dated sediment records previously published (MD07-3128 and MR05806-PC9 (Shiroya et al., 2013; Lamy et al., 2015). All graphical correlation were performed with the AnalySeries software (Paillard et al., 1996).

Multicores, giant box grabs and sediment cores were retrieved in four major study areas (Fig. 3.2.1 and 3.3.1). Transect 1 (*Pacific Chilean Margin*) is a N-S orientated core transect north of the SAF in the Southeast Pacific along the Chilean continental margin between ~52°S and ~56°S (Fig. 3.5.1). Transect 2 (*Scotia Sea Margin*) is located southeast and east of Cape Horn along the Chilean/Argentinian continental margin in the Scotia Sea (Fig. 3.5.2). Transect 3 (*Drake Passage*) extends from ~57°S to ~62.5°S from the Chilean continental margin to the Antarctic Peninsula, thereby crossing the SAF, the PF and SACCF (Fig. 3.5.3). The *DP* transect consists of cores recovered on two transects at the western Pacific entrance and within the central DP, along the Shackleton Fracture Zone. Area 4 (*Antarctic Peninsula*)

covers the continental margin north of the South Shetland Islands and Bransfield Strait (Fig. 3.5.4).

The coring locations are shown on the different maps in each sub-chapter (Fig. 3.5.1, 3.5.13, 3.5.18, and 3.5.25). Appendix A.5 to A.10 provide detailed information on sediment acoustic properties of the coring sites, photographs, graphical core descriptions, smear slide analyses and coarse fraction analyses.

3.5.1. Pacific Chilean Margin (Transect 1)

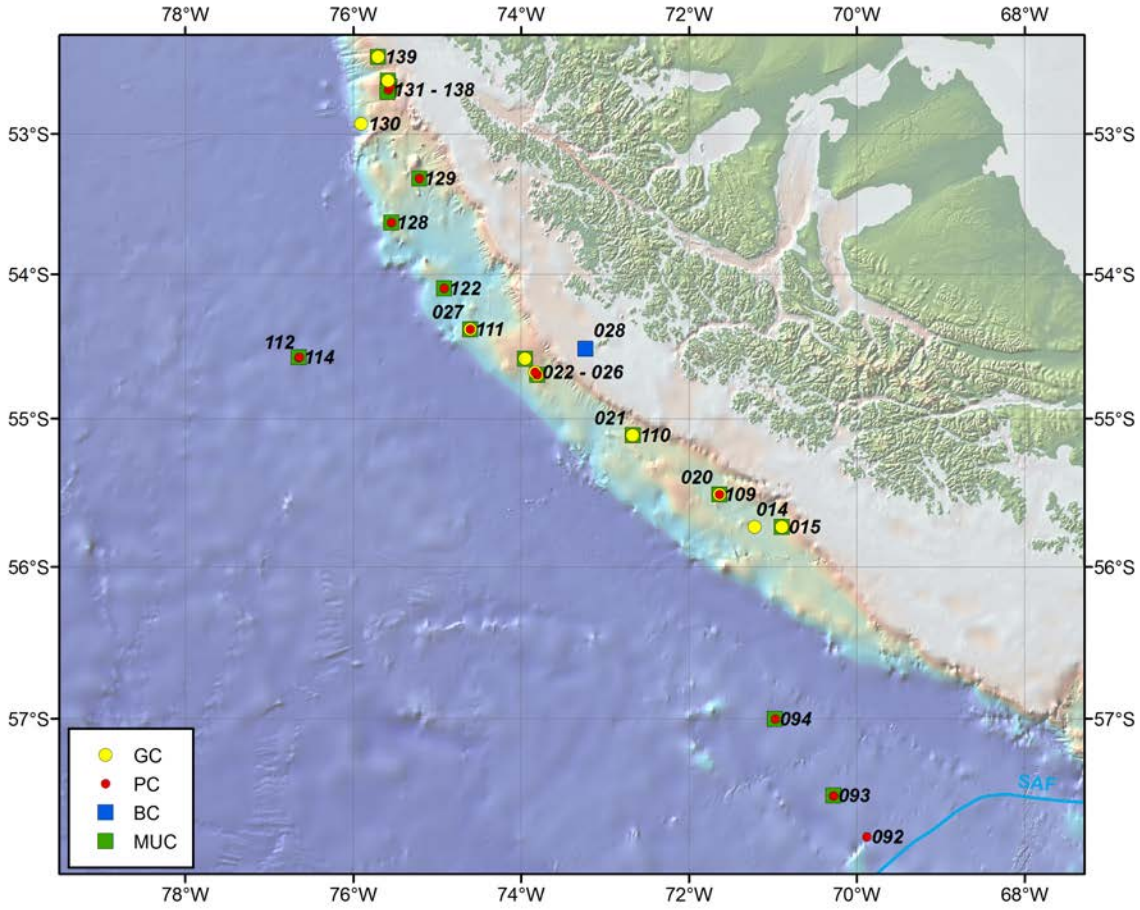

Fig. 3.5.1: Sediment core and surface sample locations at the Pacific Chilean Margin (Transect 1).

Surface sediments

Surface sediments along the Pacific Chilean Margin (Fig. 3.5.1) were successfully retrieved at 14 Multicorer stations (water depth range 637-2560 m). Additionally, one giant box corer, PS97/028-1, was collected from the shelf (105 m water depth) with surface sediments mainly composed of coarse sand, pebbles and rocks. Away from the continental margin, about 120 miles offshore, a Multicorer was deployed at a deep site (PS97/114, 3863 m water depth) where sediments are soft and characterized as foraminifer and diatom-bearing nannofossil ooze. Surface sediments at two additional pelagic stations further to the southeast about 30 to 70 nm northwest of the SAF (stations PS97/093 and PS97/094) are characterized as nannofossil-bearing silty clay (Fig. 3.5.2).

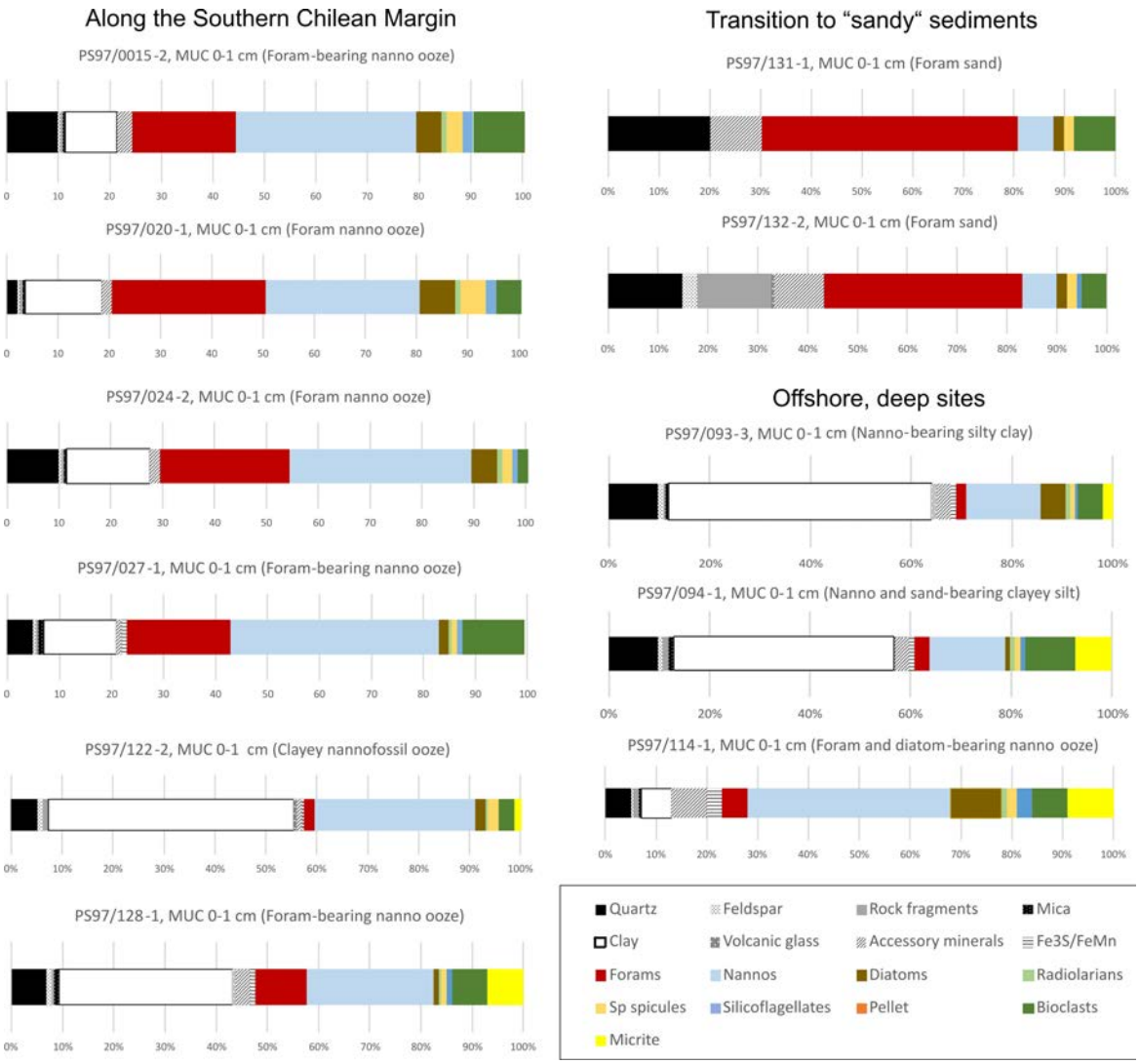

Fig. 3.5.2: Overview of surface sediment composition in the Pacific Chilean Margin, based on smear slide analysis.

Coring

An extensive coring program was carried out along the Pacific Chilean Margin. Sediment cores were retrieved from a large range of water depths between ~600 and 3900 m from the upper continental slope to the deep basin west of the Peru-Chile trench (Fig. 3.5.3). The water depths cover all major water masses along of the Southeast Pacific from Antarctic Intermediate Water across Circumpolar Deep Water/Pacific Deep Water and potentially down to Antarctic Bottom Water (at least for glacial times) (Fig. 3.5.4).

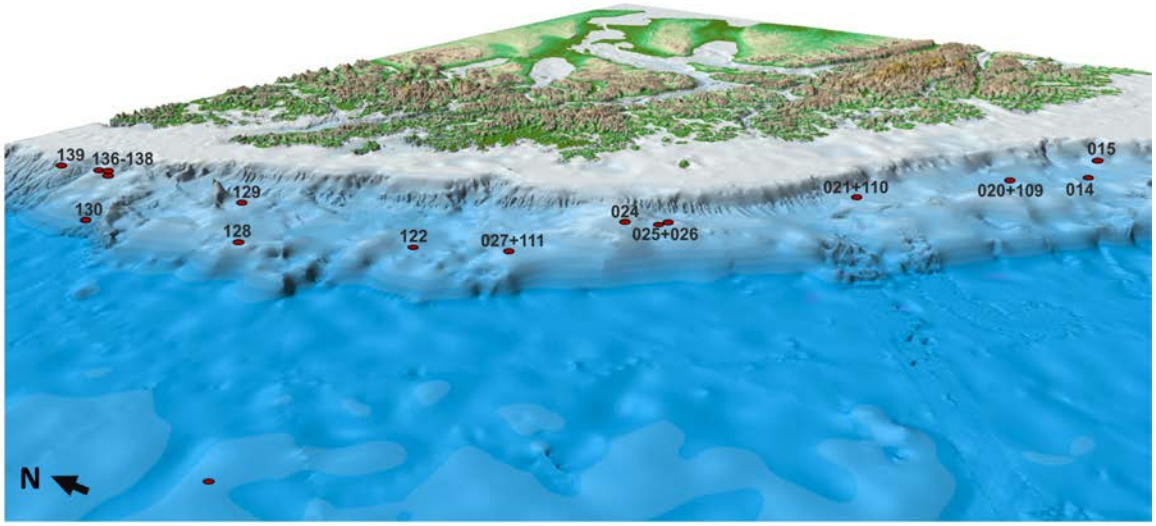

Fig. 3.5.3: 3-D view of the Pacific Chilean margin. Numbers indicate PS97 MUC and coring stations.

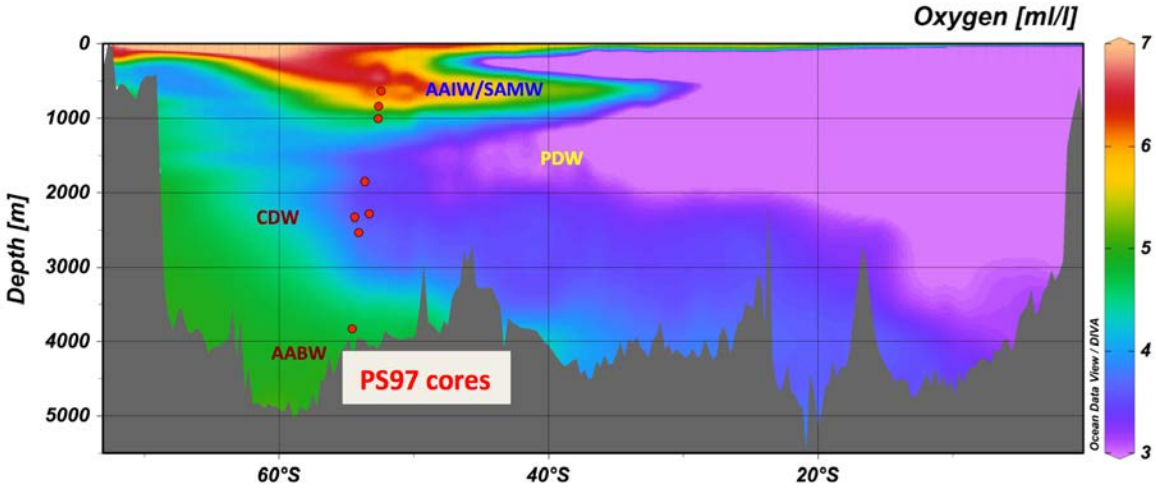

Fig. 3.5.4: The most promising PS97 Pacific Margin sediment cores plotted into an oceanographic water mass transect along South America to the Antarctic Peninsula. Shown is the modern oxygen content (Garcia et al., 2010) indicative of the major water masses (SAMW: Subantarctic Mode Water; AAIW: Antarctic Intermediate Water; PDW: Pacific Deep Water; CDW: Circumpolar Deep Water; AABW: Antarctic Bottom Water).

Continental Slope

At 56°S, cores PS97/014-1 GC and PS97/015-1GC were recovered from 2103 m and 1883 m water depth (WD), respectively, with only low recoveries of 0.44 to 0.85 m. Sediment acoustic profiling in this area also showed high-amplitude low-penetration characteristics (Fig. 3.5.5). Further to the northwest, between ~55° and 56°S, cores PS97/109-1 PC (equivalent to site PS97/020) and PS97/110-1 GC (equivalent to Site PS97/021) were taken from 2100 m and 1845 m WD.

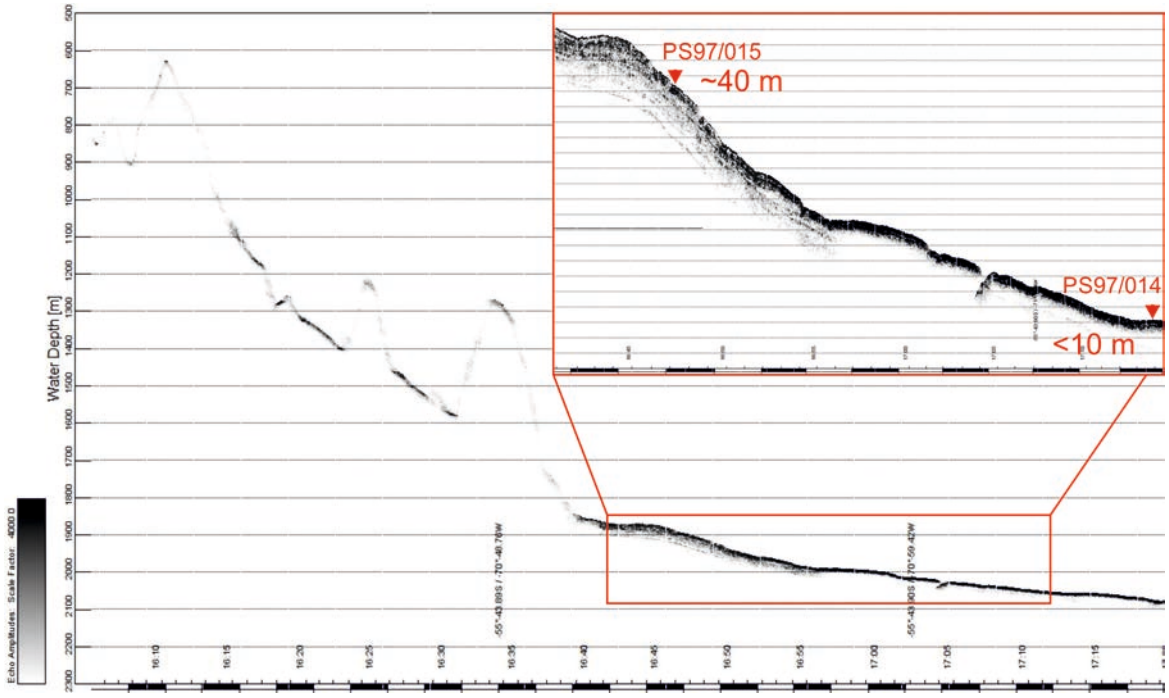

Fig. 3.5.5: Sediment acoustic downslope profile at the Southern Chilean Continental Margin showing high-amplitude low-penetration signals (most of the time less than 10 m) characteristic for coarser-grained sandy surface sediments.

Between ~54° and ~55°S, gravity cores PS97/020-1 (2105 m WD), PS97/021-2 (1840 m WD; no recovery), PS97/022-2 (1617 m WD), PS97/023-1 (1600 m WD), PS97/024-1 (1273 m WD), PS97/025-1 PC (1619 m WD), PS97/026-1 (1619 m WD), and PS97/027-2 (2352 m WD) achieved core lengths of 0.44 cm to 5.43 cm. Only the piston cores PS97/025-1 and PS97/026-1 reached core lengths of up to ~6 m (1620 m WD). The PARASOUND profile connecting these two stations (Fig. 3.5.6) shows generally good acoustic penetration depths (40 m). Station PS97/25 represents an extended section located in a sediment-filled trough-like structure and Station PS97/26 reveals a more condensed sediment sequence located at the shoulder of the structure (Fig. 3.5.6). Core PS97/027-2 (2.01 m) was repeated on the way back to Punta Arenas, and achieved a considerablby larger recovery (PS97/111-1; 9.93 m).

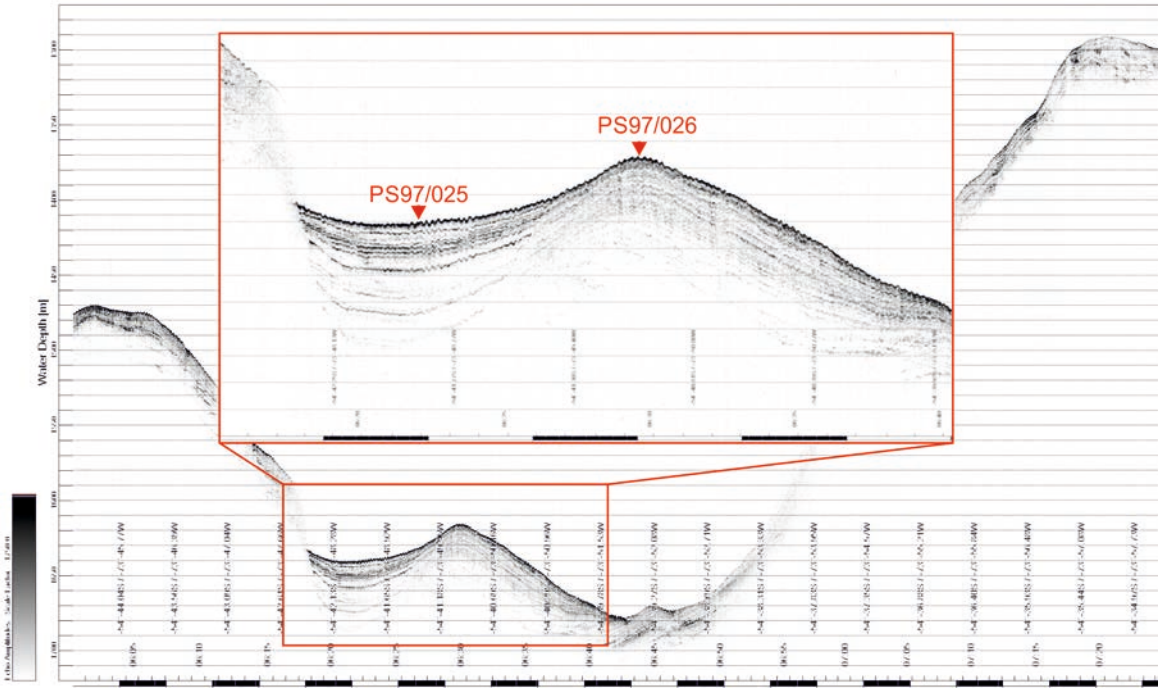

Fig. 3.5.6: Sediment acoustic profile at the Southern Chilean Continental Margin showing rel. high penetration signals (40 m) at the coring sites PS97/25 and 26.

Core PS97/122-1 from 2558 m water depth has been retrieved form the Chilean continental slope and reached 10.77 m length. Further to the north at ~53.5°S, cores PS97/128-2 (2305 m WD) and PS97/129-1 PC (1873 m WD) achieved core lengths of 10.69 m and 7.32 m, respectively. At ~53°S, a very short 1 m-gravity core was recovered from 3250 m water depth at the lower continental slope (PS97/130-1). Sediment cover was generally sparse in this area.

The continental slope at ~52.5°S was previously cored by RV Marion Dufresne (core MD07-3128; Kissel et al., 2007). A detailed PS/HS survey in this region revealed an elongated at least 40 m thick sediment prism (Fig. 3.5.7) (see chapter 6.3). During PS 97, we retrieved cores PS97/137-1 (8.5 m recovery), PS97/138-1 GC (2.71 m), and PS97/139-1 GC (4.54 m) from intermediate water depths (~600-1000 m). Piston corer PS9/136-1 from 1065 m water depth was empty.

Mostly, the uppermost sediments along the Pacific Chilean Margin across all water depths covered by our cores, consist of coarse, soupy, light greenish brown to light whitish gray foraminiferal sand, which is up to ~1 m thick. Only in a few cases, the foraminiferal sand is missing at the top (e.g., PS97/024-1). The contact to the sediment below is rather gradual, covers ~10-20 cm, and is strongly bioturbated. Below the foraminiferal sand, the sediment changes into dark greenish gray diatom-bearing clayey silt, which is mostly weakly bioturbated, and contains occasional dropstones. The top-most foraminiferal sand most likely represents the Holocene and the lower part reaches into the last glacial section.

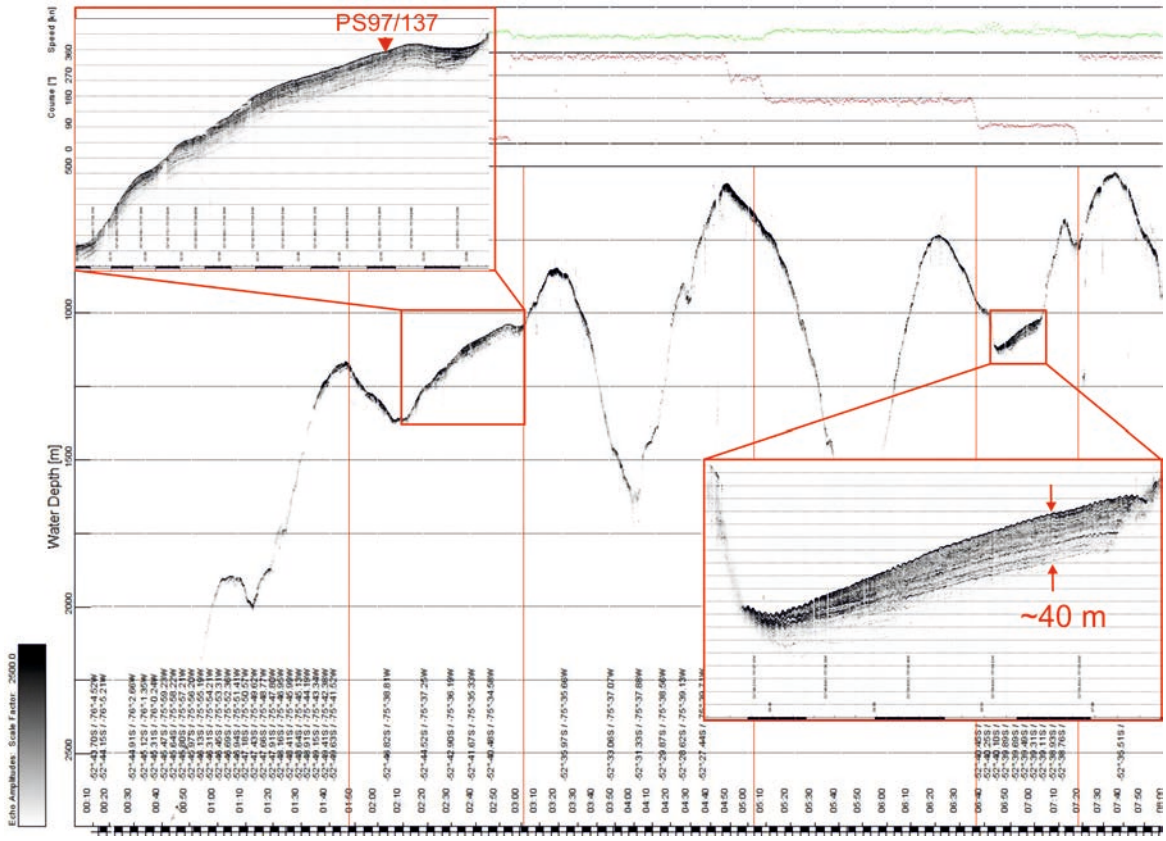

Fig. 3.5.7: Sediment acoustic profile crossing several times the sediment prism on the upper continental slope that has been drilled previously during the Pachyderm cruise of RV Marion Dufresne.

Our long cores PS97/025-1 and PS97/026-1 show mainly terrigenous sediments below the foraminferal sand with cyclic variations in the content of biogenic carbonate. The magnetic susceptibility records show lowest values within the more carbonate containing sequences, and can easily be correlated among cores. Also, the magnetic susceptibility records correspond to the dated sediment record of core MD07-3128 (Kissel et al., 2007; Caniupán et al., 2011,), providing an age of ~45 ka for core PS97/026-1 and ~20 ka for core PS97/025-1 suggesting sedimentation rates that are suitable to reconstruct millennial-scale fluctuations (Fig. 3.5.8).

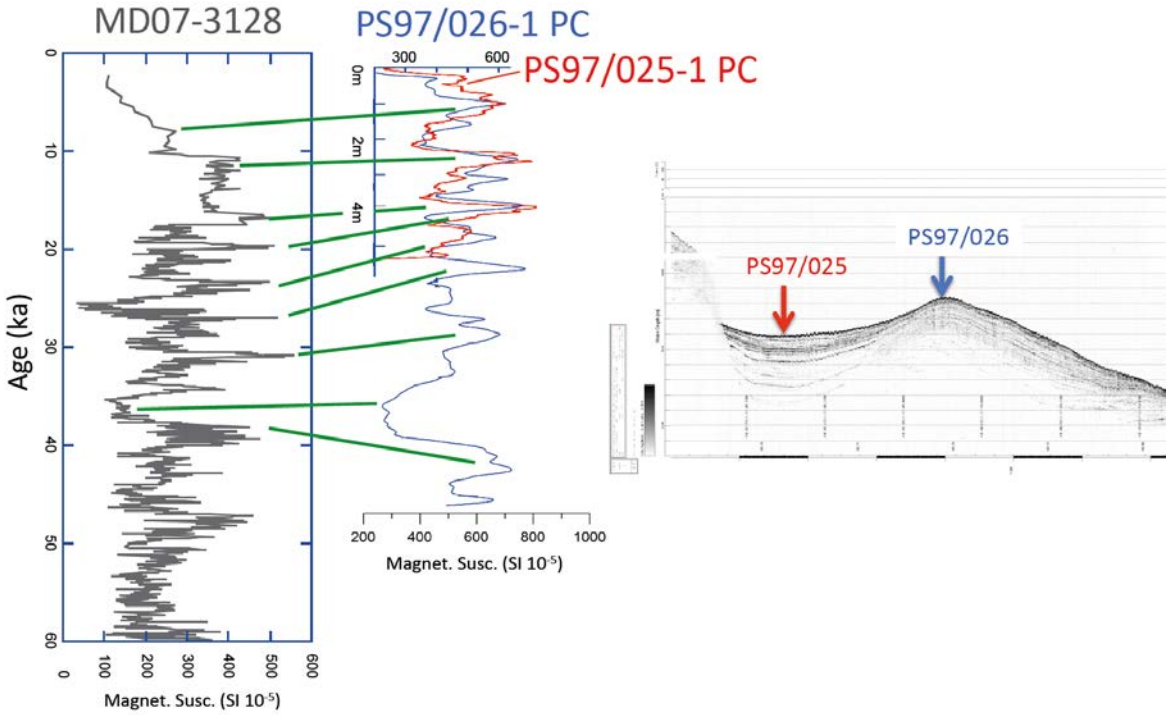

Fig. 3.5.8: Left: Correlating magnetic susceptibility records of Pacific Chilean Margin cores PS97/025-1 and PS97/026-1 in comparison to the record of core MD07-3128 (Caniupan et al., 2011, Kissel et al., 2007). The tentative correlation suggests that PS97/25-1 and PS97/26-1 reach back to ~20 and ~45 ka, respectively. They thus exhibit millennial-scale temporal resolution. Right: PARASOUND profile showing coring sites.

West of the Peru-Chile Trench

Cores PS97/112-1 and PS97/114-2 were cored in 3860 m water depth in the deep Southeast Pacific (~55°S) ~120 nm off the Chilean coast. Double coring (PC15 and PC20) achieved 14.58 m and 22.37 m, respectively. Sediment acoustic profiles and later also the seismic survey from this region revealed well-stratified deposits with acoustic penetration depths of more than 70 m (Fig. 3.5.9) (see chapter 6.3).

With respect to major lithologies, cores PS97/112-1 and PS97/114-2 from ~3860 m water depth in the deep Southeast Pacific are different from the shallower continental margin cores further to the east. Overlain by a light brownish foraminifera, coccolith, and diatom-bearing calcareous ooze, dark greenish gray to dark blueish gray clays dominate the sequence. The dark clay is partly changing into a transitional diatomaceous fine-grained sediment. The clay sequence is intercalated with whitish calcareous oozes, the base of which is commonly strongly bioturbated. In core PS97/112-1, calcareous oozes are present at 7-8.5 m core depth. In core PS97/114-2 PC calcareous oozes are found at ~6-8 m and 13.5 m. At 20-21 m, a compact, stiff, white nannofossil ooze is visible, reaching a thickness of 0.5 m. Calcareous and oozes are quite similar to those described in cores PS97/092-1 and 093-2 further to the south from comparable water depths of ~3800 m. Calcareous oozes and the well-preserved nannofossil ooze in core PS97/114-2 displays lowest magnetic susceptibilities, approaching even null-values. The records of both cores correlate convincingly. The tentative correlation to the Lisiecki & Rymo (2005) isotope stack and to the Antarctic climate records suggests that core PS97/114-2 reaches Marine Isotope Stage 11, while the shorter core PS97/112-1 only covers Marine Isotopes Stages 1-7 (Fig. 3.5.10).

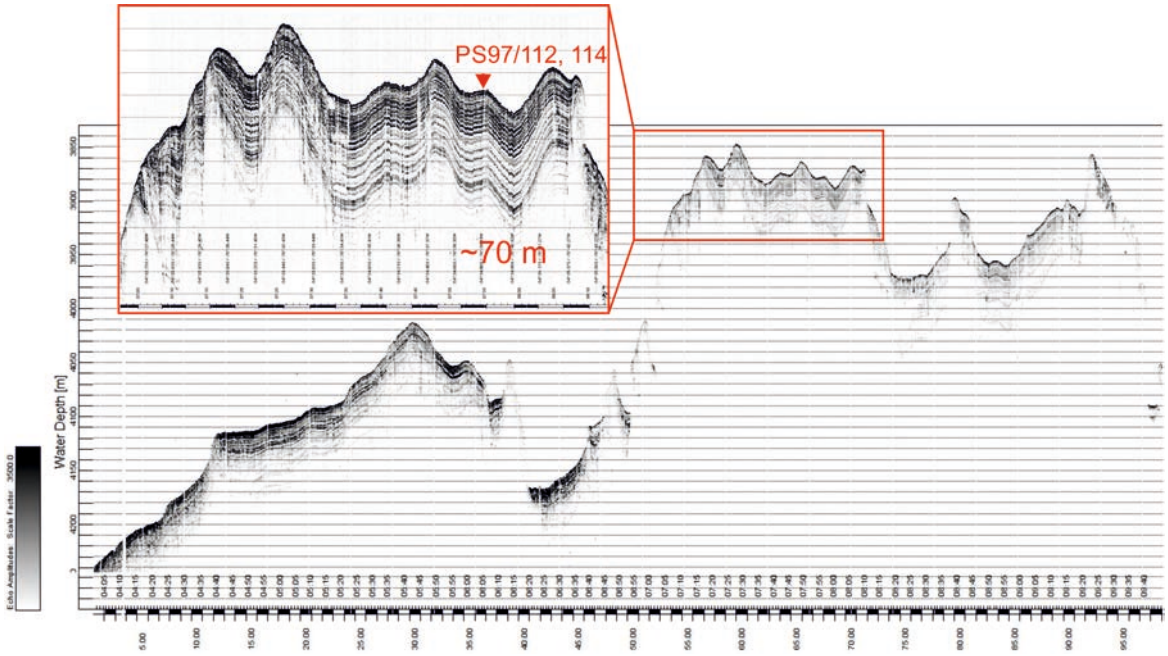

Fig. 3.5.9: Sediment acoustic profile west of the Chilean Trench showing deep sediment penetration (more than 70 m) in well-stratified laterally homogenous pelagic sediment cover.

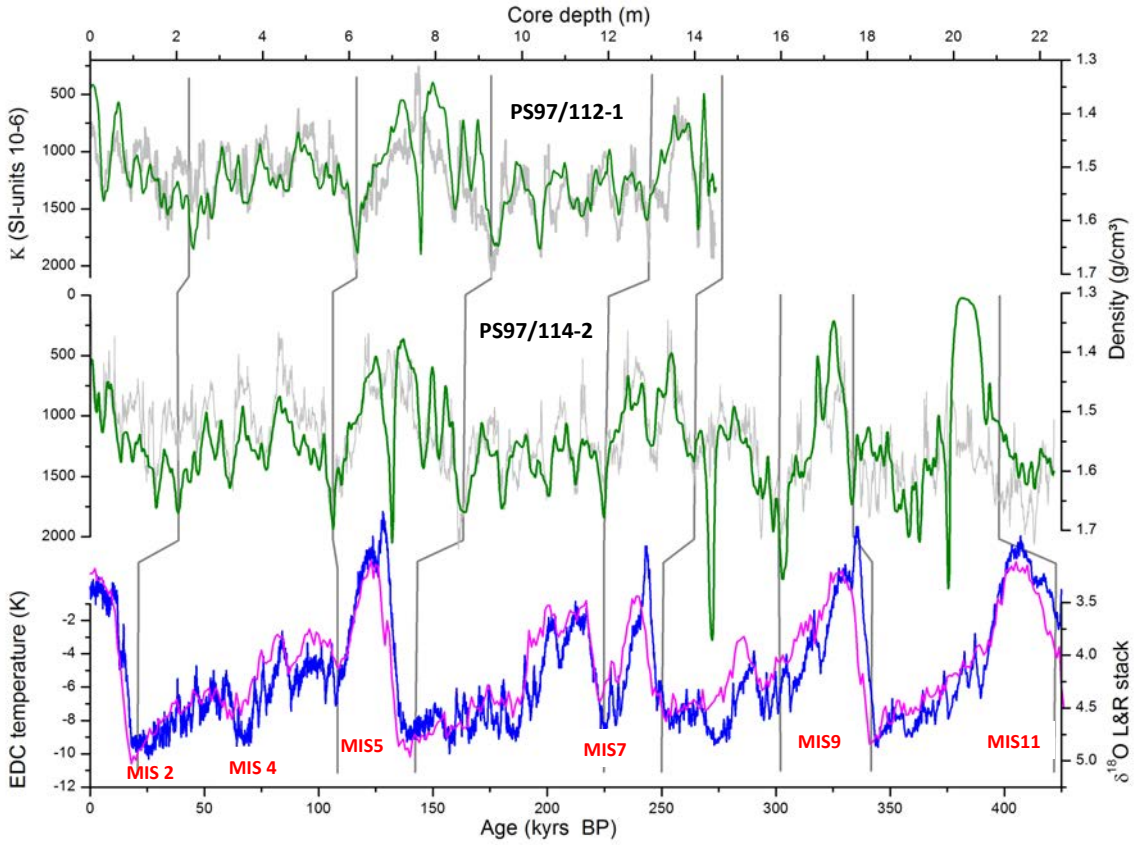

Fig. 3.5.10: Magnetic susceptibility (green) and density records (gray) of cores PS97/112-1 and PS97/114-2 from the deep Southeast Pacific (~3800 m water depth). Tentative correlations among cores and to dated reference records (blue = EPICA Dome C temperature record; pink = LR04 isotope reference stack) are indicated by vertical gray lines.

Additional pelagic sediment cores located relatively close to the continental margin and therefore grouped into this transect were taken at the beginning of the western DP transect (see chapter 3.5.3). This transect started at the upper continental slope at around 55°40'S / 71° 30'W. After passing the steep continental slope, more than 50 m of slightly deformed and faulted trench deposits were encountered in the ~4400 m deep Chilean Trench (Fig. 3.5.11). Most likely active normal faulting is responsible for vertical displacements of several meters in the trench sediments. South of the trench, until a latitude of about 57°30'S, the sea floor topography and sediment acoustic data suggest a rather uniform sediment cover of at least 40 m. Here, several sites (PS97/092 to PS97/094) were successfully cored revealing condensed pelagic sediments. With increasing distance to the trench, the seafloor becomes rough and sedimentation is starved.

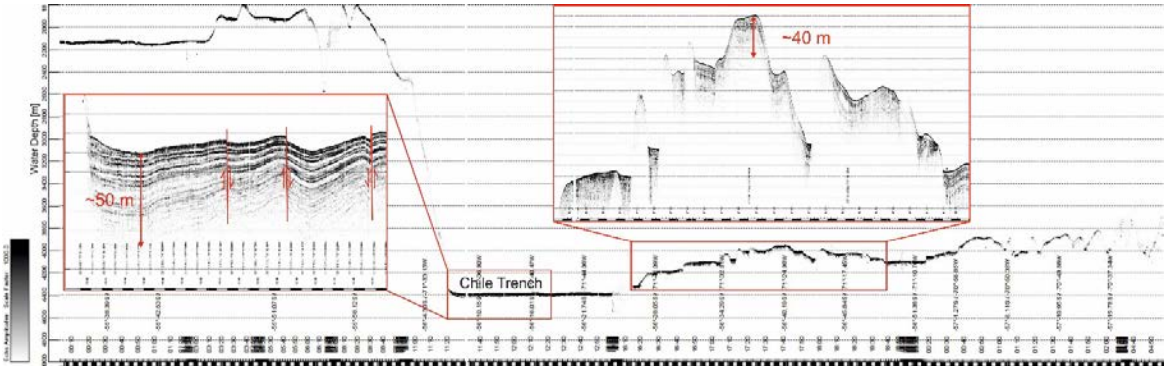

Fig. 3.5.11: PARASOUND profile downslope the Chilean Continental margin crossing the Chile Trench southward.

The sediment cores are located between 57°S and 58°S at water depths of ~3780 to ~4000 m water depth. Cores PS97/092-1, 093-1 and -2, and 094-2 reached core lengths from 7.89 m to 16.45 m. Double coring was accomplished at site PS97/093 (11.16 m and 16.45 m).
Sediment cores PS97/092-1 and 093-2 typically consist of a recurring sequence of distinct lithologies: At the base of such a sequence, a whitish gray calcareous ooze is developed, which is pervasive of coccoliths and planktonic foraminifera with only minor portions of diatoms. In parts, the calcareous ooze develops into a pure, white nannofossil ooze, which is compact, stiff, and difficult to cut. In core PS97/92-1, the nannofossil ooze is up to 80 cm in thickness, while it is only 20 cm thick in core PS97/93-2. Either, the commonly strongly bioturbated calcareous (nannofossil) ooze changes rapidly into a weakly bioturbated dark clay void of biogenic components, or a transitional diatomaceous fine-grained sediment of various thickness is intercalated. The dark gray clay gradually changes into a diatomaceous silt, which is moderately bioturbated and clearly more greenish gray. Subsequently, calcareous ooze is deposited again, with the transition zone to the sediment below being very strongly bioturbated. The calcareous oozes are clearly reflected in the magnetic susceptibility records by minimum values (Fig. 3.5.12). In core PS97/93-2, we observe ~10 well-define calcareous oozes, while only 4 oozes are present in core PS97/92-1. Both cores can be correlated easily using the magnetic susceptibility records (linear correlation r = 0.93), suggesting that the base of core PS97/92-1 at ~7.9 m correlates with the core depths of ~4.1 m in core PS97/93-2. Apparently, although being from similar water depths, core PS97/92-1 has nearly twice as high sedimentation rates as core PS97/93-2 (Fig. 3.5.12).

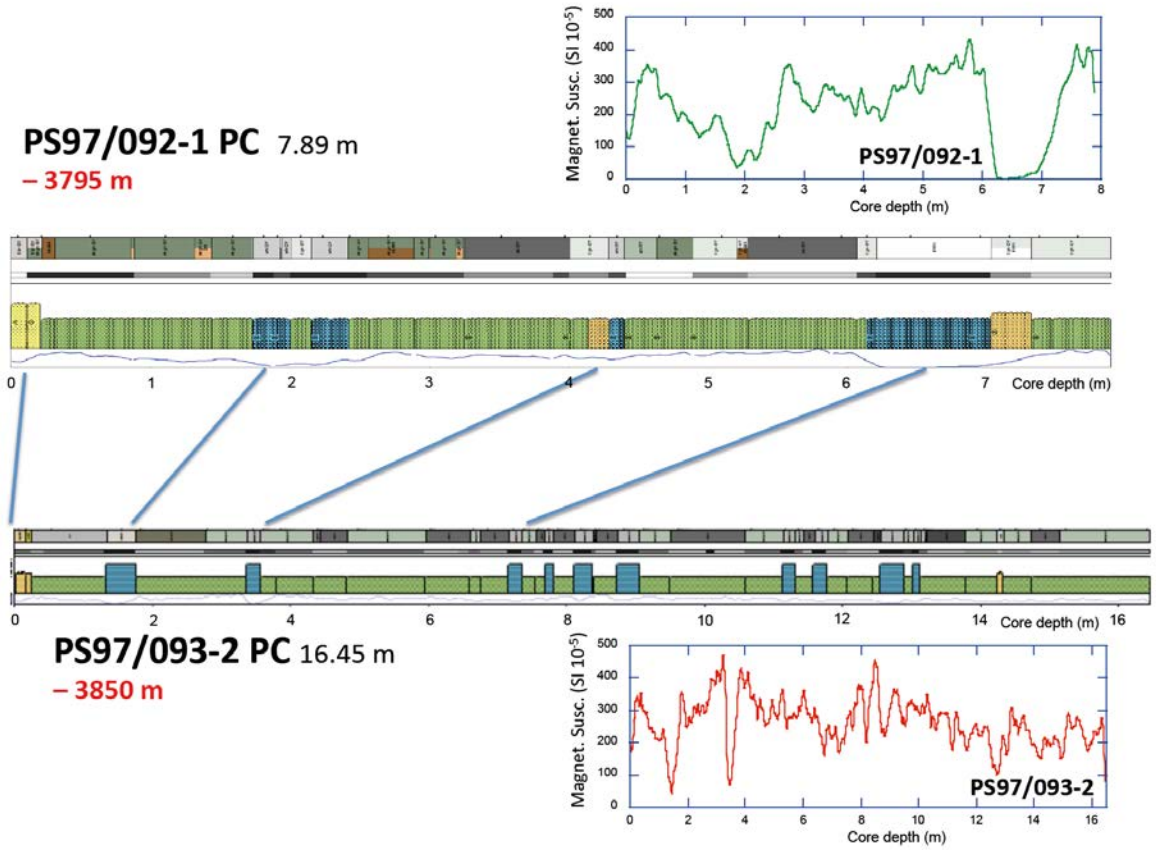

Fig. 3.5.12: Schematic lithology logs and magnetic susceptibility records of cores PS97/92-1 and PS97/93-2. A tentative correlation is indicated by the blue lines.

The rapid development of the prominent calcareous (nannofossil) oozes in the Southeast Pacific affords significant oceanographic changes. Prominent nannofossil oozes have also been encountered further west in the South Pacific during PS75 (Gersonde, 2011).

3.5.2. Scotia Sea Margin (Transect 2)

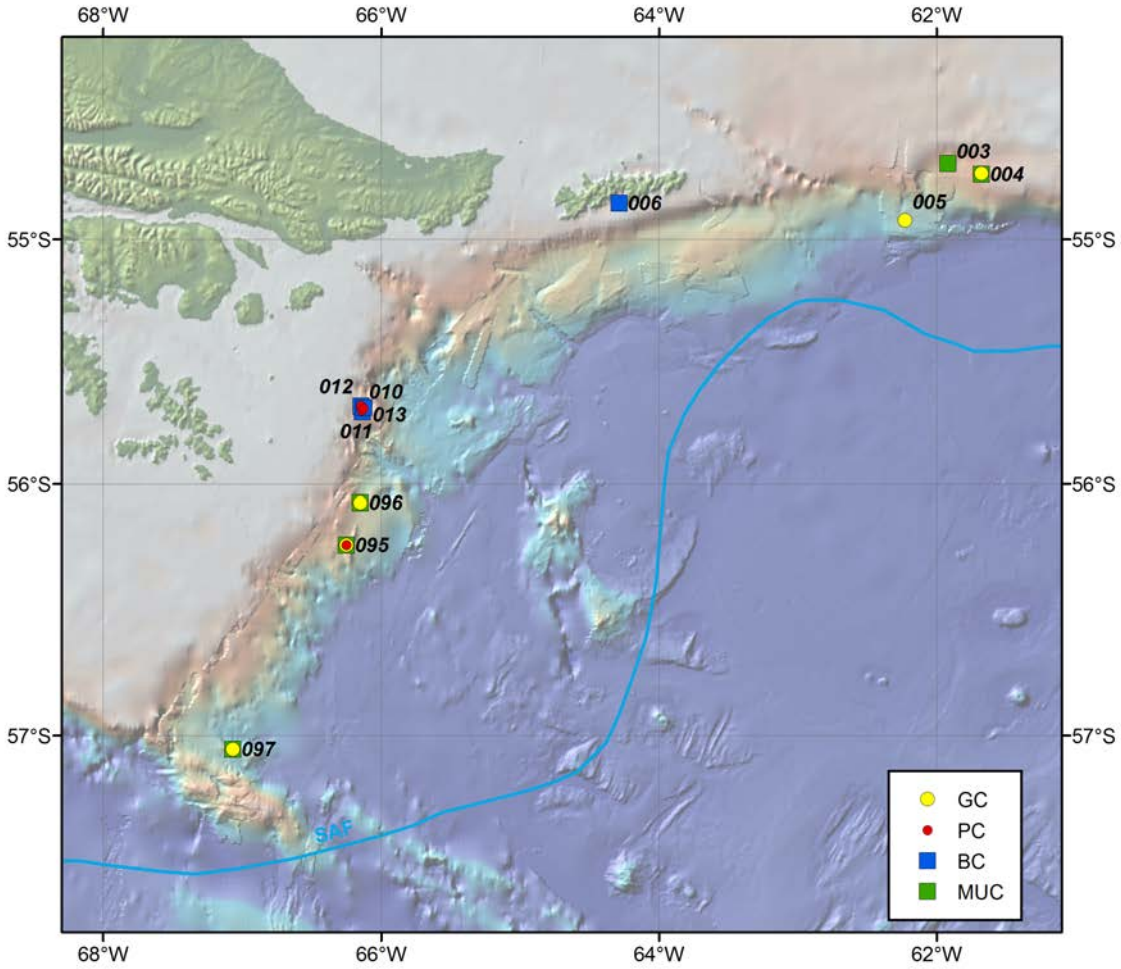

Fig. 3.5.13: Sediment core and surface sample locations at the Scotia Sea Margin (Transect 2).

Surface Sediments

Surface sediments along the Chilean/Argentinian continental margin in the Scotia Sea (Fig. 3.5.13) were collected at water depths ranging from ~670 m to ~2320 m. They are rich in terrigenous particles (quartz, rock fragments and accessory minerals) and calcareous microfossils (mainly foraminifers), and are characterized as calcareous microfossil-bearing silt (northernmost station PS97/011-2 sampled with a giant box corer; 667 m WD) or foraminifera sand. Rock fragments were particularly more abundant at station PS97/095-1 (1652 m WD). The lithology of the surface sediments is consistent with strong bottom current winnowing (Fig. 3.5.14).

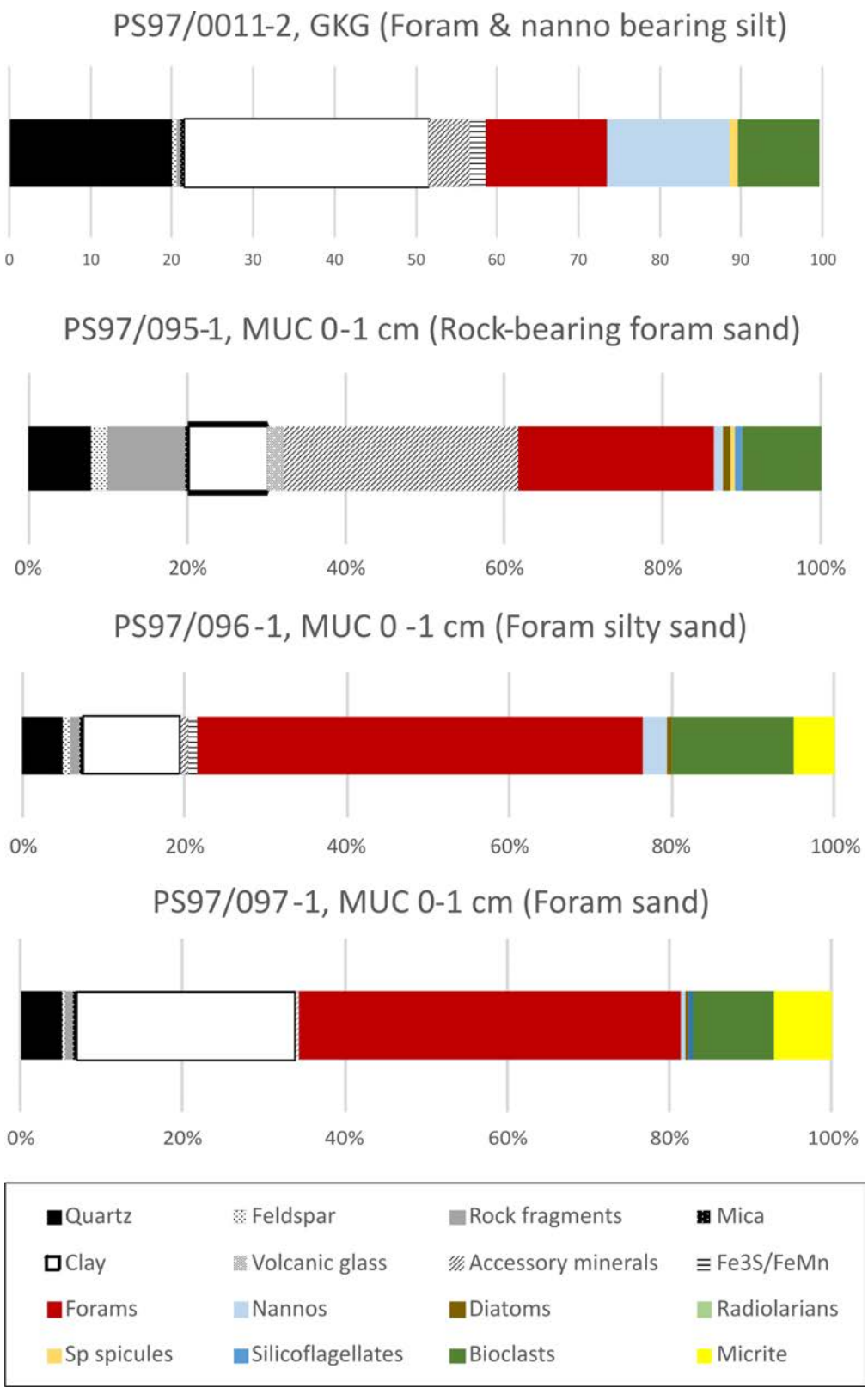

Fig. 3.5.14: Overview of surface sediment composition along the Argentinian/Chilean Margin (Scotia Sea) based on smear slide analysis.

Coring

Coring at the Scotia Sea Margin was difficult due to the hard and compacted surface sediments, in particular at shallow depths (Fig. 3.5.15). Piston coring partly suffered from bending of coring devices, while short gravity cores from ~750 m (PS97/004-2), ~1610 m (PS97/096-2), and ~2430 m (PS97/005-1) did not recover sediment due to missing penetration or wash-out of relative coarse sediment.

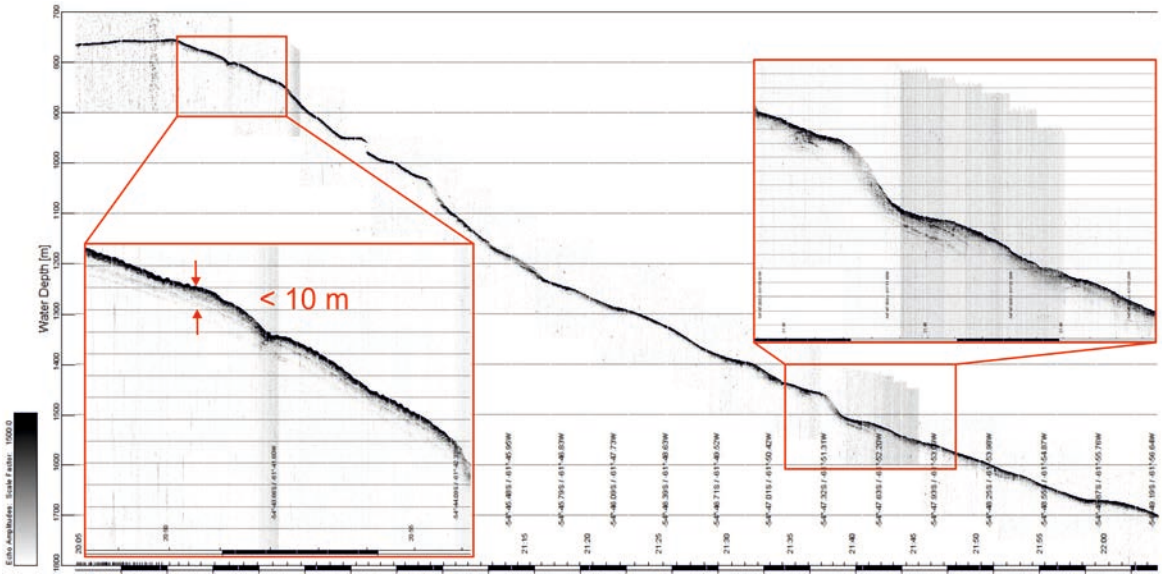

Fig. 3.5.15: Sediment acoustic downslope profile at the Argentinian Continental Margin showing high amplitude low penetration signals (less than 10 m) characteristic for coarser-grained sandy surface sediments.

From intermediate water depths (~560 to ~620 m), we recovered longer undisturbed sedimentary records (PS97/009-2, 9.04 m; PS97/011, 6.53 m; PS97/010-1, 6.91 m). From greater depth, we retrieved cores PS97/095-2 (1645 m WD), PS97/096-2 (1612 m WD), PS97/097-2 and 097-3 (2315 m and 2300m WD). Cores PS97/009-2 and PS97/010-1 were located on a NW-SE-oriented transect perpendicular to the Argentinian slope, while PS97/011 was offset from this transect by a few nautical miles to the east (see chapter 6.1; Fig. 6.1.4 and 6.1.5). Sediment sequences within this sediment body are largely expanded at the shallowest site, condensing further downslope. Sediment acoustic patterns of this sediment drift suggest four times higher sedimentation rates at the shallower site (Fig. 3.5.16). The sediment package is sharply truncated at 680 m WD, which might be related to the lower boundary of Southern Ocean Intermediate Water. Above, the low current velocities of Southern Ocean Intermediate Water could favor preferential sediment accumulation.

All cores are composed of mainly terrigenous sediments. The silty to fine sands and sandy silty clays bear only minor biogenic components, mainly planktonic foraminifera and diatoms. Ice rafted debris and large dropstones (>1 cm in diameter) are rarely but continuously present in the sediment records. At all core locations, up to 30 cm thick coarse sand layers regularly interrupt the hemipelagic sedimentary sequences. The contacts to below are even and rather sharp, while the upper contacts are mostly gradual. Dropstones and calcareous shell fragments are common within these well-sorted sand layers. The magnetic susceptibility values reach highest values within the soupy, dewatering sand layers. Magnetic susceptibility values gradually increase towards the core tops. The pattern of all magnetic susceptibility records is similar in all sediment cores allowing for correlation of the records across the slope (Fig. 3.5.17). The record of core PS97/009-2 correlates to that of the dated

RV Mirai core MR0806PC9 (Lamy et al., 2015, Shiroya et al., 2013). According to our tentative correlation, the PS PS97/009-2 record covers the time interval from ~47 to 23 ka BP, with millennial-scale temporal resolution. Accordingly, sedimentation rates are highest at the shallowest site location (30 cm/ka), decreasing gradually downslope to 20 cm/ka and 13 cm/ka. The uppermost, i.e. deglacial and Holocene sequences are apparently missing or very condensed in all three sediment cores, either due to coring disturbance and/or erosional processes on the continental slope. The magnetic susceptibility records consistently imply that the terrigenous flux towards the continental slope varied significantly over time, but steadily increased during MIS 3 and culminated prior to the Last Glacial Maximum. The soupy sand layers point to re-occurring instantaneous and short-lasting events, either episodic current winnowing or debris flows transporting coarse shelf material across the slope.

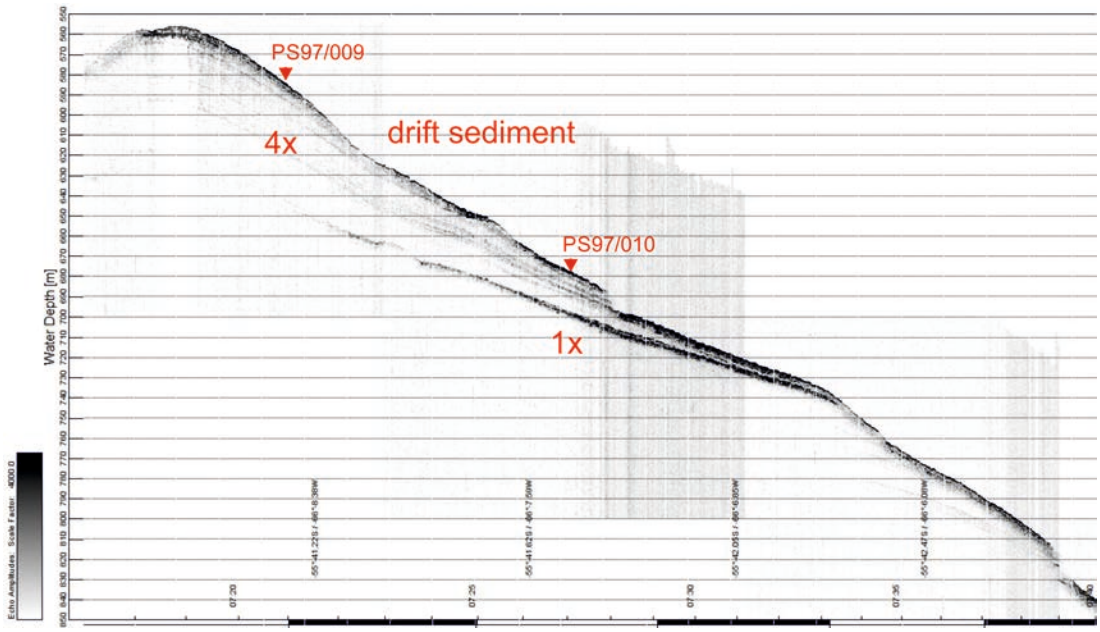

Fig. 3.5.16: Sediment drift at 560 to 760 m water depth on the upper Argentinian continental slope showing up to four times higher sedimentation rates at the shallower coring site PS97/009 compared to the deeper site PS97/010.

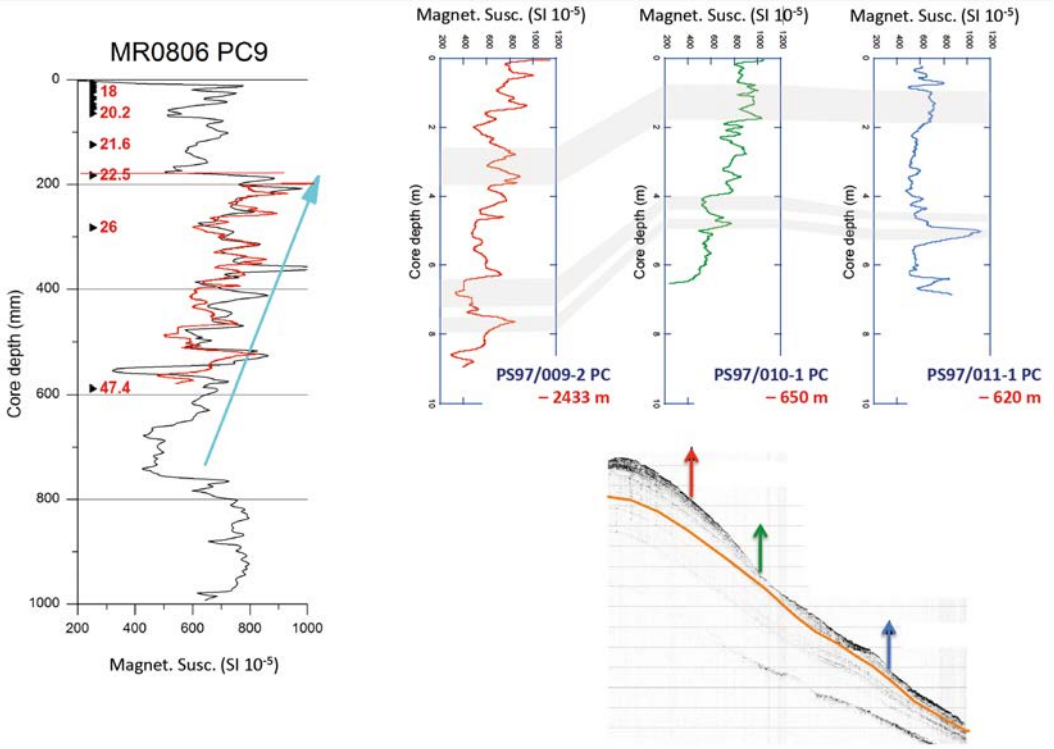

Fig. 3.5.17. Upper right: Tentative correlation of magnetic susceptibility records from Argentinian/Chilean Margin (Scotia Sea) sediment cores PS97/009-2, PS97/010-1, and PS97/011-1. Lower right diagram shows site locations along the continental slope. Left: Preliminary correlation of the PS97/009-2 magnetic susceptibility record to the dated RV Mirai core MR0806 PC9.

Cores PS97/095-2, PS97/096-2, PS97/097-2 and 097-3 retrieved from south of Cape Horn, show a similar lithology to cores from further to the east (PS97/009-011), with prominent and thick black sand layers, suggesting considerable mass flow from the shelf areas into the deep sea. In particular, core PS9/095-2 is quasi completely composed of black coarse sand, intercalated with three greenish-gray silty clay layers and the PC bent during coring. In the deepest core from the Scotia Sea Margin at the Tierra del Fuego Spur, PS97/097 (2300 m WD), coarse black sand layers are clearly thinner (few cm), and the hemipelagic sediment, although predominantly coarse, shows colorful and sharp lithological changes.

3.5.3. Drake Passage (Transect 3)

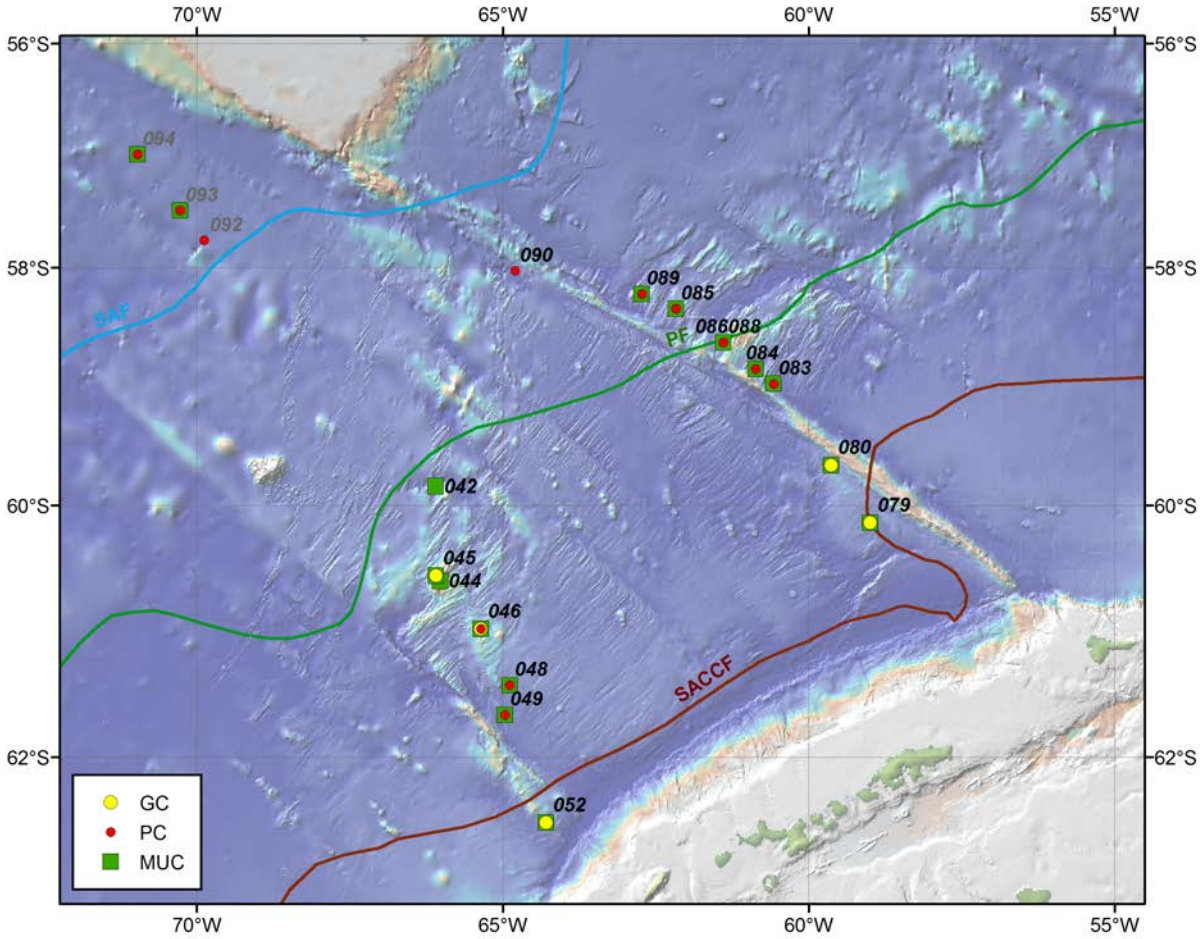

Fig. 3.5.18: Sediment core and surface sample locations in the DP (Transect 3).

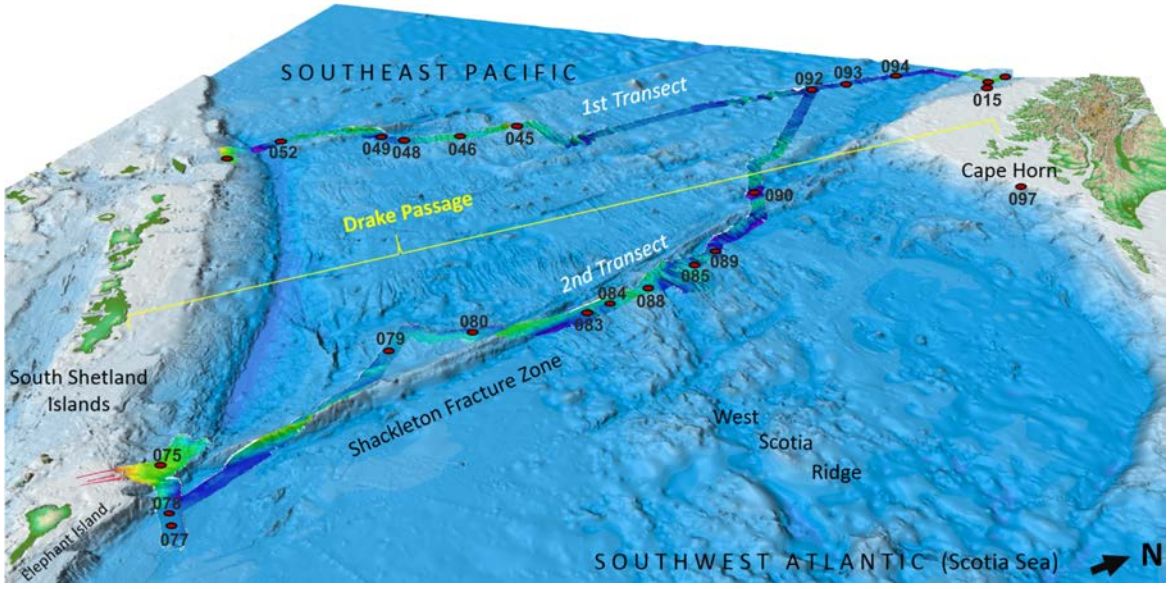

Fig. 3.5.19: 3D view of the DP with surface sample locations and coring stations.

The DP transect consists of cores recovered on two traverses: (1) at the western Pacific entrance and (2) within the central DP, roughly along the Shackleton Fracture Zone. We combine results from both transects from north to south, including from the Polar Frontal Zone (PFZ) to just south of the SACCF (Fig. 3.5.18 and 3.5.19). The subantarctic sediment cores and surface samples at stations PS97/092 to PS97/094 are discussed in the Pacific Chilean Margin chapter (3.5.1).

Surface sediments

In general, surface sediments obtained from north of or close to the PF contain higher amounts of foraminifers, coccoliths and bioclasts (mainly fragmented foraminifera), while sediments from south of the PF are characterized by a higher content of biosiliceous compounds (Fig. 3.5.20). This distribution pattern is consistent with the extent of the circum-Antarctic opal belt.

Sediments recovered along the Hero Fracture Zone and south of the present PF are dominated by biogenic oozes and sands. Foraminifer sand characterized only the shallowest station PS97/044 at 1202.8 m water depth. Whereas sediments at stations shallower than 3500 m water depth bear >20% of foraminifers (PS97/045, PS97/046 and PS97/048), diatom oozes almost devoid of calcareous microfossils characterized the deeper stations PS97/042 and PS97/049. Compared to these sediments from the western DP, surface sediments collected along the Shackleton Fracture Zone in the central DP have higher contents of silt and clay and, in general, can be characterized as diatomaceous clay or diatomaceous silt. South of the SACCF and approaching the Antarctic Peninsula continental slope (PS97/052-3), a higher content of rock fragments, probably ice-rafted, is recorded.

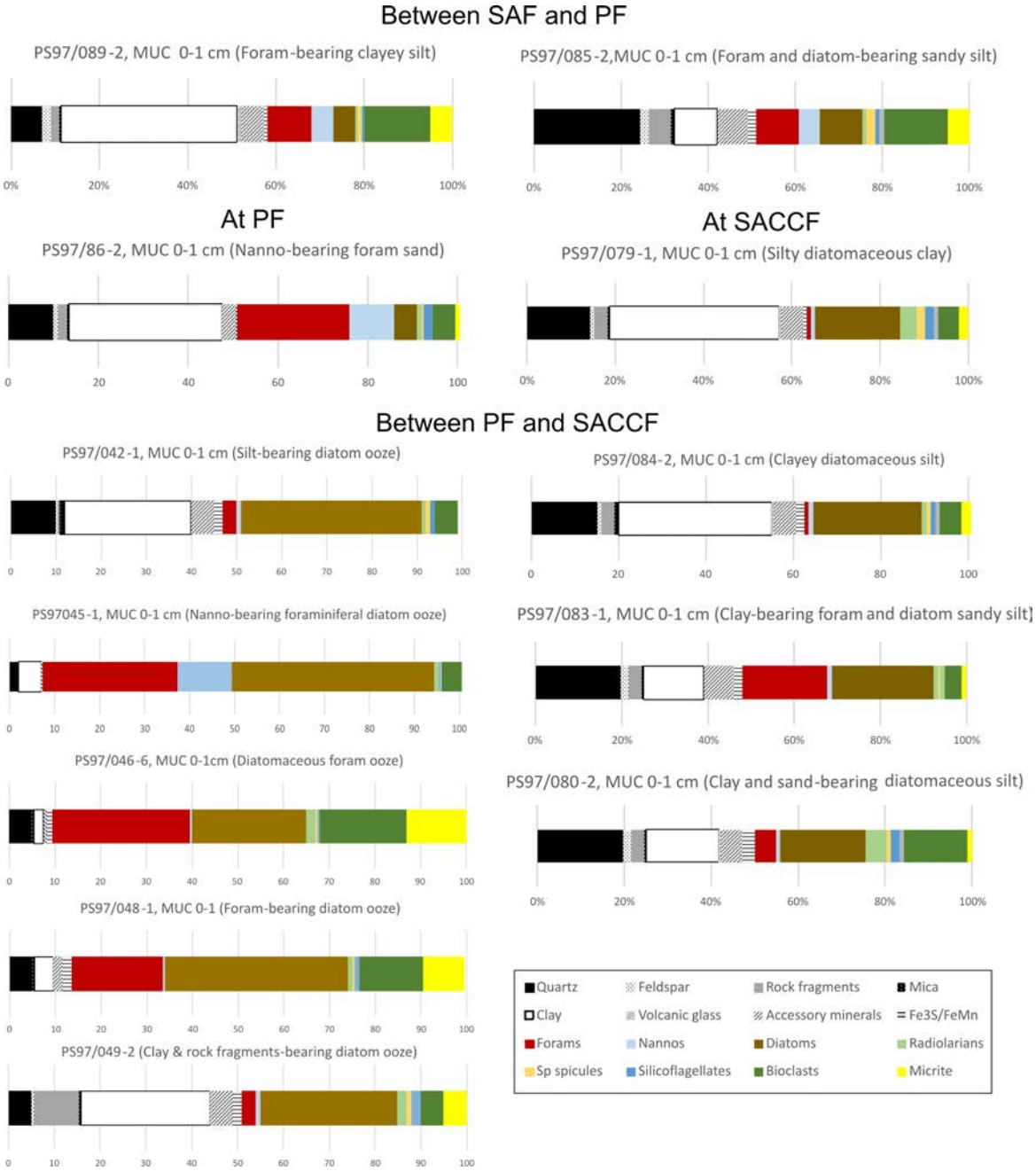

Fig. 3.5.20: Overview of surface sediment composition in the DP, based on smear slide analysis.

Coring

At the western DP transect, the sediment cover abruptly disappeared south of the SAF. Sediment were absent across the PFZ and only south of the PF at a latitude of about 61°20'S the sediment cover starts to increase again. A downslope PARASOUND profile connecting the Antarctic Phoenix Ridge with the southern part of the Hero Fracture Zone (Fig. 3.5.21) shows a faint sediment cover that tends to level out the generally rough topography. Acoustic penetration at two selected coring sites (PS97/48 and PS97/49) is 25 to 35 m and shows planar-bedded sediment layers.

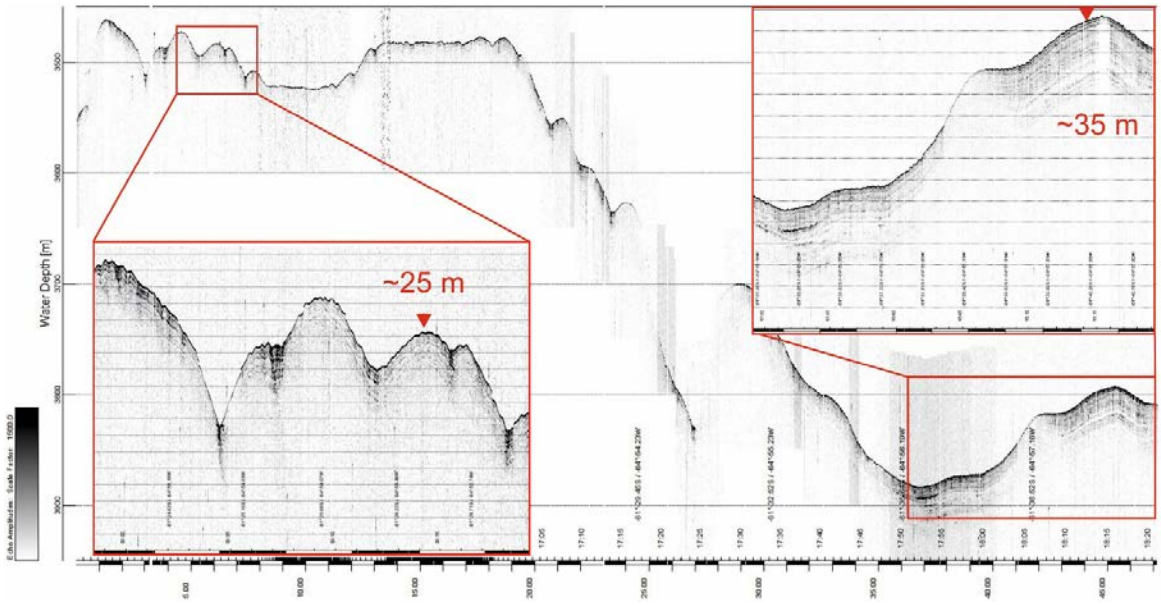

Fig. 3.5.21: PARASOUND profile downslope the Antarctic Phoenix Ridge towards the southern part of the Hero Fracture Zone.

While the central part of the western DP transect is largely barren of sediments and not suitable for coring, the sediment cover further east, at the central DP transect, along the Shackleton Fracture Zone and across the Scotia Ridge shows acoustic penetration depths of up to 60 m and coring turned out to be very successful. Fig. 3.5.22 shows the two coring sites PS97/85 and PS97/88 that lie at about the same water depth (ca. 3000 m) and distance north and south to the spreading center of the Scotia Ridge.

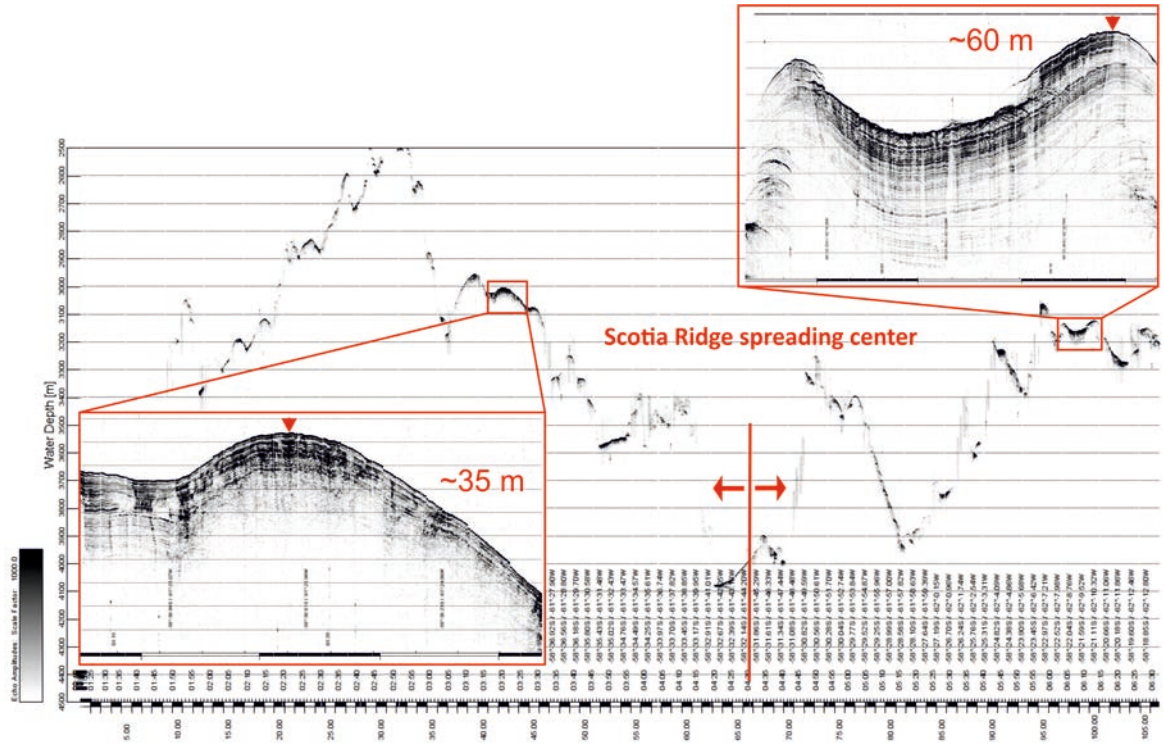

Fig. 3.5.22: PARASOUND profile across the Scotia Ridge east of the Shackleton Fracture Zone with the two coring sites PS97/085 and PS97/088.

Polar Frontal Zone

The PFZ is represented by sediment cores exclusively from the central DP transect (PS97/085-1, 088-1, 089-1, 090-1) between 58°S and 59°S. Cores were retrieved from 2960 m to 4162 m water depth with core recoveries from 7.76 m to 14.43 m. At site PS97/085-1, double coring was accomplished. At site PS97/086-1, the piston corer was lost at the seafloor (2968 m water depth). Core PS97/088-1 PC was recovered directly at the present PF. Cores PS97/089-1 and PS97/090-1 are from the central PFZ (Fig. 3.5.18 and 3.5.19).

The central PFZ sediment cores PS97/089 and PS97/090 are lithologically very similar and are characterized by, in part, by high foraminifera abundances. The occurrence of foraminiferal oozes is the central difference to cores from south of the PF. Core PS97/090-1 consists of a sequence of brownish, strongly bioturbated diatom-bearing sandy silty and dark (bluish) gray, weakly bioturbated silty clay, intercalated by prominent light gray foraminiferal oozes/sands. Magnetic susceptibility records reveal large fluctuations, with particularly low values within the foraminiferal oozes/sands. In core PS97/090-1, a prominent two-meter thick foraminiferal sand is present (termed „Zebra"-foraminifera sand due to the abundant black streaks) at the core base, most likely resulting from sediment focussing. Based on the preliminary stratigraphic correlations shown in Fig. 3.5.23, core PS97/89-1 contaians an expanded late glacial to Holcene sedimentary sequence.

In core PS97/088-1, which is located further south directly at the PF, the foraminiferal sands are reflected by comparatively low magnetic susceptibility values. The magnetic susceptibility record shows 5 prominent minima, which most likely relate to interglacial marine oxygen isotope stages 1, 5, 7, 9, and 11 (Fig. 3.5.23), and reflect southward displacements of the PF. Note, that south of the PF, foraminiferal sands disappear (see PS97/083-3).

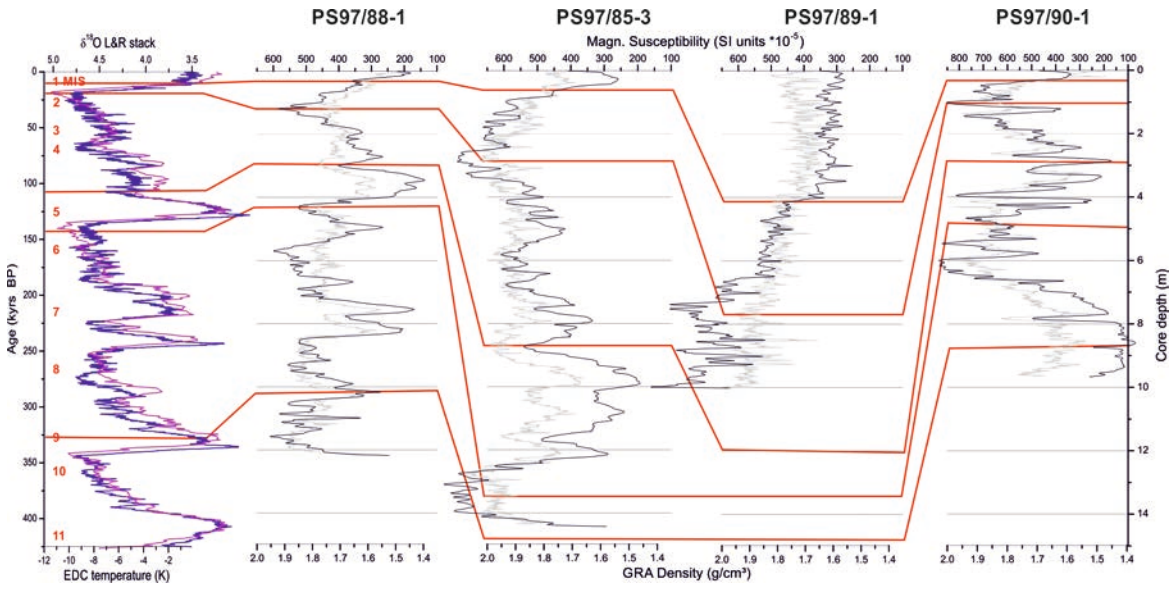

Fig. 3.5.23: Tentative correlation of magnetic susceptibility and GRA density records of cores PS97/088-1, 085-3, 089-1, and 090-1 to dated reference records (blue = Epica Dome C temperature record; pink = LR04 isotope reference stack of Lisiecki and Raymo, 2005).

Between Polar Front and Southern ACC Front

Within the area of the western DP transect (Fig. 3.5.18 and 3.5.19**)**, we successfully recovered gravity and piston cores from below 2000 m water depth. Coring was restricted to 61°S and 62°S (cores PS97-045, 046, 048, 049, 052, 053). Minimum core recovery is 1.37 m, maximum core length is 13.65 m. Core PS97/045-2 closest to the PF was empty. On the central DP transect, in the vicinity of the Shackleton Fracture Zone, core recovery was more successful than on the western DP transect. Three stations were cored between ~58°S and 60°S (PS97/080, 083, 084). Three cores were retrieved from 3106 m to 3759 m water depth. Maximum core recovery was 10.94 m and the minimum core recovery was 1.24 m.
On the western transect, cores PS97/046-3 and 046-4 from ~2800 m water depth were relatively short with 1.37 m and 2.26 m core length, respectively, while cores PS97/048-2 and 049-1 reached considerable lengths of 8.22 m and 13.65 m. These cores are from further to the south from clearly below 3500 m water depth (3448 m and 3759 m, respectively) and best reflect the temporal changes in the depositional environment.
The site location PS97/046 at ~2800 m WD is within an area of rough topography largely barren of sediment or with only local patches of sediment. The light to dark grayish brown coarse to silty sand at the top changes to clearly finer and dark greenish gray clayey sandy silt, which appears strongly bioturbated. Planktonic foraminifera and diatoms are present although not at high abundances. Ice rafted debris (single large dropstones -6 cm and dropstone layers with dropstones 1-3 cm in size) appear over the entire sediment columns. Although from the same coring location, the magnetic susceptibility records of cores PS97/046-3 and 046-4 appear different. Magnetic susceptibility values are comparatively low and only reach higher values when large dropstones are present. A convincing correlation of magnetic susceptibility records could not be achieved. Stratigraphical information is not available apart from the color change within the upper 0.5 m pointing to rather oxygenated conditions in the uppermost layers, which may represent the late Holocene.

Core sites PS97/048-2 and 049-1 are located at greater water depth (3448 m and 3759 m). The seafloor in the region is characterized by a relatively smooth topography and considerable sediment deposition. Downcore, brownish and strongly bioturbated diatom-bearing clayey silts intercalate with dark gray to dark bluish gray silty clays, which are only weakly bioturbated. Sediments are mainly terrigenous, with only minor (<10%) portions of biogenic components (diatoms, foraminifers, bioclasts) and IRD. The magnetic susceptibility values show overall higher values in core PS97/049-1. Both magnetic susceptibility records can be easily correlated, suggesting that the condensed 8 m-record of core PS97/048-2 is represented within the deeper, but expanded 14 m-record of core PS97/049-1. Recurring lithological changes between brownish, coarser and dark gray finer sediments argue for various glacial/interglacial changes covered by the sediment records.

Close to the Shackleton Fracture Zone, we recovered core PS97/083-2 from 3750 m water depth and core PS97/084-1 from 3602 m water depth. Very similar to core PS97/048-2 from further to the west, these high quality cores exhibit an undisturbed sequence of intercalating brownish, strongly bioturbated diatom-bearing clayey silts and dark bluish gray silty clays, which are only weakly bioturbated. The magnetic susceptibility data of core PS97/083-2 are similar to those recorded in core PS97/048-2, and allow the close correlation of the distant cores (Fig. 3.5.24).

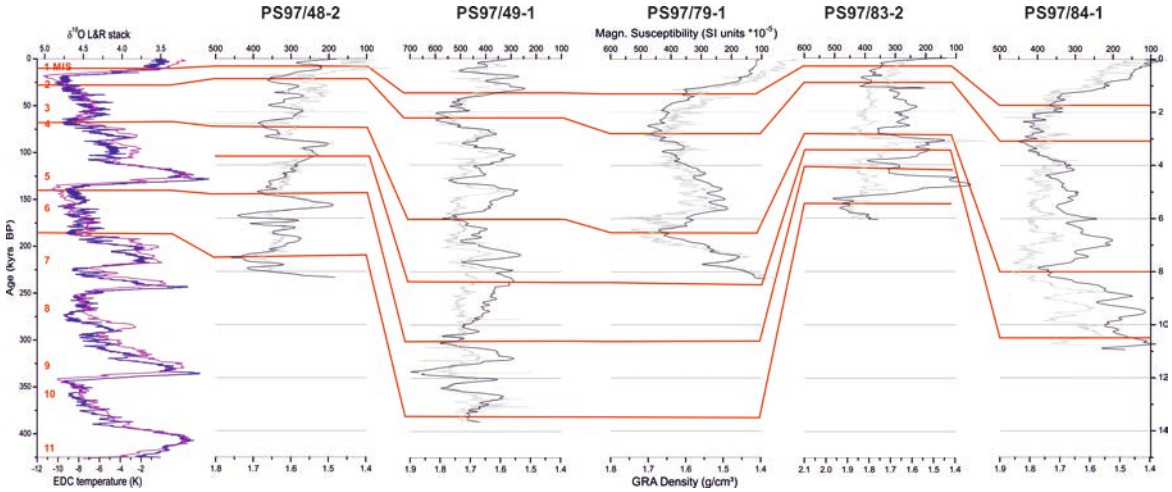

Fig. 3.5.24: Tentative correlation of magnetic susceptibility and GRA density records of cores PS97/48-2 and 49-1 from the western DP transect with cores 79-1, 83-2, and 84-1 from the central DP transrect to dated reference records (blue = Epica Dome C temperature record; pink = LR04 isotope reference stack of Lisiecki and Raymo, 2005).

3.4.5. Antarctic Peninsula

The Antarctic Peninsula working area encompasses three main sub-areas: the continental slope of the WAP, the Bransfield Strait.and the coastal and fjord areas of the South Shetland Islands.

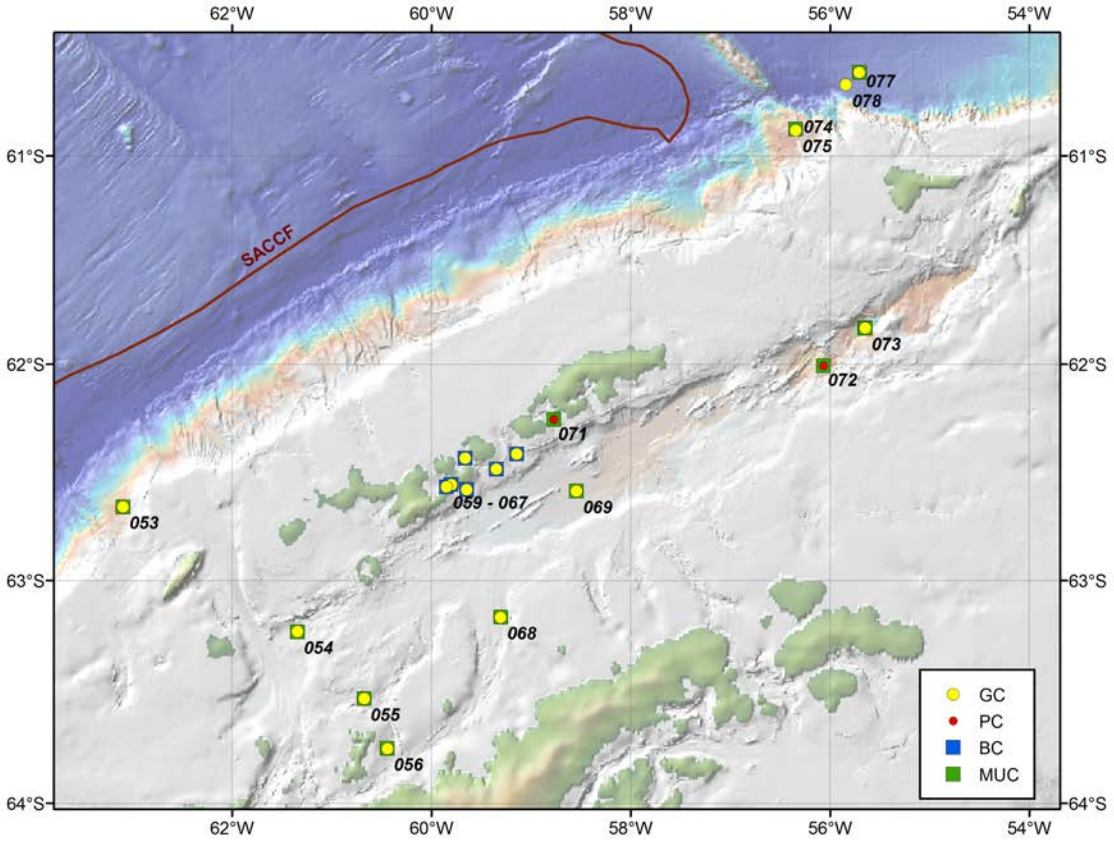

Fig. 3.5.25: Overview of coring sites along the northern continental margin of the Antarctic Peninsula, in the Bransfield Strait and the South Shetland Islands.

Surface sediments

Five giant box cores and 10 multicores were recovered in this working area. Surface sediments collected with the giant box corer in the coastal and fjord areas of the South Shetland Islands are composed of fine to coarse sand with variable amounts of biogenic fragments (Fig. 3.5.26).

Onboard smear slide analysis of the multicores obtained in Maxwell Bay (King George Island) and the Bransfield Strait reveal that the surface sediments can be characterized as silt-bearing diatomaceous clay or silt-bearing diatom ooze (Fig. 3.5.28). Diatom abundances range from 10 to 40% and are very well preserved, reflecting modern phytoplankton communities. A higher content of clastic material as well as benthic and epiphytic diatom species is recorded at more coastal sites. At almost all sites, the lower 30 cm of the multicores are black colored, which may point to either anoxic depositional conditions or early diagenetic alterations. Multicores at stations PS97/074 and PS97/077 from the continental margin of the Antarctic Peninsula are composed of clay-bearing sandy silt and silty diatomaceous clay.

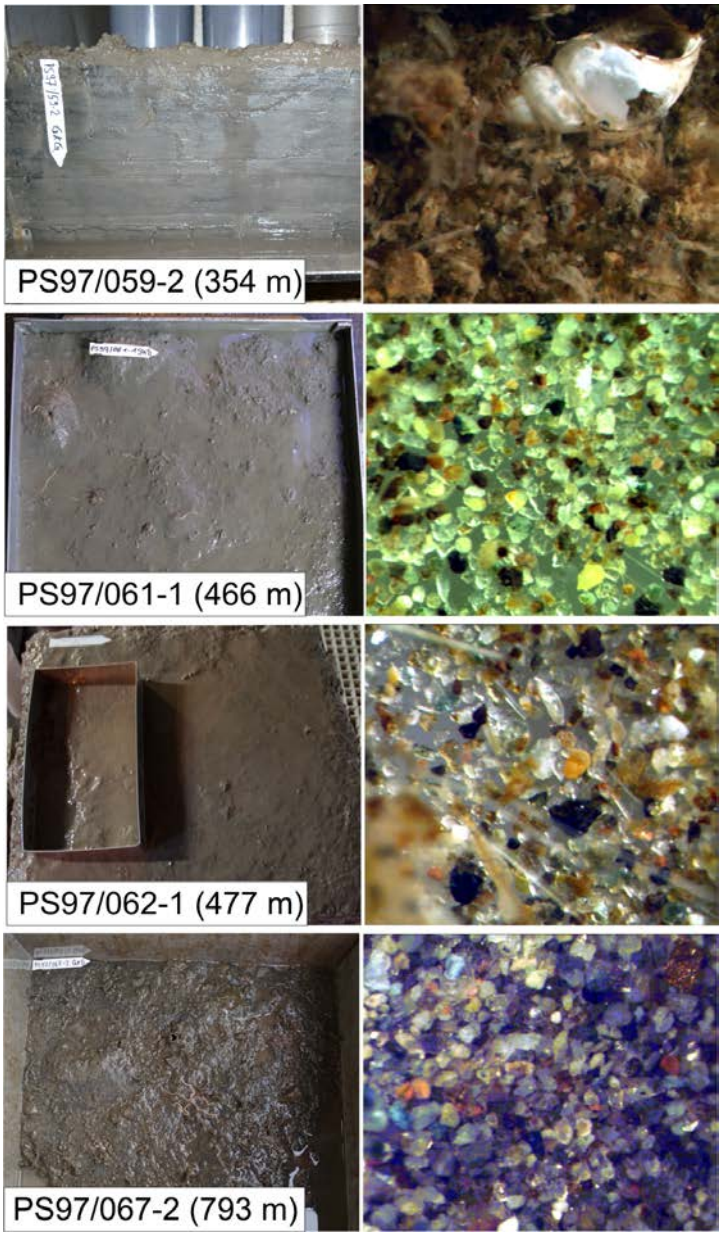

Fig. 3.5.26: Giant box corers retrieved in the South Shetland Islands and microscope images of the coarse fraction of the surface sediments.

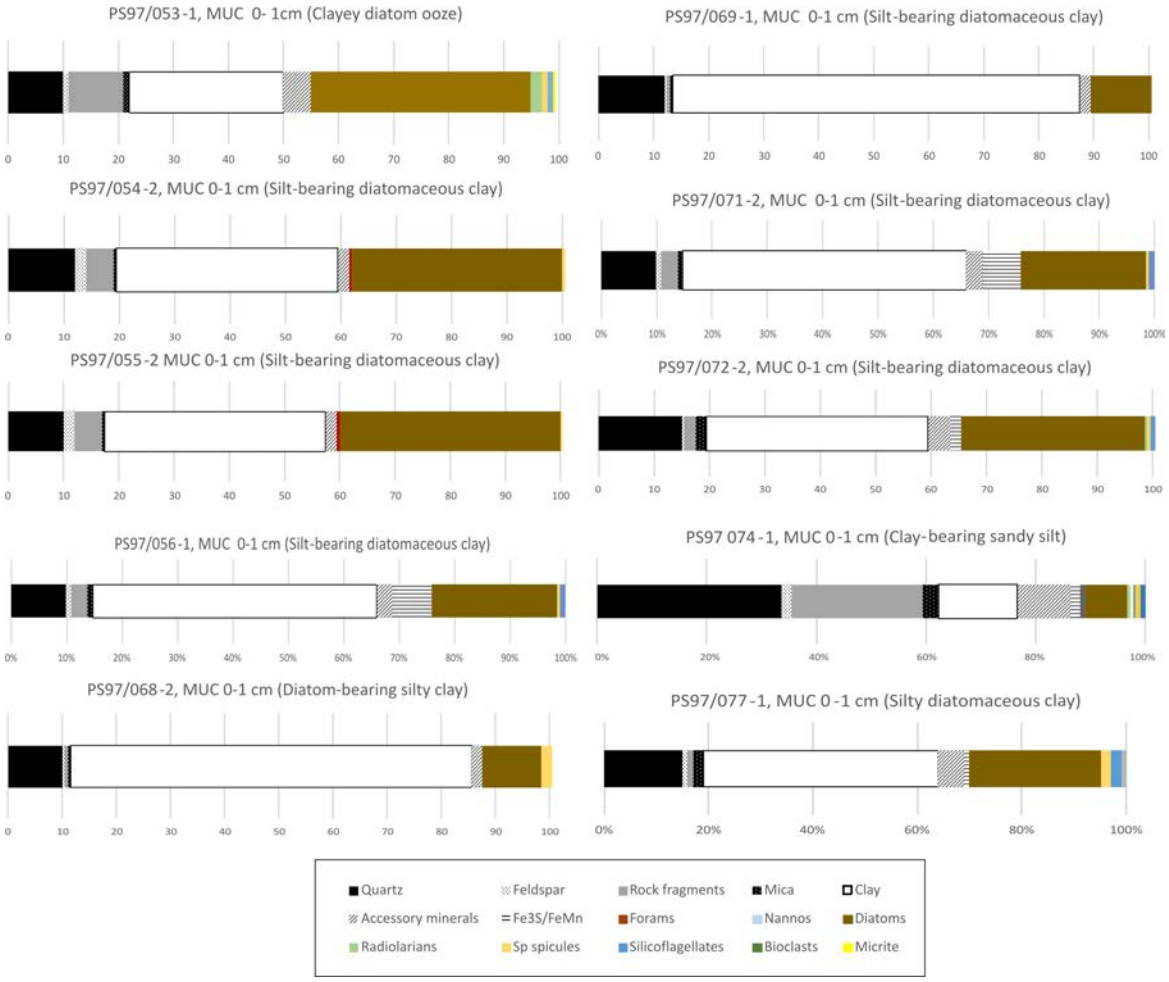

Fig. 3.5.27: Composition of fine fractions of surface sediments collected on the continental slope of the WAP, in the Bransfield Strait and the South Shetland Islands.

Coring

In total, 17 gravity cores and 2 piston cores were recovered in the Antarctic Peninsula working area. Aside from the two sediment cores retrieved along the continental slope of the WAP northwest of Elephant Island (stations PS97/077 and PS97/078), none of sediment cores obtained in the Bransfield Strait and the South Shetland Islands have been opened onboard. These cores will be opened, described and sampled for multidisciplinary investigations during a sampling party at the AWI laboratories.

Continental margin WAP

Cores PS97/052-4 (2890 m WD) and 053-2 (2016 m WD) from south of the SACCF are quite different from the cores to the north, as they are affected by downslope mass transport processes from the nearby Antarctic continental slope. The shallower core PS97/053-2 exhibits a succession of sediments, which is most likely recurring through time perhaps representing a glacial/interglacial sedimentation cycle. The depositional cycle begins with the rapid deposition of sandy silt (glacial), enriched with many dropstones, well-sorted gravel and sand layers and underlain by light brownish gray diatomaceous ooze (interglacial). The sand and gravel layers mostly have a sharp although uneven basal contact, grade upwards, and possibly represent rapid depositon by debris flows originating from the upper Antarctic continental slope. The glacial-type sediment changes upcore into a dark to moderately (deglacial?) dark silty clay partly rich in diatoms. Diagenetically altered stiff and greenish

horizons are typical for the uppermost centimetres of this sediment type. A rather thin light brownish gray diatom ooze completes the sedimentary cycle to above. The magnetic susceptibility record ranging between 500 and 1600 (Si * 105) nicely reflects the described lithological changes.

The short core PS97/052-4 entirely consists of moderately light brownish unsorted material of all grain sizes from clay up to large dropstones (-8 cm in diameter). The magnetic susceptibility values range from 300 to 800 (Si * 105) with highest values where dropstones are found. The deep location of this glacial till facies at 2890 m water depth implies that the moraine material was transported downslope over long distances. The term of „bulldozing“ best describes this process, by which the Antarctic glaciers push their moraines across the shelf far into the deep sea.

Further to the northeast close to where the Shackleton Fracture Zone intersects with the Antarctic continent, cores PS97/77-2 13.02 m length) and 078-1 (2.23 m length) were recovered from 3540 m and 3660 m water depth across the SW-NE trending continental slope. In contrast to the two cores described before, both cores exhibit largely undisturbed hemipelagic sediments. The upper parts of both cores consist of weakly bioturbated dark gray silty clay. Biogenic sediment components are rare. The dark colors and the H_2S odor imply high organic carbon contents at suboxic bottom water conditions. Dropstones are largely absent. Below this succession, the sediment coarsens to greenish to brownish clayey sandy silt, with abundant dropstones. The sedimentary sequence is condensed to ~2 m in core PS97/078-1, while expanded to ~13 m in the shallower core PS97/077-2. Stratigraphical information is not yet available for these cores.

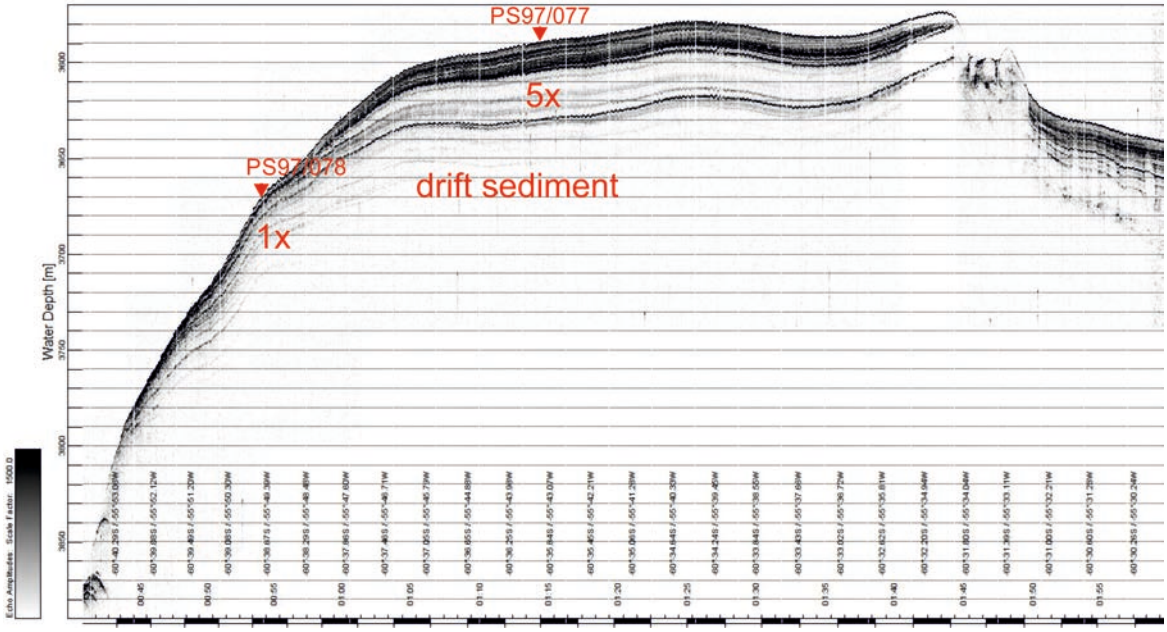

Fig. 3.5.28: PARASOUND profile on the Antarctic continental slope showing drift sediments at a water depth of around 3600 m with the two coring sites PS97/077 and PS97/078.

Bransfield Strait

The Bransfield Strait between the Antarctic Peninsula and the South Shetland Islands constitutes an ideal study area for the evaluation of biomarkers (e.g. highly branched isoprenoids) as potential sea surface temperature and sea ice proxies. The area experiences seasonal sea ice cover permitting high primary productivity in summer. Warm waters from the Bellingshausen Sea enter the Bransfield Strait from the west and are confined to the

northern part of the strait, while cold waters originating from the Weddell Sea dominate the southern part of the strait (Gordon & Nowlin 1978).

The surface sediments and gravity cores obtained along the NW-SE transect at stations PS97/054, PS97/055 and PS97/056 hence should reflect both warm- and cold-water dominated environments in the Bransfield Strait and provide a unique opportunity to identify shifts in the spatial extent of these water masses associated with past climate changes. Previous expeditions in the 1980s and 1990s successfully retrieved sediment cores from the central and northeastern Bransfield Strait that provided high-resolution records of Holocene sea ice variability (e.g. Barcena & Gersonde 1998; Barcena et al., 2002; Heroy et al., 2008). To obtain new sediment material, required for novel biomarker analyses, three gravity and one piston corer were deployed at these sites (PS97/068, PS97/069, PS97/073 and PS97/072) and successfully recovered long (up to 15.83 m) sediment cores. Preliminary magnetic susceptibility data of these cores indicate that they may not only cover the entire Holocene but even the late deglacial time interval (Fig. 3.5.29). Furthermore, smear slide analyses document high abundances and very good preservation of diatoms in Holocene sediments (diatom oozes) whereas lowest abundances and fragmented diatoms are observed for the deglacial interval characterized as silty clay with variable amounts of rock fragments (PS97/072).

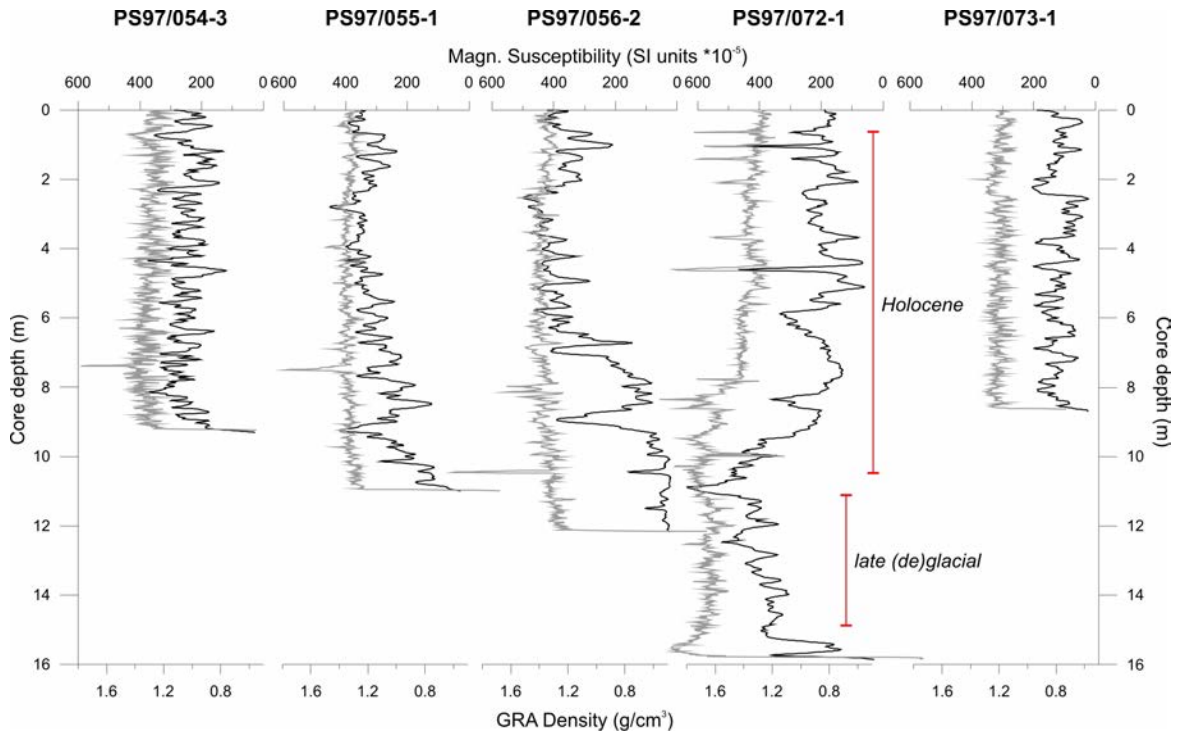

Fig. 3.5.29: Magnetic suseceptibility records from different cores recovered within the Bransfield Strait.

South Shetland Islands

The vertical sediment flux in Maxwell Bay (MB) is controlled by summer melting processes that cause sediment-laden meltwater plumes to form in the tributary fjords. These leave a characteristic signature in the sediments downstream, which can be used to distinguish summer and winter-dominated periods through the past two millennia (Hass et al., 2010). In the frame of this expedition, we investigated bays similar to MB further south of King George

Island (KGI) to improve the reconstruction of the climate of the past 2,000 years (and beyond) and its impact on delicate coastal systems.

Aerial photographs reveal mud plumes produced by tidewater glaciers in fjords such as Potter Cove (south KGI) and the straits between the islands south of KGI. These mud plumes appear to exit the bights along the bights' left coastlines (in flow direction), possibly as a result of the Coriolis force. The straits south of Maxwell Bay were investigated using HYDROSWEEP and PARASOUND to find sediment accumulations similar to those known from Maxwell Bay (Fig. 3.5.30).

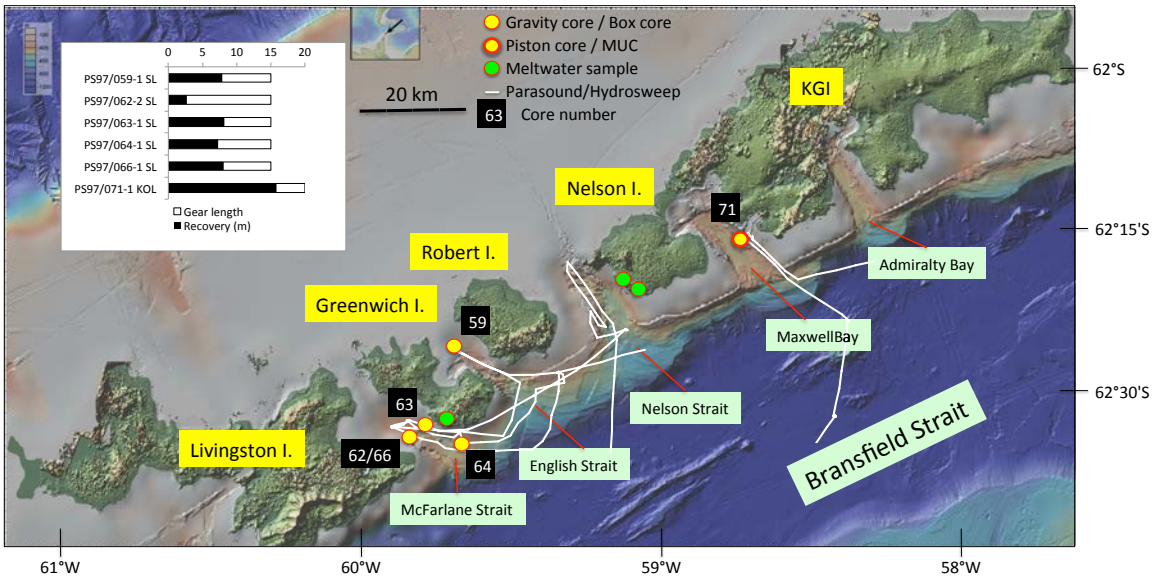

Fig. 3.5.30: South Shetland Islands. White lines mark PARASOUND and HYDROSWEEP transects, yellow/red dots mark core locations, and green dots mark locations where meltwater samples were collected.

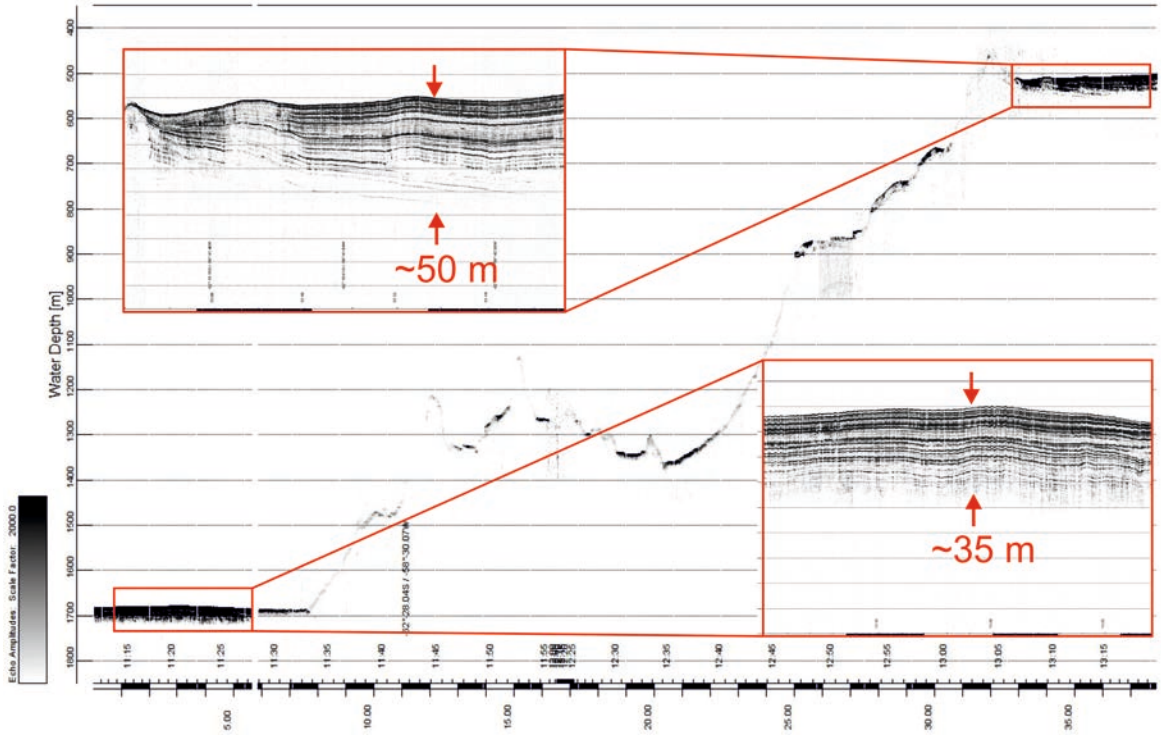

Fig. 3.5.31: PARASOUND transect from the center part of the Bransfield Strait to the shallow Maxwell Bay showing expanded Holocene sedimentary units.

Whereas Maxwell Bay shows thick, acoustically well-layered Holocene sediments (Fig. 3.5.31), the PARASOUND survey revealed less sediment cover in the Nelson, English and McFarlane straits most likely as a result of the smaller size of the surrounding Nelson, Robert, Greenwich and Livingston islands when compared to King George Island. During the survey, smaller sub-basins with acoustically well-stratified sediments were detected. Meltwater samples from three locations on land close to the glaciers of Greenwich and Nelson islands were sampled to gain information on the grain-size distribution of the suspended sediment as this can be traced in the sediment cores.

References

Asmus T, Frank M, Kaschmieder C, Frank N, Gersonde R, Kuhn G, Mangini A (1999) Variations of biogenic particle flux in the southern Atlantic section of the Subantarctic Zone during the late Quaternary: Evidence from sedimentary 231Paex and 230Thex. Marine Geology ,159 (1-4), 63-78.

Anderson RF, Ali S, Bradtmiller LI, Nielsen SHH, Fleisher MQ, Anderson B, Burckle LH (2009) Wind-Driven Upwelling in the Southern Ocean and the Deglacial Rise in Atmospheric CO2. Science, 323 (5920), 1443-1448.

Bamber JL, Alley RB, Joughin I (2007). Rapid response of modern day ice sheets to external forcing. Earth and Planetary Science Letters, 257, 1-13.

Barbara, L., Crosta, X., Schmidt, S., Massé, G. (2013). Diatoms and biomarkers evidence for major changes in sea ice conditions prior the instrumental period in Antarctic Peninsula. Quaternary Science Reviews 79, 99-110.

Barcena, M.A., Isla, E., Plaza, A., Floresa, J.A., Sierro, F. J., Masque, P., Sanchez-Cabeza, J.A., Palanques, A., 2002. Bioaccumulation record and paleoclimatic significance in the Western Bransfield Strait. The last 2000 years. Deep-Sea Research II 49, 935–950.

Barcena, M.A., Gersonde, R., Ledesma, S., Fabres, J., Calafat, A.M., Canals, M., Sierro, F.J., Flores, J.A., 1998. Record of Holocene glacial oscillations in the Bransfield Basin as revealed by siliceous microfossil assemblages. Antarctic Science 10 (3), 269–285.

Barker S, Diz P, Vautravers MJ, Pike J, Knorr G, Hall IR, Broecker WS (2009) Interhemispheric Atlantic seesaw response during the last deglaciation. Nature, 457 (7233), 1097-U1050.
Benz, V., Esper, O., Gersonde, R., Lamy, F., Tiedemann, R. (in press) Last Glacial Maximum sea surface temperature and sea-ice extent in the Pacific sector of the Southern Ocean. Quaternary Science Reviews.
Beal LM, De Ruijter WPM, Biastoch A, Zahn R, 136 SWIWG (2011) On the role of the Agulhas system in ocean circulation and climate. Nature, 472(7344), 429-436.
Best, A. I. & Gunn, D. E. (1999). Calibration of marine sediment core loggers for quantitative acoustic impedance studies. *Mar. Geol.* 160, 137-146
Caniupán M, Lamy F, Lange CB, Kaiser J, Arz HW, Kilian R, Baeza-Urrea O, Aracena C, Hebbeln D, Kissel C, Laj C, Mollenhauer G, Tiedemann R (2011). Millennial-scale sea surface temperature and Patagonian Ice Sheet changes off southernmost Chile (53°S) over the past ~60 kyr. Paleoceanography, 26, PA3221.
Chaigneau A, Pizarro O (2005) Surface circulation and fronts of the South Pacific Ocean, east of 120 degrees W. Geophysical Research Letters, 32, L08605, doi:08610.01029/02004GL022070.
Collins, L.G., Allen, C.S., Pike, J., Hodgson, D.A., Weckström, K., Massé, G. (2013) Evaluating highly branched isoprenoid (HBI) biomarkers as a novel Antarctic sea-ice proxy in deep ocean glacial age sediments. Quaternary Science Reviews 79, 87-98.
De Deckker P, Moros M, Perner K, Jansen E (2012) Influence of the tropics and southern westerlies on glacial interhemispheric asymmetry. Nature Geoscience, 5(4), 266-269.
Denton GH, Anderson RF, Toggweiler JR, Edwards RL, Schaefer JM, Putnam AE (2010) The Last Glacial Termination. Science, 328 (5986), 1652-1656.
Diekmann B, Kuhn G, Rachold V, Abelmann A, Brathauer U, Fütterer DK, Gersonde R, Grobe H (2000) Terrigenous sediment supply in the Scotia Sea (Southern Ocean): response to Late Quaternary ice dynamics in Patagonia and on the Antarctic Peninsula. Palaeogeography, Palaeoclimatology, Palaeoecology, 162, 357-387.
England MH, Godfrey JS, Hirst AC, Tomczak M (1993) The Mechanism for Antarctic Intermediate Water Renewal in a World Ocean Model. Journal of Physical Oceanography, 23, 1553-1560.
Euler C, Ninnemann US (2010) Climate and Antarctic Intermediate Water coupling during the late Holocene. Geology, 38(7), 647-650.
Garcia, H. E., R. A. Locarnini, T. P. Boyer, J. I. Antonov, O. K. Baranova, M. M. Zweng, and D. R. Johnson, 2010. World Ocean Atlas 2009, Volume 3: Dissolved Oxygen, Apparent Oxygen Utilization, and Oxygen Saturation. S. Levitus, Ed. NOAA Atlas NESDIS 70, U.S. Government Printing Office, Washington, D.C., 344 pp.
Garreaud RD (2007) Precipitation and circulation covariability in the extratropics. Journal of Climate, 20 (18), 4789-4797.
Gersonde R, Abelmann A, Brathauer U, Becquey S, Bianchi C, Cortese G, Grobe H, Kuhn G, Niebler H-S, Segl M, Sieger R, Zielinski U, Fütterer DK (2003) Last glacial sea surface temperatures and sea-ice extent in the Southern Ocean (Atlantic-Indian sector): A multiproxy approach. Paleoceanography, 18, doi:10.1029/2002PA000809.
Gersonde R, Crosta X, Abelmann A, Armand L (2005) Sea-surface temperature and sea ice distribution of the Southern Ocean at the EPILOG Last Glacial Maximum - a circum-Antarctic view based on siliceous microfossil records. Quaternary Science Reviews, 24 (7-9), 869-896.
Gille S (2002) Warming of the Southern Ocean Since the 1950s. Science, 295, 1275-1277.
Gersonde, R. (2011). The expedition of the research vessel "*Polarstern*" to the polar South Pacific in 2009/2010 (ANT-XXVI/2 - BIPOMAC), Berichte zur Polarforschung (Reports on Polar Research). Alfred Wegener Institute for Polar and Marine Research, Bremerhaven, p. 330.
Goodell, H.G. (1965). The Marine Geology of the Southern Ocean: 1. Pacific-Antarctic and Scotia basins, Marine Geology USNS Eltanin cruises 9-15. Contribution 11 Sedimentology Research Laboratory, Department of Geology, Florida State University.
Gordon, A.L. (1986) Interocean exchange of thermocline water. Journal of Geophysical Research, 91, 5037-5046.
Gordon, A.L. & Nowlin, W.D., 1978. The basin waters of the Bransfield Strait. Journal of Physical Oceanography, 8, 258-264
Gunn, D. E. & Best, A. I. (1998). A new automated non destructive system for high resolution multi-sensor core logging of open sediment cores. *Geo-Marine Letters* 18, 70-77.
Hanawa K, Talley LD (2001) Mode Waters, in Ocean circulation and climate. Edited by Siedler G, Church J, Gould J, Academic Press, London, 715 pp.

Hass H C, Kuh, G, Monien P, Brumsack H-J, Forwick M (2010). Climate fluctuations during the past two millennia as recorded in sediments from Maxwell Bay, South Shetland Islands, West Antarctica. Geological Society, London, Special Publications 344, 243-260.
Herb, R. (1968) Recent planktonic Foraminifera from sediments of the Drake Passage, Southern Ocean. Eclogae Geol. Helv., 61 ,467–480
Heroy, D.C., Sjunneskog, C., Anderson, J.B., 2008. Holocene climate change in the Bransfield Basin, Antarctic Peninsula: evidence from sediment and diatom analysis. Antarctic Science 20 (1), 69–87.
Kaiser J, Lamy F, Hebbeln D (2005) A 70-kyr sea surface temperature record off southern Chile (ODP Site 1233). Paleoceanography, 20, PA4009, doi:10.1029/2005PA001146.
Kissel et al., 2007. Cruise report “Pachiderme” MD159, Punta Arenas-Punta Arenas, Insititute Polaire Francaise.
Knorr G, Lohmann G (2003) Southern Ocean origin for the resumption of Atlantic thermohaline circulation during deglaciation. Nature, 424 (6948), 532-536.
Knorr G, Lohmann G (2007) Rapid transitions in the Atlantic thermohaline circulation triggered by global warming and meltwater during the last deglaciation. Geochemistry, Geophysics, Geosystems, 8, Q12006.
Lamy F, Hebbeln D, Wefer G (1999) High-resolution marine record of climatic change in mid- latitude Chile during the last 28,000 years based on terrigenous sediment parameters. Quaternary Research, 51 (1), 83-93.
Lamy F, Kaiser J, Ninnemann U, Hebbeln D, Arz H, Stoner J (2004) Antarctic Timing of Surface Water Changes off Chile and Patagonian Ice Sheet Response. Science, 304, 1959-1962.
Lamy F, Kaiser J, Arz HW, Hebbeln D, Ninnemann U, Timm O, Timmermann A, Toggweiler JR (2007) Modulation of the bipolar seesaw in the southeast pacific during Termination 1. Earth and Planetary Science Letters, 259 (3-4), 400-413.
Lamy, F., Arz, H.W., Kilian, R., Lange, C.B., Lembke-Jene, L., Kaiser, J., Beaza-Urrea, O., Hall, I., Harada, N., Tiedemann, R. (2015). Glacial reduction and millennial-scale variations in Drake Passage throughflow. Proceedings of the National Science Academy.
Lisiecki, L.E., Raymo, M.E., 2005. A Pliocene-Pleistocene stack of 57 globally distributed benthic delta O-18 records. Paleoceanography 20.
Lorrey AM, Vandergoes M, Almond P, Renwick J, Stephens T, Bostock H, Mackintosh A, Newnham R, Williams PW, Ackerley D, Neil H, Fowler AM (2012) Palaeocirculation across New Zealand during the last glacial maximum at similar to 21 ka. Quaternary Science Reviews, 36, 189-213.
Marshall J, Speer K (2012) Closure of the meridional overturning circulation through Southern Ocean upwelling. Nature Geoscience, 5(3), 171-180.
Mazzullo, J.M., Meyer, A., and Kidd, R.B., 1988. New sediment classification scheme for the Ocean Drilling Program. In: Mazzullo, J., and Graham, A.G. (Eds.), Handbook for Shipboard Sedimentologists. ODP Tech. Note, 8:45–67.
McCave, I.N., Crowhurst, S.J., Kuhn, G., Hillenbrand, C.D., and Meredith, M.P., 2014. Minimal change in Antarctic Circumpolar Current flow speed between the last glacial and Holocene. Nature Geoscience, 7, 113-116, doi: 10.1038/ngeo2037
Monien P, Schnetger B, Brumsack H-J, Hass HC, Kuhn G (2011). A geochemical record of late Holocene palaeoenvironmental changes at King George Island (maritime Antarctica). Antarctic Science, 23, 255-267.
Moreno PI, Lowell TV, Jacobson GL, Denton GH (1999) Abrupt vegetation and climate changes during the last glacial maximum and last termination in the Chilean Lake District: A case study from Canal de la Puntilla (41 degrees S). Geografiska Annaler: Series A, Physical Geography, 81A (2), 285-311.
Müller, J., Wagner, A., Fahl, K., Stein, R., Prange, M., Lohmann, G., 2011. Towards quantitative sea ice reconstructions in the northern North Atlantic: A combined biomarker and numerical modelling approach. Earth Planet Science Letters 306, 137-148.
Orsi AH, Whitworth T, Nowlin WD (1995) On the meridional extent and fronts of the Antarctic Circumpolar Current. Deep-Sea Research Part I, 42 (5), 641-673.
Piola AR, Georgi DT (1982) Circumpolar properties of Antarctic Intermediate Water and Subantarctic Mode Water. Deep Sea Research, 29, 687-711.
Polonia A, Torelli L, Brancolini G, Loreto MF (2007). Tectonic accretion versus erosion along the southern Chile trench: Oblique subduction and margin segmentation. Tectonics, 26(3).
Rincón-Martínez D, Lamy F, Contreras S, Leduc G, Bard E, Saukel C, Blanz T, Mackensen A, Tiedemann R (2010) More humid interglacials in Ecuador during the past 500 kyr linked to latitudinal shifts of the Equatorial Front and the Intertropical Convergence Zone in the eastern tropical Pacific. Paleoceanography, 25, PA2210.

Rojas M, Moreno P, Kageyama M, Crucifix M, Hewitt C, Abe-Ouchi A, Ohgaito R, Brady E C, Hope P (2009) The Southern Westerlies during the last glacial maximum in PMIP2 simulations. Climate Dynamics, 32 (4), 525-548.

Russell JL, Dixon KW, Gnanadesikan A, Stouffer RJ, Toggweiler JR (2006). The Southern Hemisphere westerlies in a warming world: Propping open the door to the deep ocean. Journal of Climate, 19(24), 6382-6390.

Schneider W, Fuenzalida R, Rodriguez-Rubio E, Garces-Vargas J, Bravo L (2003) Characteristics and formation of eastern South Pacific intermediate water. Geophysical Research Letters, 30 (11), 1581, doi:1510.1029/2003GL017086.

Strub PT, Mesias JM, Montecino V, Ruttlant J, Salinas S (1998) Coastal ocean circulation off Western South America. In: A. R. Robinson and K. H. Brink (Eds.), The global coastal ocean. Regional studies and syntheses, pp. 273-315. Wiley, New York.

Stuut J-BW, Lamy F (2004) Climate variability at the southern boundaries of the Namib (southwestern Africa) and Atacama (northern Chile) coastal deserts during the last 120,000 yr. Quaternary Research, 62 (3), 301-309.

Toggweiler JR, Rusell JL, Carson SR (2006) Midlatitude westerlies, atmospheric CO2, and climate change during ice ages. Paleoceanography, 21, doi:10.1029/2005PA001154.

Vaughan D G, Marshall G J, Connolley W M, King J C, Mulvaney R (2001) Devil in the detail. Science, 293, 1777-1779.

Verleye T, Louwye S (2010) Late Quaternary environmental changes and latitudinal shifts of the Antarctic Circumpolar Current as recorded by dinoflagellate cyst from offshore Chile (41°S). Quaternary Science Reviews, 29, 1025-1039.

Walter HJ, Hegner E, Diekmann B, Kuhn G, Rutgers van der loeff MM (2000) Provenance and transport of terrigenous sediment in the South Atlantik Ocean and their relations to glacial and interglacial cycles: Nd and Sr isotope evidence. Geochimica et Cosmochimica Acta, 64 (22), 3813-3827.

Well R, Roether W, Stevens DP (2003) An additional deep-water mass in Drake Passage as revealed by ^{3}He data. Deep-Sea Research, 50, 1079-1098.

Wentworth, C.K., 1922. A scale of grade and class terms of clastic sediments. J. Geol., 30, 377–392.

Zielinski, U., Gersonde, R., 2002. Plio-Pleistocene biostratigraphy from ODP Leg 177, Atlantic Sector of the Southern Ocean. Marine Micropaleontology 45, 225-268.

Zielinski, U., Bianchi, C., Gersonde, R., Kunz-Pirrung, M., 2002. Last occurrence datums of the diatoms Rouxia leventerae and Rouxia constricta: indicators for marine isotope stages 6 and 8 in Southern Ocean sediments. Marine Micropaleontology 45, 127-137.

4. GEOSCIENTIFIC WORK ON LAND

4. 1. Paleoenvironmental records from Chilean islands

Rolf Kilian[1], Frank Lamy[2], Helge W. Arz[3], Marcelo Arevalo[4], Alessa Geiger[5], Sascha Plewe[3], Mark Wengler[2]

[1]U. Trier,
[2]AWI,
[3]IOW,
[4]Punta Arenas,
[5]U. Glasgow

Background and objectives

In most off-shore marine sediment cores recovered during Expedition PS97 the Holocene period is represented by just 30 to 50 cm core depth and thus provides a limited time resolution. Furthermore, perturbations of such surface sediments are very common due to its often very soft composition. Lake and fjord sediment records from the Chilean cost include in general 5-10 m of Holocene sediments providing a much better time resolution. This was one of the reasons to obtain complementary high resolution sediment records for the Holocene and Late Glacial from lakes on islands situated next the open Pacific Ocean (Fig. 4.1.1). Such records can depict further important information concerning Holocene changes in the position and intensity of the southern westerly wind belt (SWW which have been controversially discussed (Lamy et al. 2010; Kilian & Lamy, 2012;). Despite commonly applied sedimentological, biological, and geochemical proxies, the islands are well suited for investigating new proxies such as changes sea spray-related halogens in organic matter and or salinity sensitive diatom assemblages. Such sea spray proxies potentially provide direct indicators for changes of westerly wind intensities.

Sites of previously investigated lake sediment records from the Magallanes region are shown in Fig. 4.1.1. In most of these sediment records the transition of organic-rich sediments to organic-free glacial clay deposits have been dated (e.g. Kilian et al. 2007, Francois 2015, Breuer et al. 2013) and thus they document the time when glacier tongues have been in close vicinity. For the western cost of the southernmost South American continental margin, the maximum westward extend of the Patagonian Ice field as well as the timing of its retreat phase are poorly explored. The red numbers in Fig. 4.1.1 indicate minimum ages for the late glacial ice retreat deduced from fjord and lake sediment records. The sediment records of the investigated islands from the outermost western shelf area have the potential to document the westward extend of the ice sheet and how far these island could have provided partially ice-free ecological refugees during the last glacial.

Work at sea

Within the former scientific context it was the aim to reach selected island (Islands Recalada, Noir, and Hornos shown in the insets of Fig. 4.1.1) by helicopter during the PS97 cruise including an equipment to obtain 4-10 m long lake sediment cores. The Islands Recalada, Noir and Hornos have been selected for lake drilling since they are situated nearest to the westernmost margin of the shelf and next to the open Pacific Ocean. To avoid the influence of a possible marine transgression during more elevated cost lines in the past, the selected lakes were at more than 100 m a.s.l. Morphological criteria from aerial photographs were used to select lakes with a high ratio between depth and surface area. The reason was that wind-induced rework of the sediments by bottom currents within the lakes should be absent as well as preferentially anoxic conditions to prevent bioturbation. Furthermore, the accessibility and possible landing places for the helicopter have been considered.

Groups of 4-5 scientists and technicians have been transported by helicopter to the lakes together with equipment to stay autonomously for 2-3 days. On the lake, two rubber boats were fixed together and a 3.4 m high tripod was installed to carry the piston coring equipment

from UWITEC (www.uwitec.at) with a principal 5 m long steel tube which could be closed by the piston. During this time, work with *Polarstern* continued within the reach of the helicopter.

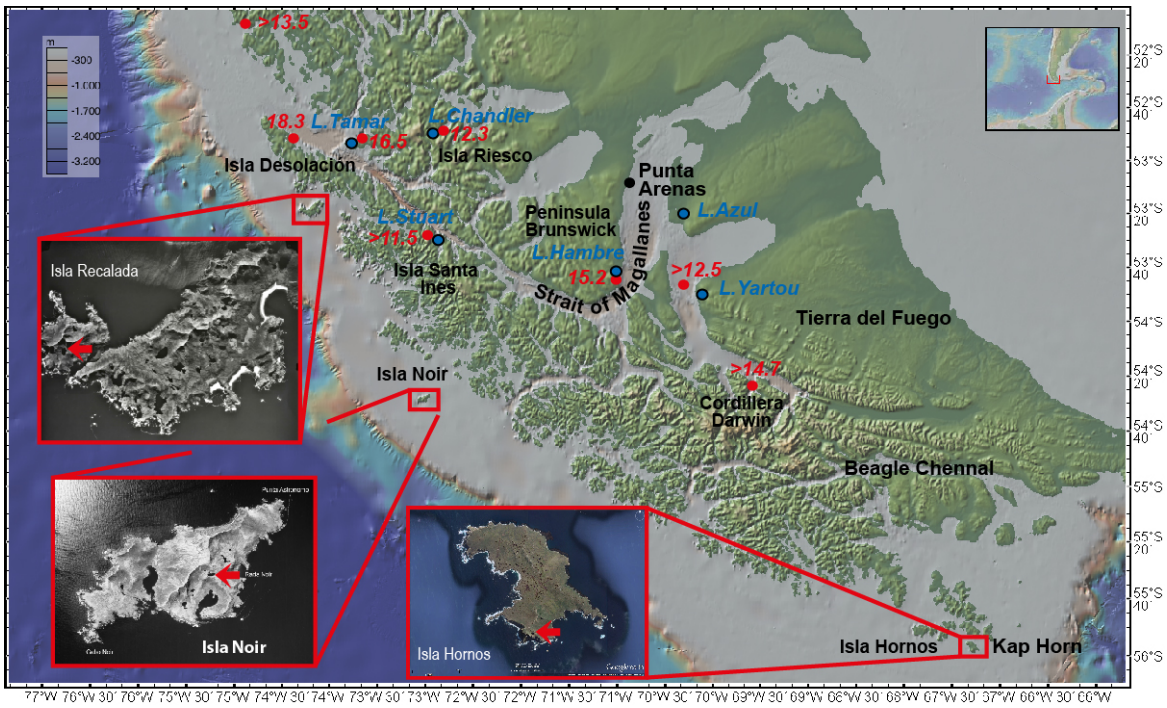

Fig. 4.1.1: The Southern tip of South America with insets for the investigated lakes on the Island Hornos and Noir and the planned site on Isla Recalada which could not be realized due to bad weather conditions. Previously investigated more easterly lake sites (Lake Azul, Chandler, Hambre, Stuart, Tamar and Yartou: Breuer et al. 2013, Kilian et al. 2007, Francois 2015) are also shown. Red dots and numbers indicate minimum ages for the Late Glacial glacier retreat based on fjord and lake sediment records (e.g. Kilian & Lamy 2012).

Isla Noir (position 1 and 2)

On Isla Noir an elongated nameless lake with 95 x 285 m surface extension at 180 m a.s.l. (54°28.505' S; 72°59.934' W) was selected (red arrow in Fig. 4.1.1 and Fig. 4.1.2). The lake has a catchment of ~1.5 km^2 and is mainly covered by 3-8 m thick peaty soils. Its northern sector with steeper slopes includes a *Nothofagus Antarctica*-dominated forest. Very small tributaries enter the lake without cutting down to the basement rocks. Basement rocks consist of a fine-grained tonalite (sample MZ 16-07 se Chapter 4.3.) and are exposed on an erosional terrace, which has been formed around the lake near to the present lake level. The deepest part of the lake has up to 7.6 m water depths. The first drilling site (KL-1) is located at the deepest lake sector, which is nearly in the middle of the lake (Fig. 4.1.2). At this location, a 55 cm long gravity core was obtained. Than a piston core was drilled into the sediment, starting a 30 cm sediment depth to get an overlapping of 25 cm with the very soft sediments recovered by the gravity core (see sediment core list below). However, the piston core was penetrated until reaching the basement of gravel and bedrock at around 94 cm corrected core depth. Thus a second drilling site (KL-2) was selected about 80 m further to the west where the water depth was 6.5 m (Fig. 4.1.2). Here the piston core reached again the basement at a corrected core depth of 2.4 m.

Tab. 4.1.1: Sediment cores from Isla Noir with core sections and corrected depths.

Sediment core		***Corrected depth***
PS97/NO-Grav-1	*0-55 cm*	0-55
PS97/NO-Grav-2	*0-56 cm*	0-56
PS97/ NO KL-1	*0-64 cm*	30-94
PS97/ NO KL-2	*0-100 cm*	40-140
PS97/ NO KL-2	*100-200 cm*	140-240
PS97/ NO-Peat 1	*0-50 cm*	0-50
PS97/ NO Peat 2	*0-71 cm*	0-71

Fig. 4.1.2: The investigated nameless lake on the Noir Island with the drilling platform in the foreground. The lake position on the island is marked by a red arrow in Fig. 4.1.1. The upper left image shows the positons of the two drilling sites (KL-1 and KL-2). Insets document the drilling operation (upper right foto) and the camp during the three-day work (Photos from M. Arevalo (AWI) and S. Plewe (IOW)).

Isla Hornos

The selected nameless lake on Isla Hornos is situated on the southwestern side of the island (55°58.535' S and 67°16.999' W) at 156 m a.s.l. (Figs. 4.1.1 and 4.1.3). The lake has N-S extension of 107 m and a W-E extension of 120 m. Its western and northern side is formed by a steep glacial kar next to the highest mountain of the island (315 m a.s.l.). The lake´s shores are completely covered by dense peat with a thickness of at least a few meters. Rocky outcrops from the steepest hill slopes consist of a fined-grained tonalite (sampled; see Chapter 4.3). No erratic blocks were visible in the catchment. If there have been some, they could have been overgrown by peat. Despite the pronounced morphology there are no tributaries cutting until basement rocks. The southern rims of the lake are formed by a moraine that contains meter-sized blocks. The catchment has an area of ~0.6 km^2. The deepest sector was found in the middle of the lake with a water depth up to 10.7 m. The lake

has no superficial outflow and the lowest lakeshores are 25 m higher than the present lake level. There are several subsoil drainage systems, which are formed within the moraine. Older outflow systems were detected about 15 m above the present lake level, which led to the formation of an erosional terrace which is smoothed by overgrowing of peat. This suggests significantly higher water levels (>25 m water depths), probably during the Holocene.

Fig. 4.1.3: The investigated nameless lake on the southeastern tip of the Hornos Island. The drilling site is marked in red. Insets document the transport of the equipment with a helicopter from RV Polarstern (Fotos from R. Kilian (U Trier) and S. Plewe (IOW)).

March 22, 2016 the drilling platform was fixed in the middle of the lake where we recovered a 54 cm long gravity core. Due to the soft gyttja composition of the surface sediments we opened the piston core after penetrating 35 cm, in order to obtain an overlap of 20 cm with the gravity core. The 5 m long piston corer was penetrated 470 cm into the sediment where a further penetration was hampered by very coarse gravel. Due to the gravel in the lowermost sediment sequence the coarse clastic detritus was lost so that we calculate a total recovery of 402 cm (Table 4.1.2). Due to a very restricted time schedule and very bad weather forecasts, we were not able to do further drilling operations.

Tab. 4.1.2: Sediment cores from Isla Noir with core sections and corrected depths.

Sediment core		Corrected depth
PS97/IH-Grav-1	*0-15 cm*	0-15
PS97/ IH-Grav-2	*0-54 cm*	0-54
PS97/IH-Kl-1	*0-100 cm*	35-132
PS97/IH-Kl-1	*100-200 cm*	132-232
PS97/IH-Kl-1	*200-302 cm*	232-334
PS97/IH-Kl-1	*302-372 cm*	334-402

Preliminary and expected results

The Lake Hornos site is strongly exposed to far distance as well as local sea spray that is formed along the rocky cliffs of the nearby coast. This influence is also documented by unusual high pH values of up to 7 of the lake water. Lakes that are more protected from sea spray have much lower pH values of 4 to 6. The 402 cm long Lake Hornos sediment core is very rich in organic matter (gyttja) and includes >30 wt. % of terrestrial organic components as well as up to 10 wt.% of aquatic organic matter. A few wt. % of siliciclastic components were also found in this sediment (Table 4.1.3). They may have been introduced during wind and wave-related erosion along the lakeshore lines during storm events. Smear slides show significant amount of diatoms (5 – 15 vol. %). The diatom assemblages are characterized by changes along the sediment core and they are likely to be sensitive to the distinct amount of sea spray. C/N ratios are likely to document rain-related changes in the amount of allochthonous versus autochthonous organic matter. Organic components may also represent good proxies for trace element and isotopic characteristics.

The sediment cores from the Lake Noir site have similar organic-rich compositions as that of Islas Hornos. Again diatoms represent an important micro-paleontological sediment component. Some siliciclastic components including quartz and feldspar are derived from the abrasional terraces along the lakeshore and can be used a proxy for stronger wind and storm action. Other potential proxies are similar as described for the Isla Hornos sediment core.
Pyrite was present in both sediment cores indicating anoxic conditions at least within the sediment core. However, since the drilling sites of both lakes are not very deep we expect a significant decomposition of organic matter. We can also not exclude that wind induced currents have caused some sediment rework on the lake floor. Possible laminations can be first seen after the opening of the sediment core that will be done together with a high resolution core logging (magnetic susceptibility and XRF scanning) at the IOW in collaboration with Helge Arz and Frank Lamy. Glacial clay was not detected at the transition to the underlying basement. Age constrains are difficult to make before the planned ^{14}C dating. However, comparable sediment cores from such very small catchments and with little contribution of siliciclastic components and decomposition of organic matter are consistent with records up to > 20 ka.

Tab. 4.1.3: Composition of the Lake Hornos IH-KL-1 sediment core deduced from smear slides.

Components	**IH 0 cm**	**IH 100 cm**	**IH 200 cm**	**IH 300 cm**	**IH 400 cm**
Organic matter	Abundant	Abundant	Abundant	Abundant	Abundant
Pyrite	Common	Common	Common	Common	Common
"tiny black dots"	Abundant	Abundant	Abundant	Abundant	Abundant
Accessory minerals	Rare	Common	Common	Common	Frequent
Diatoms	**7 vol. %**	**15 vol. %**	**8 vol. %**	**5 vol. %**	**7 vol. %**
Discotella (Cyclotella) stelligera	Abundant	Abundant	Abundant	Abundant	Abundant
Surirella	Present	Common	Present	Present	Common
Navicula	Present	Present	Present	Present	Present
Diploneis subovalis	Present	Present	Present	Present	Present
Achnanthes	Present	Present	Present	Present	Present
Pinnularia	Present	Present	Present	Present	Present
Amphora	Present	Present	Present	Present	Present
Cocconeis	Present	Present	Present	Present	Present

Data management

All data will be uploaded to the PANGAEA database. Unrestricted access to the data will be granted after about three years, pending analysis and publication.

4. 2. PATAGONIAN ICE SHEET DYNAMICS

Alessa Geiger[1], Frank Lamy[2], Rolf Kilian[3], Helge W. Arz[4]

[1]U. Glasgow,
[2]AWI,
[3]U. Trier,
[4]IOW,

Objectives

During most of the last glacial cycle (11.7-115 kyrs) the Patagonian Ice Sheet stretched ca. 2000 kilometres along the Patagonian Andes (38-56°S), recorded by an extensive network of glacial moraines east of the Andean divide. Incidentally the majority of studies providing geochronological constraints of glacier extent are located here, due to the favourable preservation potential of glacial landforms and relative ease of access (Fig. 4.2.1). At only two sites west of the Andean divide are constraints of glacier extent available (Fig. 4.2.1).

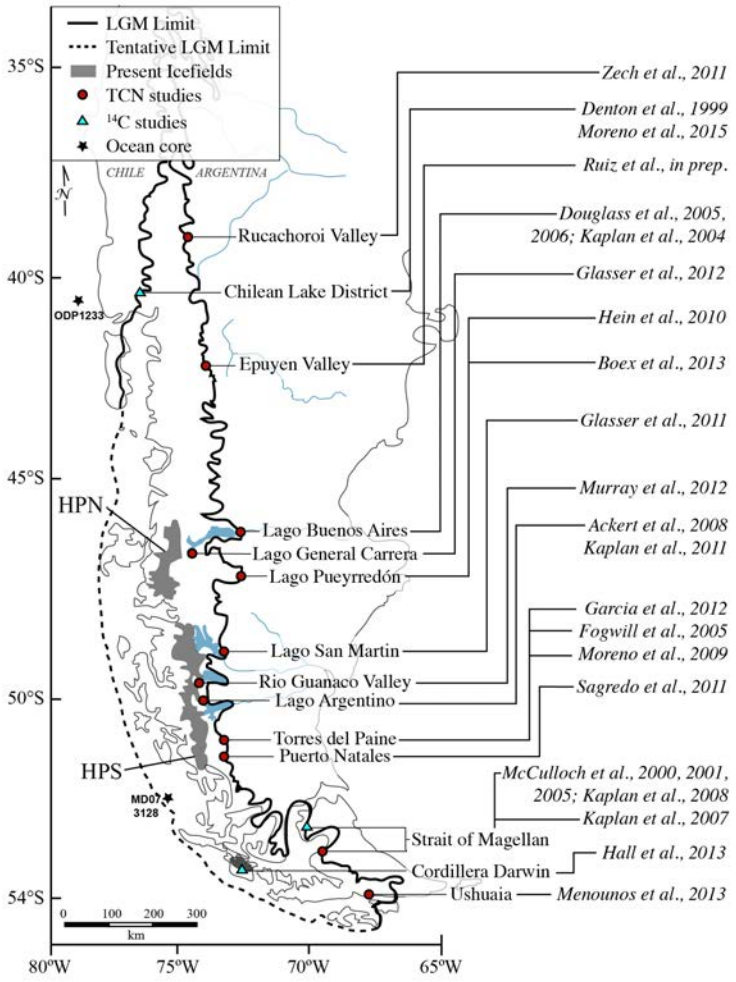

Fig. 4.2.1: Compilation of geochronological studies utilizing terrestrial cosmogenic nuclide (TCN) and radiocarbon dating to constrain Patagonian Ice Sheet extent/thickness. Note stippled western Ice Sheet margin indicative of tentative glacier extent. Adapted from Geiger (2015).

Though numerical modelling exercises have been utilized to understand Patagonian Ice Sheet dimensions and dynamics from the Last Glacial Maximum (LGM: 19-26 kyrs; Hulton et al. 2002) empirical data of ice thickness, extent and rate of recession from the western portions of the Patagonian Ice Sheet are lacking between 43-54°S. This substantially hinders our understanding of Patagonian Ice Sheet dynamics toward the west, broader internal glaciological feedbacks as well as the interaction between the Patagonian Ice Sheet and the regional to global climatic forcings during the late Quaternary.

Frontal moraines produced by the Patagonian Ice Sheet in and west of the west fjords of Chile are presently below sea-level making access problematic and establishing dating control of glacier extent difficult. In addition, dense forest cover precludes reliable remote mapping of the geomorphology marking glacier extent and dynamics on land. To address these issues, this work focuses on obtaining geochronological control of Patagonian Ice Sheet dimensions in the western fjords of Chile between 52-55°S (Fig. 4.2.2). In-situ produced terrestrial cosmogenic nuclide dating of bedrock and erratic boulders abandoned by the disintegrating Patagonian Ice Sheet is utilized. Vertical transects are built, where possible, to provide constraints of ice-thickness and palaeo-ice surface elevations. In addition, deposits marking glacier extent toward west are sampled for surface exposure dating. Exposure ages will be used to reconstruct former ice surface elevations and glacier extent. Together with the local glacial geomorphology and insights from lake and fjord sediment cores from the coastal area (Section 4.1) light will be shed onto the regional palaeo-glaciology and climate dynamics of southern South America during the last glacial.

Work on land

The *Polarstern* helicopters were used to access land sample sites in the southern west fjords of Chile between 52-55°S, 67-74°W (Fig. 4.2.2). Weather conditions along the southern west fjords of Chile, were highly variable and mostly poor during the expedition (see Section 2). Short good weather windows were exploited to obtain samples with limited time for detailed geomorphic mapping of glacial deposits. Surficial bedrock and erratic boulder samples were collected for surface exposure dating along a vertical mountain transect on Isla Londonderry & Narborough and from a glacial deposit on Isla Hornos & Desolacion (Fig. 4.2.2).

Promising sample sites were pre-selected via remote sensing, mainly based on the whale-back morphology of the bedrock and suitability for helicopter landing. Individual erratic boulders could not be identified from the imagery; hence actual sample site verification and selection occurred in the field from the helicopter with individual rock samples selected following local reconnaissance. Sampling in the field occurred by A. Geiger supported by M. Zundel. In most cases quartz-rich rock samples were obtained in order to utilize in-situ produced cosmogenic 10Be, 26Al and 14C dating (Table 4.2.1; Briner et al. 2014). A number of volcanic erratics were collected which are suitable for cosmogenic 36Cl and/or 3He dating (see Table 4.2.1). Bedrock-erratic pairs were collected at each elevational increment (limited by suitable sample availability). The vertical difference between bedrock-erratic sample pairs is a minimum of ca. 100 meters (Table 4.2.1, see Isla Londonderry & Narborough). This methodological approach has been utilized successfully in other formerly glaciated terrain to reconstruct vertical ice mass loss (e.g. Lilly et al. 2010). The upper five centimetres of the samples' rock surface, perpendicular to incoming secondary cosmic ray trajectories were sampled, obtaining up to a maximum of 1 kg per sample. A battery driven circular handsaw, chisel and hammer were used to obtain the surface samples (Fig. 4.2.4A).

Each sample was stored in a labelled fabric bag to avoid cross-contamination. Field data and observations relevant for exposure age calculations were noted in the field book (Table 4.2.1). A hand-held GARMIN 60 PS GPS was used to obtain geographical coordinate and altitude information (with accuracy of ±5 meters). Topographic shielding information of the sample sites was established using a compass and clinometer (time permitting), observations of differential weathering patterns were noted for both bedrock and erratic boulders. The overall geomorphological context of the sample sites and their surrounding were noted to aid in further interpretations. Photographs of the samples, sample sites and broader context were taken for reference (Figs. 4.2.3 and 4.2.4). Following each sampling day, the data collected was digitised and backed up.

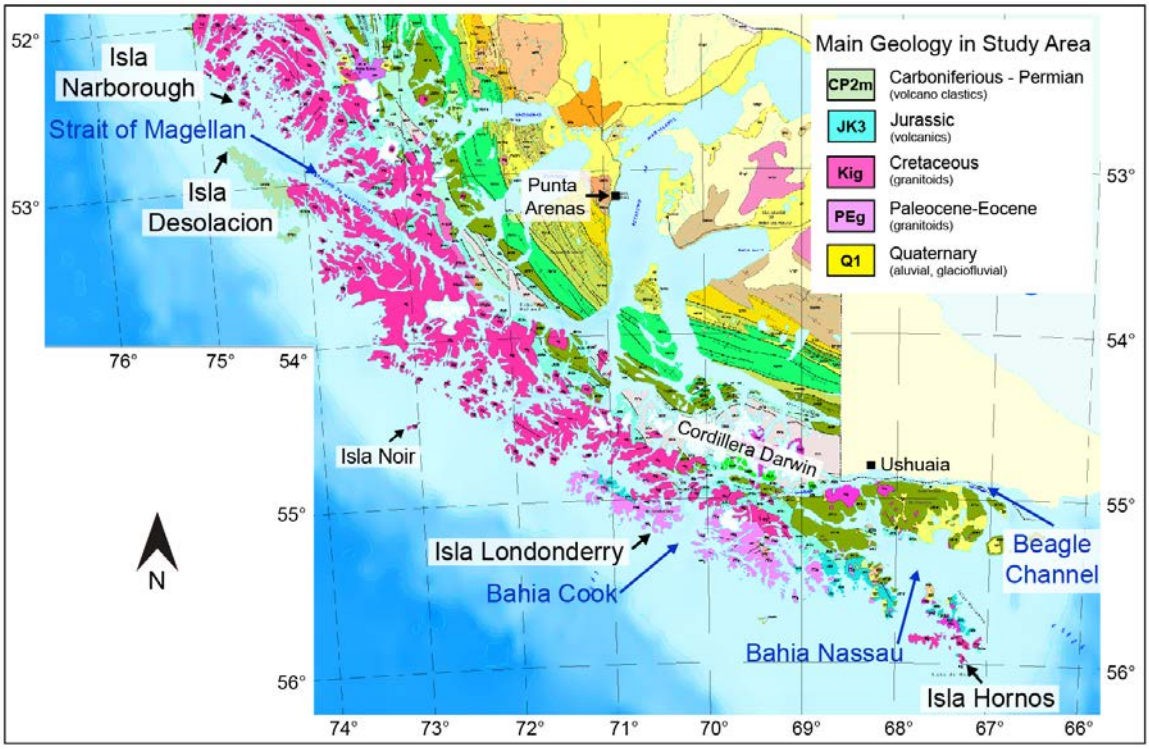

Fig. 4.2.2: Geological map of southern South America, from Sernageomin (2003). Islas Narborough, Desolacion, Londonderry and Hornos were sampled for exposure dating. At all sites except at Isla Desolacion, the bedrock is composed of quartz-rich granitoids (see Table 4.2.1). From Isla Hornos & Noir, lake cores were obtained for palaeoclimatic reconstructions (see Section 4.1), whilst all areas sampled for exposure dating and Isla Noir were also sampled for thermochronology (see Section 4.3).

Southern South America

The research area is located in south-west Chile (Fig. 4.2.2). Due to the weather conditions *Polarstern* could not exit the Magellan Strait via the Pacifc as originally planed, hence the research area could not be investigated as thoroughly as we would have liked. In addition poor weather conditions during our return track along the western Chilean margin meant a limited number of field days were available. The total amount of time spent in the field was 12 hours during which 16 samples were collected.

Isla Narborough

A vertical sample profile was established at Isla Narborough (Fig. 4.2.2). Two erratic and one bedrock sample were collected at ca. 400 m.a.s.l. and one bedrock sample at 10 m.a.s.l. (Tabel 4.2.1). Stream lined bedrock occurs from sea level to the summit of Isla Narborough with a-axis orientation from SE-NW (Fig. 4.2.3A). The bedrock on the summit shows clear

signs of mechanical and chemical weathering (Fig. 4.2.3B-C). It was difficult to identify erratic boulders on the summit, as most of the material transported and deposited here is of relatively local origin, with the same or similar geology (Fig. 4.2.2). An ice moulded bedrock sample collected at 10 m.a.s.l. is located close to a glacial till deposit which is interpreted as a ground moraine. The ground moraine is located at sea level and consists of a mixture of sub-rounded to bullet shaped boulders of different lithologies (Fig. 4.2.3D). As it is located at sea level, tide and storm action has had a significant influence on the deposit, hence it was not sampled for cosmogenic surface exposure dating due to post-depositional disturbances associated with marine activity. Along the flanks of Isla Narborough no signs of glacier still stand in the form of lateral or frontal moraines were observed, suggesting continuous glacier retreat from this location.

Fig. 4.2.3: Selection of sample locations and samples. A) View toward south from Isla Narborough summit at ca. 400 m.a.s.l. with streamlined bedrock visible toward south. B-C) Summit bedrock

sample WF1614 at Narborough showing mechanical & chemical weathering. D) Ground moraine deposit close to bedrock sample WF1616 on Narborough. E) Surface morphology and structure of bedrock at Isla Desolacion where WF1617 was collected. F) Erratic WF1619 among weathered bedrock. G) View from bedrock sample WF1617 toward SE with later-frontal moraine and streamlined bedrock in the distance.

Isla Desolacion

Three samples (1x bedrock, 2 erratics) were collected on the north-western most part of Isla Desolacion at ca. 80 m.a.s.l. (Table 4.2.1). The bedrock is a gneiss containing quartz veins of ca. 0.1-3 centimetres in thickness (Fig. 4.2.3E). The bedrock still shows some signs of glacial erosion with an overall ice-moulded morphology with the a-axis aligned SE-NW. Present weathering action has led to disintegration along the foliation planes. The quartz vein sampled protrudes the surrounding bedrock by ca. 3 centimetres. Two pebble sized erratic boulders were collected at this site. Both are sub-rounded and surrounded by frost shattered bedrock material (Fig. 4.2.3F). A latero-frontal moraine is located SE of the sample location (Fig. 4.2.3G). This landform indicates not only the likely localised ice flow direction, but also records a significant still stand and/or advance of this glacier before further retreating inland. A hanging u-shaped valley is located east of the latero-frontal moraine, which indicates high subglacial erosion and also the location of an eastern ice accumulation area.

9.2.6 Isla Londonderry

A vertical sample profile was established at Isla Londonderry up to an elevation of ca. 200 meters (Table 4.2.1; Fig. 4.2.2). The bedrock at this site shows clear signs of glacial erosion in the form of characteristic whale-back morphologies with the a-axis orientated in E-W direction (Fig. 4.2.4A). Erratic boulders were identified up to an elevation of 300 meters with morphologies ranging from rounded bullet-shaped (ie. glacially modified and transported) to angular, indicative of supra and/or englacial transport. On the slopes of Isla Londonderry the glacially transported boulders are interspersed with localised rock-fall and scree material. Visible ice moulded bedrock occurs up to an elevation of ca. 600 meters. Higher elevations could not be accessed or were not visible at the time of sampling, hence glacially modified bedrock could extend to higher elevations at Bahia Cook (Fig. 4.2.2).

In total five samples were collected: 2 erratics and 1 bedrock at ca. 90 meters and one erratic-bedrock pair at ca. 190 meters (Table 4.2.1; Fig. 4.2.4A-B). No landforms indicating glacier still stand, e.g. moraines, were identified in the field. However the localised sampling and limited time available for sampling means that subtle glacial geomorphic landforms might have been missed.

Ice flow likely emanated from the Cordillera Darwin and extended toward Bahia Cook, flowing from NE to SW (Figs. 4.2.2 and 4.2.4). The glacially moulded bedrock indicates a temperate subglacial environment capable of eroding the bedrock. The lack of lateral moraines could indicate continuous ice thinning at this site. This is supported by the similarity in the type and lithologies of erratics sampled at both elevation increments.

Isla Hornos

At Isla Hornos a glacial deposit at ca. 140 m a.s.l. was sampled which is interpreted as a glacial drift. The bedrock at this site is a tonalite whilst the deposit consists of 70% biotite granites (Table 4.2.1). The grain size of the deposit is variable from boulders to gravel and sand size fractions (Fig. 4.7C-E). The drift is located just north of a heavily weathered bedrock exposure and is interspersed with shallow lakes and low lying vegetation (Fig. 4.2.4E). Four samples were collected at this site, three erratics and a cumulative surface gravel sample with mixed lithologies (Fig. 4.2.4C-E, Table 4.2.1). The deposit was likely left behind by ice retreating N/NE-ward at this site.

Preliminary (expected) results

To present empirical data on Patagonian Ice Sheet thickness are largely unavailable along its former western margin (Fig. 4.2.1) whilst timing of glacier cover and recession has been indirectly inferred from limiting radiocarbon ages of marine sediments in selected fjords and the Pacific (e.g. Kilian *et al.,* 2013, Breuer *et al.,* 2013, Caniupan *et al.,* 2011). Submarine moraines have been identified west of the Chilean fjords hence glacier coverage was extensive in the past, however no dating control exists of these features. Based on extent studies at similar latitudes toward the east (51-54°S), glacier maxima/retreat are/is recorded from ca. 45-12 kyrs (e.g. McCulloch, *et al.* 2005; Darvill, *et al.* 2015, Garcia, 2011). Work by Hall, *et al.* 2013, indicates recession of glacier tongues into the Cordillera Darwin by 10-15 calib. ^{14}C years B.P (Fig. 4.2.2), hence exposure ages from Isla Londonderry and Hornos should be older. Lastly it has been debated whether ice reached Isla Hornos. Through the identification of erratic boulders on Isla Hornos, it is clear that ice once covered this area. Exposure ages will provide insight into the exact timing of glacier recession from the island.

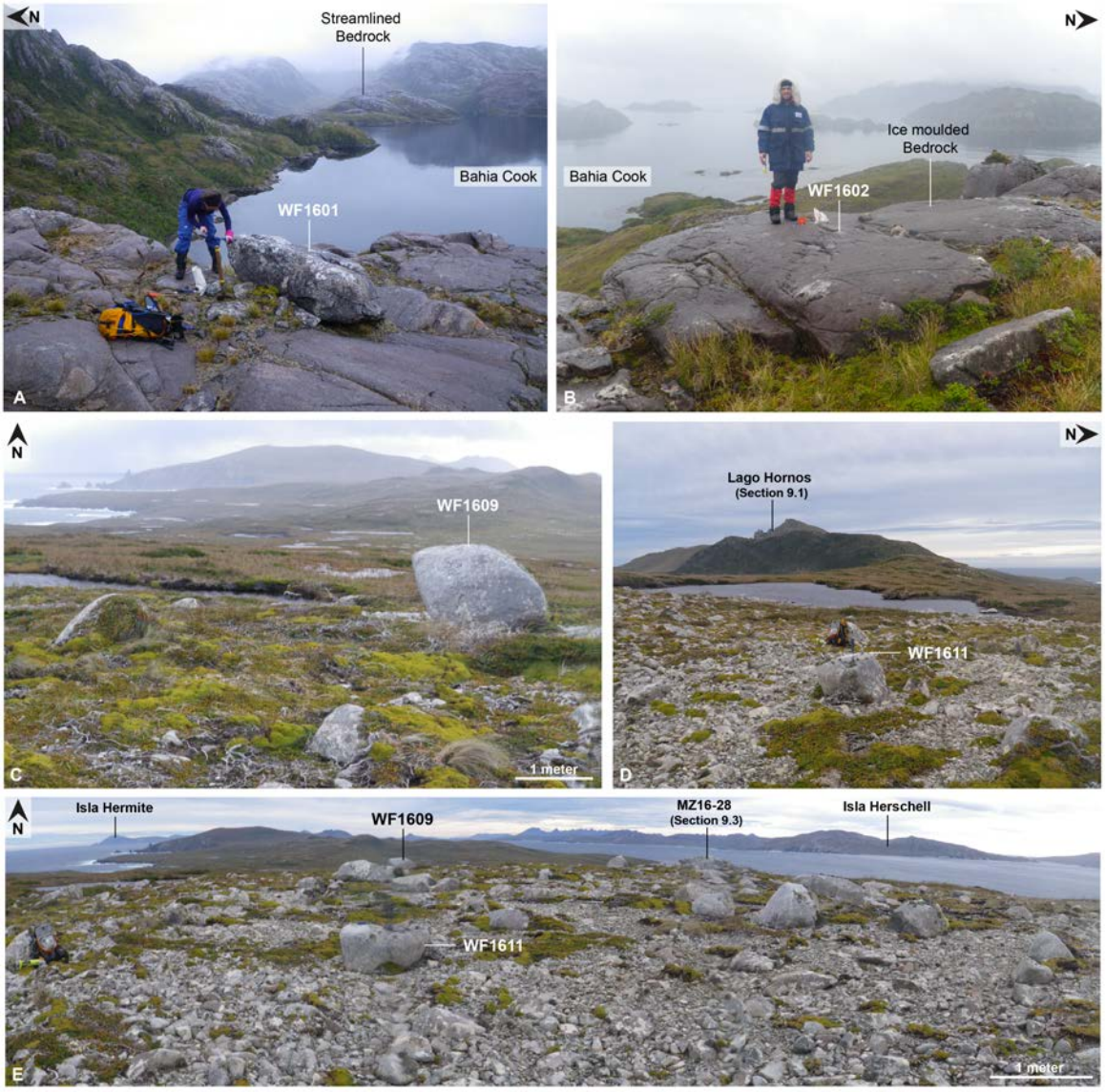

Fig. 4.2.4: Selection of samples and sample sites. A) Erratic at Isla Londonderry with streamlined bedrock in background. Ice flow from NE to SW (photo: M. Zundel). B) Ice moulded bedrock at Isla Londoderry. C) Erratic boulder on glacial till deposit, Isla Hornos. Ice flow from N/NW. D) Erratic

boulder on glacial till deposit, Isla Hornos. Majority of island is covered in peat/shrubs. E) Panorama of glacial till deposit on Isla Hornos. See Tabel 9.2.1 for further sample information.

Data management

Sample processing will be carried out at a laboratory suitable for terrestrial *in-situ* produced cosmogenic nuclide analysis (^{10}Be, ^{14}C, ^{26}Al, ^{36}Cl). Once sample processing has started, the typical time-period to obtain exposure age results is between 9-15 months, depending on laboratory and AMS priorities and availability. The results from this work will be published in peer-reviewed journal articles where all the relevant sample and target processing information will be provided for wider community access (Dunai & Stuart, 2009).

Sample ID	Location	Possible Nuclides	Sample Type	Lat. (°S)	Long. (°W)	Elev. (m a.s.l)	Spl depth (cm)	Spl hxlxw (m)	Lithology	Sample Geomorphology	Additional Info
WF1601	Londonderry	Be, Al, C	Erratic	-55.11542	-70.58126	81	4.0	0.9x1.5x1.1	granite	bullet shaped	Sitting on bedrock
WF1602	Londonderry	Be, Al, C	Bedrock	-55.11597	-70.58233	81	3.0	1.0x8.0x5.0	granite	ice moulded	
WF1603	Londonderry	Be, Al, C	Erratic	-55.11553	-70.58152	80	needs cutting	0.1x0.2x0.1	granite	bullet shaped on bedrock	Whole boulder collected. Depth will be provided.
WF1604	Londonderry	Be, Al, C	Erratic	-55.11309	-70.58567	178	2.0	0.5x0.6x0.4	granite	rounded on bedrock	
WF1605	Londonderry	Be, Al, C	Bedrock	-55.11340	-70.58609	180	3.0	1.2x1.2x0.8	granite	ice moulded	
WF1606*	Half-Moon, Ant.	Be, Al, C	Bedrock	-62.59658	-59.92043	96	1.5	0.5x4.0x1.5	quartz diorite	ice moulded	Ice flow from Livingston Island.
WF1607*	Gibbs, Ant.	Cl, He	Erratic	-61.48069	-55.63118	103	1.5	1.2x2.0x1.5	ultramafic	rounded, weathered	Same lithology as bedrock. Short transport pathway.
WF1608*	Gibbs, Ant.	Cl, He	Erratic	-61.48069	-55.63118	103	1.0	1.0x1.8x1.8	ultramafic	rounded, weathered	same as WF1607
WF1609	Hornos	Be, Al, C	Erratic	-55.95049	-67.25895	140	1.0	1.6x1.3x1.1	biotite granite	rounded, surface till deposit	Bedrock is a tonalite.
WF1610	Hornos	Be, Al, C	Pebbles	-55.95049	-67.25895	140	~4.0	varying	variety, quartz bearing	surface till deposit, gravel size	Bedrock is a tonalite.
WF1611	Hornos	Be, Al, C	Erratic	-55.95068	-67.25861	147	1.0	0.6x0.7x0.5	biotite granite	bullet shaped as glacial till deposit	Bedrock is a tonalite.
WF1612	Hornos	Be, Al, C	Erratic	-55.95068	-67.25861	147	needs cutting	0.1x0.2x0.1	biotite granite	low lying boulder as glacial till deposit	Bedrock is a tonalite. Needs cutting. Sample depth will be provided.
WF1613	Narborough	Be, Al, C	Erratic	-52.47274	-74.53468	407	1.0	1.0x1.4x1.2	granite	rounded on bedrock	Same lithology as bedrock but glacially modified.
WF1614	Narborough	Be, Al, C	Bedrock	-52.47265	-74.53426	413	1.5	1.2x6.0x3.0	granite	ice moulded	
WF1615	Narborough	Cl	Erratic	-52.47216	-74.53511	393	1.0	0.4x0.5x0.5	volcanic	sub-angular	
WF1616	Narborough	Be, Al, C	Bedrock	-52.48478	-74.5633	10	1.0	0.6x1.2x0.5	biotite granite	ice moulded	close to glacial deposit at sea level
WF1617	Desolacion	Be, Al, C	Bedrock	-52.73852	-74.72392	82	1.0	0.9x3.0x2.5	quartz vein	ice moulded	
WF1618	Desolacion	Be, Al, C	Erratic	-52.73852	-74.72392	82	5.0	0.06x0.1x0.09	granite	rounded	next to bedrock surrounded by frost shattered material

4. 3. THERMOTECTONIC & GLACIAL EVOLUTION OF CRUSTAL FRAGMENTS AROUND THE SCOTIA SEA

Maximilian Zundel U. Bremen
Not onboard: Cornelia Spiegel

Objectives

The area of the Scotia Sea mainly comprises the Scotia plate, which has essentially formed after the break-up of Gondwana and the associated divergence of the South American and Antarctic plates (Fig. 4.3.1). Thus, the opening of the Scotia Sea is of particular interest for understanding the post-Gondwana plate tectonic evolutions of the Southern Patagonian and Fuegian Andes as well as the Antarctic Peninsula. In addition, the Scotia Sea is of great significance for oceanographic, climatic, and biological research as prior to the – presumably Eocene / early Oligocene – opening, the area of the Scotia Sea was clogged by numerous crustal fragments which formed barriers blocking deep-water circulation. Subsequently, various ocean floor spreading ridges led to the opening of the Scotia Sea and the DP, respectively, and enabled the formation of the Antarctic Circumpolar Current, the largest ocean current on earth, which may have resulted in continental glaciation of Antarctica and a pronounced decrease of global temperatures (Zachos & Kump 2005). It also allowed high-latitude fauna and flora exchange between the Atlantic and Pacific oceans, and put an end to terrestrial biota migration between Antarctica and South America (e.g., Dalziel et al., 2013, Eagles & Jokat, 2014). Today, the crustal fragments surround the Scotia Sea and are separated by different basins. Although the formation of these basins is relatively well constrained (Eagles & Jokat, 2014), tectonic data of the crustal fragments are limited. Obtaining thermochronological data of these crustal is therefore crucial to better reconstruct the tectonic evolution within the Scotia Sea area. As a consequence, this project plan pursues two partly superimposed goals; one concerns the long-term (thermos)tectonic reconstruction of the Scotia Sea area (I), the other is related to a relatively short-term glacial reconstruction (II).

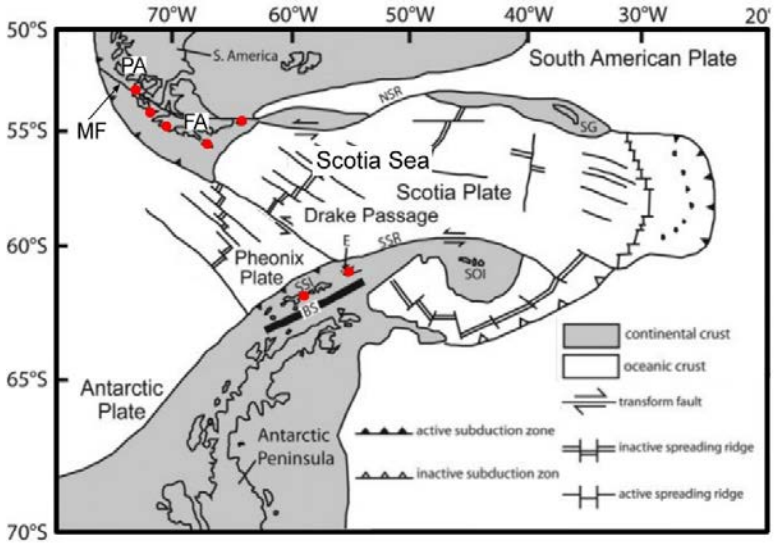

Fig. 4.3.1: Regional plate tectonic situation of the Scotia Sea, which is mainly encompassed by the Scotia Plate (modified after Lee et al. 2015). The Scotia Plate is largely comprised by oceanic crust with several continental fragments at its margin. Sampled areas during PS97 are marked in red.

Abbreviations: BS=Bransfield Strait, E= Elephant Island, FA=Fuegian Andes, MF=Magallanes Fault, NSR=North Scotia Ridge, PA=Patagonian Andes, SG=South Georgia, SOI=South Orkney Islands, SSI=South Shetland Islands, SSR=South Scotia Ridge.

(I) For deriving the thermotectonic evolution, samples were taken from (i) the Southern Patagonian and Fuegian Andes including "Isla de los Estados" and from (ii) the South Shetland Islands, including the Elephant Island Group. The samples will be analysed by means of apatite fission track and apatite (U-Th)/He analysis, which provide cooling paths through the upper ~4 km of the earth´s crust, thus recording movements, tectonic activity, and erosion of the shallow crust and close to the surface. Comparing the tectonic evolutions of the sampled crustal fragments gives evidence about common or differential movements and thus allows inferences about the timing of their separation and the opening of oceanic basins between these blocks (see, e.g., Carter et al., 2014).

(II) In addition to the Cenozoic tectonic evolution of this area (that potentially initiated southern hemisphere glaciation), we are also interested in the younger Pleistocene deglaciation history. For this, glacially eroded bedrock and erratic samples from Half Moon Island (South Shetland Islands) and from Gibbs Island (Elephant Island Group) were sampled for surface exposure dating (cf. chapter 4.2).

Work on land

For both, surface exposure dating and thermochronological analysis, the main priority was a sampling along elevation profiles, since they allow direct extraction of glacier thinning rates and exhumation rates from age-elevation-relationships. An additional goal was to collect iso-altitude horizontal profiles, because it is possible to derive lateral glacial retreat rates from them, and they reveal information on fault movements, crustal tilting, and paleotopography. For surface exposure dating, sampling of erratic boulders and/or glacially-eroded bedrock, (ideally striated) was carried out. Because surface exposure dating relies on the accumulation of 10Be in quartz, quartz-bearing lithologies such as granites and granodiorites were collected. Most of 10Be production occurs in the upper few cm of a rock and thus the surfaces of exposed rocks have been sampled. Since these are difficult to sample from unweathered, rounded bedrock or boulders, a rock saw was used to cut up to 2 cm deep grids into the rock´s surface. After sawing, the samples were removed from the surface by hammering and chiseling. For thermochronology, in-situ bedrock samples were collected. The applied thermochronological dating methods are based on the radioactive decay of U (and Th and Sm) in the mineral apatite; accordingly apatite bearing rocks were sampled, which involves essentially the same lithologies as required for surface exposure dating. Apart from sample collection, observations on structural evolution, tectonic activity and glacial geomorphology were included in the fieldwork.

Work at sea

For thermochronological analysis, the coarse grained detrital fraction from the upper ~1 m of ocean sediment was also collected (Table 4.3.1, Fig. 4.3.2. and 4.3.4). This was recovered using a box-corer of the marine geology group (see Chapter 3). Dating of this ice rafted debris yields averaged age patterns that reflect the cooling and exhumation history integrated over the whole source area. Main priority was on coring sites that can be related to well-defined glacial catchments.

Preliminary results

Due to mostly unstable weather conditions, time in the field was limited, and particularly higher elevated areas were often inaccessible because of deep clouds. However, for thermochronology 19 samples from 18 different land sites and 6 box-corers, while for surface exposure dating, 2 samples from 2 sites were collected. Additionally, two samples were

taken for thin section analysis. The samples will allow to generate thermochronological data of the respective areas around the Scotia Sea. This will provide important information on its exhumation history and tectonic evolution. Furthermore, it is possible to gather new data on the long-term dynamics and thinning history of the West Antarctic Ice Sheet, and on the general process of lithosphere – ice sheet interaction (cf. geodetic work chapter 4.4).

Southern Patagonian and Fuegian Andes

The first priority area, the western part of the Strait of Magellan in the southern Patagonian Andes could not be reached at the beginning of the cruise since very bad weather conditions caused a change in the ship track towards the eastern area of Tierra del Fuego. Thus, sampling was focused first on the Scotia Sea and southernmost Pacific margins of South America, where samples were taken close-by or from “Isla de los Estados”, “Isla Hornos”, “Isla Londonderry”, “Isla Noir”, “Isla Desolación” and “Isla Narborough” (Fig. 4.3.2).

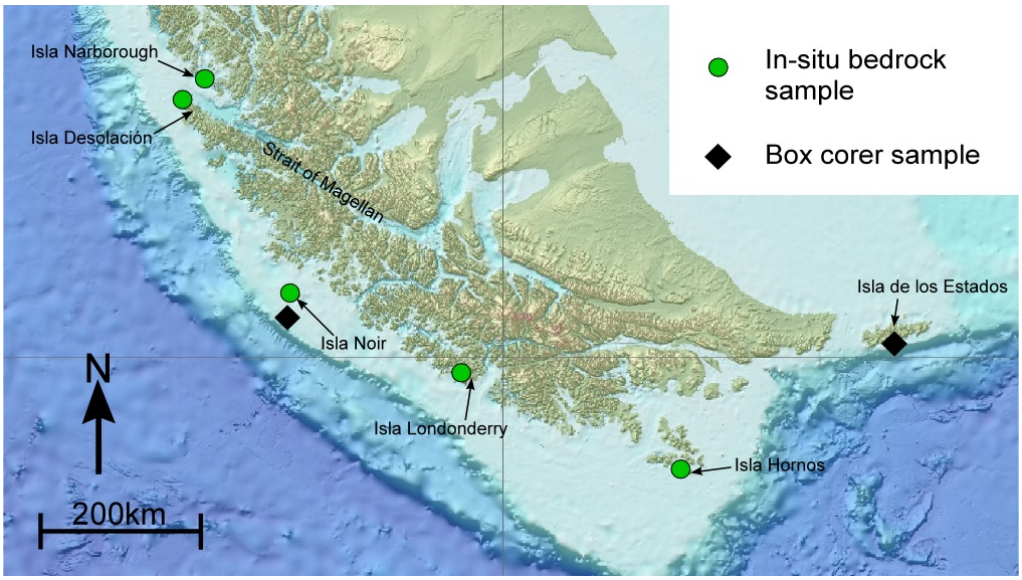

Fig. 4.3.2: Sampling area in southernmost South America. Box-corer samples MZ16-01 and MZ16-08 were collected offshore “Isla de los Estados” and “Isla Noir”, respectively. In-situ bedrock samples for thermochronology were collected on the “Isla Hornos”, “Isla Londonderry”, “Isla Noir”, “Isla Desolación” and “Isla Narborough”.

Isla de los Estados

With the deployment of a box-corer in shallow water depths of 114 m very close to “Isla de los Estados” a well-sorted sandy sediment was retrieved, yielding high proportions of carbonate materials, e.g. shells, shell fragments etc. This sample most-likely comprises detrital material from the island being reworked and mixed with biogenic carbonate. As the catchment of the sample location is well defined, thermochronological dating of extracted apatites will yield an integrated age of the island. The thermotectonic reconstruction of “Isla de los Estados” is particularly interesting regarding its location at the transition between Tierra del Fuego and the North Scotia Ridge where major strike-slip movement of the Scotia Plate are accommodated.

Isla Hornos

Two in-situ bedrock samples were taken from “Isla Hornos” by A. Geiger and R. Kilian, respectively, at 140 and 158 m a.s.l. (Table 4.3.1). These samples are of tonalitic composition with high proportions of plagioclase and minor quartz, hornblende, and biotite. They are fine-grained and equigranular with no preferential mineral orientations. These

samples will be subjected to thermochronological dating in order to constrain the exhumation history of “Isla Hornos”, which potentially resembles the history of the whole archipelago of “Islas Wollaston” being a remarkable promontory off the main coast of Tierra del Fuego.

Isla Londonderry

Sampling on “Isla Londonderry” was performed along an elevation profile. By doing so, five in-situ bedrock samples were collected covering an elevation range of 350 m (Table 4.3.1). Rock samples from 12 and 100 m a.s.l. are of granitic composition showing an equigranular medium-grained mineral assemblage comprising K-feldspar, plagioclase, quartz, and biotite. At higher elevations (200, 300, and 350 m a.s.l.) coarse-grained, occasionally porphyritic granodiorites are prevailing, containing plagioclase, K-feldspar, quartz, and biotite. The rocks are relatively fresh with occasional evidence of minor alteration, e.g. partly chloritized biotite. Conspicuous pinkish N-S- to NE-SW-striking felsic dykes of 5-20 cm thickness frequently cross-cut the granitic-granodioritic basement, showing tapering terminations (Fig. 4.3.3a). Parts of the felsic basement contained fine-grained mafic enclaves of pheno-dioritic composition.

Isla Noir

On “Isla Noir”, one fine-grained in-situ bedrock sample was taken from a blocky outcrop along the shoreline of a small lake at 179 m a.s.l. by R. Kilian. The sample is macroscopically characterized as a tonalite. It shows a slightly developed tectonic foliation by aligned mica minerals. Foliation is locally cut by whitish quartz veins indicating a hydrothermal overprint. Nevertheless, the sample will by thermochronologically dated, and thus add to understanding the exhumation and uplift history of the Pacific margin of the southern Patagonian Andes.

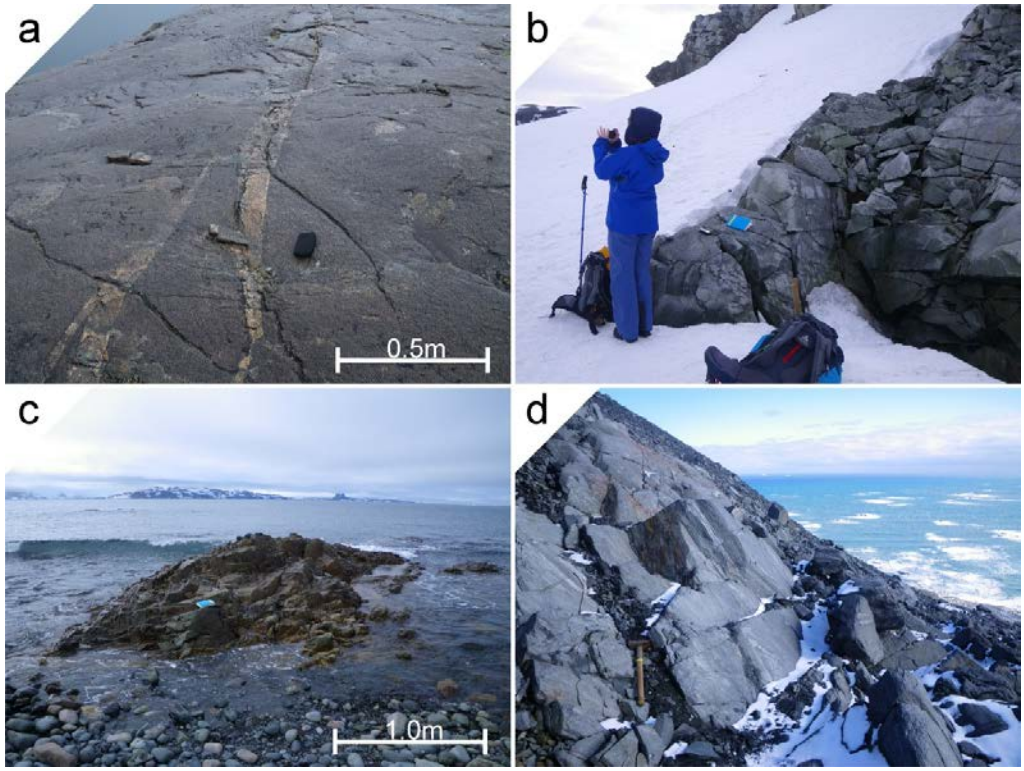

Fig. 4.3.3: Sampled rocks during the onland work: a) Dykes cross-cutting the granitic basement on “Isla Londonderry” (MZ16-02). b) On occasional ice-free spots the granitic bedrock on Half Moon Island can be accessed close to sea level (MZ16-12). c) E-W-striking, brownish rhyolite dyke shows a prominent morphological relief at the shoreline of Nelson Island (MZ16-17). d) Foliated and lineated mica-schists (MZ16-24) on Elephant Island’s SW coast (Fotos: M. Zundel).

Isla Desolación and Isla Narborough

The Magallanes Fault is a major transform structure and a Plate boundary between southernmost South America and the Scotia plate (Fig. 4.3.1). Thus, constrains on the time of such activity along the Magallanes Fault is of great interest for the reconstructing tectonic evolution of the Scotia Sea. As the western part of the Magallanes Fault is most-likely reflected by the prominent western Strait of Magallan, sampling was carried out on the southern and northern coast in order to constrain the timing of fault activity.

The southern side was sampled on “Isla Desolación” where greyish gneisses and schistose meta-volcanic rocks are exposed yielding a fine-grained grey groundmass with white plagioclase and quartz porphyroclasts of up to 1-2 mm. These rocks show a well-defined steep NW-SE-striking foliation and a shallowly NW-plunging stretching lineation majorly defined by quartz. Conspicuous several cm thick white quartz veins are frequently cross-cutting the rock fabric. The prevailing NW-SW-striking rock fabric is well reflected in the coastal morphology, which shows NW-SE-trending ridges and cliff sides.

On the other side of the Strait of Magallan, coarse-grained equigranular biotite-granites (Fig. 4.3.5) and bt-granodiorites are exposed on “Isla Narborough”. They consist of quartz and biotite with variable contents of plagioclase and K-feldspar. Locally, rounded fine-grained dioritic enclaves of up to several decimetres are incorporated in the granodioritic rocks. An ENE-WSW-striking 1 m thick dyke of basaltic composition cross-cuts a locally evident, subtle NE-dipping foliation in the granodiorites.

South Shetland Islands and Elephant Island Group

Sampling on the Antarctic side of the DP was mainly focused on the South Shetland Islands and Elephant Island Group. Potential sampling sites were identified on almost every island within the respective archipelago. However, only few sites could be sampled due to unstable weather conditions and the restricted time schedule of RV *Polarstern*. Nevertheless, sampling could be performed on four islands, namely Half Moon Island, Nelson Island, Gibbs Island, and Elephant Island (Fig. 4.3.4). Their present-day hard rock exposure probably monitors the young tectonic history related to recent subduction and basin formation processes.

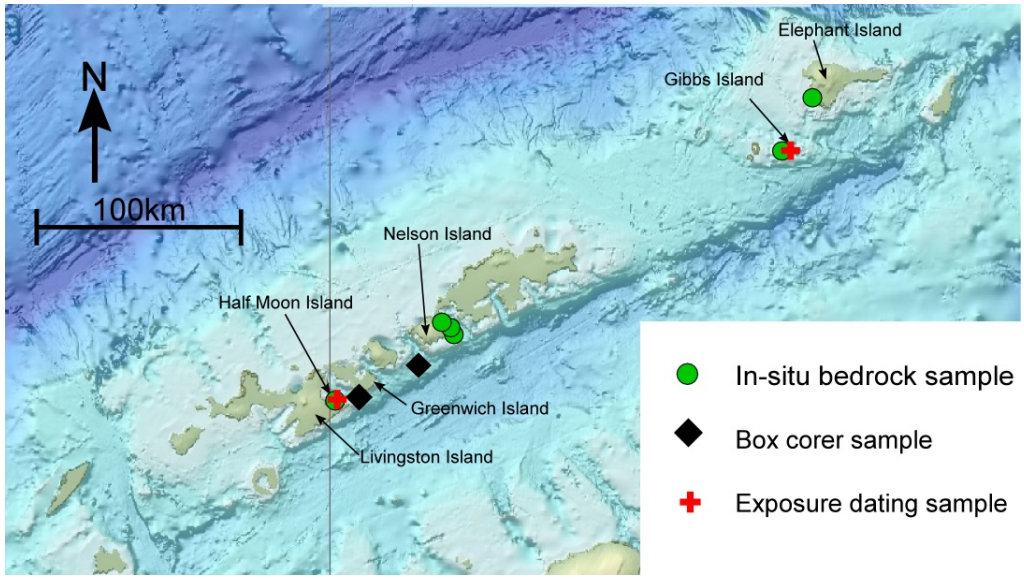

Fig. 4.3.4: Map showing samples taken on the South Shetland Islands and on the Elephant Island Group.

Additionally, four box-corer samples were retrieved offshore Nelson and Greenwich Islands (Fig.4.3.4). These samples yield a large variety of clasts of different grain sizes: (i) high proportions of volcanic clasts of most-likely basaltic composition; they presumably reflect the basalt-dominated lithologies on the South Shetland Islands. (ii) samples also contain various plutonic clasts of granitic to gabbroic composition. The batholith on Livingston Island could likely account for these plutonic rocks, especially for the tonalities and gabbros. Another potential source of plutonic rocks could be King George and Low Islands. Alternatively, all these lithologies could have been derived from the Antarctic Peninsula, too. (iii) only a small amount of metamorphic rocks was identified in the box-corer samples. They could be derived for example from the Scotia Metamorphic complex on Smith Island and from the Elephant Island Group. (iv) light brownish sandstone also shared their fraction with the sediments in the box-corer samples. Some of them probably represent reworked volcanic material from the South Shetland Islands.

Half Moon Island

Sampling of Half Moon Island was concentrated on La Morenita Hill in the South of the island. This hill exposes the north-eastern parts of a tonalite intrusion, possibly part of the larger batholith mainly located on Livingston Island. On Half Moon Island the rocks are dark coloured, fine-grained, equigranular and of tonalitic composition. They are very rich in plagioclase and biotite with lesser amounts of quartz and k-feldspar with occasional amphiboles. In total, five samples were taken from this tonalite body: (i) two in-situ bedrock samples for thermochronology, one close to sea level (Fig. 4.3.3b) and one on top of the hill (96 m), (ii) two in-situ bedrock samples for thin sections in order to better characterize the pluton petrographically, (iii) one in-situ bedrock sample for exposure dating on the hill's top. Thermochronological dating will be very essential to understand the upper crustal tectonic dynamics of the South Shetland Islands. Obtained data will therefore add to a few existing thermochronological data from Livingston and King George Island (e.g. Brix et al., 2007).

Nelson Island

The East coast of Nelson Island was quickly visited during a short weather window. The island is largely composed of Late Cretaceous to Paleogene volcanic rocks of basaltic to andesitic composition. Therefore, the sites were primarily investigated for felsic erratic boulders, which are normally well visible on a mafic basement. The visited coastal section of Nelson Island is characterized by narrow beaches and steep cliffs with small platforms on top. These platforms were primarily used as landing sites as the also provide an ideal environment for glacial erractics. However, no erratics were found and virtually no sediments were observed on these platforms. Thus, in-situ coarse-grained basaltic rocks were sampled instead for thermochronology at the first and second location. At the third location, a cobble beach at O'Cain Point, a brownish rhyolitic dyke was sampled near sea level (Fig. 4.3.3c). The E-W-striking dyke has a width of approximately 2-3 m and is characterised by a fine-grained groundmass bearing quartz phenocrysts. Whitish layers of several mm are indicated by bands of quartz presumably acquired during magma flow. Apatite is known to contribute to the mineral assemblage of dykes in this region (Kraus, 2005), thus it is forseen to date this by means of apatite thermochronology.

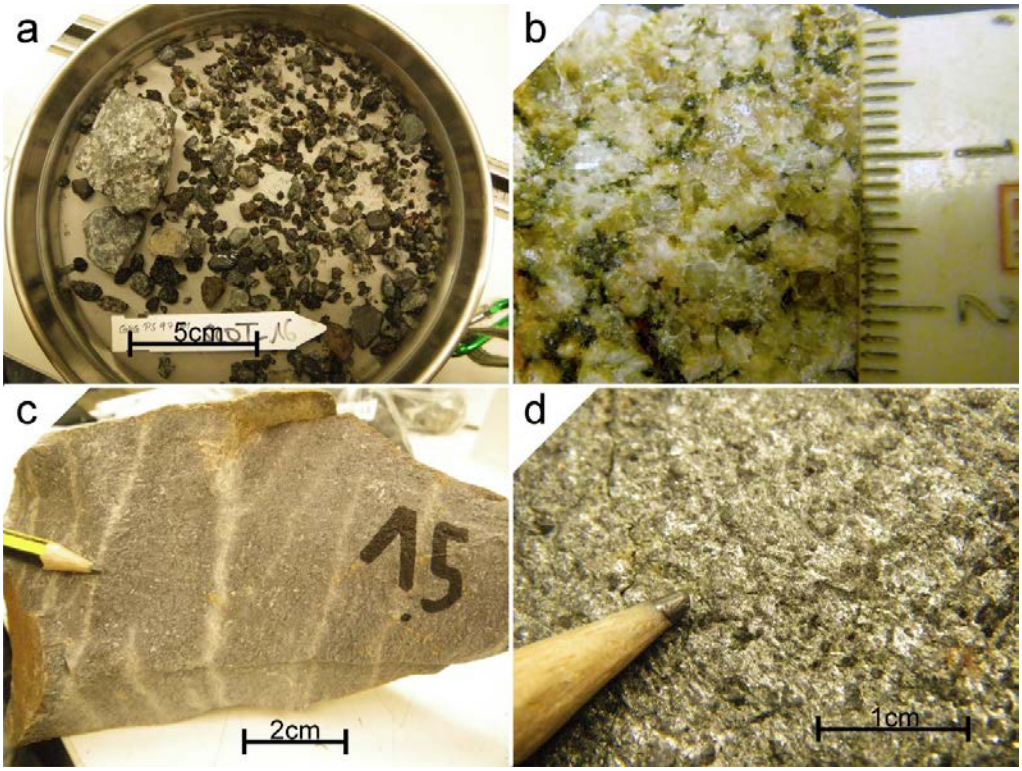

Fig. 4.3.5: a) Typical sediment retrieved by box-corer in the vicinity of the South Shetland Islands showing variable grain-size and composition (MZ16-19). b) Equigranular texture of medium-grained granite from "Isla Narborough" (MZ16-32). c) Fine grained rhyolitic dyke shows light-coloured bands which possible reflect a magmatic flow fabric (MZ16-17). d) Euhedral biotite-porphyroblasts are frequently observed on foliation plains of amphibolite-facies schist from Elephant island (MZ16-24) (Fotos: M. Zundel).

Gibbs Island

Gibbs Island was visited in cooperation with the geodetic group of TU Dresden. The Island mostly consists of rocks of ultramafic composition, in general spinel-olivine dunites (Lee et al., 2015). They show a high degree of metasomatic overprint which was recognized by the intensive serpentinization of olivine. Commonly, these rocks are lacking any apatite and are thus unsuitable for thermochronological dating methods, they were however sampled because metasomatic interactions could significantly enhance the apatite content in such rocks. As quartz is entirely absent, an exposure dating based on 10Be is also not suitable. However, two glacier erratics were sampled for potential exposure dating with Helium in olivine.

Elephant Island

On Elephant Island low- to high-grade metamorphic rocks are exposed along coastal sections and in ice-free areas in the mountains. The high relief of almost 1000 m makes the island very suitable for sampling an elevation profile for thermochronological dating. Although clouds were blocking the higher areas on the island, four sampling sites could have been reached by helicopter covering an elevation range from 0 up to 426 m a.s.l. The first stop was located at 155 m a.s.l., where coarse grained mica-schists are exposed (Fig. 4.3.3d). These rocks are largely composed by white mica, albite, and quartz with euhedral biotite porphyroblasts potentially indicating lower amphibolite-facies (Fig. 4.3.5). The obvious foliation is widely spaced and moderately N-dipping while the stretching lineation is moderately W-plunging. At the second stop, again mica-schists were sampled at sea level. Besides the previously described minerals, occasional red euhedral garnet of a few mm in

size add to the mineral assemblage indicating a slightly higher metamorphic degree or a more Al-rich precursor rock with regard to the last sample location. The foliation is sub-vertical striking NE-SW with a moderately WSW-plunging stretching lineation. The third sample location was on a relatively large plateau on top of a steep cliff along the southern coast of the island, where one sample was taken at the helicopter landing site, another sample was collected as a reference sample from a nearby outcrop, because it was somewhat unclear whether the first sample was *in-situ.* Present mica-schists reveal white mica, albite, biotite and quartz. The foliation wasn't accurately measured due to time reasons, however it was roughly E-W-striking.

Tab. 4.3.1: All samples taken during PS97 cruise. Abbreviations: bc=box-corer sample, cosmo=sample for exposure dating, bt=biotite, qz=quartz, hbl=hornblende.

Sample	alternative	type	Region	elevation in m	W	S	Lithology
MZ16-	PS97/006-	bc	Isla de los	-113.8	64° 17.01'	54° 51.00'	fine-grained carbonate
MZ16-	-	bedroc	Isla Londonderry	96	70°	55°	bt-granite
MZ16-	-	bedroc	Isla Londonderry	207	70°	55°	bt-granodiorite
MZ16-	-	bedroc	Isla Londonderry	304	70°	55°	bt-granodiorite
MZ16-	-	bedroc	Isla Londonderry	338	70°	55°	bt-granodiorite
MZ16-	-	bedroc	Isla Londonderry	12	70°	55°	bt-granite
MZ16-	-	bedroc	Isla Noir	179	73°	54°	bt-tonalite
MZ16-	PS97/028-	bc	Isla Noir	-104.6	73°	54°	sand-gravel with shells
MZ16-	-	bedroc	Half Moon Island	14	59°	62°	qz-diorite
MZ16-	-	bedroc	Half Moon Island	14	59°	62°	qz-diorite
MZ16-	-	bedroc	Half Moon Island	22	59°	62°	qz-diorite
MZ16-	-	bedroc	Half Moon Island	21	59°	62°	qz-diorite
MZ16-	-	bedroc	Half Moon Island	92	59°	62°	qz-diorite
MZ16-	-	bedroc	Half Moon Island	92	59°	62°	qz-diorite
MZ16-	-	bedroc	Nelson Island	74	58°	62°	basalt
MZ16-	-	bedroc	Nelson Island	55	58°	62°	basalt
MZ16-	-	bedroc	Nelson Island	0	58°	62°	rhyolite
MZ16-	PS97/060	bc	Greenwich Island	-462	59°	62°	gravelly sediment
MZ16-	PS97/061	bc	Greenwich Island	-466	59°	62°	gravelly sediment
MZ16-	PS97/062	bc	Greenwich Island	-477	59°	62°	gravelly sediment
MZ16-	PS97/067-	bc	Nelson Island	-793	59°	62°	gravelly sediment
MZ16-	WF1607	cosmo	Gibbs Island	103	55°	61°	serpentinized dunite
MZ16-	WF1608	cosmo	Gibbs Island	103	55°	61°	serpentinized dunite
MZ16-	-	bedroc	Gibbs Island	106	55°	61°	serpentinized dunite
MZ16-	-	bedroc	Elephant Island	155	55°	61°	bt-schist
MZ16-	-	bedroc	Elephant Island	0	55°	61°	grt-bt-sschist
MZ16-	-	bedroc	Elephant Island	426	55°	61°	bt-schist
MZ16-	-	bedroc	Elephant Island	421	55°	61°	bt-schist
MZ16-	-	bedroc	Isla Hornos	140	67°	55°	hbl-bt-tonalite
MZ16-	-	bedroc	Isla Hornos	158	67°	55°	hbl-bt-tonalite
MZ16-	-	bedroc	Isla Desolación	82	74°	52°	qz-pl-gneis
MZ16-	-	bedroc	Isla Narborough	374	74°	52°	bt-granodiorite
MZ16-	-	bedroc	Isla Narborough	0	74°	52°	bt-granite

4. 4. REPEATED GNSS MEASUREMENTS IN THE REGION OF THE ANTARCTIC PENINSULA TO INVESTIGATE NEOTECTONICS

Lutz Eberlein, Peter Busch TU Dresden
Not onboard: Mirko Scheinert

Objectives

In order to deepen the knowledge on the glacial history and on the tectonic state of Antarctica it is important to investigate recent deformations of the earth crust.

Vertical deformations are caused by changing ice loads, hence they are in particular related to the glacial history and with recent ice mass changes. The region of the Antarctic Peninsula and especially the Bransfield Strait is one of the rare active tectonic zone of the Antarctic continental margins. The Bransfield Strait is characterized by an active rift. The spreading of this rift is about 7 mm/year (Rülke et al. 2014). That means that the South Shetland Islands moves more to the west then the Antarctic Peninsula.

During the Geodetic Antarctic Project (GAP95 / GAP98) 6 station sites on bedrock was setup and measured twice (1995 and 1998) in the northern region of the Antarctic Peninsula and the South Shetland Islands. Two of these sites have now been reoccupied during the PS97 cruise. In addition, a new site has been installed on the Isla Hornos. This contributes to the investigation of recent tectonic movements near to the border between the Antarctic and Scotia plate.

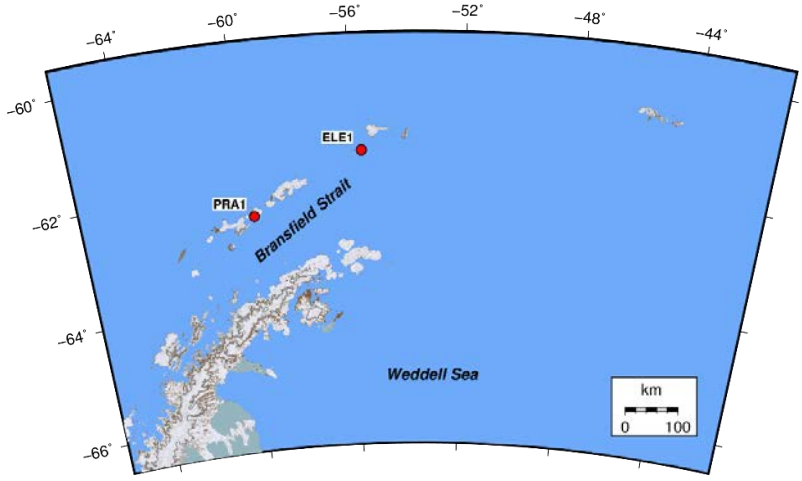

Fig. 4.4.1: Location of GPS sites PRA1 and ELE1 west of Bransfield Strait.

Work on land

As described above, the main goal was to re-occupy GPS sites on bedrock which were measured for the first time in 1995. By means of the ship-based helicopters two of four sites could be visited, and the GPS equipment was successfully installed, namely at PRA1 and ELE1 (Fig. 9.4.1.). Due to of the difficult weather conditions at both sites it was not possible to get back the equipment. The site PAR1 is close to the Chilean Navy Station Arturo Prat, so we could be organize the recover and backhaul of the equipment to Punta Arenas by the Chilean colleague's with the help of Instituto Antártico Chileno (INACH). The equipment at the site ELE1 is still there.

At the Isla Horns we could setup a new site on bedrock and successful recover the equipment after one month. More details are found in Table 4.4.1 and Figs. 4.4.1 to 4.4.5

Fig. 4.4.2: Location of GPS sites HORN on Isla Hornos.

Tab. 4.4.1: Geographical location, coordinates and observation time of the GPS bedrock sites [set-up: date of the set-up of the equipment; recover: date of the recover of the equipment; days: number of days with complete 24h measurements (24h sessions).

ID	**geographical location**	**approximate coordinates**		**observation time**		
		longitude (west)	*latitude (south)*	*setup*	*recover*	*days*
PRA1	close to Arturo Prat station on Greenwich Island	59°39,012'	62°28,656'	03-08-2016	by Chileans	??
ELE1	on bedrock plateau on the southern coastline of Gibbs Island	55°37,884'	61°28,842'	03-12-2016	still there	
HORN	on a ridge north of the light-house at Isla Horns	67°16.686'	55°58.110'	02-23-2016	03-21-2016	25

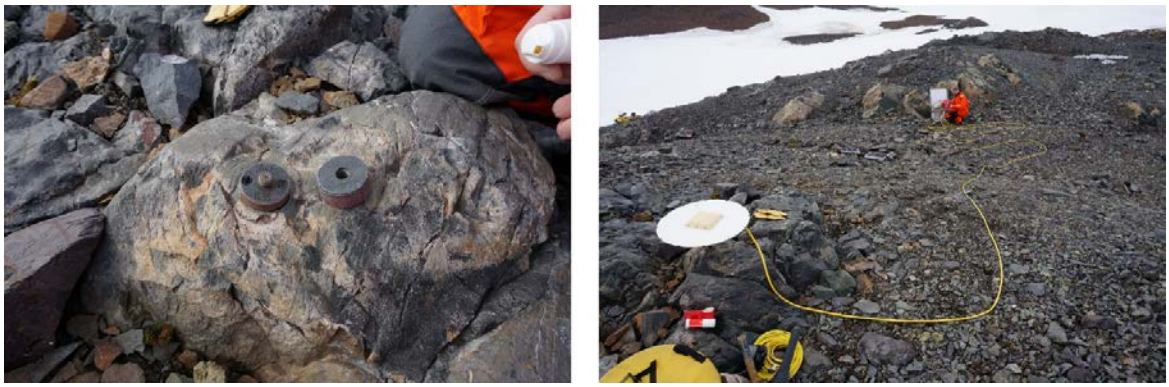

Fig. 4.4.3: Installation of the GPS equipment at the sites PRA1. The left photography shows the existing GAP (Geodetic Antarctic Project) marker from 1995. The right photo shows the mounted GPS antenna in the left foreground.

Fig. 4.4.4: Installation of the GPS equipment at the sites ELE1. The left photography shows mounted GPS antenna on the existing GAP marker from 1995. The right photography shows the solar-panels (left) for power supply of the receiver and the Zarges aluminium box (right) to protect the receiver and battery.

Fig. 4.4.5: Installation of the GPS equipment at the sites HORN. The left photography shows a solar panel and the aluminum box (the middle ground). The right photo shows the mounted GNSS antenna.

Preliminary results

The data analysis will be done at the home institution during the post-processing since further data like re-analyzed precise GPS orbits have to be utilized. Therefore, preliminary results cannot be presented in this report.

References

Briner JP, Lifton NA, Miller GH, Refsnider K, Anderson R, Finkel R (2014) Using *in-situ* cosmogenic ^{10}Be, ^{14}C, and ^{26}Al to decipher the history of polythermal ice sheets on Baffin Island, Arctic Canada. Quaternary Geochronology, 19, 4-13.

Breuer S, Kilian R, Weinrebe W, Berhmann J, Schörner D, Kissel C, Baeza O (2013) Distribution and structures of Late Glacial and Holocene sediments in the fjord system of the Magellan region (53°S) deduced form seismic profiles and sediment cores. Marine Geology, 346, 31-46.

Brix M, Faundez V, Hervé F, Solari M, Fernandez J, Carter A, Stöckhert B (2007) Thermochronologic constraints on the tectonic evolution of the westernAntarctic Peninsula in late Mesozoic and Cenozoic times. USGS, OF-2007-1047.

Caniupán M, Lamy F, Lange C, Kaiser J, Arz H, Kilian R, Baeza O, Aracena C, Hebbeln D, Kissel C, Laj C, Mollenhauer G, (2011) Millennial-scale sea surface temperature and Patagonian Ice Sheet changes off southernmost Chile (53°S) over the past 60 kyr. Paleoceanography, 26, 1-10.

Carter A, Curtis M, Schwanethal J (2014) Cenozoic tectonic history of the South Georgia microcontinent and potential as a barrier to Pacific-Atlantic through flow. Geology, G35091.1.

Dalziel I, Lawver L, Norton I, Gahagan L (2013) The Scotia Arc: genesis, evolution, global significance. Annual Revision Earth Planetary Sciences, 41, 767-793.

Darvill CM, Bentley MJ, Stokes CR, Hein AS, Rodes A (2015) Extensive MIS 3 glaciation in southernmost Patagonia revealed by cosmogenic nuclide dating of outwash sediments, Earth and Planetary Science Letters, 429, 157-169.

Dunai TJ, Stuart, FM (2009) Reporting of cosmogenic nuclide data for exposure age and erosion rate determinations. Quaternary Geochronology, 4, 437-440.

Eagles G, Jokat W (2014) Tectonic reconstructions for paleobathymetry in Drake Passage. Tectonophysics, 611, 28-50.

Francois, J.-P. (2015) *Postglacial paleoenvironmental history of the Southern Patagonian Fjords at 53°S.* PhD thesis at University of Cologne, Germany.

Garcia JL (2011) Late-Pleistocene glacial and climate fluctuations in the Torres del Paine region (51°S), southern South America, PhD thesis, University of Maine (available as download).

Geiger AJ (2015) Patagonian glacial reconstructions at 49°S. PhD thesis, University of Glasgow (unpublished).

Hall BL, Porter CT, Denton GH, Lowel TV, Bromley GRM (2013) Extensive recession of Cordillera Darwin glaciers in southernmost South America during Heinrich Stadial 1, Quaternary Science Reviews, 62, 49-55.

Hulton N, Purves R, McCulloch RD, Sugden DE, Bentley MJ (2002) The Last Glacial Maximum and deglaciation in southern South America. Quaternary Science Reviews, 21, 233-241.

Kilian, R., Baeza, O., Steinke, T., Arevalo, M., Rios, C., Schneider, C., 2007. Late Pleistocene to Holocene marine transgression and thermohaline control on sediment transport in the western Magellanes fjord system of Chile (53 degrees S). Quaternary International 161, 90-107.

Kilian R & Lamy F (2012) A review of Glacial and Holocene paleoclimate records from southernmost Patagonia (49-55°S). Quaternary Science Reviews, 53, 1-23.

Kilian R, Lamy F, Arz HW (2013) Late Quaternary variations of the southern westerly wind belt and its influences on aquatic ecosystems and glacier extend within the southernmost Andes. Z. Dt. Ges. Geowiss, 164, 279-294

Kraus S, (2005) Magmatic dyke systems of the South Shetland Islands volcanic arc (West Antarctica): reflections of the geodynamic history. Dissertation, LMU Munich.

Lamy F, et al. (2010) Holocene changes in the position and intensity of the southern westerly wind belt. Nature Geoscience 3, 695-699.

Lilly K, Fink D, Fabel D, Lambeck K (2010) Pleistocene dynamics of the interior East Antarctic ice sheet, Geology, 38, 703-706.

McCulloch RD, Fogwill CJ, Sugden DE, Bentley MJ, Kubik PW (2005) Chronology of the last glaciation in central Strait of Magellan and Bahia Inutil, southernmost South America. Geografiska Annaler, 87, 289-312.

Rülke A, et al. (2014) The Antarctic regional GPS network densification – status and results. International Association of Geodesy Symposia, IAGS-D-13-00155.

Sernageomin (2003) Mapa Geologico de Chile: version digital. Servicio Nacional de Geologia y Mineria, Publicacion Geologico Digital, No. 4, 1-15.

Zachos J, Kump L, (2005) Carbon cycle feedbacks and the initiation of Antarctic glaciation in the earliest Oligocene. Global and Planetary Change, 47, 51–66.

5 PHYSICAL OCEANOGRAPHY

Wolfgang Schneider[1], Harold Fenco[2], Gastón Kreps[3], Bruno Canella[4], Lester Lembke-Jene[5], Frank Lamy[5]
Not onboard: Alberto Piola[6]

[1]UdeC/IMO,
[2]INIDEP,
[3]CADIC-CONICET (Arg. Observer),
[4]ARA (Arg. Observer),
[5]AWI,
[6]SHN

Objectives

The first objective is to evaluate the water mass characteristics and velocity structure of the so far poorly understood Cape Horn Current which flows along the Southern Chilean Margin in the northwest DP. The Cape Horn Current is believed to be fed by the northern branch of the Antarctic Circumpolar Current which crosses the low-salinity tongue of the Southeast Pacific Ocean situated at mid latitudes. The Cape Horn Current is thought to be the main pathway of low salinity near-coastal waters in the Southeast Pacific feeding into the Southwest Atlantic (Hart, 1946).

Secondly, the volume transport through the western part of DP from the South American continent to the Antarctic Peninsula and the water mass structure therein will be estimated, as well as the vertical velocity structure of the Antarctic Circumpolar Current which flows through DP. This transect will be used together with existing historical transects for variability studies regarding the upper items.

Work at sea

The Physical Oceanography group concentrated its activities on the South Chilean Margin (Pacific) and the Western DP; hydrographic stations were also carried out on demand in the Central DP and Chilean/Argentinean (Scotia Sea) in support of the Biological Stations I-III and for the estimation of bottom currents, among others (in total 70 stations were sampled). The main instrumentation used was a SeaBird 911+ CTD, with two temperature and conductivity sensors and additional oxygen, fluorescence and turbidity sensors, integrated in the water sampling rosette and a downward looking Lowered Acoustic Doppler Current Profiler (LADCP, manufactured by RDI) also integrated in the rosette but independent from the CTD system. The difference between both temperature and conductivity sensors was < 0.003, °C and mS/cm, respectively. The GPS position at any time during the profile was added to the CTD bins by means of NMEA. The raw CTD data were processed with the SeaBird Data processing software according to SeaBird recommendations. The raw LADCP data were processed with the LDEO LADCP MATLAB software package version IX, developed by Manuel Visbeck, in which the ship's GPS position during profiling is used in order to correct for the movement of the rosette. Thus, at each station, profiles of the main hydrographic variables including current velocity were obtained. Water samples were drawn at stations and depths specified by the biological and chemical scientists.

The Antarctic Circumpolar Current was sampled when entering the Western DP starting at the northern position 56° 24' S and 71° 45' W, about 200 nm west of Cape Horn, towards the southern Shetland Islands and ending at 62° 40' S and 63° 6' W (Figure 5.1); 15 CTD/LADCP/Waterbottle stations from surface to bottom were occupied from 28th of February to 6th of March, i.e. late austral summer.

In order to shed light on the vertical velocity structure of the Cape Horn Current (which flows within the South Chilean Pacific margin) and its water mass composition four transects perpendicular to the current were carried out from the open ocean to the coast, each about 80 nm long, terminating at around 56°,55°, 54° and 52° 30' S (25 February, 24 March, 30

March and 4 April). During each transect between 8 to 12 CTD/LADCP/Waterbottle stations were sampled to bottom or 2000 m depth, whatever came first; some deep stations > 2000 m were sampled, too (for details concerning the exact positions, sampling depth, and water samples taken please consult the station book and the bottle summary to be found in the Appendices X+Y).

Capacity Building: In the beginning of the cruise HF, BC and GK were trained to operate the CTD/Rosette unit, to process the raw data with SBE-Software and to visualize the processed data with ODV.

Preliminary (expected) results

Antarctic Circumpolar Current / Western DP, Hydrography and Current Velocity

The PF which separates cold fresher Antarctic Polar Water south of it from somewhat warmer and saltier Sub-Antarctic Water north of it could be estimated to be located at around 59° S based on the strong meridional temperature gradient observed at 150 m depth along the transect through Western DP. Permanent Polar Water occupied the depth range from 100-250 m with temperature being less than 0.5° C at the PF and decreasing to -1.5° C towards the Shetland Islands, whereas the upper Polar Water had warmed to 2.5° C close to the front corresponding to the late austral summer season but only around 1°C west of the islands. The Sub-Antarctic Front was determined to be situated at around 58° S, just 60 nm north of the PF. Sub-Antarctic Surface Water north of this front was warmer than 4.5° C with rising temperatures (> 6.0° C) towards the South American continent. Antarctic Intermediate Water was present between the two fronts and below the surface waters while the sub-surface waters north of the Sub-Antarctic Front were occupied with Sub-Antarctic Mode Water (Figure 3.1b). Below this mode water Upper Circumpolar Deep Water was present with salinity > 34.2 and followed in depths > 2000 m and all the way to the bottom by Lower Circumpolar Deep Water with salinity > 34.65. The Circumpolar Deep Water shoaled towards the Shetland Islands and the Antarctic Divergence and got in contact with Polar Water (Figure 3.1b). This shoaling of Circumpolar Deep Water in the here in the Western DP towards the Antarctic Divergence is also typical for the Central DP (Naviera et al., 2009). Currents, measured 5 m above the bottom, along the transect crossing Western DP were around 5 cm/s and predominantly in north-eastern direction.

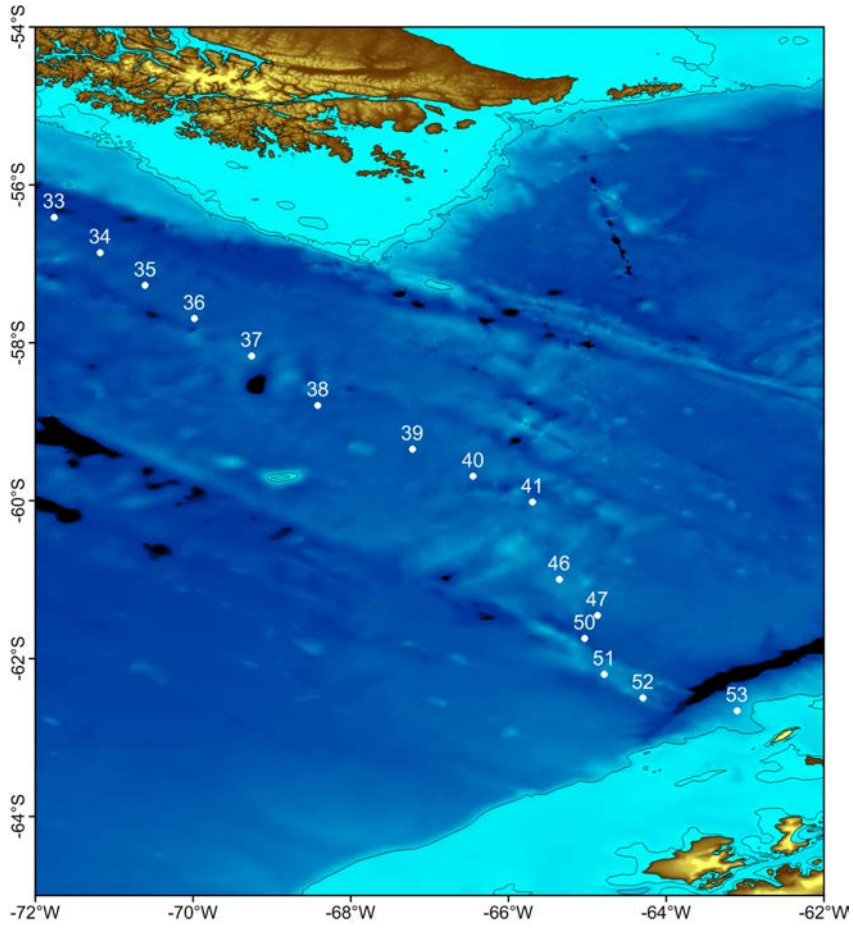

Fig. 5.1: Geographic positions and station numbers (PS97/XX) for the transect through the western DP

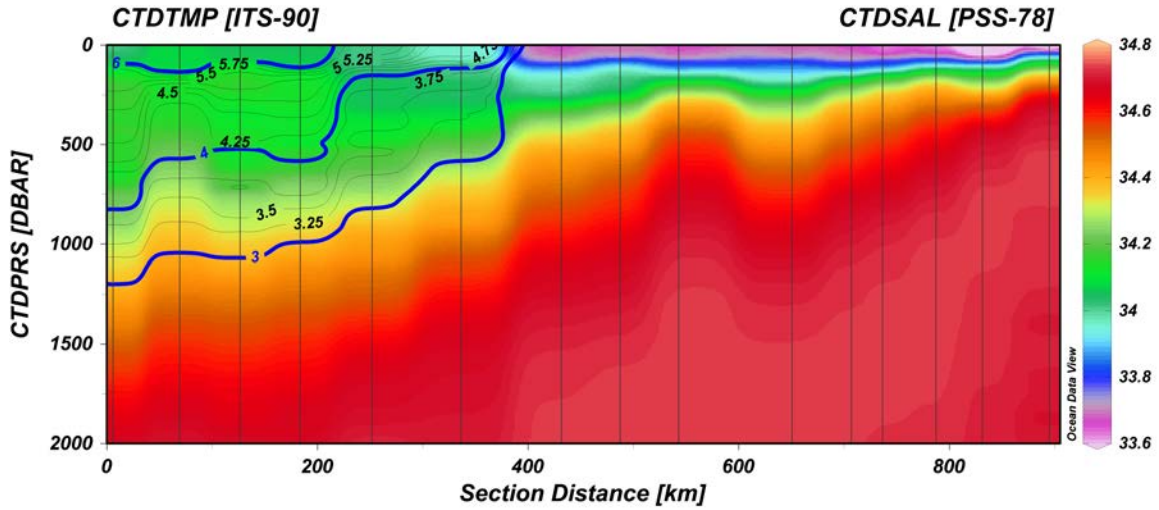

Fig. 5.2: below. Transect Western DP. The transect runs from north, about 200 nm west of Cape Horn (56° 24' S and 71° 45' W, Station PS97/33), towards the southern Shetland Islands and ending at 62° 40' S and 63° 6' W (Station PS97/53). The vertical black lines mark the stations occupied. Salinity is color-coded according to the right hand side colorbar. Iso-therms from 3-6 °C are overlaid as black

contour lines. AAIW is constrained from 3-4 °C and SAMW from 4-6 °C, high lightened by blue contour lines.

Cape Horn Current / South Chilean Margin (Pacific), Hydrography and Current Velocity

Out of the 4 transects across the Cape Horn Current, the most complete one spanning from the Chilean coast at 54° S about 125 km towards the open ocean is presented (Figures 5.3 and 5.4). As expected the upper layer (100 m) of the water column on the shelf and continental slope (the first ~80 km from the coast) wss occupied by low salinity water (< 33.6). Salinity slightly increases towards the outer part of the section (> 33.8). This salinity threshold confines the extent of the Cape Horn Current. In addition the iso-pycnals, which follow the salinity structure, outcrop at the deeper part of the continental slope thus indicating a geostrophic control of the current down to 300 m depth and parallel to the coast on the shelf and along the continental slope. A sub-meso scale eddy appeared at about kilometre 90 interrupting the flow of the Cape Horn Current. Preliminary estimates of current velocity derived from the lowered Acoustic Current Profiler are depicted in Figure 3.3. In the centre of the transect the flow is parallel to the coast line in southeast direction. Current velocities were relatively uniform from surface to 2000 m and were in the order of 10 cm/s. A narrow counter current with speeds around 15 cm/s was observed in the LADCP data above the continental slope. Velocities were again in southeast directions on the continental shelf. Velocities were to the northwest (~20 cm/s) at the most offshore portion of this transect.

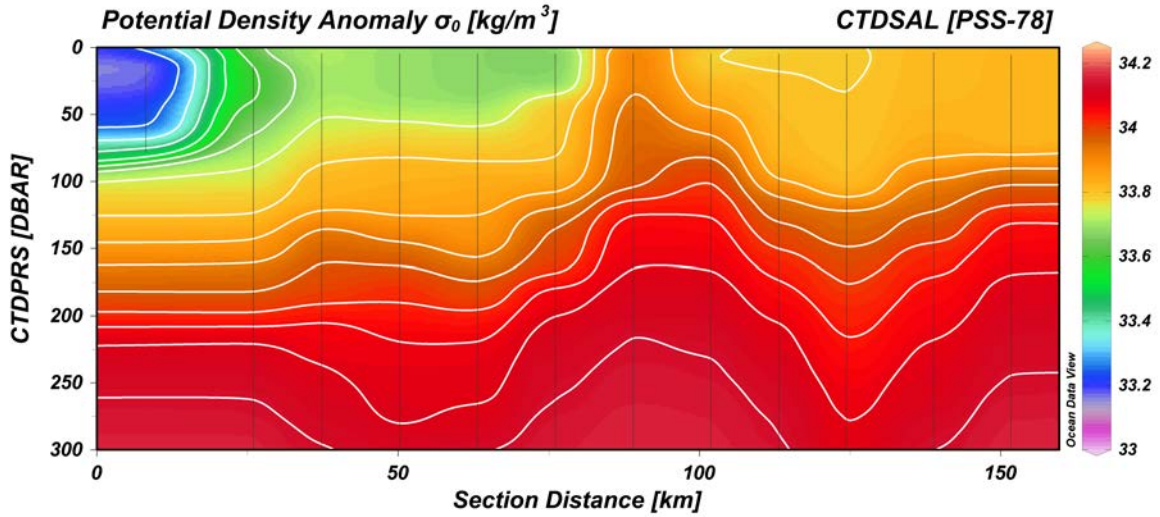

Fig. 5.3: Cape Horn Current cross-section. The section starts ~10 nm off the coast of South Chile at 54° S (left) and ends at 54° 45' S and 75° 30' W (right). Salinity is color-coded according to the right hand side colorbar. Isopycnal are overlaid as white contour lines starting at 25.5 kg/m^3 and increasing in intervals of 0.1 kg/m^3.

A detailed analysis of the CTD/LADCP data set (vertical velocity profiles) will continue on land according to the objectives outlined above. Upper layer current velocity was measured on the way with an ADCP installed in the haul of the ship. These raw data will be processed and included in the analysis. Sea surface temperature and salinity measured routinely by "*Polarstern*" together with the navigational data will be incorporated in the analysis. The co-operation with the water user community will continue on land.

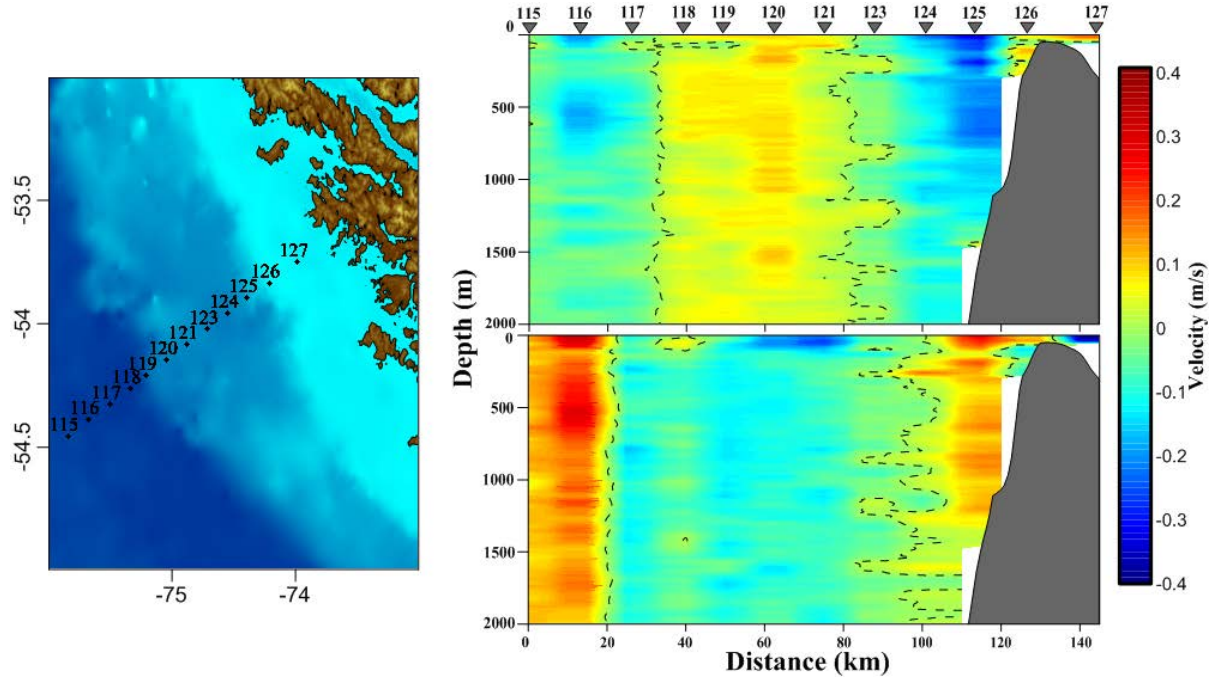

Fig. 5.4: The geographic position of the "Cape Horn Current 54°S" transect is shown in the left panel. The zonal velocity component, from surface to 2000 m depths, as derived from the LADCP data, is shown in the upper right column; the meridional velocity component in the lower right column. Velocities are color coded according to the colorbar shown on the right hand side of the figure.

6 HYDRO-ACOUSTICS

6.1 Bathymetric Investigations

Laura Jensen[1], Svenja Papenmeier[1], Friedrich Artel[1], Jürgen Goßler[2], Henrik Grob[3], Sjard Stratmann[3]

[1] AWI, [2] KUM GmbH
[3] U Hamburg

Objectives

Accurate knowledge of the seafloor topography, hence high resolution multibeam swath bathymetry data, is key information necessary to understand several marine processes. It is of particular importance for the interpretation of oceanographic, geological and biological data in a spatial context. For example, potential sediment depo-centres and areas of erosion as well as glacial and current-induced seabed features can be identified by means of multibeam bathymetry data.

Although repeatedly visited by research vessels, large parts of the DP have not been mapped with multibeam echosounder and thus lack of high resolution multibeam swath bathymetry. The same holds true for the study areas offshore Southern Chile, Southern Argentina and some parts of the Antarctic Peninsula. The bathymetric models for these areas are to a large extent derived from satellite altimetry measurements, which have a limited spatial resolution (maximum 1000 m). On this scales the identification of small- to meso-scale topographic features, for example depressions acting as sediment traps or glacial-geomorphological features, is hardly possible. Also sedimentological features related to bottom currents, such as scours and sediment waves, cannot be resolved from satellite altimetry data. Therefore, ship-borne high resolution bathymetry surveys in the study area are crucial for understanding and interpreting (palaeo-)oceanographic, hydrodynamic and sedimentological processes.

The main task of the bathymetry group on this expedition was the continuous collection and processing of high-resolution seafloor topography data in the research area. The data are basis for detailed working maps supporting other working groups to identify sampling sites and in station planning.

Work at sea

Technical settings

Multibeam data were recorded with the ATLAS Hydrographic Hydrosweep DS3 multibeam echo sounder permanently installed on *Polarstern*. Data acquisition was performed using the ATLAS Hydromap Control (AHC) software version 2.8.5.0 with the following relevant parameter settings: Swath width portside/starboard mainly “250%”, in rough sea conditions and water depths deeper than 4000 m sometimes reduced to “200%”, which results in a coverage of 4-5 times the water depth. Beam spacing was set to “Equal Footprint”, desired number of beams to “960”, C-keel source to “System C-keel”, and Pulse Type to “Frequency Modulated (Chirped)”. Generally, the transmission sequence “Single Pulse”, and the Multi Ping Mode “2 Swathes desired” was used, in order to achieve an optimal spatial coverage also during surveys with rather high ship’s speed of 10 kn or more. In shallow water depths (<300 m) the transmission sequence was switched to “Equidistant Transmission”, with a desired time interval of 1000 ms, and the multi ping mode was set back to “1 Swath” in order to limit the data amount.

For online visualisation of the raw data, the Hypack software package version 15.0.1.1 was used. Raw data were stored in *.asd-format in 30 minute blocks using the ATLAS Parastore software version 3.4.0.0. In addition it was stored in *.hsx-format with Hypack (in 30 minute

blocks as well). No water column data were collected. As no significant artefacts related to interferences between PARASOUND PS70 and Hydrosweep DS3 were visible, Hydrosweep was not used to trigger the PARASOUND on this expedition.
North of 60°S (outside the region of the Antarctic Treaty), the sonar operation was running continuously during survey and station work. In the latter case the "Wait Time" in the acquisition control was set to 120 s to avoid an overload of data but to guarantee gapless data sets during vessel drift. South of 60°S the sonar operation was switched to "Standby" when marine mammals were observed during surveying and during station work following the regulations of the German "Umweltbundesamt" (UBA). For the sound velocity corrections sound velocity profiles were obtained from 70 CTD casts (see Chapter 3), and 6 Valeport SVP casts (Table 6.1.1). As the Valeport SVP was tied to the wire during Multicorer casts, no additional ship's time was needed for the operation. The sound velocities were applied in AHC, Hypack and during postprocessing.

Tab. 6.1.1: Casts where the Valeport SVP was tied to and lowered with the Multicorer (MUC).

Station	Device	Date	Time [UTC]	Latitude	Longitude	Depth [m]
PS97/011-02	SVP (MUC)	23/02/15	10:54	55°41.301 S	66°08.668 W	570
PS97/056-01	SVP (MUC)	06/10/15	18:18	63°32.170 S	60°40.491 W	726
PS97/072-01	SVP (MUC)	10/03/15	03:23	62°00.372 S	56°03.868 W	1992
PS97/074-01	SVP (MUC)	12/03/15	05:15	60°55.623 S	56°15.812 W	1898
PS97/085-02	SVP (MUC)	16/03/15	16:04	58°21.274 S	62°10.039 W	3092
PS97/0114-01	SVP (MUC)	29/03/15	09:39	54°34.720 S	76°38.834 W	3865

Operation

Data acquisition started on February 20th, 2016 at 23:07 UTC on the Argentinian shelf and lasted until April 6th, 2016, 16:28 UTC on the Chilean Shelf near the Strait of Magellan. From March 10th, 2016, 18:06 UTC to March 11th, 2016, 18:10 UTC and on March 12th, 2016, from 07:24 to 19:20 UTC the system was switched off because *Polarstern* was outside the UBA permitted area at the Antarctic Peninsula near Elephant Island. It was switched off again on March 25th, 2016, from 10:23 to 13:42 UTC and on March 26th, 2016, from 09:46 to 17:23 UTC while staying in the 3 nm zone of Chile near Cape Horn Island and in the Bahia Cook (due to bad weather conditions). Eventually, the system was switched off in the 3 nm zone in the Strait of Magellan from April 4th, 2016, 19:07 UTC to April 6th, 2016, 03:57 UTC, when *Polarstern* had a weather related stop. The echo sounder was operated fully supervised by three operators in a 24/7 shift mode.

Generally, the system was running stable and continuous data recording was possible. However, during the cruise the system had to be restarted several times, which caused data gaps with a total duration of about 1.5 hours. Furthermore, several smaller data gaps (1-2 min) occurred due to CM Recovery actions automatically performed by the echo sounder. Especially on steep slopes (deep sea – shelf transition) the bottom detection sometimes did not work properly which lead to additional data gaps in these regions.

For data processing, the *.asd-files were imported in the software CARIS HIPS&SIPS Version 9.0. All raw data were already processed during the cruise. Data were corrected for

refraction errors using the sound velocity profiles and cleaned from severe depth errors using the “Swath Editor”, a ping-by-ping data-cleaning editor. Occasionally the “Subset Editor” was used for data cleaning, where data can be viewed and cleaned region-based in a 2D- or 3D-view. The processed data were exported to ASCII-files, gridded and – for data access, station planning and further use – integrated into an ESRI ArcGIS project. Furthermore, maps were produced with ESRI ArcGIS and 3D-visualizations were obtained with QPS Fledermaus.

Preliminary results

During PS97, an area of about 69,128 km² with a track length of about 5,886 nm was mapped within 46 days. Figure 6.1.1 shows an overview of the acquired multibeam data coverage. The data were mainly recorded to search suitable coring sites. The focus was set to sediment drifts, depressions acting as sediment traps and glacial-geomorphological features especially on the continental shelf. In the following, for each of the four working areas an overview map and examples for characteristic and task features are represented. The Global Multi-Resolution Topography synthesis (GMRT, Ryan et al., 2009) data set is used as background data for all overview maps.

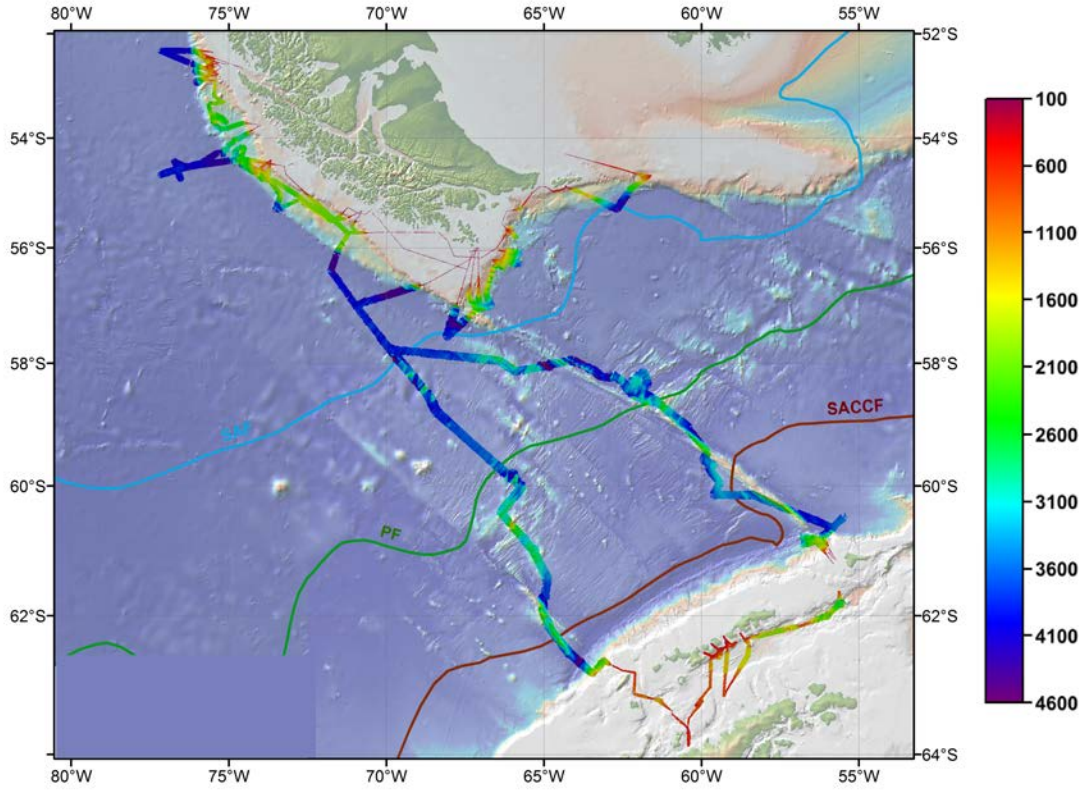

Fig. 6.1.1: Overview map of the multibeam data coverage for PS97 (Map projection: World Mercator, Background data: GMRT (Ryan et al., 2009))

Scotia Sea Margin

From February 21st, 2016 to February 24th, 2016, and from March 21st, 2016 to March 25th, 2016, *Polarstern* operated in the working area *“Scotia Sea Margin”*. Figure 6.1.2 shows an overview of the multibeam data collected in this region. Water depths range between 70 m and 4548 m comprising the continental shelf, the slope and parts of the deep sea. Glacial-geomorphological bed forms have been observed northeast of *Isla de los Estados* (Figure

6.1.3). South of *Cape Horn Island* the continental slope is characterized by several submarine canyons. Drift controlled sediment structures suitable for coring have been observed for example 40 nm northeast of *Cape Horn Island* in about 650 m water depth (Figure 6.1.4 and 6.1.5) and 65 nm south of *Cape Horn Island* in about 2300 m water depth.

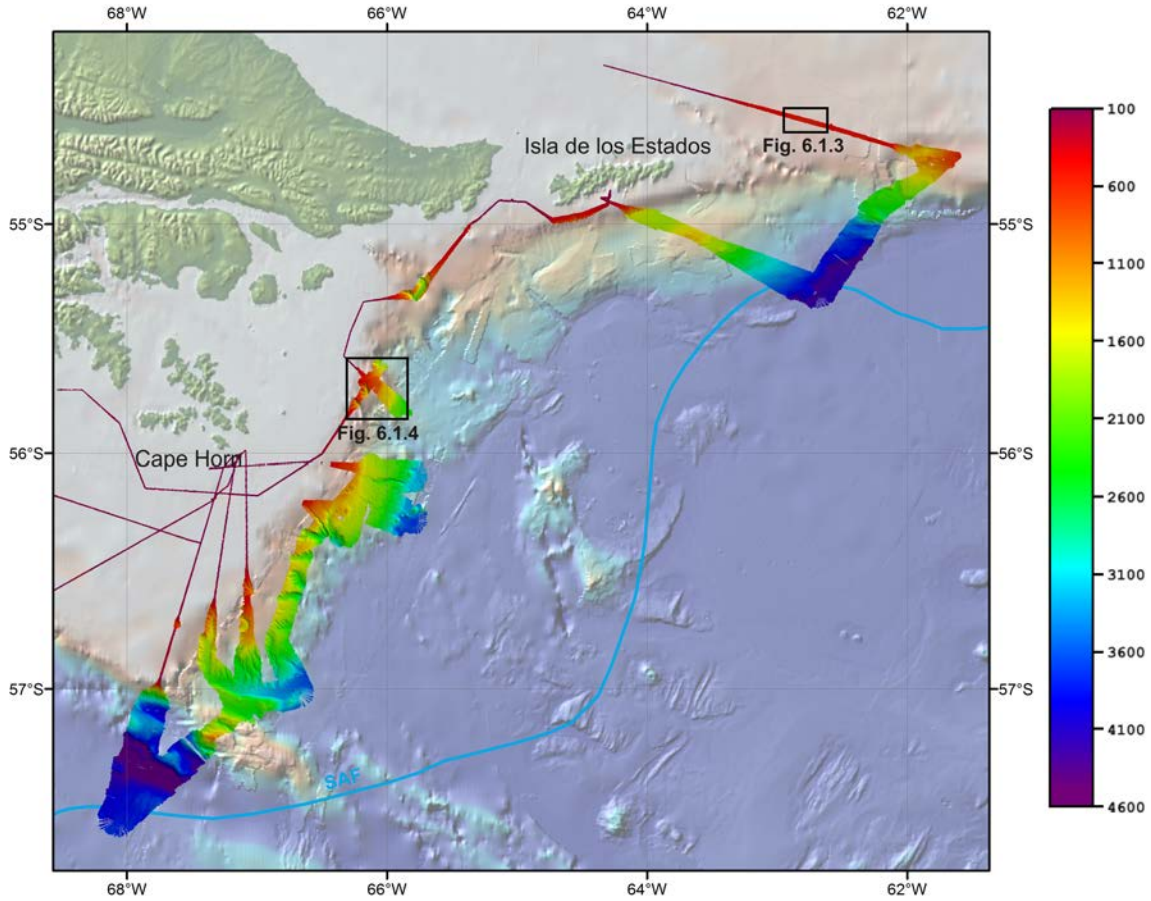

Fig. 6.1.2: Overview map of multibeam data collected in the working area Scotia Sea Margin (Map projection: World Mercator, Background data: GMRT (Ryan et al., 2009)). The black boxes mark the locations of the detail maps in Figure 6.1.3 to 6.1.5.

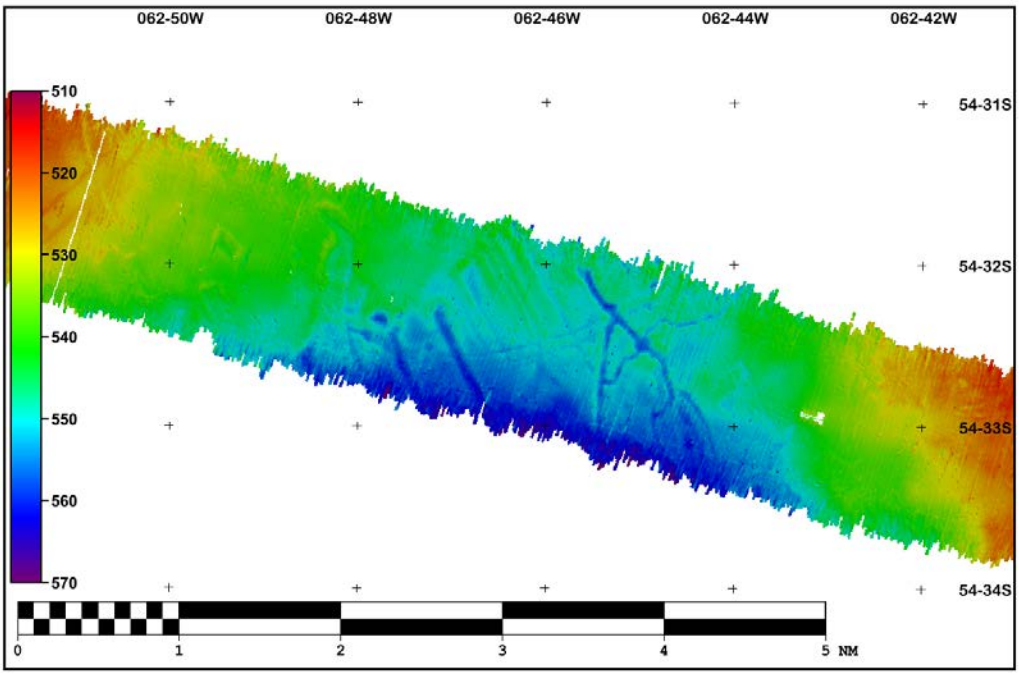

Fig. 6.1.3: Detail map (grid cell size: 20 m) of glacial features observed northeast of Isla de los Estados (Map projection: UTM Zone 20S).

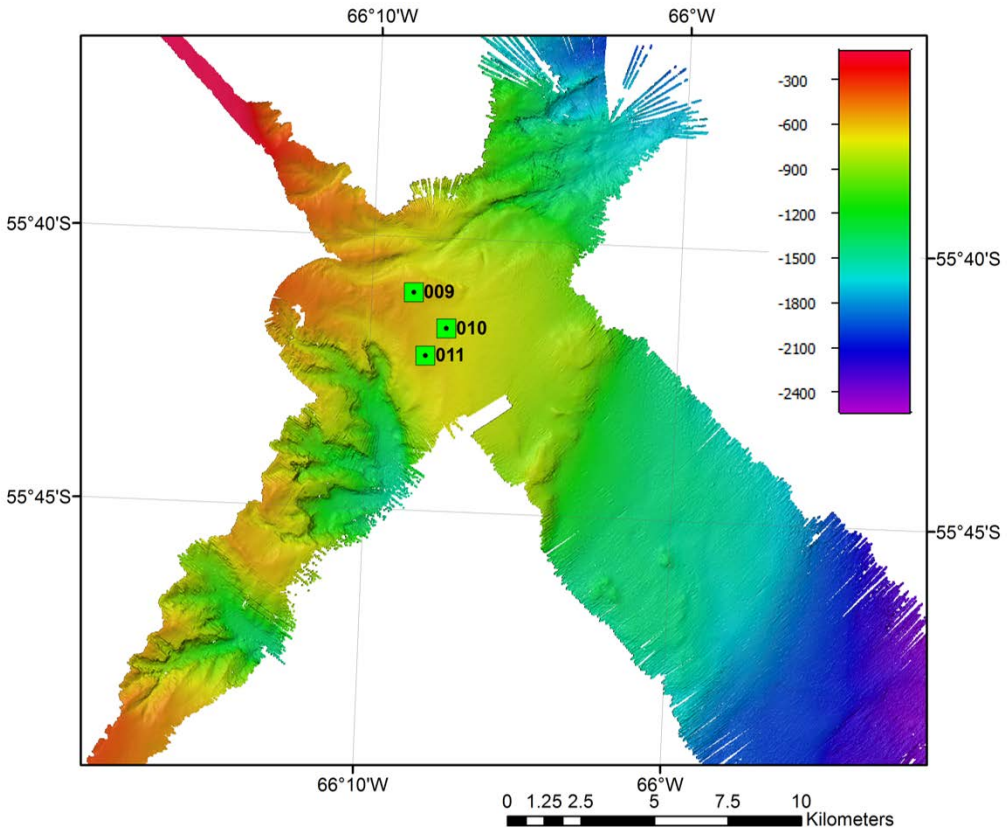

Fig. 6.1.4: Detail map (grid cell size: 40 m) with bathymetry data collected 40 nm northeast of Cape Horn Island (Map projection: UTM Zone 19S). Green squares indicate core locations.

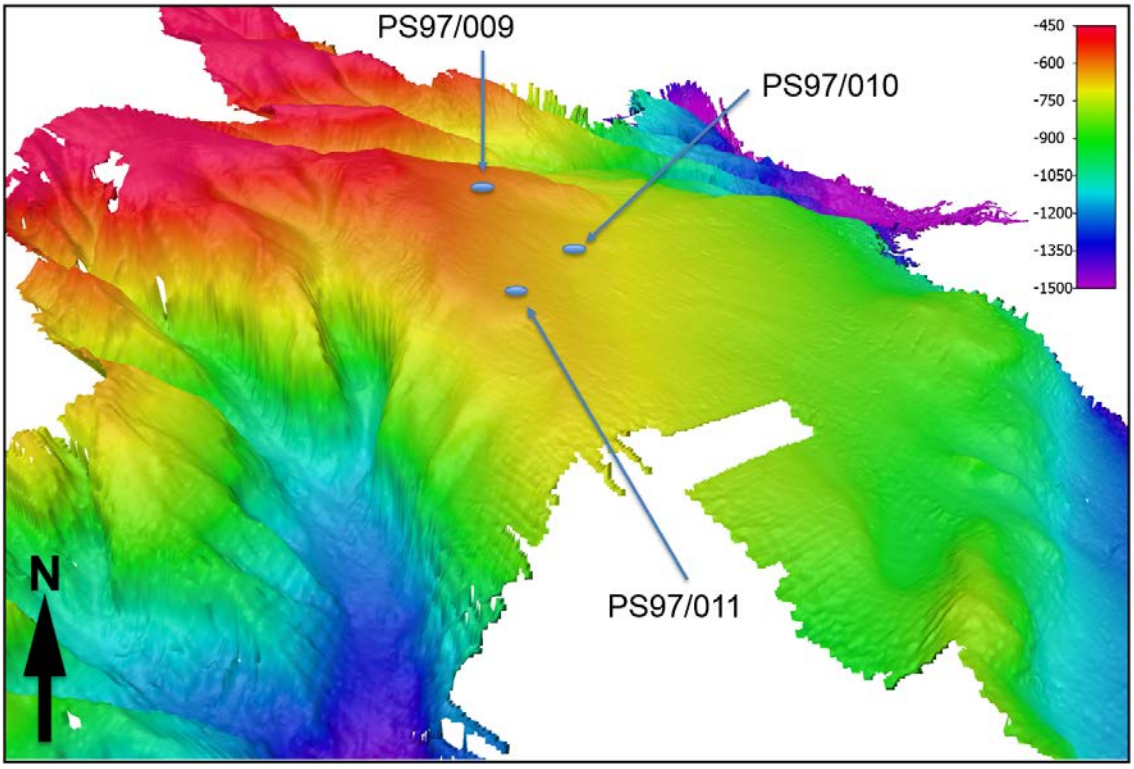

Fig. 6.1.5: 3D view of the bathymetry data shown in Figure 6.1.4 (grid cell size: 40 m)

Pacific Chilean Margin

The working area "Pacific Chilean Margin" was visited by *Polarstern* from February 25th, 2016 to February 28th, 2016, and from March 26th, 2016 to April 06th, 2016 (Figure 6.1.6). Water depths range between 56 and 4389 m comprising the continental shelf, the slope with submarine canyons and two transect of 90 nm and 48 nm to the deep sea crossing the Chile Trench. The trench with a maximum depth of 4389 m seems to be levelled by sediment accumulations. Bathymetric elevations along the margin associated with sediment accumulations and hence suitable for coring have been observed around 32 nm west of Isla Noir (Figure 6.1.7).

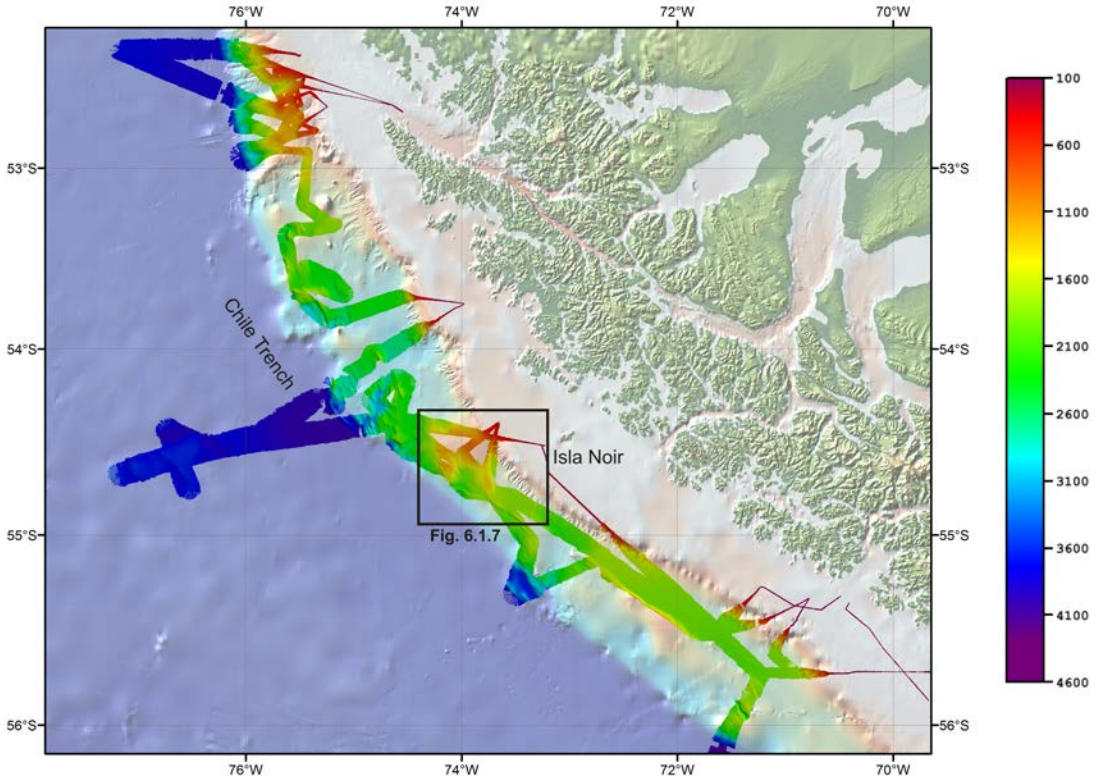

Fig. 6.1.6: Overview map of multibeam data collected in the working area Pacific Chilean Margin (Map projection: World Mercator, Background data: GMRT (Ryan et al., 2009)).

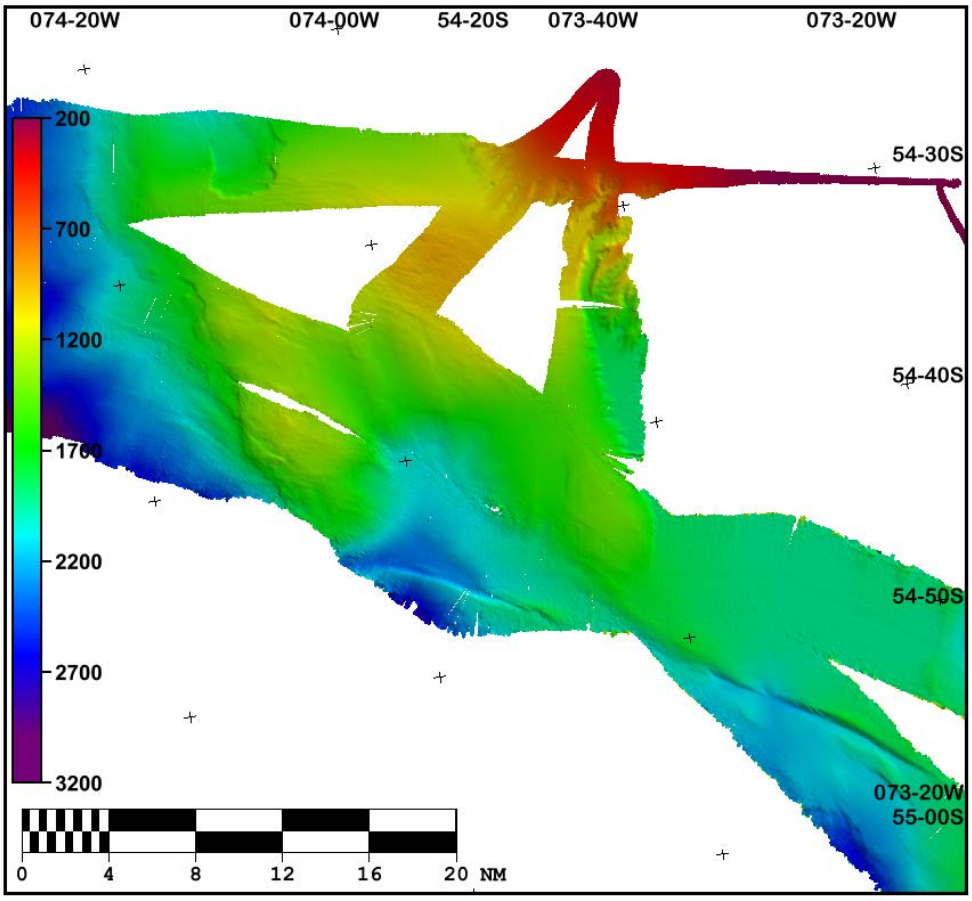

Fig. 6.1.7: Detail map (grid cell size 100m) of multibeam data collected west of Isla Noir (Map projection: UTM Zone 20S).

Drake Passage

The working area "DP" was visited by *Polarstern* from February 28th, 2016 to March 5th, 2016, and from March 14th, 2016 to March 20th, 2016 (Figure 6.1.8). Water depths range between 976 m and 4913 m. The DP was crossed once in southern ("Western DP") and once in northern direction ("Central DP"). A prominent feature observed in the "Western DP" is the Antarctic Phoenix Ridge with a minimum observed water depth of 976 m (Figure 6.1.9). The track through the "Central DP" was set along the Shackleton Fracture Zone. In total, the zone was crossed three times. In the centre of the DP, at the Scotia Ridge (west of the Shackleton Fracture Zone) a local high with promising sediment accumulations has been observed (Figure 6.1.10).

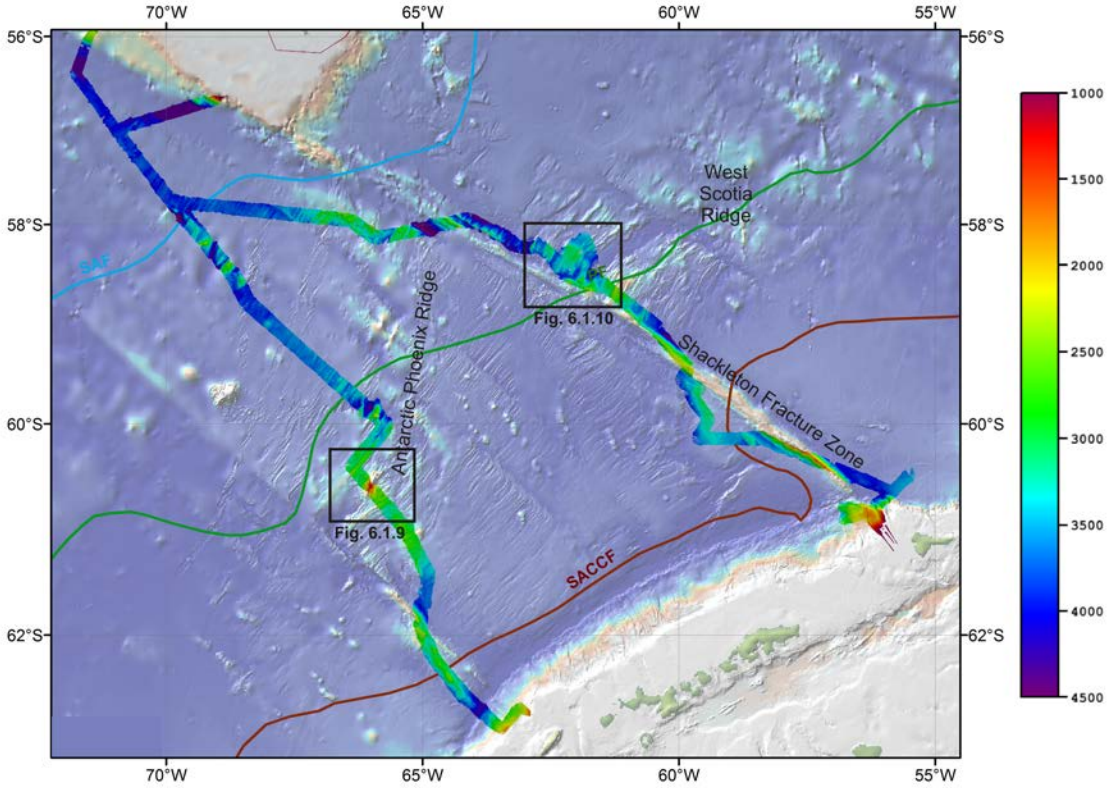

Fig. 6.1.8: Overview map of multibeam data collected in the working area DP (Map projection: World Mercator, Background data: GMRT (Ryan et al., 2009)).

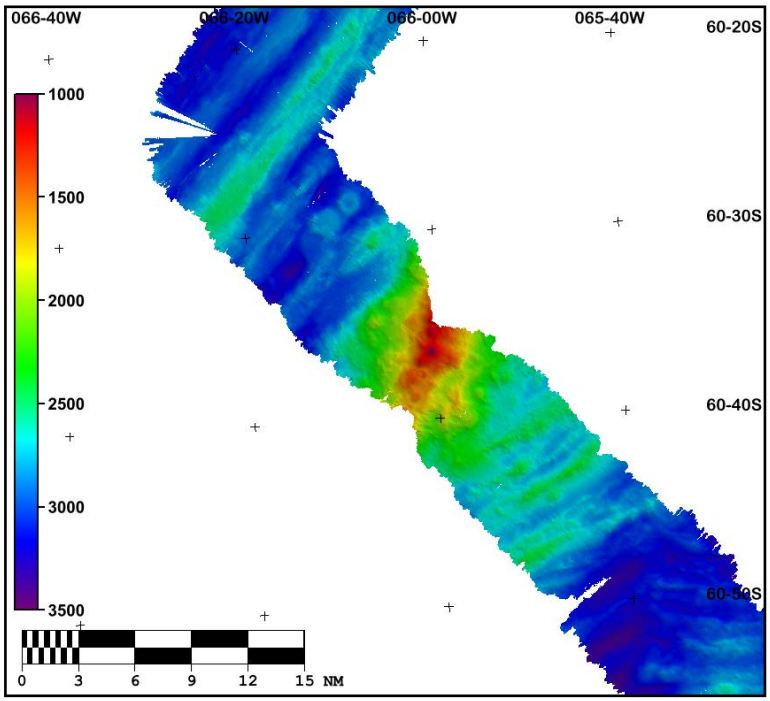

Fig. 6.1.9: Detail map (grid cell size 200 m) of multibeam data collected at the Antarctic Phoenix Ridge (Map projection: UTM Zone 20S).

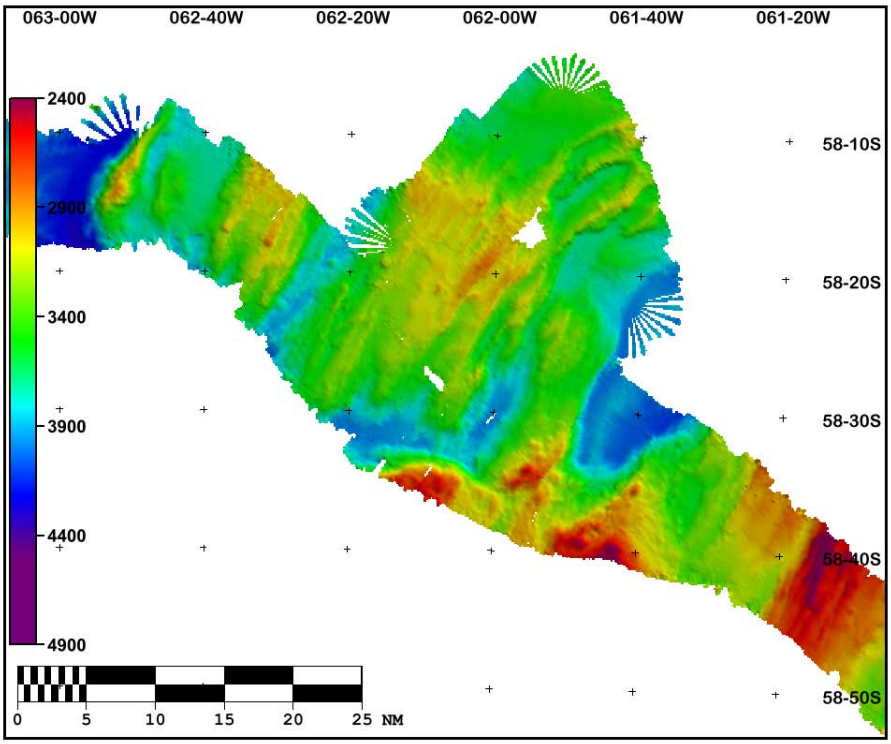

Fig. 6.1.10: Detail map (grid cell size 200 m) of multibeam data collected at the Scotia Ridge, west of the Shackleton Fracture Zone (Map projection: UTM Zone 20S).

Antarctic Peninsula

The working area "Antarctic Peninsula" was visited by *Polarstern* from March 6th, 2016 to March 13th, 2016 (Figure 6.1.11). In this region area wide data sets of multibeam swath bathymetry already exist. The data recorded in course of this cruise were used to fill small gaps in the existing data set and to provide up-to-date water depth during coring. Water depths range between 86 m and 2858 m. The shallowest water depth has been observed in the straits between the Southern Shetland Islands and in Maxwell Bay. The deepest observed point is located in the Wordie Caldera about 35 nm south of Elephant Island. Glacial-geomorphological features were identified at several locations, especially at the entrances of the straits between the South Shetland Islands at water depths between 500 m and 800 m. Figure 6.1.12 and 6.1.13 show some glacial formed deposits (e.g. drumlins) in the Nelson Strait.

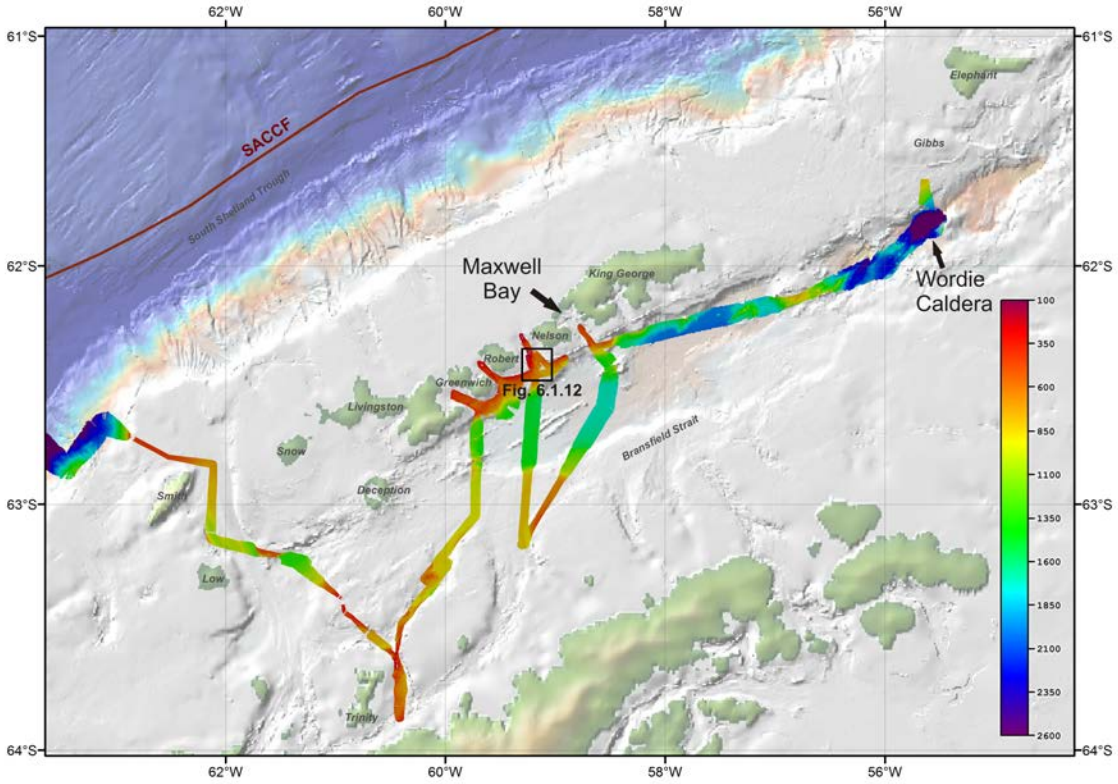

Fig. 6.1.11: Overview map of multibeam data collected in the working area Antarctic Peninsula (Map projection: World Mercator, Background data: GMRT (Ryan et al., 2009)).

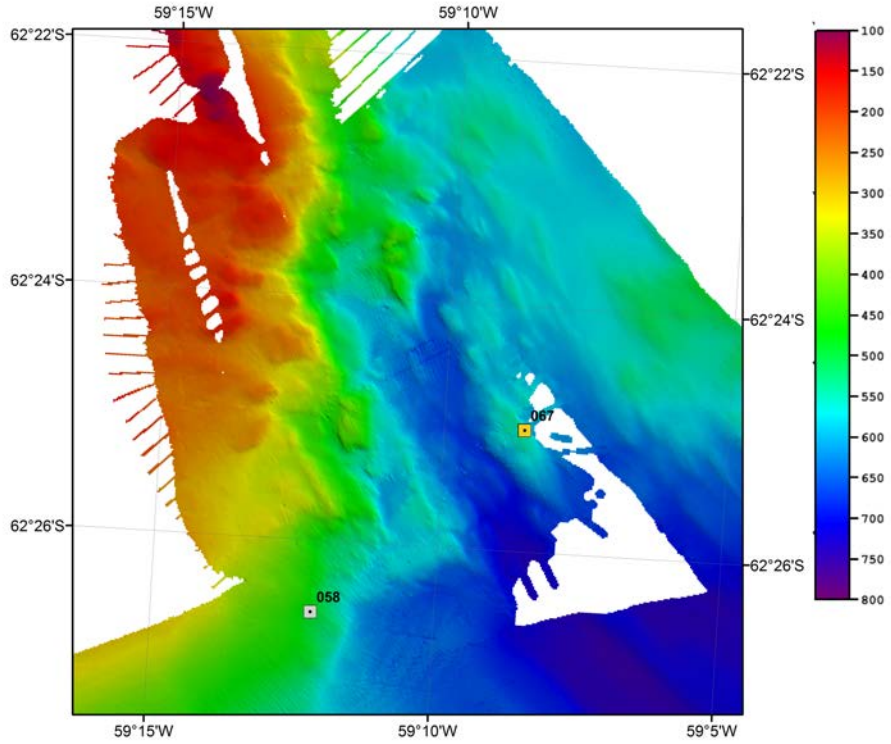

Fig. 6.1.12: Detail map (grid cell size 50 m) of multibeam data collected in the Nelson Strait (Map projection: UTM Zone 19S). The yellow square indicates the location of the Giant Box Grab taken at one of the drumlins. The gray square represents the station PS97/058 (GO-FLO).

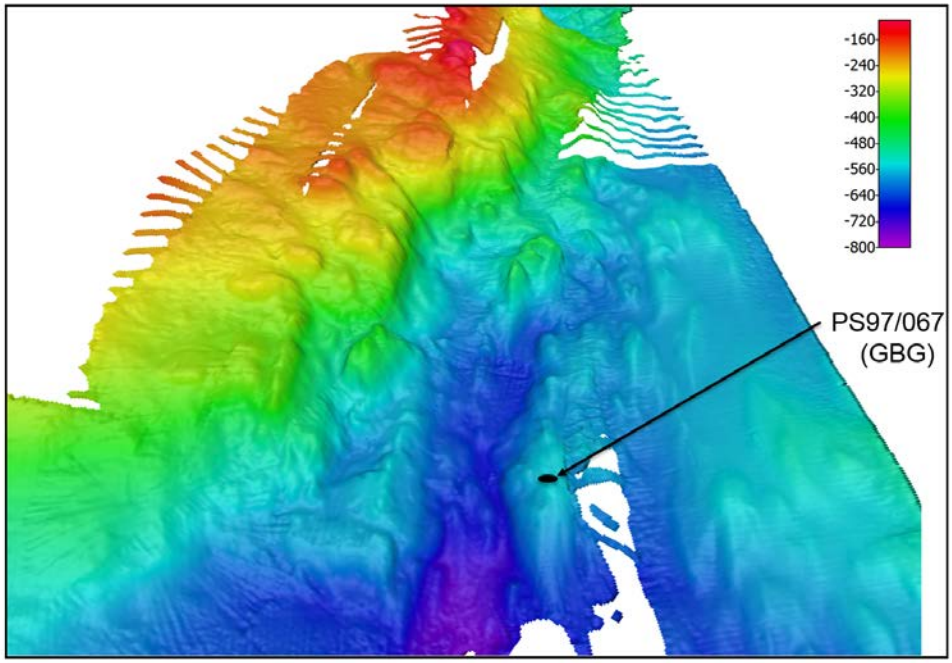

Fig. 6.1.13: 3D view of the bathymetry data shown in Figure 6.1.12 (grid cell size: 50 m)

Data Management

The recorded multibeam raw data will be stored in the long-term archive PANGAEA and will be available on request. The processed data will be stored in the bathymetric archive of the AWI bathymetry group and can be requested at infobathy@awi.de. Bathymetric data sets will be provided to mapping projects and added to regional data compilations, such as the International Bathymetric Chart of the Southern Ocean (IBCSO) and the General Bathymetric Chart of the Oceans (GEBCO).

References

Ryan, W.B.F., Carbotte, S.M., Coplan, J.O., O'Hara, S., Mekonian, A., Arko, R., Weissel, R.A., Ferrini, V., Goodwillie, A., Nitsche, F., Bonczkowski, J., Zemsky, R. (2009). Global Multi-Resolution Topography synthesis. Geochem. Geophys. Geosyst., 10, Q03014, doi: 10.1029/2008GC002332.

6.2 Marine sediment echosounding (PARASOUND)

Helge Arz[1], Jürgen Gossler[2], Henrik Grob[3], Sjard Stratmann[3], Gerhard Kuhn[4]

[1]IOW, [2]KUM GmbH, [3] U Hamburg, [4]AWI

Objectives

The objectives of sediment echosounding during cruise PS97 included:

- Selection of coring stations based on acoustic patterns and backscatter,
- Obtaining different pattern of high-resolution acoustic stratigraphy useful for lateral correlation over shorter and longer distances thereby aiding correlation of sediment cores retrieved during the cruise,
- Providing a high-resolution supplement of the uppermost sediments as part of the IODP seismic pre-site survey,
- Improvement of information on the sediment distribution in the DP

Work at sea

Technical settings

The sediment echosounder PARASOUND DS III - P70 (Atlas Hydrographic, Bremen, Germany) is permanently installed aboard *Polarstern*. It records sea floor and sub-bottom reflection patterns and thus characterizes the upper sediment layers according to their acoustic behaviour.

A transducer array is mounted in the ship's hull. It transmits an acoustic signal, which propagates through the water column down to the sea floor where parts of the signal are reflected. Other parts penetrate the sea floor and are reflected at boundaries between sediment layers. In Fig. 6.1, a comparison of the returning echo, the PARASOUND online echogram and the density record of core PS97/114-2 is shown. The correlation between the size of amplitude of the returning echo and the density of the upper sediment layers can be seen clearly. The denser a sediment layer the larger the reflected signal.

PARASOUND uses the parametric effect. It produces additional frequencies through non-linear acoustic interactions of finite amplitude waves. By emitting two primary sound waves of higher frequency (18.8 and 22.8 kHz) a signal of the differential frequency (4 kHz) is generated. Due to its longer wavelength the secondary low frequency (SLF) signal allows a sub-bottom penetration up to 200 m (depending on the thickness of the sediment cover and its density and composition) with a vertical resolution of 30 cm. Due to the parametric effect the pulse is generated within the narrow emission cone (4°) of the primary high frequencies (PHF) and thereby a very high lateral resolution compared to conventional 4 kHz-systems is provided. The secondary high frequency (SHF) is a sum signal of the primary frequency and was not used during PS97.

The PARASOUND system is controlled by two operator software packages (ATLAS HYDROMAP CONTROL, ATLAS PARASTORE-3) and server software running in the background. These processes are running simultaneously on a PC using a Windows XP operating system. ATLAS HYDROMAP CONTROL is the control software for the echosounder. It is used to set the modes of operation, sounding options and ranges. ATLAS PARASTORE-3 is an acquisition and visualisation software.

During profiling and station work south of 60°00' S, whale watching was carried out. In the event that marine mammals would have been observed close to the vessel, the PARASOUND system would have been switched to "Standby" following the regulations of the German "Umweltbundesamt" (UBA).

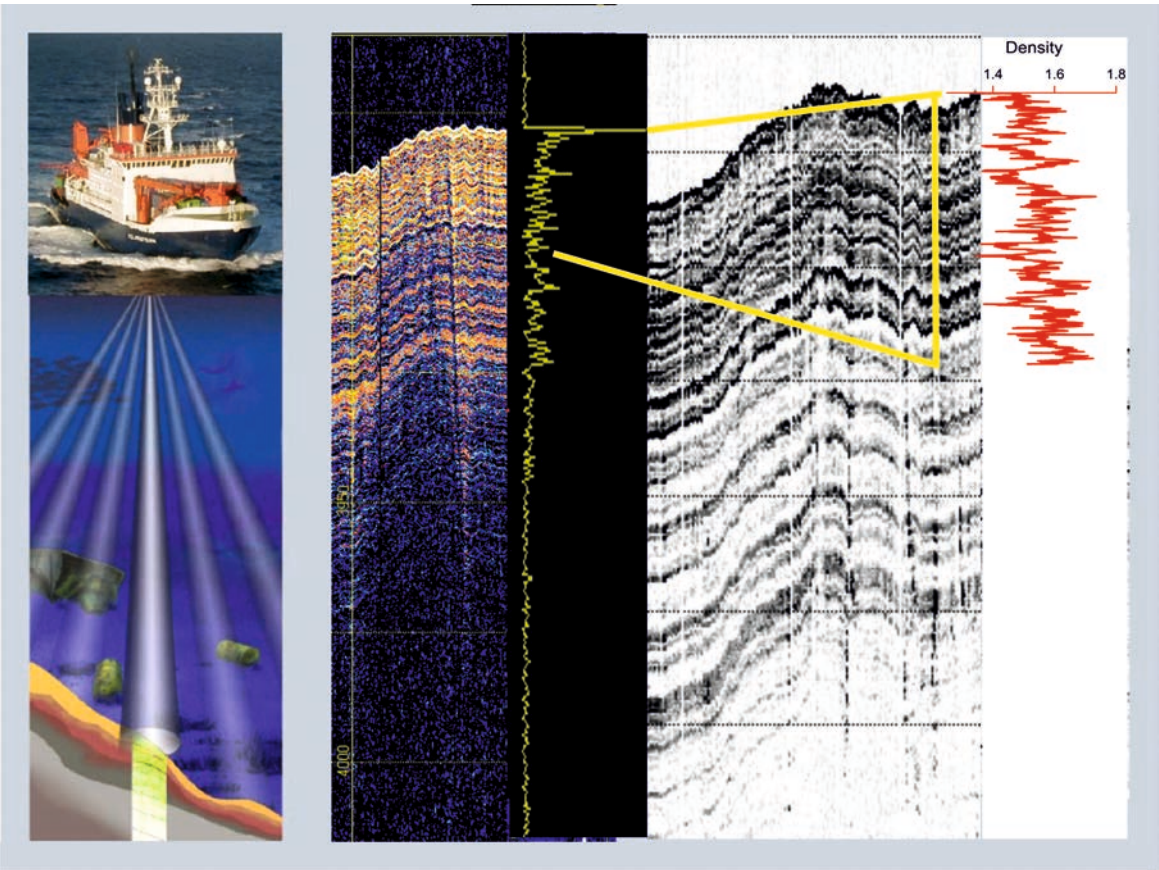

Fig. 6.2.1: Comparison of returning echo, PARASOUND online echogram and GRA-density record of core PS97/114-2

Time windows with data of special interest (e.g. geological structures at or near stations) were replayed during the cruise using optimal settings of ATLAS PARASTORE-3. The software SeNT (University of Bremen) was used for visualizing PS3 files of the SLF signal for interesting areas. Representative examples from all working areas are shown in the Marine Geology and Paleoceanography Chapter 3.5. The echograms of all coring stations are shown in A. 10.

Data acquisition and storage was generally on all the time; except for transits outside the permitted working areas of the Chilean and Argentinian EEZ. Acquisition included PHF and SLF data. Both frequencies were stored in ASD (Atlas Sounding Data) format. This is a raw file format and stores the complete sounding profiles including reflections from the water column, the seafloor, and the subsurface echoes down to 200 m bottom penetration. The SLF signal was additionally stored in PS3 and SEG-Y format. These formats only save data that are displayed in the PARASTORE reception window (200 m depth window). Both PHF and SLF traces were visualized as online profiles on the screen and additionally stored as screen shots. Furthermore, navigation data and general PARASOUND settings as well as ATLAS PARASTORE-3 settings were stored in ASCII format for the duration of data acquisition. SLF profiles (200 m depth window) and online status prints were printed on A4 pages.

While steaming, the quasi-equidistant transmission mode for signal transmission was used. The desired time interval between signal transmissions was set between 1000 and 2000 ms. During station work, the transmission mode was set to single pulse in order to reduce data

volume. The system was operator-controlled during PS97 (watch keeping). Book keeping was carried out including basic PARASOUND system settings, some navigation information, various kinds of remarks.

The system depth source was set to the multibeam echosounder HYSROSWEEP DS2. Depth measurements in steep slope areas were, however, not always stable and occasional failures occurred. As documented already in a detailed PS95 heave analysis report, most of the recorded sediment-acoustic profiles of PS97 show wave-like artefacts related to the delayed arrival of the motion sensor heave data.

Preliminary results

After pre-selection of working areas based on oceanographic and marine geological background information, PARASOUND acoustic profiles played an important role in locating coring stations. Site selection was based on acoustic patterns such as the strength of characteristic reflectors, their spacing, and the total sub-bottom penetration. A short outline regarding the general sediment cover and sub-bottom penetration as well as special geological structures recorded with the PARASOUND system within the individual working areas of PS97 is given in the respective subchapters of the preliminary results in the Marine Geology and Paleoceanography Chapter 3.5.

Data Management

The recorded PARASOUND data will be stored in the long-term archive PANGAEA and will be available on request.

6.3 Seismic imaging for IODP pre-site survey

Frank Lamy[1], Sjard Stratmann[2], Henrik Grob[2], Jürgen Gossler[3],
Not onboard: Christian Hübscher[2], Karsten Gohl[1], Alina Polonia[4]

[1]IOW, [2]KUM GmbH, [3] U Hamburg, [4]AWI

Objectives

The Subantarctic Southeast Pacific (SEP) is a particularly sensitive region where atmosphere-ocean changes between high-, mid- and low latitudes are strongly coupled. The SEP provides a unique opportunity to obtain exceptionally highly-resolved sediment records to document millennial and orbital-scale Plio/Pleistocene ocean-atmosphere changes and their implications for global climate. The deactivated IODP drilling proposal SUBANTPAC targeted two drilling area, at the southernmost Chilean Margin and in the central Pacific Southern Ocean. Both regions likely provide sediment records with high sedimentation-rates that allow resolving orbital and millennial-scale variations throughout the Pleistocene and at least parts of the Pliocene.

The following primary objectives are targeted by the SUBANTPAC IODP proposal:

- Paleoceanographic role of the DP for Plio/Pleistocene global climate.
- High-low latitude linkages in the Subantarctic SEP.
- Plio/Pleistocene temperature evolution in the Subantarctic Pacific.
- Paleoceanographic changes associated with the Subantarctic Front.
- Changes in Subantarctic productivity, nutrient consumption/utilization, and dust fluxes.
- Patagonian Ice Sheet changes and their role in global climate.

In addition to the completion of seismic surveys, Expedtion PS97 collected bathymetric and PARASOUND information as well as sediment cores at potential IODP sites. This combination of hydroacoustic surveys and piston coring will produce the appropriate pre-site survey database needed for drilling of Cenozoic sediments in the Subantarctic Pacific Ocean. Based on these newly acquired data, a revised full proposal for drilling in the SEP will be submitted by October ^{t}, 2016.

Work at sea

Multi-channel reflection seismics (MCS) - Seismic source, triggering and timing

A multichannel seismic (MCS) survey has been realised to image the seismic record of sediments and basement in the area of the proposed IODP sites at the upper continental slope in front of the Strait of Magellan (Fig. 6.3.1b) and further south west of the Chile trench in a deep sea in a deep sea environment (Station PS97/112; Fig. 6.3.1a). Over all more than 120 nm were multichannel seismics were acquired.

Both sites were surveyed with a cross profile with each axis of about 20 nm profile length. The high-resolution reflection lines were shot using one GI-Gun (Fig. 6.3.2). A GI-Gun produces a highly reproducible primary seismic signal. GI-Guns consist of two chambers – the generator and the injector. Here, both were used with volumes of 105 in^3 each. They were filled with compressed air at 160 bar. By firing the first chamber (generator) it produces an expending, oscillating air bubble. The bubble signal results from oscillation of the air bubble. This bubble pulses are undesirable noise. For prevention of this oscillation and for

stabilizing the air volume, it is necessary to release the highly compressed air in the second chamber (injector) and inject it into the first air bubble with a delay of 24 ms.

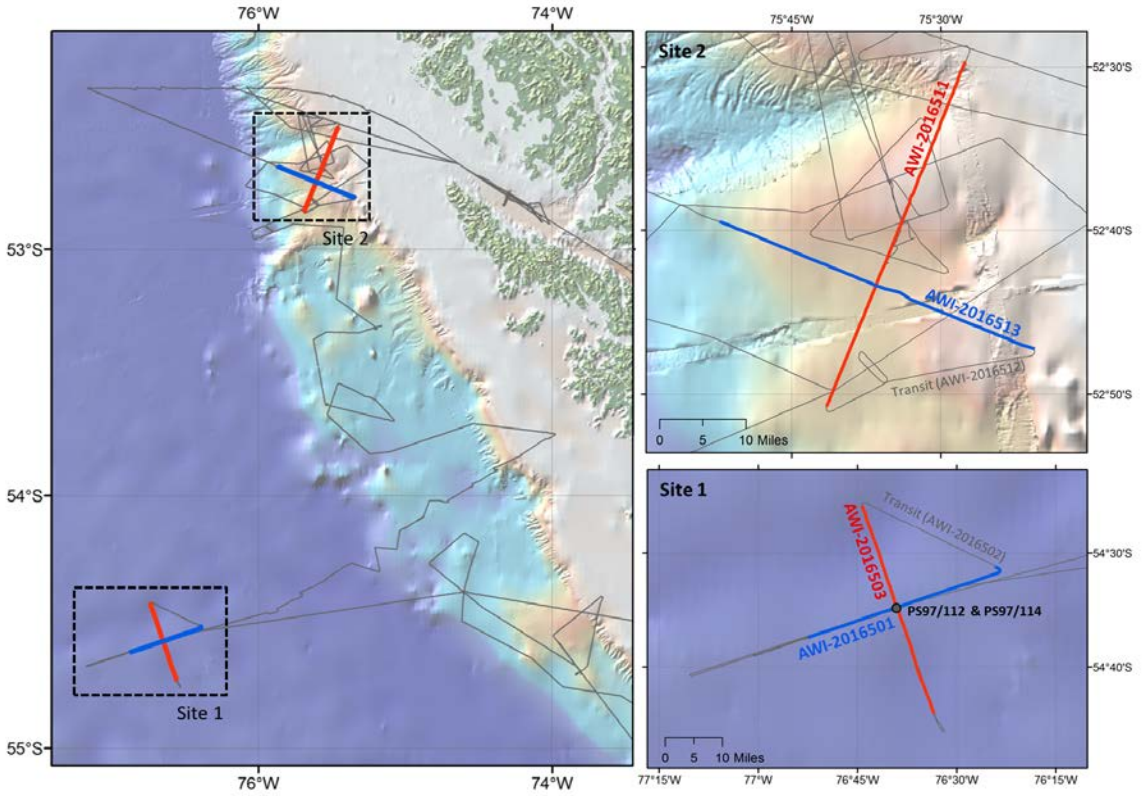

Fig. 6.3.1: Location of seismic profiles for potential IODP drill sites in the Southeast Pacific. a) First cross transect in the off the Chilean margin. b) Second cross transect at the upper continental slope off the Strait of Magellan.

The GI-Guns were towed circa 30 m behind the vessel in 5 m depth. With a shot interval of 10 s and 15s and for cruise velocity of 5 knots the shot distance is 25 m or 37.5 m respectively. This provides a good lateral resolution.

Fig. 6.3.2: GI-Airgun used for the seismic survey (Photo: Thomas Ronge (AWI)).

Seismic data acquisition requires very precise timing systems, because seismic sources and recording systems must be synchronised. A combined electric trigger-clock system was in operation in order to provide the firing signal for the electric airgun valves and the time-control of the seismic data recording. The clock is synchronised by GPS data.

Fig. 6.3.3: The 600 m long analogue streamer (front) (Type PRAKLA) (Photo: ?).

Multi-channel reflection recording system

As part of the multi-channel reflection data acquisition system, a 600 m long (active sections), 96 channel (hydrophones groups) analogue streamer (Type Prakla) was used (Fig. 6.3.3). Multi-channel streamers enhance data quality because translational accelerations are eliminated and due to signal summation the signal-to-noise ratio (S/N-Ratio) increases.
The analogue signals were digitized by analogue-digital (A/D) converter (Geodes). The seismic data were sampled with 1 ms in SEG-Y file format to a Geometrics™ acquisition system.

Processing of multi-channel reflection seismic data

A single streamer acquisition layout is a 2D geometry. This acquisition layout is designed for common-midpoint (CMP) sorting and CMP-based processing. On-board CMP coordinates were calculated and traces were binned. For quality control (QC) single- and multi-channel sections were processed.

Additionally, a first frequency filtering, gaining, time-invariant trace balancing and also dip filtering were applied. Normal moveout was corrected with constant velocity and all data were stacked afterwards, so that primary signals are constructively enhanced and incoherent noise is destructively eliminated. The resulting so-called brutestack presents the very first image of the subsoil in the time-domain (Fig. 6.3.5, Fig. 6.3.7). Only near-offset channel sections were time-migrated with constant velocity to reduce time-consuming computation

time. Nevertheless, to obtain a fully high resolution, noise-reduced seismic image of the subsurface a detailed onshore post-processing is imperative.

Fig. 6.3.4: Photo of RV Polarstern with the towed airgun and 600 m multi-channel streamer (Photo: ?).

Preliminary results

Potential IODP Site 1

The potential deep sea IODP site in front of the Chilean Margin is located nearly 95 miles off the Chilean Shelf in circa 3900 m water depth (Fig. 6.3.1a). The profiles AWI-20160501 and AWI-20160503 are perpendicular to each other. Both profiles have a length of ~20 nm. Unfortunately, while transit from profile AWI-20160501 to AWI-20160503 data recording system had to be shut down a few times because of hardware problems. This provided a continuous recording on the profiles itself. Measuring with one GI-Gun only at depth up to 4000 m is of course not ideal. The signal-to-noise-ratio becomes weak and much noise is significant within the data. Hence, a good processing is indispensable.

The brutestack plots show a first high resolution image of the sedimentary layers and the acoustic basement at ~5.6 s TWT (Fig. 6.3.5). The sedimentary layers have been resolved clearly.

Fig. 6.3.5a shows the seismic line AWI-20160501 in SW-NE direction. The sediment layers are sub-parallel and well stratified until the acoustic energy is absorbed by the acoustic

basement indicated by diffraction hyperbolas. Sediments are shown in a homogeneous thickness of ~500 – 625 m.

Profile AWI-20160503 in NW-SE direction is shown in Fig.6.5b. The sediment is less wavy and more parallel in the upper sediment layers. The thickness of sediment is with 600 – 750 m and thus thicker than in profile AWI-20160503. Estimated sediment thicknesses may differ from real thicknesses because we approximated with velocities of 2000 – 2500 m/s.

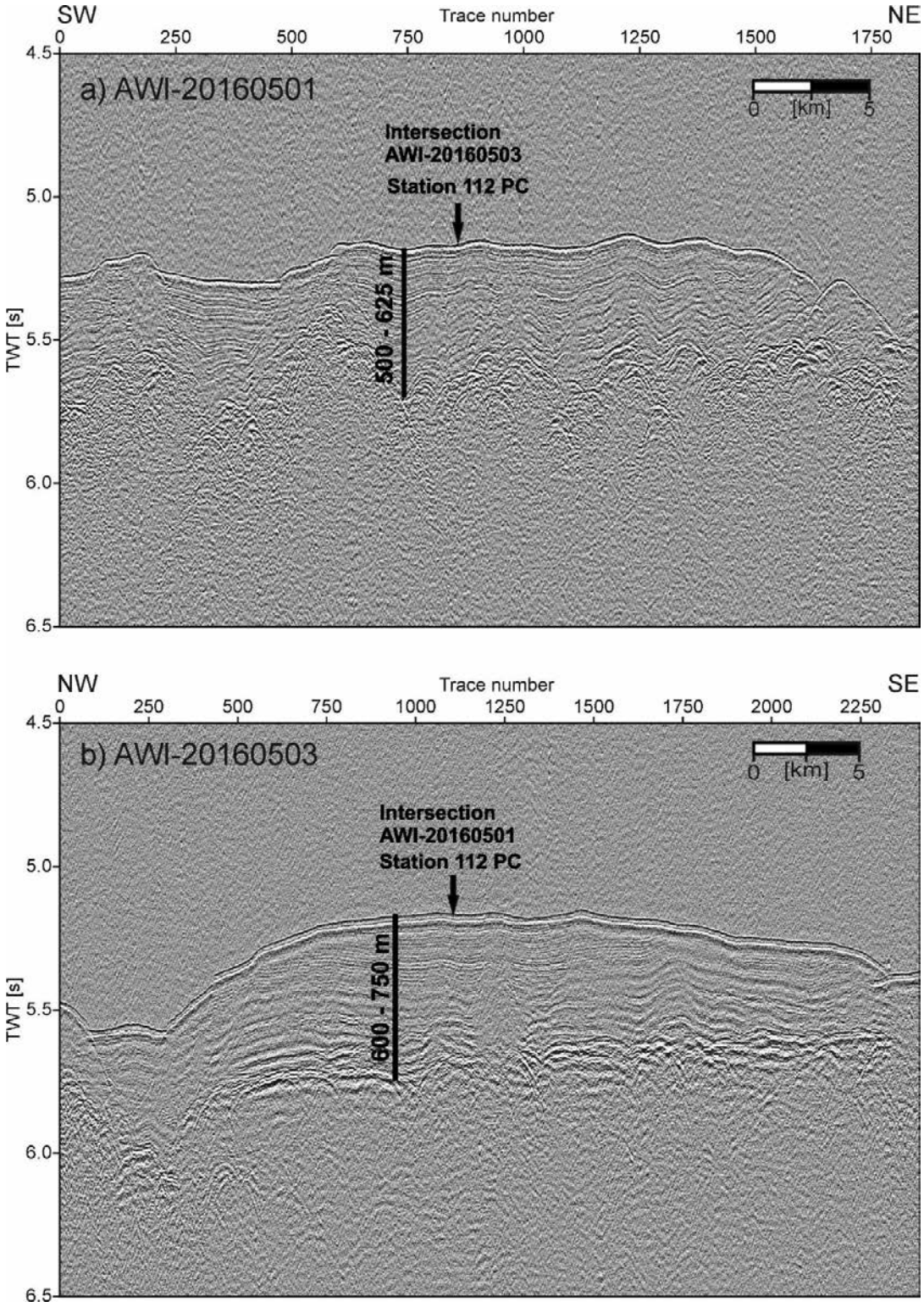

Fig. 6.3.5: Multi channel reflection sections potential IODP site 1. See Fig. 6.3.1a for localisation. a) Seismic line AWI-20160501 in SW-NE direction. b) Seismic line AWI-20160503 in NW-SE direction. The seismograms are shown as time-section with two-way traveltime (TWT) at y-axis. At the x-axis trace numbers are shown. Depth values are estimated with a sound velocity of 2000 - 2500 m/s. The arrows mark the location of piston core PS97/112-1 and PS97/114-1 and the intersection points.

Potential IODP Site 2

The second cross transect was performed at the Chilean Margin in front of the Strait of Magellan (Fig. 6.3.1b). Before doing seismics we discovered the intersection point with a multibeam and PARASOUND survey to ensure that the profiles are well selected. The PARASOUND offered high penetration of 50 m at well stratified drift controlled sediments (Fig. 6.3.6) at circa 1030 m water depth.

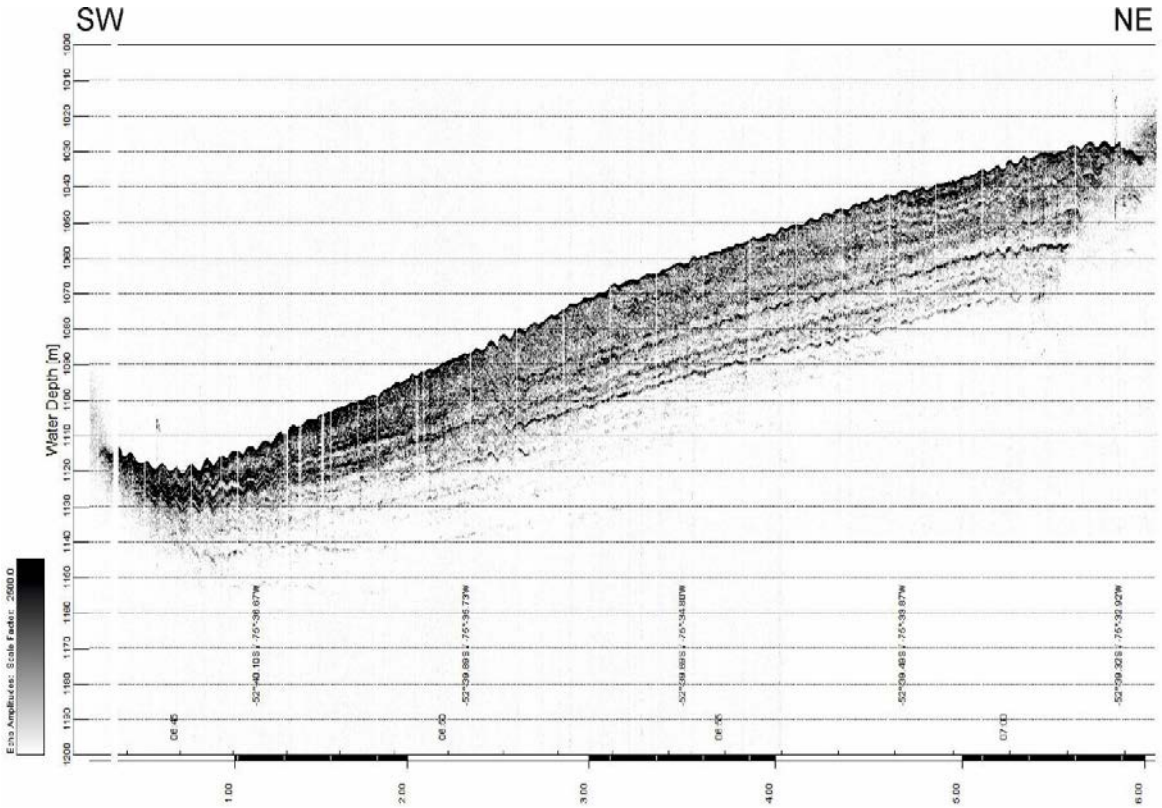

Fig. 6.3.6: PARASOUND profile from the pre-survey. The penetration amounts 50 m. The sediments are parallel and a relative deep penetration without strong impedances could indicate soft sediments.

Afterwards, we decided to perform the seismic survey along the PARASOUND track in order to extend the PARASOUND data to deeper than the first 50 m (Fig. 6.6). Profile AWI-20160511 (Fig. 6.3.7a) is orientated in NW-SE direction and shows a high-resolution image of the sediment distribution. The elongated drift body is imaged very well with a penetration down to the basement at ~2.2 s TWT (Fig. 6.3.7a). Due to the lower water depth of about 1030 m, noise is far weaker and reflections are much more distinct.

The drift body is characterized by sigmoidal, parallel sediment layers. It thins out towards north-east and is terminating at the basement with onlap terminations (Fig. 6.3.8). The thickest point is located at ~CMP 4400. By calculating the thickness with constant velocities of 2000 and 2500 m/s results in estimated 700 – 875 m sediment thickness.

Originally, the cross section was defined at ~CMP 3100. After finishing the first line and processing a first seismic line, we noticed that the position of the intersection provides only relatively thin sediment cover. Hence, the intersection was redefined further south to the position with deepest penetration at ~CMP 4400. Line AWI-20160513 (Fig. 6.3.7b) crosses

line AWI-20160511 at thickest part of the sediment drift. It is orientated in SE-NW direction. The sediments thin towards SE and SW. Internal reflections determinate at the borders of the channel-formed basement. The thickest location is at ~CMP 3200. Calculated thickness conforms approximately 750 – 940 m (Fig. 6.8).

Data Management

The recorded seismic data will be stored in the long-term archive PANGAEA and will be available on request.

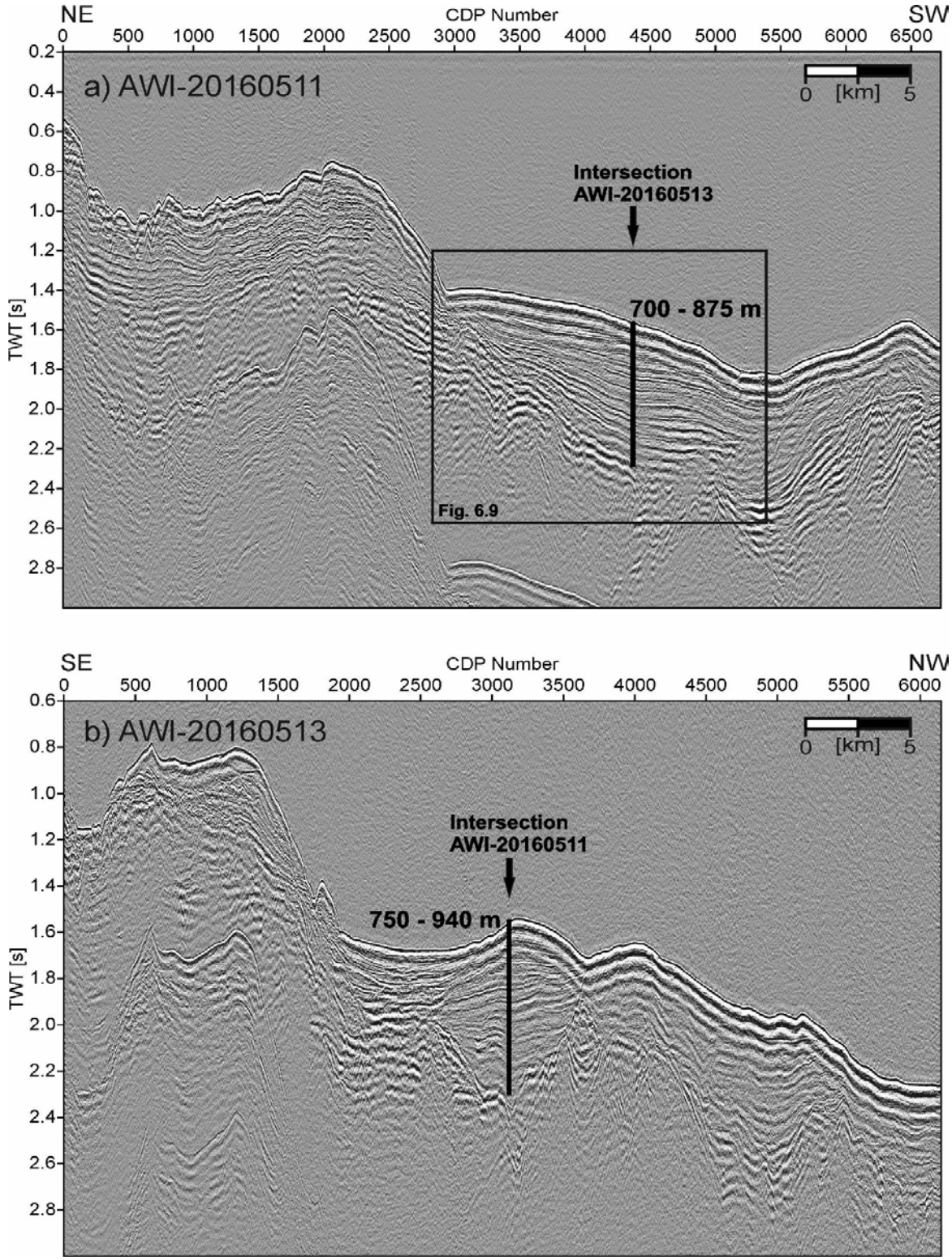

Fig. 6.3.7: Multi-channel reflection sections of potential IODP site 2. a) Seismic line AWI-20160511 in NE-SW direction. b) Seismic line AWI-20160513 in SE-NW direction. The seismograms are shown as time-section with two-way traveltime (TWT) at y-axis. At the x-axis CMP numbers are shown. Depth values are estimated with a sound velocity of 2000 - 2500 m/s.

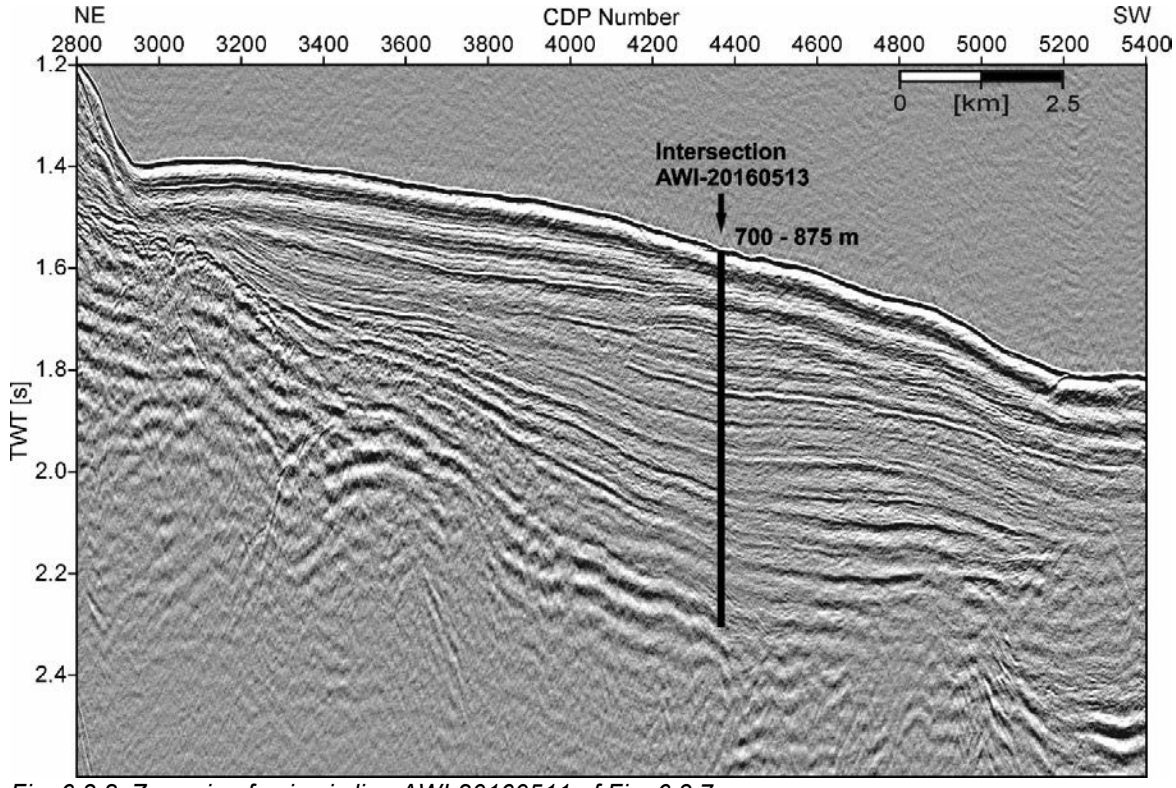

Fig. 6.3.8: Zoom-in of seismic line AWI-20160511 of Fig. 6.3.7a.

7. BIOLOGY

S. Blanco-Ameijeiras[1], D. Cabanes[1], C. Hassler[1], J. P. Heiden[2,3], P. Karitter[2], F. Koch[2], F. Lelchat[1], M. Sieber[4], H. Simon[5], S. Trimborn[2,3], C. Völkner[2], R. Zimmermann[2]

[1] U Geneva
[2] AWI
[3] U Bremen
[4] ETHZ
[5] U Oldenburg

Objectives

Southern Ocean phytoplankton are major drivers of global carbon cycling accounting for 20% of the global annual primary production. One of the most challenging issues is to understand how trace metal limitation and cycling operates and how global change will impact the Southern Ocean ecosystem. The availability of trace metals, in particular iron, is considered the key factor governing Southern Ocean phytoplankton productivity and community composition. However, since phytoplankton are part of a complex food web, their interactions with other trophic levels can have profound effects on the dynamics of the system. This project aims to study the interconnected microbial processes that are driving the biogeochemical cycles of carbon as well as of trace metals such as iron, zinc, cobalt and manganese and B-vitamins. Our work will focus on viral-bacterial-phytoplankton interactions considering biologically excreted organic matter as a control for trace metal chemistry, the bioavailability of these trace metals to the plankton community, their effects on primary productivity and species composition and succession. The increase in atmospheric CO_2 has already resulted in a significant increase in aquatic CO_2 concentrations and thus lower pH values ('ocean acidification') compared to pre-industrial times, potentially affecting plankton community structure as well as iron chemistry. This study will also evaluate the sensitivity of phytoplankton of different regions to climate change scenarios and trace metal availability in order to predict the response of the plankton community to these future changes. This project will carry out ship-board incubation experiments with water collected from contrasting Southern Ocean sites; namely the naturally iron-enriched waters of the Antarctic Peninsula and the open ocean and iron-limited waters of the DP. Given that organic matter drives the biogeochemical cycle of carbon and trace metals, in-situ marine dissolved organic carbon will be sampled for further characterization back in the laboratory. The proposed research will improve our current understanding of how trace metals and carbon biogeochemical cycles inter-connect, characterize organic materials present at the contrasting sites and establish how microbial interactions control the biogeochemical cycle of trace metals in the Southern Ocean under current and future climatic conditions.

Work at sea

The proposed work involved chemical and biological methods to isolate and purify dissolved organic matter (DOM), bacteria and viruses. In addition, incubation experiments were conducted to assess the bioavailability and chemistry, as well as the limitation imposed on phytoplankton by Fe, Zn, Co, Mn and vitamins and measured their impact on bacterial dynamics. We conducted the incubation experiments at three different sites, two in the high nutrient low chlorophyll (HNLC) waters of the DP (PS97/043 (BIO 1) and PS97/076 (BIO 2) and another site north of Elephant Island (PS97/087 (Bio 3)) using the same initial batch of trace metal limited seawater pumped from an approximate depth of 25 m. In order to ideally locate our stations (Table 7.1; Fig. 7.1) with respect to our scientific questions, we used the map of weekly chlorophyll a to identify area with low chlorophyll and the surface water temperature (below 2°C) to identified region south of the PF that typically presents a high nutrient signature. Additional stations were sampled using a Teflon-coated 25 L Go-Flo bottle deployed on a Dyneema non-contaminating line to study the cycling of trace metals and vitamin. Samples were collected from 25 m using trace metal clean techniques.

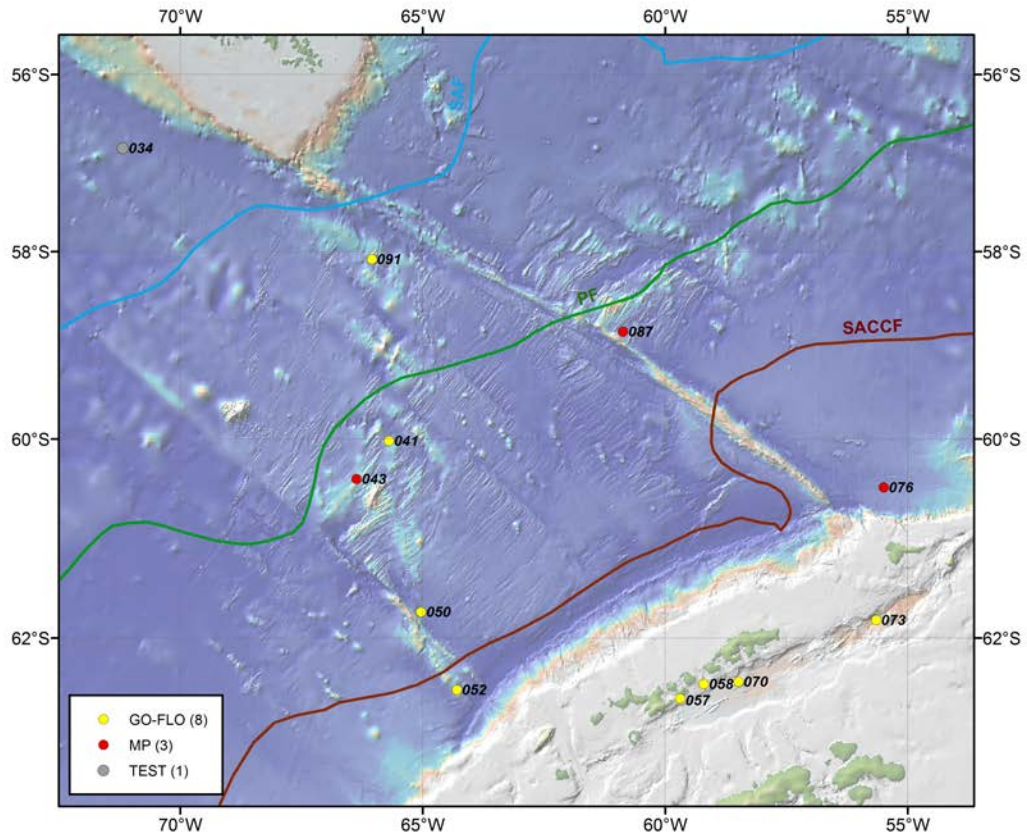

Fig. 7.1: Station map. The stations sampled with the membrane pump (called BIO stations) where most experiments were carried out are indicated in red, whereas stations sampled with the Go-Flo bottles for additional work on trace metal and vitamin recycling are shown in yellow. The station to test our equipment (test station) is shown in grey. In total 11 stations were sampled.

Tab. 7.1.: List of stations for experimental work.

Station No.		Gear	Date UTC	Start (in the water) UTC	Latitude in the water (deg/min)	Longitude in the water (deg/min)	Area
PS97/034	Pump Test	MP	28.02.16	18:58	56° 50.78' S	71° 10.97' W	DP
PS97/041	pump	MP	01.03.16	15:10	60° 1.08' S	65° 41.63' W	DP
PS97/043	BIO 1	MP	02.03.16/03.03.16	8:08	60° 24.78' S	66° 21.85' W	DP
PS97/050	GoFlo#2	GO-FLO	05.03.16	1:44	61° 44.73' S	65° 2.00' W	DP
PS97/052	GoFlo#3	GO-FLO	05.03.16	15:13	62° 29.90' S	64° 17.66' W	DP
PS97/057	GoFlo#4	GO-FLO	07.03.16	15:17	62° 35.03' S	59° 41.33' W	AP
PS97/058	GoFlo#5	GO-FLO	07.03.16	19:33	62° 26.57' S	59° 12.24' W	AP
PS97/070	GoFlo#6	GO-FLO	09.03.16	12:04	62° 25.32' S	58° 29.35' W	AP
PS97/073	GoFlo#7	GO-FLO	10.03.16	16:47	61° 49.53' S	55° 39.02' W	AP
PS97/076	BIO 2	MP	13.03.16	6:21	60° 29.94' S	55° 29.70' W	AP
PS97/087	BIO 3	MP	17.03.16	11:08	58° 52.17' S	60° 51.92' W	DP
PS97/091	GoFlo#8	GO-FLO	19.03.16	18:34	58° 5.01' S	66° 3.00' W	DP

Bacterial and viruses isolation

Natural community of viruses specific of their DOM-producing hosts were concentrated by tangential ultrafiltration (100 kDa cut-off), following sterile filtration. The viral natural community was also isolated from filtered seawater following flocculation in presence of $FeCL_3$ for metaviromes analysis at each BIO station (1-3). Bacteria were isolated using a sterile 10 L Niskin bottle deployed on the regular rosette from depths of 25 m and 300 m at each site. The selection of psychrophilic bacterial candidates was realized at sea following a phenotypic screening on agar plate kept at 4 °C. Specific agar media with a low N/C ratio allowed us to determine the probable EPS-excreting bacteria by selecting the most mucoid strains. This biological material will then be characterized back at the University of Geneva in collaboration with the CERMAV (CNRS), the University of Western Brittany and the INRA (France). This bioprospection will be used to produce large quantity of bacterial EPS, isolate new EPS-degrading psychrophilic viruses and measure viral degradation rates of EPS isolated *in-situ* including impact for Fe biogeochemistry. This data will thus be vital to complement information gathered at sea.

DOM isolation

Large volume (1000 L) of 0.2 µm filtered seawater was collected to isolate natural organic matter (NOM) larger than 100 kDa contributing to small organic particle and colloids. The role of such compounds on Fe biogeochemistry is widely recognised. The NOM collected at BIO1 was then used in incubation experiments at sea at BIO 3. Material will be brought back for further work in the laboratory in order to characterize the nature of marine DOM with respect to Fe biogeochemistry. For that purpose, state-of-the art techniques will be collaboratively used at the AWI and the University of Geneva. To complement this approach of DOM isolation based on size, we carried solid phase extraction using C_{18} cartridges with filtered and ultra-filtered seawater in order to better characterise organic compounds associated with the colloidal and the soluble fraction, respectively. Elution was sequentially performed at pH 8 and pH 2 in order to collect basic as well as acidic DOM compounds. These will be characterized back at our home laboratories (AWI, University of Oldenburg, University of Geneva, CERMAV (CNRS), Brest University).

Trace elements competition for organic ligands binding

T

o date we know that association with organic compounds (termed ligands) is paramount to define trace elements biogeochemistry. However whether different trace elements of biological importance can compete for the binding of similar organic ligands in the Southern Ocean remains largely unknown. For this purpose, we sampled filtered sweater to measure whether iron, zinc and copper can react with the same organics. Analysis will be done back at University of Geneva in collaboration with University of Southampton, University of Liverpool and University of Otago (New-Zealand).

Effect of EPS on Fe microbial recycling and phytoplankton physiology

The effect of freshly isolated EPS amendments on Fe bioavailability, the bacterial and phytoplankton community composition and productivity was assessed using 24h up to 6 days *in-situ* experiments on size-fractionated planktonic communities (pre-filtered on a 200 *µ*m mesh: large and small phytoplankton as well as bacterioplankton). The organic carbon source used for heterotrophic bacteria and Fe binding ligands was carbohydrates (glucuronic acid as a model monosaccharide and carraghenane as a model marine polysaccharide), EPS (a polysaccharidic form of DOM, isolated from two marine bacteria) and a widely studied siderophore (desferrioxamine B). Moreover, as viruses can degrade EPS from bacteria we measure the effect of virally degraded and native bacterial EPS. The bioavailability for the phytoplankton community of the different forms of Fe was determined

using ^{55}Fe uptake rates and sequential filtration. Growth will be measured using flow cytometry for bacteria and POC for phytoplankton. The structure of the plankton community will be described as above using flow cytometry and light microscopy. *In-situ* Fe limitation was assessed using F_v/F_m. As Fe biology and Fe chemistry are tightly coupled we also sampled for Fe chemistry, humic substances-like polysaccharides and others biopolymers in addition of dissolved trace metal concentrations. These analyses will be done in collaboration with the AWI and University of Zagreb (Croatia).

Impact of Fe limitation on Si and Zn isotopic signature

Because diatoms are a dominating phytoplankton group in the SO and the Si associated with their frustules is slow to remineralize, the SO acts as an Si trap with consequences for the global Si distribution. Thus Fe limitation, by controlling the growth of diatoms across the SO, has also consequences for the global Si distribution and primary productivity. Zn and Cd may also be impacted as it is required for the biological uptake of Si and $Cd:PO_4$ ratio are influenced by Fe limitation. Here, we checked how Fe enrichment affects the isotopic signatures of Si, Cd and Zn following 7 days incubations. As isotopic signatures can be used to track processes, comparison of our results with isotopic signatures measured worldwide will provide a unique insight of the influence of Fe limitation in the SO at large. This study is done in collaboration with the ETH Zurich and the Australian National University.

Incubation experiments with Fe, light and pCO2

Shipboard perturbation experiments with natural phytoplankton communities from the **DP** site BIO 1 (PS97/043) were performed to address the question of how CO_2-related changes in carbonate chemistry (e.g. ocean acidification) in combination with Fe and light limitation will affect primary productivity and phytoplankton species composition. To this end, 80 L seawater containing the starting phytoplankton community (filtered through a 200 µm mesh to avoid zooplankton inside the experimental bottles) were sampled at station 97/043 using a teflon membrane pump sampling from 24 m depth. To ensure prolonged exponential phytoplankton growth, in addition 100 L of iron-limited seawater were sampled using acid-cleaned 0.2 µm filter cartridges. This water was used to dilute the incubations when nitrate concentrations went below 10 µmol L^{-1}. For all experiments, triplicate incubation bottles were bubbled with pCO_2 levels representing values of present-day (~380 *µ*atm) and those projected for the year 2100 (~980 *µ*atm) using a porTab. gas mixing system. To also test the influence of iron availability, incubations were grown under natural iron concentrations of 0.1 nM and under iron enrichment though addition of 0.9 nM $FeCl_3$. No additional macronutrients were added to the incubation bottles. To also elucidate the impact of light, experiments were conducted under light-limiting (30 *µ*mol m^{-2} s^{-1}) and saturating (80 *µ*mol m^{-2} s^{-1}) daylight irradiance under a light-dark cycle of 16:8 h. The experiments were run up to for 4 weeks in a temperature-controlled growth chamber (1 °C). Nitrate and silicate concentrations were measured at latest every third day over the course of the experiments. Similarly, the physiological state of the cells was determined via a fast repetition rate fluorometer (FRRF, Chelsea). At the beginning, dilution and end of the experiments, samples for taxonomic species composition, cell density and chemical parameters were taken that will be more described in the following.

To determine taxonomic composition aliquots of 200 ml or 100 ml unfiltered seawater were preserved with both hexamine buffered formalin solution at a final concentration of 2% and lugol at a final concentration of 1%. Preserved samples were stored at 4 °C in the dark until further analysis by light and epifluorescence microscopy back at the AWI. For bacterial composition, seawater was transferred into cryovials to which gluteraldehyde of a final concentration of 0.1% was added. These samples were then stored at -80 °C until they will

be analysed at home. For the determination of the seawater carbonate chemistry, samples for alkalinity, dissolved inorganic carbon (DIC) and pH were collected. Alkalinity samples were taken after filtration (Whatman GFF filter, 0.6 mm), fixed with $HgCl_2$ and stored in 100 mL borosilicate flasks at 4 °C until further analysis by potentiometric titration at the AWI. DIC samples were sterile-filtered (0.2 mm), fixed with $HgCl_2$ and stored in 13 mL borosilicate flasks free of air bubbles at 4 °C until they will be measured with a Quaatro Autoanalyzer (Seal Analytical). Seawater pH was measured onboard using a calibrated pH/ion meter (Methrom, three-point calibration). From these three parameters the carbonate system will be calculated using the program CO2Sys (Lewis and Wallace 1998). Information on the efficiency of photochemistry in PSII after dark acclimation for 1h and during varying light exposure was obtained using FRRf by exposure to increasing irradiance (from 11 up to 500 μmol photons m^{-2} s^{-1}).

Moreover, pigment samples were collected, filtered and stored at -80 °C until high performance liquid chromatography (HPLC) analysis will be performed at the university of Bremen. Samples for particulate organic (POC) were filtered onto precombusted (500° C; 12 h) GFF filters and stored in precombusted petri dishes (500° C; 12 h) at -20 °C. Samples for the determination of biogenic silicate were taken, filtered and stored at -20 °C until further analysis. Samples for dissolved organic carbon (DOC) were filtered through precombusted (500° C; 12 h) GFF filters and the filtrate was kept and stored in acid-cleaned bottles at -20 °C until further analysis at the AWI. Samples for RNA analysis were filtered and stored at -80 °C in sterile vials until analysis at the AWI.

Regarding the characterisation of the iron chemistry, filtered seawater samples for the determination of iron dissolved, iron speciation, humic acid-like compounds and ligands were taken. While iron dissolved samples are stored at room temperature until further analysis by ICP-MS, samples for iron speciation, humic acid-like compounds and ligands were stored at -20 °C until further analysis. Samples for iron speciation and humic-acid-like compounds will be analysed using voltammetry (CLE-AdSV) at the AWI while ligand samples will be measured by reversed-phase high performance liquid chromatography hyphenated to inductively coupled plasma sector field mass spectrometry (HPLC-ICP-MS).

Incubation experiments with Fe and light

To investigate how the availability of light influences phytoplankton growth and community composition two perturbation experiments were carried out, one with from the iron-limited DP site BIO1 (PS97/043) as well as one with a naturally iron-limited phytoplankton community at site BIO 2 north of Elephant Island. These short-term shipboard perturbation experiments took place between 10-14 days depending on experimental conditions. Phytoplankton incubations were exposed to undersaturating (30 µE), saturating (80 µE) and oversaturating (150 µE) irradiance. All light treatments were carried out either under the *in situ* Fe concentration (0.1 nM) or after addition of 0.9 nM $FeCl_2$. From the effects on species composition (phytoplankton and bacteria taxonomy, pigment composition), particulate organic carbon, biogenic silica, RNA and total iron dissolved concentrations were assessed using the same parameters as described for the experiments with Fe, light and pCO_2.

Incubation experiments with Fe, Zn, Co, Mn and vitamin B12

This research project aimed to identify whether Zn, Co, Mn and B12 are limiting or co-limiting factors together with Fe and thus impact primary productivity or influence the plankton community composition in two DP waters sites BIO 1 and 3 (Stations PS97/043 and PS97/087, respectively). In order to identify the limiting or co-limiting trace metal/vitamins, short-term shipboard amendment experiments with the in situ phytoplankton communities

using single or multiple trace metal additions were conducted. Experiments were carried out in triplicate 2.5L polycarbonate bottles. The treatments consisted of either 0.9 nM inorganic Fe, 4 nM Zn, 100 pM Co, 1 nM Mn, 100pM B_{12} by themselves while a combination of Fe with the other four trace metals/vitamins was also added to investigate potential co-limitation. The duration of the experiments ranged between 14-17 days, depending on the community growth rates. The same set of parameters as described for the incubation experiments with Fe, light and pCO_2 was collected. Additionally, samples were taken to determine the cellular quota of Fe, Zn, Co and Mn by ICP-MS as well as dissolved vitamin concentrations which will be analysed using HPLC coupled MS.

Trace metal/vitamin dynamics and cycling

In order to elucidate the cycling and dynamics of trace metals and vitamins in the Southern Ocean, a novel mass balance approach using radioisotopes was tested. 11 stations in the open ocean, including HNLC regions (PS97/034, PS97/041, PS97/043, PS97/050, PS97/087 and PS97/091), and coastal areas of the Bransfield Straight off the Antarctic Peninsula (PS97/052, PS97/057, PS97/058, PS97/070, PS97/073 and PS97/076) were sampled. A multifaceted approach was used to characterize the phytoplankton community composition including light microscopy, size fractionated pigments (HPLC) and particulate carbon as well as flow cytometry. To shed light on the trace metal requirements of the plankton community, samples for the cellular content of Fe, Zn, Co and Mn were taken and stored frozen for subsequent analysis by ICP-MS. In addition dissolved metals, ligands and macronutrient concentrations were analysed using ICP-MS, voltammetry and conventional photo spectrometric methods, respectively. Removal of dissolved trace metals by the plankton was measured using triplicate 250mL PC bottles, spiked with either 50 nCi $^{57}Co\text{-}B_{12}$, $^{57}CoCl$, $^{55}FeCl$ $^{65}ZnCl$ and incubated in an on deck flow through incubator. Bottles were covered with neutral density screening allowing for 50% of light to penetrate, corresponding to light levels at a depth of 20-30m. In order to determine primary productivity rates triplicate bottles were spiked with 4µCi of sodium bicarbonate. Experiments were terminated after 24 hours by filtering each bottle onto 0.2 and 2um polycarbonate filters and uptake rates of each isotope was determined by subsequent quantification on a liquid scintillation counter. A 2.5L untreated bottle of whole water was allowed to incubate along the spiked bottles and dissolved vitamin and trace metals concentrations were determined after 24-48 hours as described above.

Preliminary (expected) results

At this stage it is very difficult to discuss preliminary results as most of the taken samples still need either to be analysed or to be processed. However, the research carried out addressed several outstanding challenges with respect to trace metal biogeochemistry and the ecosystem functioning of the SO under current and future climatic conditions. Regarding chemistry, a better characterisation of the link of Fe biogeochemistry with DOM will help to characterise the nature of organic ligands – a prerequisite to develop tracers and improve our understanding as well as the modelling of iron biogeochemistry. Our results will also help to better understand the role of viruses on biogeochemistry. The different experiments will further indicate how simultaneous changes in multiple parameters will affect the productivity and the biodiversity of SO phytoplankton. The joint effect of trace metals, vitamins, organics, light as well as pCO_2 will therefore provide a better understanding of the dynamic of primary producers in the SO. Finally, by measuring the impact of Fe limitation on isotopic signature we will contribute to enhance our understanding of the impact that the SO exerts at a global scale.

8. WATER COLUMN AND SURFACE SEDIMENT SAMPLING FOR MICROFOSSIL-BASED PROXY CALIBRATIONS

Lester Lembke-Jene[1], José Luis Iriarte[2] Hartmut Schulz[3], Vania Carrera[4], Carina Lange[2], Helge W. Arz[5], Wolfgang Schneider[6], Harold Fenco[7], Gastón Kreps[8], Bruno Canella[9], Dirk Nürnberg[10]

Not on board: Edith Maier[1], Andreas Mackensen[1], Mariem Saavedra[11]

[1]AWI,
[2]UdeC/COPAS/IDEAL,
[3] U Tübingen,
[4]U Valparaíso,
[5]IOW,
[6]UDEC/IMO ,
[7]INIDEP,
[8]CADIC-CONICET,
[9]ARA,
[10]Geomar,
[11]U Bremen

Background and Objectives

The oceanographic processes on the southern Chilean margin, in Drake Passage and the Scotia Sea have a fundamental influence on the Pacific – Atlantic – Southern Ocean inter-basin exchange of water masses and thus on the global Meridional Overturning Circulation (e.g. Meredith et al., 2011). Biogeocheochemical and physical processes in the Southern Ocean play a crucial role in initiating and shaping climatic changes not only on modern, but also on geological, i.e. millennial and orbital timescales. As the Southern Ocean is the largest High-Nutrient-Low Chlorophyll (HNCL) area in the World Ocean, it thus has the potential to act as a major CO_2 sink, when the efficiency of the biological pump increases, as proposed for glacial periods (e.g. Kohfeld et al., 2005, Yu et al., 2014, Anderson et al., 2014). In addition, the region acts as a major junction of the Antarctic Circumpolar Current with associated oceanographic fronts and currents, leading to an intensely dynamic and heterogenous ecological setting for both calcareous and siliceous planktic and benthic species that are widely used as signal carriers in paleoceanographic proxy reconstructions.
These proxy methods available to paleoceanographers, which do not only allow to qualitatively reconstruct changes in the oceans' nutrient inventories and physical dynamics, but also permit to quantify such variations have increased in their sophistication over recent years.

Planktic and benthic foraminifera are widely used to understand the responses of the species assemblages to changes in physical and chemical oceanographic parameters. Apart from such species assemblage and established stable oxygen and carbon isotope analyses, additional geochemical and isotope-based tools that use foraminiferal test carbonate have opened new avenues towards the quantitative reconstruction of physical paleoceanographic parameters. The application of Mg/Ca elemental ratios, when combined with stable oxygen isotopes, permits the reconstruction of upper and deep ocean water temperatures, and as a result allows to differentiate effects of temperature, salinity and ice sheets on geological time scales. However, while already some of the earliest works on Mg/Ca – temperature relationships from planktic foramininfera used samples from the subpolar latitudes (Nürnberg, 1995), large ucertainties in using both planktic and benthic foraminifera, especially in the high latitudes remain (Kozdon et al., 2009). Recent studies point to complex inter-dependencies of Mg/Ca and other trace metal signals in *N. pachyderma* (s) with secondary environemental effects (sea ice – CO_3^{2-}) in polar and subpolar southern latitudes (Hendry et al., 2009). On the other hand, benthic foraminiferal stable oxygen and carbon isotopes, and trace metal/elemental ratio such as Cd/Ca, B/Ca and their isotopes deliver the means, to disentangle the complex signals of physical (T, S) and chemical (CO_3^{2-}, PO_4, O_2) changes of deep water masses through Earth's history. Such results provide critical information to understand past variations in the Southern Ocean's carbon cycle dynamics

and the nature of the southern-sourced branch of the meridional overturning circulation (e.g. Yu et al., 2010; Elderfield et al., 2012).

In addition, new tools based on the use of stable isotopes ($\delta^{30}Si$, $\delta^{18}O$) from siliceous microfossils have emerged (diatoms, radiolarians, sponge spicules), which can be used to reconstruct changes in environmental conditions such as ice volume, surface salinity and nutrient dynamics (cf. e.g. Egan et al., 2012; Hendry et al., 2012; Maier et al. 2013). For the interpretation of the geochemical data obtained from siliceous microfossils and the understanding of the complex mechanisms ecological information (e.g. depth habitat) of living species in combination with hydrographic data, chlorophyll and nutrient measurements as well as stable isotope data ($\delta^{30}Si$, $\delta^{18}O$) from the water column (surface to bottom) are needed.

However, highly fluctuating and drastic conditions, e.g. strong winds stress, high mixing rate, low light availability throughout the water column and seasons, low temperature, the ecophysiological adaptations play a key role in the growth of phytoplankton assemblages. Previous phytoplankton studies have been carried out in this region, including phytoplankton composition (Villafañe et al 1995; Kang et al 2002; Olguin & Alder 2011), size-fractionated chlorophyll-a and primary productivity estimates (Varela et al 2002; Holm-Hansen et al 2004; Vernet et al 2014). These studies pointed out distinctive marine ecological provinces along the Drake Passage, Bransfield Strait and Antarctic Penninsula. In general, high chlorophyll-a biomass are associated to diatoms (>20 um cell size) dominated phytoplankton assemblages during summer months, whereas pico-and nanoplankton are associated to very low biomas with a strong spatial gradient between water masses (Holm-Hansen et al., 2004; Hewes 2009). The nature of processes associated with water types/currents around Antarctica has a dominant influence on the water column structure, nutrient supply and the overall productivity of the system.

Any of these proxy methods is critically dependent on their established relationship to actual tracers and quantitative parameters in the modern ocean. Especially the subpolar and polar Southern Ocean is seriously undersampled both in the water and sediment domain, thus remains in critical need for precise calibration of proxies under modern conditions, next to the necessity for validating and mechanistically understanding the proxydata — instrumental data relationships. Previous works in the Southern Ocean have so far mostly focussed only on the subpolar Atlantic sector and the Weddell Sea, thereby leaving large areas upstream the ACC towards the Pacific effectively unsampled. We aim to close this gap and supplement existing water and sediment surface data (e.g. Mackensen, 2012), using the acquired samples to refine existing, or establish new proxy calibration datasets. Particularly in this study region, a focus will be put on (1) locations along the subantarctic and mesopelagic Chilean margin due to its importance for the export Southern-sourced intermediate to deep water masses into the South Atlantic and (2) on the Drake Passage transect to better resolve North — South physical and chemical oceanographic gradients across the ACC.

In this High Nutrient Low Chlorophyll (HNLC) region autotrophic biomass varies widely over four orders of magnitude (0.01 to 189 mg Chl. m^{-3}), both geographically and seasonally, throughout the Southern Ocean (Villafane et al. 1995, Kang et al 2002), being usually higher in regions associated to islands (Ebersbach and Trull 2008), frontal zones especially in the Polar Front (Laubscher et al. 1993), at the ice edge (Comiso et al. 1990) and relatively high near icebergs (Vernet et al 2011). Recent studies, using long-term phytoplankton data, have indicated spatial (regional) and temporal (inter-annual) changes in phytoplankton structure (as chlorophyll, and taxa composition), associated negatively with water temperature (Olguin & Alder 2011) and major Antarctic regions (Drake Passage, Polar Front, Weddell Sea). Most dramatically, Monte-Hugo et al (2009) have suggested that ocean chlorophyll-a

concentration has significantly changed (12% declined) along Western Antarctic Peninsula, especially during summertime surface chlorophyll-a over the past 30 years.

Work at sea

Water Column sampling – Instrumentation

A rosette with 24 x 12 L Niskin bottles (Ocean Test Equipment Inc.) is attached to the shipboard CTD Seabird SBE911plus set up. The system consists of the Seabird SBE9 CTD underwater unit, an SBE11 CTD board unit, with Niskin bottles fired by an SBE32 carousel. The rosette sampler was used on 57 stations along the cruise track (Fig. 8.1.). Water samples were taken with the 24 x 12 L Niskin bottles (*cf*. chapter) according to sample protocols. In general, stations were either designated “shallow” or “deep” hydrocasts, with the latter sampling the upper c. 200 m for surface water analyses, while a deep casts extended across the entire water column down to bottom depth. These latter deep stations were scheduled less frequently, due to the significantly higher amount of time needed on station and our maximum sampling capacity for deep water isotope samples. We used the hydrocasts on the first two stations (PS97/001-1 and PS97/002-1) to establish all standard sampling and laboratory procedures. A complete list of all hydrocasts, comprising all sampled water depths and the according oceanographic data at bottle depths is given in Appendix A.11 for reference.

Our sampling programmes focused of the following topical groups:

- Chlorophyll a – surface water sampling and filtration
- Primary production and incubation experiments – surface water sampling
- Calcareous plankton, suspension – Surface,deep sea water filtration, net tows, pumping
- Silicon isotopes of silicate – surface, deep water sampling and filtration
- Oxygen, carbon (of DIC) isotopes, nutrients – surface, deep water sampling
- Oxygen, carbon (of DIC) isotopes, nutrients – bottom water sampling MUC deployments

Chlorophyll-a (Chl-a)

On 39 hydrographic stations, seawater was collected for chlorophyll-a measurements between Cabo de Hornos and south Drake Passage conducted on board the R/V POLARSTERN (AWI - Germany) between 19 February and 8 April 2016. Water samples were obtained at standard depths (5, 10, 20, 40, 60, 80, 100 m and sometimes 300 and 500 m) from the Niskin bottles attached to the rosette with CTD-profiling sensors. Between 300 and 500 mL of seawater were filtered (Sartorius Polycarbonate filters, 0.4 µm nominal pore size) without replicate and immediately frozen (-20°C) until later analysis via fluorometry (Parsons et al 1984), using acetone (90% v/v) for the pigment extraction (Turner Design TD-700). The chlorophyll-a measurements are expected to be analyzed at IDEAL Center in Universidad Austral de Chile.

The work at sea comprised the analyses of autotrophic biomass (measured as Chlorophyll-a) along several transects of Cabo de Hornos and Drake Passage. Specifically, Drake Passage has been indicated as a region of High Nutrient Low Chlorophyll (HNLC) with the lowest chlorophyll-a concentration (<0.5 mg m^{-3}) in surface waters, and a deep chlorophyll-a maximum close to 75 m (Holm-Hansen et al 2004). The main objectives were (1) to estimate the vertical (5 – 100 m) and horizontal (transects) distributions of phytoplankton biomass, and (2) to estimate surface gross primary production (GPP) and community respiration (CR) along the Drake Passage during late summer.

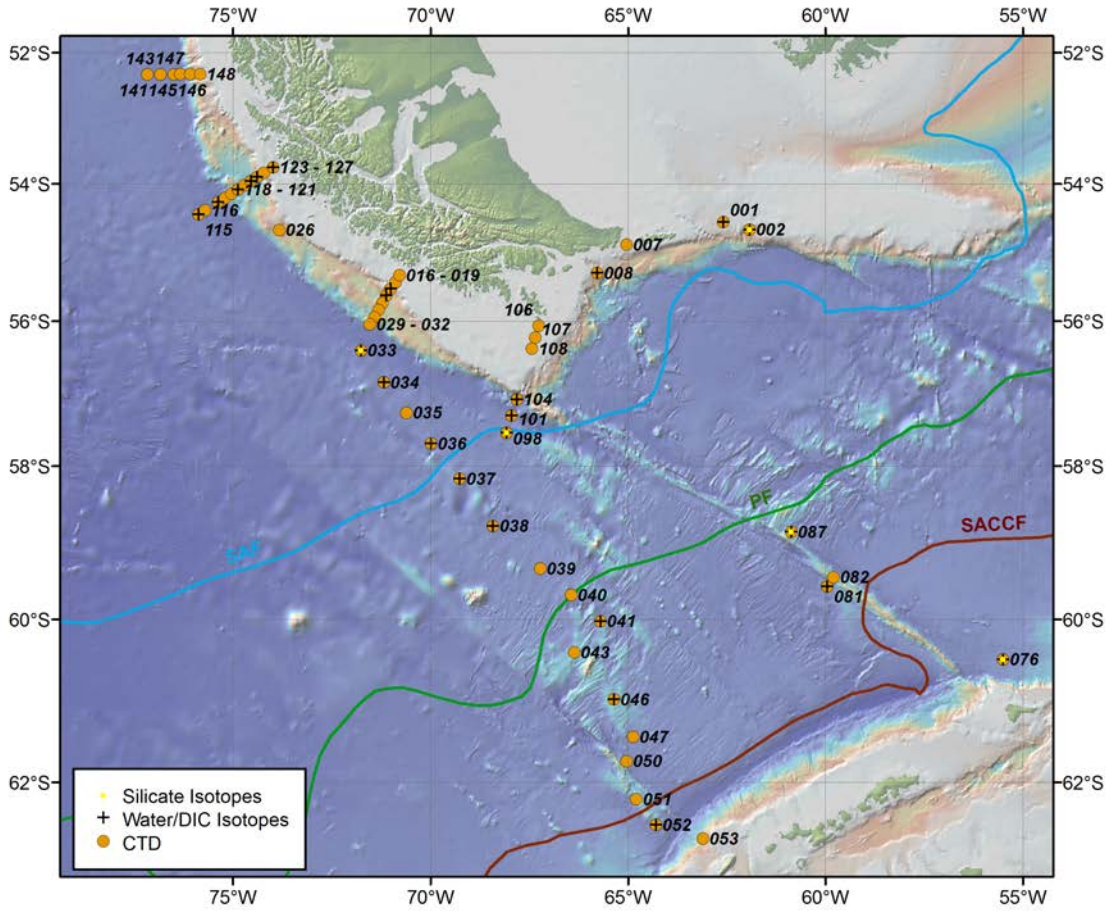

Fig. 8.1: Map of PS97 stations for sea water sampling. Markers provide information according to principal sampling, orange filled circles show surface water sampling stations, additional black crosses mark added deep water sampling. Yellow inserted dots mark stations with additional water sampling for silicate isotope analyses.

Gross Primary Production (GPP) and Community Respiration (CR) incubations

Gross Primary Productivity (GPP) and Community Respiration (CR) incubations (on-deck) were conducted as on-deck incubations, carried out with water from a surface depth of 5 or 10 m at five oceanic and one shallow stations at Cabo de Hornos and Drake Passage areas. Estimations of GPP and CR were based on changes in dissolved oxygen concentrations observed after the incubations of light and dark bottles (Strickland, 1960). Water from the Niskin 10 L bottles was transferred to gravimetrically calibrated borosilicate bottles with a nominal volume of 125 mL using a silicone tube. Four time-zero bottles, four light bottles, and four dark bottles were used for each incubation set. Samples of on-deck experiments were incubated in a transparent container. In all experiments, water samples were collected at dawn (05:30 h) and were incubated throughout the whole light period for 10 or 12 h (daylight). Time-zero bottles were read at the beginning of each experiment.

Net community production (NCP) and community respiration (CR) were measured as oxygen production and consumption at selected stations during the PS97 track cruise. Oxygen concentration was measured before and after incubation using the Fibox4-a optode system (PreSens) with the O -sensitive membrane glued to the inside wall of the BOD bottles. The average coefficient of variation for replicate (n = 8) samples was 0.05%. GPP values were converted from oxygen to carbon units using a conservative photosynthetic quotient (PQ) of

1.25 (Williams and Robertson, 1991) and the CR values were converted from oxygen to carbon units using a respiration quotient (RQ) of 1.

Sea water filtration

50 casts of the shipboard CTD-Rosette, equipped with 24 x 10l-Niskin bottles, were sampled at different depths in order to obtain water sample for the four participating institutions IOW, AWI, Universität Tübingen and Universität Bremen (see table 8.2.). Focus was on the upper (150 to 0m) and deepest (bottom to 1000m above) water masses in the Drake Passage. Two filtration techniques and different filters were used. Filtration for IOW (Sascha Plewe) was through an IsoporeTM Membrane Filters Filter Type 0.4µm HTTP, diameter 47mm by a MCP peristaltic pump at a flow rate of 4 liters. Filtration for coccolithophores for Bremen University (Saveedra-Pellitero et al., 2014) was by a specifically designed bench (Bollmann et al., 2002) of five parallel filter stations (47mm in diameter) using sartorius Polycarbonte Track-Etch Membrane or Whatman Nucleopore Track-Etch Membrane filters, both with a pore size of 0.4µm. Coccolithophore filtration was at a pressure of -0.4 bar. A volume of 2 L took about 1 h of filtration which was started in less than few hours after sampling of the CTD-Rosette.

For the biomarker analysis water samples of 4.5 l were filtered through Whatman Glass Microfiber Filters GF/F, diameter 47 mm at a pressure of > -0.2 bar, packed into aluminium foil, and frozen at -80°C, whereas the coccolithophore- and IOW-filters were stored in plastic petri dishes (60 mm) and dried in an oven at 40°-45°C for 24h. All filter samples will be transported by R/V POLARSTERN to Bremerhaven.

We extracted a sum of 405 filters. In a few cases filtration was not successful because filter was damaged, or there was water flow out at the sides of the gasket. Durations did not exceed 4 hours. There were no cases where filtration had to be stopped due to clogging of the filter. Standard depths for Bremen coccolithophore sampling was 10, 20, 40, 60, 100, 150 m . A shallow 5 m deep smapling interval, often situated in the wavy shallow layer was often not possible, depending on the sea and wind state. An additional number of samples were taken at 80 depth, similar to the sampling schemes in Saveedra-Pellitero et al. (2014). The chlorophyll maximum was in most cases above 100 water depth so that a dense sampling of the entire upper ocean surface can be expected. This scheme was corroborated by the light-yellowish to greenish staining of the GF/C and polycarbonate filters, reflecting highest phytoplankton densities between 20 m and 100 m water depth.

Fig. 8.2: Filtration plant set-up for water samples to determine chlorophyll a and silicate in shipboard wet chemistry laboratory, filtration device for coccolithophore filtrations samples in the background (left). Peristaltic pump set up for suspension filtration of IOW water samples (right).

Examination under the light microscope at 650X magnification through the Isopore filters of 3 µm pore size revealed a homogeneous filter coverage by isolated particles that could be identified as coccospheres, diatoms, silicoflagellates, radiolarian and uvenile planktic foraminifera. Further, lithic matter like quartz, feldspar or volcanic material, including dark grey basaltic pumices (pale grey to olive green colors), could be revealed by slide analysis using a petrographic microscope. Glass fiber filter GFF were used to extract biomarkers at AWI from two stations (total of 16 filters) off southern Chile, parallel to the coccolithophore samples (Table 8.2.).

Filtration with shipboard seawater supply (rotary pump), membrane pump (MP)

For the last weeks of the cruise, from 19 March 2016, 14h (ship time) to 04 April 2016 (14h) water volumes between 1,300 and 10,750 liters were rinsed through a 63 µm-metal sieve which was fixed in a plastic tank to assure that the catch stayed continuously under water. The flow of water was repeatedly measured during the sampling period, to shift between 300 and 350 liter per hour. The inlet of seawater to the ship is at a water depth of about 5 m. The volume was calculated from the duration of the cast. After the filtration, the sieve was washed with fresh seawater from the pump and the residue was scanned and photographed in a petri dish under a binocular linked to a digital microscope camera (*cf.* for results Figure 8.5.).

Tab. 8.1 Statistics for sea water pumping during March/April 2016 on PS97.

Sample Number	Start (ship time)	End (ship time)	Time interval (h)	Pumped Liters (L)
1	19.03.14h	20.03.14h	24	720
2	21.03.14h	22.03.08h	18	5800
3	22.03.09h	22.03.17h	8	2600
4	22.03.19h	23.03.07h	12	3900
5	23.03.11h	23.03.23h	12	3900
6	23.03.23h	24.03.11h	12	3900
7	24.03.12h	24.03.23h	11	3575
8	24.03.23h	25.03. 09h	10	3250
9	25.03.10h	26.03.00h	14	4550
10	26.03.01h	26.03.09h	8	2600
11	26.03.10h	26.03.22h	12	3900
12	26.03.10h	26.03.22h	12	3900
13	27.03.01h	27.03.11h	10	3250
14	28.03.01h	28.03.10h	9	2925
15	28.03.11h	29.03.01h	12	3900
16	29.03.01h	29.03.10h	9	2925
17	29.03.10h	29.03.19h	9	2925
18	29.03.19h	30.03.10h	15	4875
19	30.03.17h	31.03.10h	17	5525
20	31.03.10h	01.04.01h	15	4875
21	01.04.01h	01.04.11h	10	3250
22	01.04.13h	02.04.09h	20	6500
23	02.04.11h	03.04.20h	33	10725
24	03.04.23h	04.04.10h	11	3575

25	04.04.10h	04.04.14h	4	1300

Plankton tows by small plankton net

In total, six plankton tows (PLA) were taken during the cruise, using a Apstein-type plankton net (HYDRBIOS Kiel) with an opening of 17 cm (0.0227 m^2), which was towed vertically through the water column with a speed of 0.2 or 0.3 m/s. The nets could only be deployed at suitable wind and sea conditions. Depth was the upper 30 m of the surface water layer, using a net with 10 µm for diatom observations. A second net of a mesh size of 41 µm for PF was towed from 300 m water depth. The latter had only a very small yield of PF. Samples were preserved in a formaline solution of 18 %. (for details see PS97 station list).

Unfortunately, the originally planned deployment of the Multi-Net (Type MPS 92 B, "Hydrobios" Kiel, Germany) with defined depth catch intervals was first postponed and ultimately cancelled, due to (1) the time-demanding nature of deployments for silicious plankton (10-12 h) in light of the significant delay and changes to the expedition track at the start of the cruise (2) regular weather condition beyond the safe standard operating parameters (i.e. sea state higher than 3-4 m and winds in excess of 5 Bft).

Filtration of water samples for Si isotope analysis

Samples for measurements of sea water δ^{30}Si (of silicate) were taken on four depth profiles, with a total of 44 samples. Due to the larger sample volume (4–10 L) that was needed in conjunction with the higher amount of preparatory work, the sampling remained limited. Priority for silicate water sampling was given to sites where complementary studies were carried out (Biology stations), Multicorer for surface sediment sampling were closely located, or with water sampling at depths similar to the depth levels for other stable isotope analyses, to optimally study the relationship between hydrography, nutrient availability, isotope fractionation of the different nutrients (C, Si).

The four stations were sampled at the following bottle depths:
PS97/033-1 (S' Chile): 5, 20, 60, 100, 250, 500 m;
PS97/076-1 (BIO-2): 10, 60, 100, 200, 500, 1000, 1500, 2000, 2500, 3000, 3500 m;
PS97/087-1 (BIO-3): 10, 60, 100, 200, 500, 1000, 1500, 2000, 2500, 3000, 3500 m;
PS97/098-1 (near SAF): 10, 50, 150, 250, 450, 550, 1000, 1500, 2000, 2500, 3500 m.

Narrow-necked 2 L plastic bottles were used for taking water samples from the CTD rosette, filtration of water samples was begun immediately after sampling and continued un-interrupted until all samples for the station were processed. Prior to each sample, the filtration plant was rinsed with milli-Q water without filter paper, average filtration time of water samples varied around 45–90 min. for each water sample, depending on sample volume (4 L vs. 10L). After filtration, filters were removed, wrapped in aluminium foil for light protection, and stored in the shipboard cold storage at –20°C. The filtered sea water for isotope analyses was filled into pre-acidified (with HCl) wide-necked plastic bottles (2L), and stored under dark conditions (in aluminium boxes) in a reefer container at +4°C.

Surface & deep water sampling for O and C (of DIC) isotope and nutrient analyses

We sampled sea water from a total of 24 CTD stations with the rosette sampler deployments, for the characteriziation of modern physical (δ^{18}O) and chemical (PO_4, DIC, NO_3, δ^{13}C) oceanographic parameters. The choice of stations we targeted corresponded to the transects along two tracks of the Cape Horn Current and a latitudinal transect across the ACC and frontal systems in the Drake Passage. Compared to a total pre-cruise planning maximum of 400-450 samples from CTD casts, we took a total of 466 unique samples, plus a total of 16

replicates from three stations to enable QA/QC tests, thus sampling to the maximum capacity of the consumables available (glas and plastic bottles, stoppers, etc.).

Tab. 8.2 Station list of CTD stations used for water sampling with numbers of samples nd types of sampling carried out, hydrocast data with bottle depths are given in Appendix 11.

Station	Max. water depth [m] & no. of sampled depths	*Chl. a* depth interval [m]	Primary Product.	Samples silicate isotopes	Samples water/DIC isotopes	Samples for nutrients	plankton samples (UT / UB)	suspension samples (IOW)
PS97/001-1	400 (24)*	5 - 100	X	-	4	4	24 / 0	-
PS97/002-1	1280 (18)	5 - 500	-	4	18	18	0 / 7	7
PS97/007-1	104 (7)	5 - 100	-	-	-	-	7 / 0	2
PS97/008-1	1658 (20)	5 - 100	-	-	19	19	8 / 7	3
PS97/016-1	1980 (17)	5 - 100	-	-	12	12	0 / 7	-
PS97/017-1	786 (14)	5 - 80	-	-	13	13	0 / 7	-
PS97/018-1	130 (8)	5 - 100	-	-	-	-	0 / 7	-
PS97/019-1	80 (5)	10 - 80	X	-	-	-	0 / 7	-
PS97/026-2	200 (21)*	5 - 40	-	-	-	-	20 / 7	-
PS97/029-1	150 (8)	5 - 100	-	-	-	-	0 / 7	-
PS97/030-1	150 (8)	5 - 100	-	-	-	-	0 / 7	-
PS97/031-1	150 (8)	5 - 100	X	-	-	-	0 / 7	-
PS97/032-1	150 (8)	5 - 100	-	-	-	-	0 / 7	-
PS97/033-1	4000 (17)	5 - 100	-	7	17	17	0 / 7	-
PS97/034-1	4060 (23)	5 - 100	-	-	20	20	0 / 7	-
PS97/035-1	150 (8)	5 - 100	-	-	-	-	0 / 7	-
PS97/036-1	3882 (23)	5 - 100	X	-	21	21	0 / 7	21
PS97/037-1	3122 (23)	5 - 100	-	-	23	23	17 / 7	-
PS97/038-1	3750 (23)	5 - 100	-	-	21	21	0 / 7	-
PS97/039-1	150 (8)	5 - 100	-	-	-	-	0 / 7	-
PS97/040-1	150 (8)	5 - 100	X	-	-	-	0 / 7	-
PS97/041-1/3	300 (20)*/3380 (23)	10 - 100	-	-	24	24	15 / 7	-
PS97/043-3	150 (8)	5 - 100	X	-	-	-	8 / 7	-
PS97/046-7	2500 (23)	5 - 100	-	-	23	23	-	9
PS97/047-1	150 (8)	5 - 100	-	-	-	-	0 / 7	-
PS97/050-2	150 (8)	5 - 100	-	-	-	-	2 / 7	-
PS97/051-1	150 (8)	5 - 100	X	-	-	-	2 / 7	-
PS97/052-1	2830 (22)	5 - 100	-	-	20	20	2 / 7	-
PS97/053-3	150 (8)	5 - 100	-	-	-	-	-	-
PS97/076-1	3577 (18)	5 - 100	-	11	18	18	0 / 7	-
PS97/081-1	3700 (24)	5 - 500	-	-	24	24	0 / 7	-
PS97/082-1	150 (8)	-	-	-	-	-	0 / 7	-
PS97/087-1	3578 (18)	5 - 100	-	11	20	20	-	12
PS97/098-1	3800 (22)	5 - 100	-	11	21	21	-	13
PS97/101-1	4370 (24)	5 - 500	-	-	24	24	0 / 7	10
PS97/104-1	3860 (24)	5 - 500	-	-	24	24	2 / 7	3
PS97/106-1	88 (8)	5 - 80	-	-	-	-	2 / 7	-
PS97/107-1	91 (8)	5 - 80	-	-	-	-	0 / 7	-
PS97/108-1	100 (7)	5 - 100	-	-	-	-	2 / 7	-
PS97/115-1	4000 (24)	5 - 100	-	-	24	24	2 / 7	10
PS97/116-1	150 (8)	5 - 100	-	-	-	8	(8)** 0 / 7	-
PS97-118-1	4241 (24)	5 - 100	-	-	24	24	0 / 7	12
PS97-119-1	150 (8)	5 - 100	-	-	-	-	0 / 7	-
PS97/120-1	150 (8)	5 - 100	-	-	-	-	2 / 7	-
PS97/121-1	2574 (16)	5 - 100	-	-	16	16	-	7
PS97/123-1	150 (8)	5 - 100	-	-	-	-	-	-
PS97/124-1	1000 (15)	5 - 100	-	-	13	13	0 / 7	-
PS97/125-1	1800 (22)	5 - 100	-	-	22	22	-	-
PS97/126-1	150 (8)	5 - 100	-	-	-	-	(8)** 0 / 7	-
PS97/127-1	77 (6)	5 - 100	-	-	-	-	0 / 6	

* High-resolution surface ocean sampling station

** Biomarker filter samples taken for AWI (amount in brackets)

UT: University of Tübingen

UB: University of Bremen

Samples for isotope and nutrient analyses were taken according to standard protocols immediately after the CTD rosette was retrieved into the hangar of R/V POLARSTERN. Clean glas bottles with screw lids were flushed three times with sea water from the Niskin bottles, before fully filling the bottles bubble-free in overflow without air reservoir. From each sampled bottle depth (cf. table 8.2. and appendix 11 for bottle depths) we took the following standard series of samples: (1) one 100 ml glas bottle for oxygen isotope analysis, (2) one 50 ml glas bottle for stable carbon isotope analysis of Dissolved Inorganic Carbon ($\delta^{13}C_{DIC}$) and DIC concentrations, and (3) one 50 ml wide-necked PE plastic bottle with screw caps for phosphate and nitrate concentrations. All 50 mL samples for $\delta^{13}C_{DIC}$ were fixed with 200 µL of saturated $HgCl_2$ solution under a fume hood to stop biological activity. All glas bottles with screw caps were sealed airtight after sampling with a heated stearin/beeswax mixture to inhibit gas leakage during long-term storage. Samples were thereafter stored refrigerated in the cold rooms at +4°C (stable istotopes) or deep-frozen at –20°C (nutrients).

Multicorer water and sediment surface sampling

To connect water column-based data to the conditions recorded in microfossil proxy carriers within the sediment record, we sampled the bottom waters retrieved during Multi-Corer (MUC) deployments. Whenever possible, duplicate sample series for shore-based analyses of $\delta^{18}O$, $\delta^{13}C_{DIC}$ and nutrients (PO_4, NO_3) were taken from the two tubes assigned to benthic studies (cf. Chapter 3.2, Figure 8.3. and table 8.3. for MUC locations).

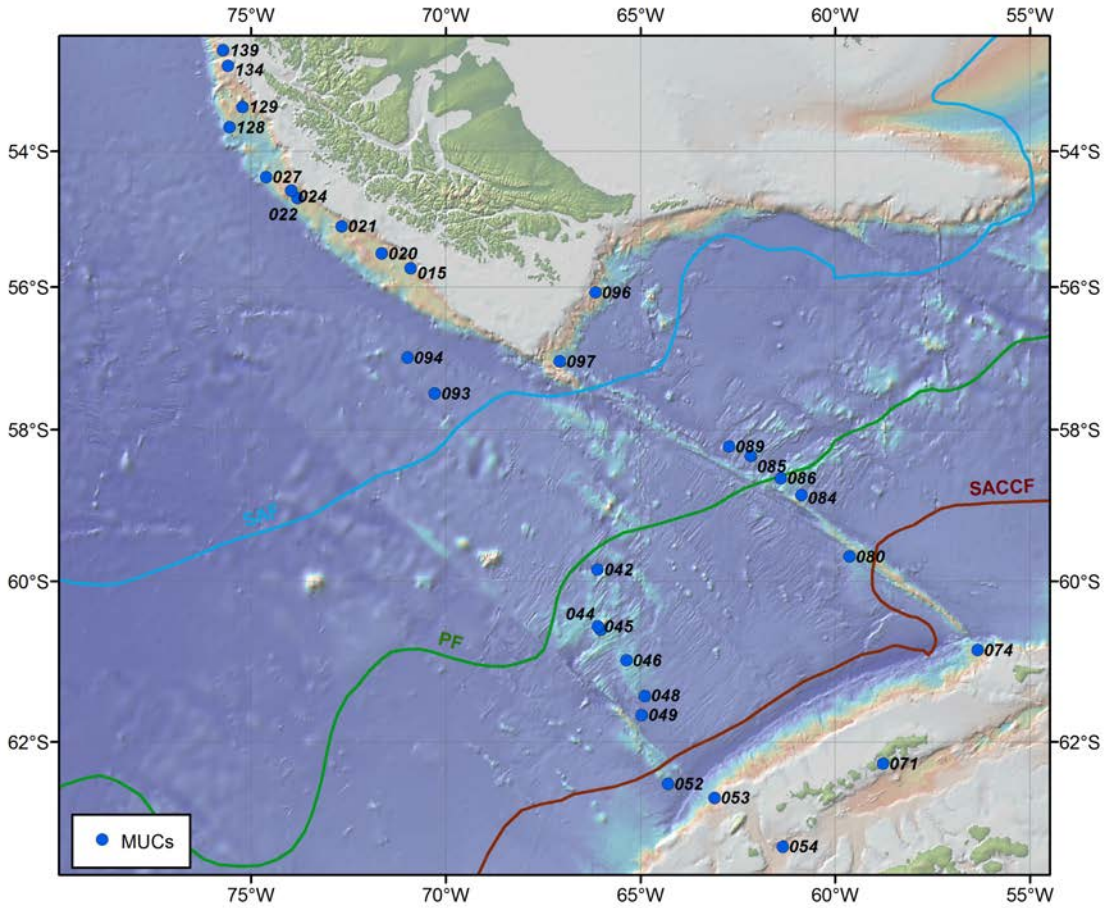

Fig. 8.3: Map of PS97 Multi-Corer stations that were sampled for bottom water nutrient concentrations, and stable oxygen and carbon isotope chemistry, as well as for live benthic foraminiferal assemblages.

Sampling was carried out immediately after the MUC was back on deck, before the tubes were retrieved from the sampling device, to minimize exposure and contamination of samples by interaction with ambient air. The sampling protocols given above for sea water stable isotope and nutrient samples were as well followed for all MUC bottom water samples. On PS97, a total of 32 surface sediment MUC stations were sampled for combined bottom water and sediment surface proxy analyses. Minimum requirement was to retrieve at least two rose Bengal-stained “live” benthic species MUC profiles across the upper 10-15 cm sampled in 1 cm intervals to characterize the interaction of sea water chemistry, habitat information in foraminifera, diatom, radiolarian tests and coccoliths prior to modification during sediment burial, in order to facilitate the interpretation of paleoproxy records.

Tab. 8.3 Overview of PS97 Multi-Corer stations sampled for bottom water stable O and C isotope, and nutrient analyses. Note that geographic coordinates given in decimal degrees.

Station	Longitude [°E]	Latitude [°S]	Bot. Depth [m]
015-2	-70.893	-55.732	1886
020-1	-71.637	-55.513	2104
020-1	-71.637	-55.513	2104
021-1	-72.668	-55.115	1840
022-1	-73.806	-54.701	1615
024-2	-73.955	-54.588	1273
027-1	-74.605	-54.384	2349
042-1	-66.096	-59.844	4172
044-1	-66.022	-60.613	1203
045-1	-66.095	-60.571	2292
046-6	-65.360	-60.997	2803
048-1	-64.888	-61.440	3455
049-2	-64.962	-61.671	3752
052-3	-64.294	-62.499	2890
053-1	-63.095	-62.663	2021
054-2	-61.344	-63.233	1283
071-2	-58.772	-62.258	441
074-1	-56.342	-60.869	1831
077-1	-55.703	-60.591	3587
080-2	-59.631	-59.675	3113
084-2	-60.865	-58.869	3617
085-2	-62.168	-58.355	3091
086-2	-61.397	-58.644	2969
089-2	-62.727	-58.227	3432
093-3	-70.276	-57.499	3782
094-1	-70.972	-57.003	3993
096-1	-66.149	-56.076	1621
097-1	-67.067	-57.055	2319
128-1	-75.545	-53.634	2294
129-1	-75.214	-53.321	1879
134-1	-75.581	-52.683	1075

139-1	-75.707	-52.442	639

In the case of benthic foraminiferal samples, the upper 10-15 cm were sampled into KAUTEX plastic bottles and fixed with Ethanol (98 %, with 1% MEK) admixed with rose Bengal (min. 2 g L^{-1}) for sample conservation and later identification of benthic foraminifera specimen that were alive during sampling. The remaining deeper parts of the MUC profiles were sampled into conventional sealable, plastic bags (Whirlpack®). On MUC deployments, apart from the two tubes for benthic foraminifera, one for other microfossil species work, one for additional isotope studies (requiring larger volumes), and – on selected stations – one to two tubes for siliceous microfossil studies were sampled in 1 cm sample intervals accordng to the procedures outlined in Chapter 3.1. about the surface sediment sampling.

Preliminary Results

Results from water column sampling are limited to the small amount of ship-based analytical work carried out on primary productivity estimations, quality control of filter residue samples and retrieved sea-water profiles. As the vast majority of the analytical work will be carried out at a later stage in shore-based laboratories, results are limited in this reporting. No shipboard results were obtained for water sampling for isotope and nutrient analyses, all filter samples for plankton and suspension load studies will also be analysed entirely shore-based.

Gross Primary Production (GPP) and Community Respiration (CR) calculations

The obtained gross primary productivity (GPP) estimates for the studied region of Cabo de Hornos and Drake Passage showed low GPP estimates with values between two and 16 mgC m^{-3} d^{-1}, with a median of 7.4 mgC m^{-3} d^{-1} at surface waters (i.e. 5 and 10 m). The low estimates of GPP in oceanic stations were similar to those reported in the Drake Passage of 3 to 9 mgC m^{-3} d^{-1} for offshore stations (Trimborn et al., 2015), and near icebergs in Antarctica 2 – 6 mgC m^{-3} d^{-1} at surface waters (Vernet et al 2011, Holm-Hansen et al. 2004). Only at one station near the Argentinian margin (PS97-001) with highest GPP value, community respiration (CR) showed an increase (i.e. negative values representing oxygen consumption).

Tab. 8.4. Estimates (mean values of 4 replicates and 4 pseudo-replicates) of Gross Primary Production (GPP), Community Respiration (CR) and GPP/CR ratio during PaleoDrake PS97 cruise (Cabo de Hornos, Drake Passage, February – March 2016).

Date	Lat. S	Long. W	Station	Depth (m)	GPP ug C L^{-1} d^{-1}	CR ug C L^{-1} d^{-1}	GPP/CR
21 Feb 16	54º36'204''	62º23'0.88''	PS97-001	5	16.2	-6.2	2.61
25 Feb 16	55º20'401''	70º46'5.23''	PS97-019	10	6.7	14.6	0.45
29 Feb 16	54º41'639''	69º58'0.99''	PS97-036	10	10.6	8.4	1.26
01 Mar 16	59º41'276''	66º26'0.493''	PS97-040	5	2.3	6.7	0.34
05 Mar 16	62º11'944''	64º47'186''	PS97-051	10	8.2	3.3	2.48
15 Mar 16	59º27'540''	59º47'560''	PS97-082	10	1.9	5,7	0.33

Net production (NP), estimated as GPP-CR, tended to increase at the inshore station, with oxygen production at the Cabo de Hornos station. The GPP/CR ratio, used as an index for the trophic status of the system, ranged from 0.3 to 2.5 (Table 8.4.) and showed a median value of 0.8 (n = 6). This result may suggest a close coupling between the synthesis of organic matter (photosynthesis) and its usage by the heterotrophic community (i.e. microzooplankton grazers) in the study area.

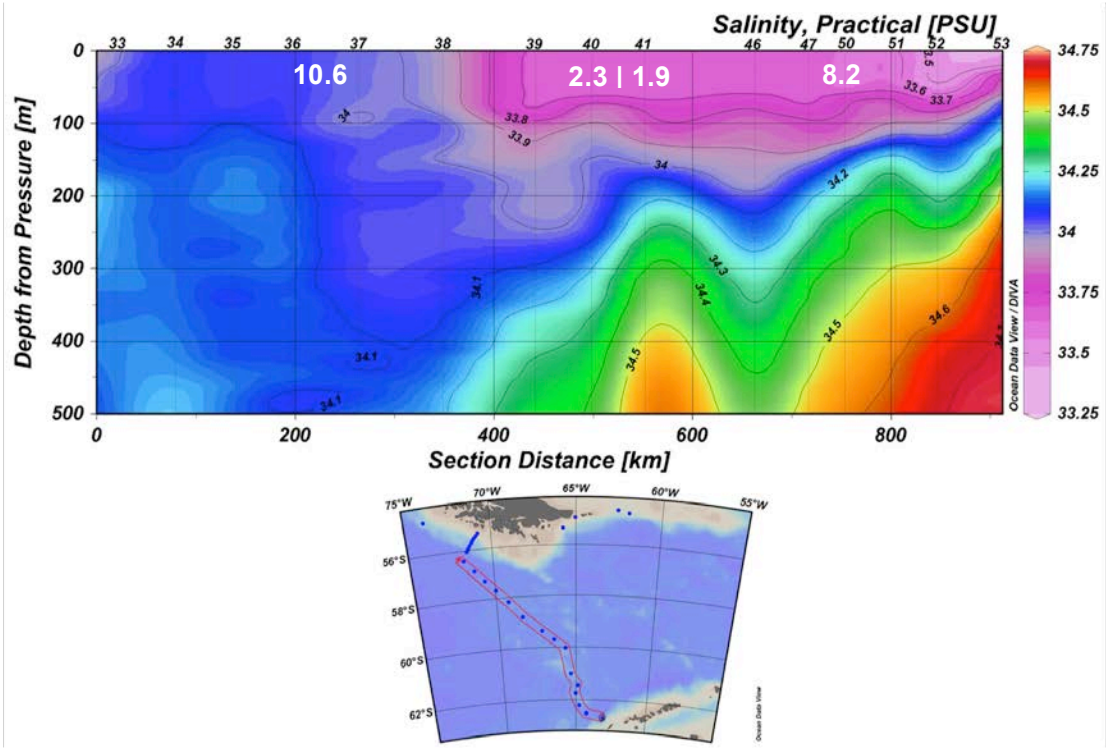

Fig. 8.4: Section showing salinity of the upper 500 m as measured on PS97 (see chapter 6) across western Drake Passage with oceanographic stations (bottom and as small numbers on top panel). Values for GPP (in µg C L^{-1} d^{-1}) are marked in bold white numbers in the approximate sampling locations of incubation experiments.

Plankton Sampling

In all catches, an estimated number of 50 to several 100 of small planktic foraminifera among other plankton was obtained. We estimate that most specimens are in the size of 100-150 µm with about 5-10 % being larger (100 to 250 µm). The small sizes can be explained by the shallow sampling depth, where mostly juveniles can be found, prior to their sinking to greater depth for reproduction (Hemleben et al., 1989). The specimens in many cases were completely filled with cytoplasma. Showing different coloration from dark green-olive to orange-brown to red, some outer chambers from the last whorl in some specimens were not completely filled with cell plasma or empty, suggesting that the plasma was retracted to the inner test space. Coloration of the chamber plasma was different in in the same specimen, showing, for example two dark-green chambers in the last whorl whereas the rest of the dark-orange cytoplasma (Fig. 8.5.). From the number and volume of water, we estimate a population density of about 1 specimen in 30 to 100 L of sea water as a first guess.

Comparison of the catches from the ships rotary pump with those sampled from waters pumped through a membrane pump MP (Scarlett Trimborn, pers. comm.) clearly showed the negative effects of the first to the plankton (Fig. 8.5.). From the ship pump, we found in the checked plankton samples many cases, where fragile antennae and other body segments were broken or disrupted, whereas the MP from the AWI Biology group produced samples with largely fully intact plankton specimens. We observed that the foraminifer spines were longer and much better preserved using the MP. However, numbers of well preserved test could be also recovered from the waters using the ships pump. Some empty shells were

found in all samples. However, no broken tests were noticed. The plankton extract as a whole was dilutes to 50% fixed with ethanol, sealed in 100ml-NUNC-beakers, and will be wet picked in Tübingen in a few months for TEM- and stable isotope analyses (AWI, L. Lembke-Jene, A. Mackensen). Photographs from the plankton pumping are stored in PANGAEA.

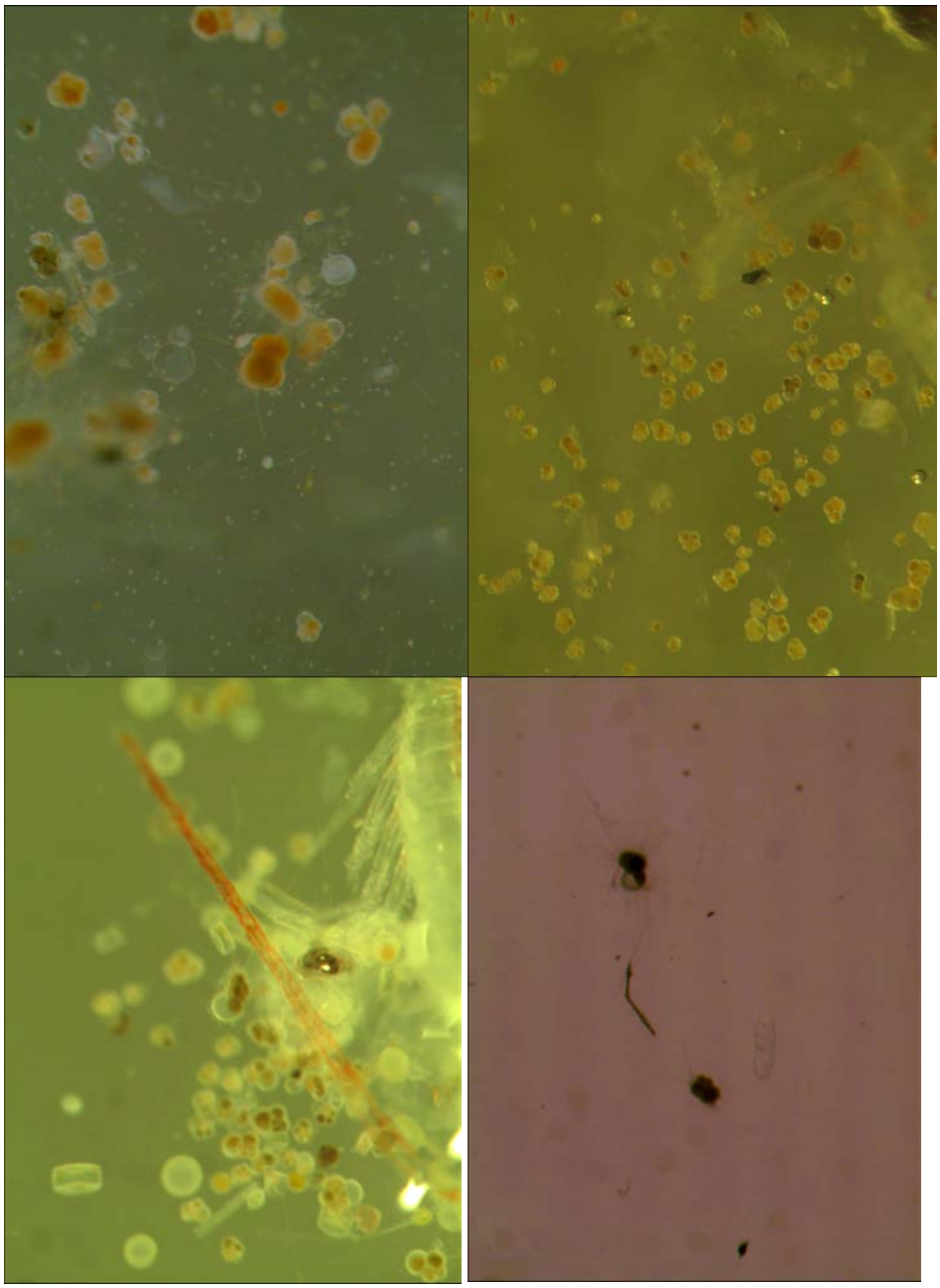

Fig. 8.5: Planktic foraminifera PF from plankton pumping during PS97, mostly as living juvenile specimens (see text). Note that some PF have empty chambers. Lower right: 2 PF with well preserved spines, in length doubling the body diameter (membrane pump sample PS97/034-1 of 28.02.2016). Lower left: specimen in the center of the picture with short spines (<< body diameter, rotary pump sample of 19.03.2016). White to transparent circles and "boxes" are centric diatoms, large debris is of shriops/copepods.

Surface and deep-water sampling for stable O and C isotope characteristics

The planned onshore works will address several outstanding questions with respect to nutrient biogeochemistry and the dynamics of the subantarctic Southern Ocean and narrow, jet-like structure of the Cape Horn Current under modern climate conditions. With the newly acquired samples we expect to better map the isotope and nutrient characteristics of the surface ocean, the major mid-depth water masees, especially the Antarctic Intermediate Water (AAIW), as well as provide data on the Upper and Lower Circumpolar Deep Water (CPDW) patterns. By enlarging the data coverage in this sparsely sampled region, we hope to increase our understanding of the scaling of paleoceanographically relevant tracers ($\delta^{13}C_{DIC}$, $\delta^{18}O$, PO_4, NO_3, $\delta^{19}O_{Sil}$, $\delta^{30}Si$), to mechanistically link their recording in proxy carriers to present environmental conditions, and assess their sensitivity in the temporal and spatial domain on modern and geological time scales.

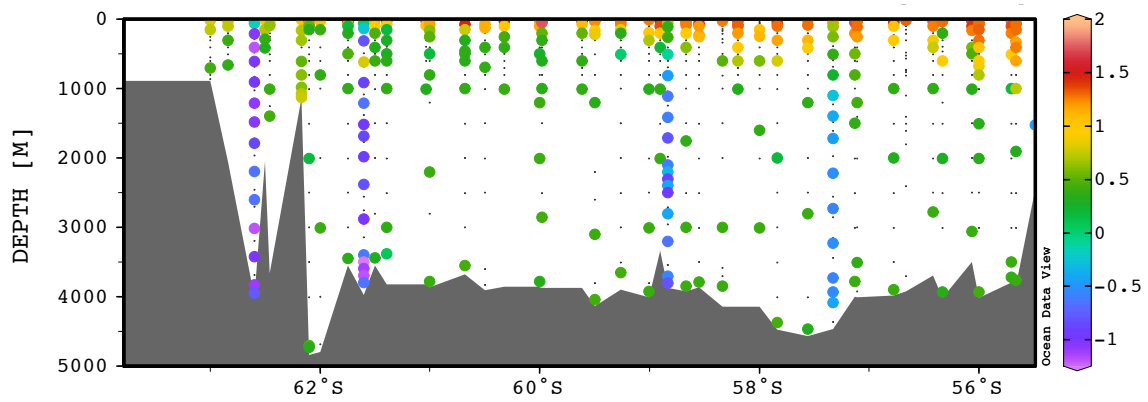

Fig. 8.6: Latitudinal section across Drake Passage, shown are $\delta^{13}C_{DIC}$ data from stations available through the GLODAP v2 database. Note the scarcity of data below 2000 m.

As of now, only a limited dataset of published $\delta^{13}C_{DIC}$ and $\delta^{18}O$ isotope profiles exists in the Drake Passage section of the Southern Ocean, despite its importance for inter-oceanic exchange. Within the current GLODAP database (Key et al., 2004, http://cdiac.ornl.gov/oceans/glodap/), less than 3% of the available oceanographic station data contain e.g. $\delta^{13}C_{DIC}$ and $\delta^{18}O$ data. In fact, below 2000 m water depth less than 100 such measurements (> 2000 m) have been published to date from the study region (Fig. 8.6).

The planned analyses with the collected sea water sample profiles will significantly enhance this coverage. Comparison between the selected station profiles and the resutls from the PS97 CTD casts (Fig. 8.7) show that we have successfully sampled the major water masses across the major frontal systems along the major oceanographic target transects, e.g. the western Drake Passage. In conjunction with both carbonaceous and siliceous microfossil groups and their elemental and isotope chemistry, we hope that shore-based results will show how changes in multiple oceanic parameters might affect the productivity, the biodiversity of Southern Ocean phytoplankton and their bentho-pelagic coupling through time.

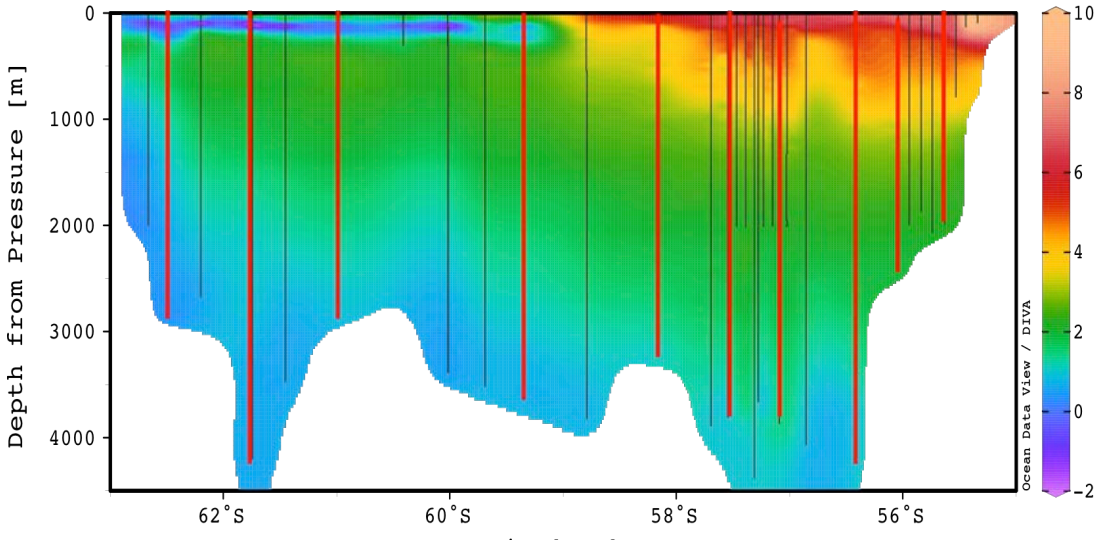

Fig. 8.7: Cross section of Drake Passage, stations as in Figure 8.4, but for entire water column and plotted against latitude. Colour shading shows temperatures as measured on PS97 gridded with the ODV DIVA function, black vertical lines reference the station hydrocasts, red lines mark the selected stations sampled for O and C isotope and nutrient measurements.

Data Management

ABC

References

Anderson R.F., Barker, S., Fleisher, M., Gersonde, R., Goldstein, S.L., Kuhn, G., Mortyn, P.G., Pahnke, K., Sachs, J.P., 2014. Biological Response to Millennial Variability of Dust and Nutrient Supply in the Subantarctic South Atlantic Ocean. Philosophical Transactions of the Royal Society A: Mathematical, Physical & Engineering Sciences 372 (2019), 20130054–54.

Bollmann J, Cortés MY, Haidar AT, Brabec B, Close A, Hofmann R, Palma S, Tupas L, Thierstein HR (2002) Techniques for quantitative analyses of calcareous marine phytoplankton. Marine Micropaleontology, 44, 163-185.

Comiso C, McClain CR, Sullivan CW, Ryan JP and Leonard CL. (1993). Coastal Zone Color Scanner pigment concentrations in the Southern Ocean and relationships to geophysical surface features. Journal of Geophysical Research 98: 2419-2451.

Ebersbach, F., Trull, T.W.(2008). Sinking particle properties from polyacrylamide gels during the Kerguelen Ocean and Plateau compared Study (KEOPS): Zooplankton control of carbon export in an area of persistent natural iron inputs in the Southern Ocean. Limnology and Oceanography. 53: 212-224.

Egan KE, Rickaby REM, Leng MJ, Hendry KR, Hermoso M, Sloane HJ, Bostock H, Halliday AN (2012) Diatom Silicon Isotopes as a Proxy for Silicic Acid Utilisation: a Southern Ocean Core Top Calibration. Geochimica Et Cosmochimica Acta, 96, 174-192. doi:10.1016/j.gca.2012.08.002.

Elderfield H, Ferretti P, Greaves M, Crowhurst S, McCave IN, Hodell DA, Piotrowski AM (2012) Evolution of Ocean Temperature and Ice Volume Through the Mid-Pleistocene Climate Transition. Science, 337 (6095), 704–709.

Hemleben C., Spindler, M., and Anderson R., 1989. Modern planktonic foraminifera, Springer Verlag, 380pp.

Hendry KR, Rickaby REM, Meredith MP, Elderfield H (2009) Controls on stable isotope and trace metal uptake in Neogloboquadrina pachyderma (sinistral) from an Antarctic sea-ice environment. Earth and Planetary Science Letters, 278 (1-2), 67–77. doi: 10.1016/j.epsl.2008.11.026.

Hendry KR, Robinson LF (2012) The Relationship Between Silicon Isotope Fractionation in Sponges and Silicic Acid Concentration: Modern and Core-Top Studies of Biogenic Opal. Geochimica Et Cosmochimica Acta, 81, 1-12. doi:10.1016/j.gca.2011.12.010.

Hewes, C.D. (2009). A quantitative analysis of sources for summertime phytoplankton variability over 18 years in the South Shetland Islands (Antarctica) region. Deep-Sea Research I 56:1230-1241.
Holm-Hansen, O., Naganobu, M., Kawaguchi, S., Kameda, T., Krasovski, I., Tchernyshkov, P., Pridle, J., Korb, R., Brandon, M., Demer, D., Hewitt, R.P., Kahru, M., Hewes, C.D. (2004). Factors influencing the distribution, biomass, and productivity of phytoplankton in the Scotia Sea and adjoining waters. Deep-Sea Research II 51: 1333-1350
Kang, J.S., Kang, S.-H., Lee, J.H., Lee, S.H. (2002). Seasonal variation of microalgal assemblages at a fixed station on King George Island, Antarctica, 1996, Marine Ecology Progress Series. 229: 19–32.
Kohfeld KE, Le Quere C, Harrison SP, Anderson RF (2005) Role of Marine Biology in Glacial-Interglacial CO2 Cycles. Science, 308 (5718), 74-78. doi:10.1126/science.1105375.
Kozdon R, Eisenhauer A, Weinelt M, Meland MZ, Nürnberg D (2009) Reassessing Mg/Ca temperature calibrations of Neogloboquadrina pachyderma (sinistral) using paired d44/40Ca and Mg/Ca Measurements. Geochemistry Geophysics Geosystems, 10 (3), Q03005.
Laubscher RK, Perissinotto R, McQuaid CD. (1993). Phytoplankton production and biomass at frontal zones in the Atlantic sector of the Southern Ocean. Polar Biology. 13: 471- 481.
Key, R. M., Kozyr, A., Sabine, C.L., Lee, K., Wanninkhof, R., Bullister, J.L., Feely, R.A., Millero, F.J., Mordy, C., Peng, T.H., 2004. A Global Ocean Carbon Climatology: Results From Global Data Analysis Project (GLODAP). Global Biogeochemical Cycles 18 (4). GB4031.
Mackensen A (2012) Strong Thermodynamic Imprint on Recent Bottom-Water and Epibenthic δ13C in the Weddell Sea Revealed: Implications for Glacial Southern Ocean Ventilation. Earth and Planetary Science Letters, 317-318, 20-26. doi:10.1016/j.epsl.2011.11.030.
Maier E, Chapligin B, Abelmann A, Gersonde R, Esper O, Ren J, Friedrichsen H, Meyer H, Tiedemann R (2013) Combined Oxygen and Silicon Isotope Analysis of Diatom Silica From a Deglacial Subarctic Pacific Record. Journal of Quaternary Science, 28 (6), 571-581, doi:10.1002/jqs.2649.
Marshall J and Speer K (2012) Closure of the Meridional Overturning Circulation Through Southern Ocean Upwelling. Nature Geoscience, 5 (3), 171–180, doi:10.1038/ngeo1391.
Meredith MP, Woodworth PL, Chereskin TK, Marshall DP, Allison LC, Bigg GR, Donohue K, Heywood KJ, Hughes CW, Hibbert A, McC. Hogg A, Johnson HL, Jullion L, King BA, Leach H, Lenn Y-D, Morales Maqueda MA, Munday DR, Naveira Garabato AC, Provost C, Sallée J-B, Sprintall J (2011) Sustained Monitoring of the Southern Ocean at Drake Passage: Past Achievements and Future Priorities. Reviews of Geophysics, 49 (4), RG4005. doi: 10.1029/2010RG000348.
Montes-Hugo, M., Doney, S., Ducklow, H.W., Fraser, W., Martinson, D., Stammerjohn, S.E., Schofield, O. (2009). Recent changes in phytoplankton communities associated with rapid regional climate change along the western Antarctic Peninsula. Science 323: 1470-1473.
Nürnberg D (1995) Magnesium in tests of Neogloboquadrina pachyderma sinistral from high northern and southern latitudes, Journal of Foraminiferal Research, 25, 350-368.
Olguin, H.F., Alder, V.A. (2011). Species composition and biogeography of diatoms in Antarctic and subantarctic (Argentine shelf) waters (37-76S). Deep-Sea Research II 58: 139-152.
Parsons, T.R., Maita, Y., Lalli, C.M., 1984. Counting, media and preservatives. Chapter 8. In: A manual of chemical and biological methods for seawater analysis (pp. 173). Pergamon Press, Toronto.
Saavedra-Pellitero, M., Baumann, K.-H., Flores, J. A., Gersonde, R., 2014. Biogeographic Distribution of Living Coccolithophores in the Pacific Sector of the Southern Ocean. Marine Micropaleontology 109, 1-20.
Trimborn, S, Hoppe, CJM, Taylor, BB, Bracher, Hassler, C. (2015). Physiological characteristics of open ocean and coastal phytoplankton communities of Western Antarctic Peninsula and Drake Passage waters. Deep-Sea Research I, 98; 115-124.
Varela, M., Fernandez, E., Serret, P. (2002). Size-fractionated phytoplankton biomass and primary production in the Gerlache and south Bransfield straits (Antarctic Penninsula) in austral summer 1995-1996. Deep-Sea Research II 49: 749-768.
Vernet, M, Sines, K, Chakos, D, Cefarelli, AO, Ekern, L. (2011). Impacts on phytoplankton dynamics by free-drifting icebergs in the NW Weddell Sea. Deep-Sea Research II. 58: 1422-1435
Villafane, V.E., Helbling, E.W., Holm-Hansen, O. (1995). Spatial and temporal variability of phytoplankton biomass and taxonomic composition around Elephant Island, Antarctica, during summers of 1990–1993, Marie Biology. 123: 677–686.

Williams, P. J. LeB., Robertson, J.E., 1991. Overall planktonic oxygen and carbon dioxide metabolisms: the problem of reconciling observations and calculations of photosynthetic quotients. Journal of Plankton Research 13 (suppl.), 153–169

Yu J, Broecker WS, Elderfield H, Jin Z, McManus JF, Zhang F (2010) Loss of Carbon From the Deep Sea Since the Last Glacial Maximum." Science, 330 (6007), 1084–1087. doi: 10.1126/science.1193221.

Yu J, Anderson RF, Rohling EJ (2014) Deep Ocean Carbonate Chemistry and Glacial-Interglacial Atmospheric CO2 Changes. Oceanography, 27 (1), 16-25.

A.1 TEILNEHMENDE INSTITUTE / PARTICIPATING INSTITUTIONS

	Address
ARA	Armada Argentina Mar del Plata Buenos Aires Argentina
AWI	Alfred-Wegener-Institut Helmholtz-Zentrumfür Polar- und Meeresforschung Postfach 120161 27515 Bremerhaven Germany
U Bergen	Department of Earth Sciences Postboks 7803 5020 Bergen Norway
U Bremen	Universität Bremen Bibliothekstraße 1, 28359 Bremen Germany
CADIC-CONICET	Centro Austral de Investigaciones Cientificas Ushuaia, Tierra del Fuego Argentina
COPAS	Center for Oceanographic Research in the eastern South Pacific COPAS Sur-Austral Program University of Concepción Chile
TU Dresden	Technische Universität Dresden Institut für Planetare Geodäsie 01062 Dresden Germany
DWD	Deutscher Wetterdienst Geschäftsbereich Wettervorhersage Seeschifffahrtsberatung Bernhard Nocht Str. 76 20359 Hamburg Germany
U Geneva	Université de Genève Institut F.A. Forel Université de Genève 10, route de Suisse 1290 Versoix Switzerland
U Glasgow	School of Geographical & Earth Sciences Main Building, East Quadrangle University of Glasgow Glasgow, G12 8QQ United Kingdom
U Hamburg	Universität Hamburg

	Bundesstrasse 55 20146 Hamburg Germany
HeliService	HeliService International GmbH Am Luneort 15 27572 Bremerhaven Germany
HIDRO	Servicio de Hidrografía Naval Av. Montes de Oca 2124, C1270ABV Buenos Aires, Argentina
IDEAL	Centro de Investigación: Dinámica de Ecosistemas marinos de Altas Latitudes oder auf English: Research Center: Dynamics of High Latitude Marine Ecosystems University of Concepción Chile
IMO	Instituto Milenio de Oceanografía University of Concepción Chile
INIDEP	Instituto Nacional de Investigación y Desarrollo Pesquero,, Paseo Victoria Ocampo 1 7600 Mar del Plata, Argentina Argentina
IOW	Leibniz Institute for Baltic Sea Research, Seestraße 15 18119 Rostock-Warnemünde Germany
ISMAR/CNR	Istituto di Scienze Marine – Consiglio Nazionale delle Ricerche Via Gobetti, 101 40129 Bologna Italy
KUM	K.U.M. Umwelt- und Meerestechnik Kiel GmbH Wischhofstr. 1-3, Geb. 15 24148 Kiel - Germany
U Oldenburg	Universität Oldenburg Ammerländer Heerstraße 114-118 26129 Oldenburg Germany
SHN	Servicio de Hidrografía Naval (SHN), Buenos Aires Argentina
UdeC	Universidad de Concepción Chile
U Trier	Fachbereich Geographie/ Geowissenschaften (FB VI) Behringstraße 54286 Trier Germany
U Tübingen	Universität Tübingen Hölderlinstraße 12 72076 Tübingen Germany

ETH Zürich	ETH Zürich Rämistrasse 101 8092 Zürich Switzerland

A.2 FAHRTTEILNEHMER / CRUISE PARTICIPANTS

Name/ Last name	Vorname/ First name	Institut/ Institute	Beruf/ Profession
Arevalo	Marcelo	AWI	Technician, Geology
Artel	Friedrich	AWI	Student, Hydroacoustics
Arz	Helge	IOW	Scientist, Geology
Blanco-Ameijeiras	Sonia	U Geneva	Scientist, Biogeochemistry
Busch	Peter	TU Dresden	Technician, Geodesy
Cabanes	Damien	U Geneva	Scientist, Biogeochemistry
Canella	Bruno	ARA	Observer, Argentina
Carrera	Vania	Valparaiso	Observer, Chile
Eberlein	Lutz	TU Dresden	Technician, Geodesy
Ehrhardt	Sophie	AWI	Student, Geology
Fenco	Harold	INIDEP	Scientist, Oceanography
Geiger	Alessa	U Glasgow	Scientist, Land-Geology
Gossler	Jürgen	AWI	Scientist, Hydroacoustics
Grob	Henrik	U Hamburg	Student, Hydroacoustics
Hass	Christian	AWI	Scientist, Geology
Hassler	Christel	U Geneva	Scientist, Biogeochemistry
Heiden	Jasmin	AWI/U Bremen	Scientist, Biogeochemistry
Iriarte Machuca	José Luis	UdeC/COPAS/IDEAL	Scientist, Geology
Jager	Harold	HeliService	Pilot, Helicopter
Jensen	Laura	AWI	Scientist, Hydroacoustics
Karitter	Pascal	AWI/U Bremen	PhD-student, Biogeochemistry
Kilian	Rolf	U Trier	Scientist, Land-Geology
Koch	Florian	AWI/U Bremen	PhD-student, Biogeochemistry
Kreps	Gaston	CADIC-CONICET	Observer, Argentina
Kuhn	Gerhard	AWI	Scientist, Geology
Lamy	Frank	AWI	Scientist, Geology
Lange	Carina	UdeC/COPAS/IDEAL	Scientist, Geology
Lelchat	Florian	U Geneva	Scientist, Biogeochemistry
Lembke-Jene	Lester	AWI	Scientist, Oceanography
Lensch	Norbert	AWI	Technician, Geology
Miller	Max	DWD	Meteorologist
Müller	Juliane	AWI	Scientist, Geology
Nürnberg	Dirk	GEOMAR	Scientist, Geology
Papenmeier	Svenja	AWI	Scientist, Hydroacoustics
Plewe	Sascha	IOW	Technician, Geology
Rebolledo	Lorena	UdeC/COPAS/IDEAL	Scientist, Geology
Richter	Roland	HeliService	Technician, Helicopter

Ronge	Thomas	AWI	Scientist, Geology
Rothenburg	Mark	HeliService	Technician, Helicopter
Schneider	Wolfgang	UdeC/IMO	Scientist, Oceanography
Schröder	Simon	AWI	PhD-student, Geology
Schulz	Hartmut	U Tübingen	Scientist, Geology
Sieber	Matthias	ETH Zürich	Scientist, Biogeochemistry
Simon	Heike	U Oldenburg	Scientist, Biogeochemistry
Sonnabend	Hartmut	DWD	Technician, Meteorology
Stratmann	Sjard	U Hamburg	Student, Hydroacoustics
Trimborn	Scarlett	AWI/U Bremen	Scientist, Biogeochemistry
Vaupel	Lars	HeliService	Pilot, Helicopter
Völkner	Christian	AWI/U Bremen	Scientist, Biogeochemistry
Wengler	Marc	AWI	PhD-student, Geology
Zimmermann	Raphael	AWI/U Bremen	Scientist, Biogeoechmistry
Zundel	Max	U Bremen	Scientist, Land-Geology

A.3 SCHIFFSBESATZUNG / SHIP'S CREW

No.	Name	Rank
		Master
		1. Offc.
		Ch. Eng.
		2. Offc.
		2. Offc.
		3. Offc.
		Doctor
		R. Offc.
		2. Eng.
		2. Eng.
		2. Eng.
		Elec. Eng.
		ELO
		ELO
		ELO
		ELO
		Boatsw.
		Carpenter
		A.B.
		A.B.
		A.B.
		A.B.
		A.B.
		A.B.
		A.B.
		A.B.
		Storek.

		Mot-man
		Mot-man
		Mot-man
		Mot-man
		Mot-man
		Cook
		Cooksmate
		Cooksmate
		1. Stwdess
		Stwdess/N.
		2. Stwdess
		2. Steward
		2. Stwdess
		2. Steward
		2. Stwdess
		Laundrym.

A.4 STATIONSLISTE / STATION LIST PS 97

Station	Date	Time (UTC)	Gear	Action	Position Lat	Position Lon	Water depth (m)
PS97/001-1	21.02.16	07:35	CTD/RO	on ground/max depth	54° 33.90' S	62° 34.97' W	502
PS97/002-1	21.02.16	11:45	CTD/RO	on ground/max depth	54° 40.51' S	61° 55.34' W	1299.3
PS97/003-1	21.02.16	17:26	MUC	on ground/max depth	54° 41.09' S	61° 54.94' W	1333.7
PS97/004-1	21.02.16	19:28	MUC	on ground/max depth	54° 43.78' S	61° 40.58' W	750.5
PS97/004-2	21.02.16	20:18	GC	on ground/max depth	54° 43.58' S	61° 40.51' W	747.7
PS97/005-1	22.02.16	00:57	GC	on ground/max depth	54° 55.33' S	62° 13.58' W	2439.8
PS97/006-1	22.02.16	13:53	GKG	on ground/max depth	54° 51.00' S	64° 17.01' W	113.8
PS97/007-1	22.02.16	19:44	CTD/RO	on ground/max depth	54° 53.71' S	65° 2.31' W	123.2
PS97/008-1	22.02.16	01:42	CTD/RO	on ground/max depth	55° 18.40' S	65° 46.47' W	1695.8
PS97/009-1	23.02.16	12:08	MUC	on ground/max depth	55° 41.07' S	66° 8.61' W	561.3
PS97/009-2	23.02.16	14:10	PC	on ground/max depth	55° 41.02' S	66° 8.65' W	555.5
PS97/010-1	23.02.16	18:22	PC	on ground/max depth	55° 41.66' S	66° 7.55' W	691.2
PS97/011-1	23.02.16	20:37	PC	on ground/max depth	55° 42.17' S	66° 8.19' W	626
PS97/011-2	23.02.16	22:11	GKG	on ground/max depth	55° 42.49' S	66° 8.04' W	667.4
PS97/012-1	23.02.16	23:01	GKG	on ground/max depth	55° 41.14' S	66° 8.59' W	563.5
PS97/013-1	24.02.16	00:08	GKG	on ground/max depth	55° 41.52' S	66° 7.43' W	665
PS97/014-1	24.02.16	18:33	GC	on ground/max depth	55° 43.93' S	71° 12.94' W	2102.6
PS97/015-1	24.02.16	21:02	GC	on ground/max depth	55° 43.88' S	70° 53.54' W	1872.1
PS97/015-2	24.02.16	22:16	MUC	on ground/max depth	55° 43.89' S	70° 53.55' W	1886.3
PS97/016-1	24.02.16	00:42	CTD/RO	on ground/max depth	55° 37.81' S	71° 7.34' W	2000.9
PS97/017-1	25.02.16	02:44	CTD/RO	on ground/max depth	55° 31.79' S	71° 0.22' W	804.6
PS97/018-1	25.02.16	04:10	CTD/RO	on ground/max depth	55° 26.44' S	70° 53.41' W	140.7
PS97/019-1	25.02.16	05:18	CTD/RO	on ground/max depth	55° 20.41' S	70° 46.62' W	101.7
PS97/020-1	25.02.16	10:38	MUC	on ground/max depth	55° 30.80' S	71° 38.22' W	2104.3
PS97/020-2	25.02.16	12:00	GC	on ground/max depth	55° 30.79' S	71° 38.22' W	2070.4
PS97/021-1	25.02.16	17:49	MUC	on ground/max depth	55° 6.91' S	72° 40.09' W	1840.4
PS97/021-2	25.02.16	19:15	GC	on ground/max depth	55° 6.93' S	72° 40.14' W	1839.2
PS97/021-3	25.02.16	20:08	GC	on ground/max depth	55° 6.90' S	72° 40.15' W	1822.7
PS97/022-1	26.02.16	12:06	MUC	on ground/max depth	54° 42.03' S	73° 48.38' W	1615.1
PS97/022-2	26.02.16	13:15	GC	on ground/max depth	54° 42.03' S	73° 48.41' W	1615.9
PS97/023-1	26.02.16	14:26	GC	on ground/max depth	54° 40.86' S	73° 49.94' W	1597.8
PS97/024-1	26.02.16	16:01	GC	on ground/max depth	54° 35.28' S	73° 57.29' W	1278
PS97/024-2	26.02.16	16:57	MUC	on ground/max depth	54° 35.27' S	73° 57.30' W	1272.8
PS97/025-1	26.02.16	19:23	PC	on ground/max depth	54° 42.03' S	73° 48.44' W	1620.4
PS97/026-1	26.02.16	22:10	PC	on ground/max depth	54° 40.84' S	73° 49.98' W	1604.3
PS97/026-2	26.02.16	23:25	CTD/RO	on ground/max depth	54° 40.83' S	73° 49.85' W	1599.3
PS97/027-1	27.02.16	08:02	MUC	on ground/max depth	54° 23.05' S	74° 36.30' W	2349.2
PS97/027-2	27.02.16	10:06	GC	on ground/max depth	54° 23.09' S	74° 36.35' W	2341.8
PS97/028-1	27.02.16	16:02	GKG	on ground/max depth	54° 31.22' S	73° 14.02' W	104.6
PS97/029-1	28.02.16	02:11	CTD/RO	on ground/max depth	55° 44.33' S	71° 13.07' W	2099.6
PS97/030-1	28.02.16	04:34	CTD/RO	on ground/max depth	55° 50.25' S	71° 19.10' W	1887.2
PS97/031-1	28.02.16	07:09	CTD/RO	on ground/max depth	55° 56.32' S	71° 25.34' W	1989
PS97/032-1	28.02.16	09:50	CTD/RO	on ground/max depth	56° 2.28' S	71° 31.89' W	2455.4
PS97/033-1	28.02.16	14:25	CTD/RO	on ground/max depth	56° 24.47' S	71° 45.65' W	4345.9
PS97/034-1	28.02.16	18:59	MP	on ground/max depth	56° 50.78' S	71° 10.96' W	4089.5
PS97/034-2	28.02.16	22:00	CTD/RO	on ground/max depth	56° 51.27' S	71° 10.78' W	4089.5
PS97/035-1	29.02.16	03:25	CTD/RO	on ground/max depth	57° 16.43' S	70° 36.51' W	3759.4
PS97/036-1	29.02.16	08:38	CTD/RO	on ground/max depth	57° 41.63' S	69° 59.06' W	3911.5
PS97/037-1	29.02.16	14:27	CTD/RO	on ground/max depth	58° 9.95' S	69° 15.54' W	3163.3
PS97/038-1	29.02.16	20:55	CTD/RO	on ground/max depth	58° 47.51' S	68° 24.97' W	3858.9
PS97/039-1	01.03.16	04:25	CTD/RO	on ground/max depth	59° 20.84' S	67° 13.31' W	3673.1
PS97/040-1	01.03.16	09:56	CTD/RO	on ground/max depth	59° 41.28' S	66° 26.48' W	3542.2
PS97/041-1	01.03.16	14:45	CTD/RO	on ground/max depth	60° 1.16' S	65° 41.75' W	3437.1
PS97/041-2	01.03.16	15:27	MP	on ground/max depth	60° 1.14' S	65° 41.66' W	3459

PS97/041-3	01.03.16	18:03	CTD/RO	on ground/max depth	60° 1.00' S	65° 41.71' W	3442.5
PS97/042-1	02.02.16	00:14	MUC	on ground/max depth	59° 50.62' S	66° 5.77' W	4172
PS97/043-1	03.03.16	08:19	MP	on ground/max depth	60° 24.79' S	66° 21.70' W	
PS97/043-2	03.03.16	08:59	CTD/RO	on ground/max depth	60° 24.70' S	66° 21.73' W	3141.1
PS97/044-1	03.03.16	11:54	MUC	on ground/max depth	60° 36.80' S	66° 1.34' W	1202.8
PS97/045-1	03.03.16	13:30	MUC	on ground/max depth	60° 34.27' S	66° 5.67' W	2292
PS97/045-2	03.03.16	14:49	GC	on ground/max depth	60° 34.25' S	66° 5.66' W	2293
PS97/046-1	03.03.16	19:46	PLA	on ground/max depth	60° 59.91' S	65° 21.86' W	2766.4
PS97/046-2	03.03.16	20:04	PLA	on ground/max depth	60° 59.88' S	65° 21.79' W	2776.4
PS97/046-3	03.03.16	20:51	GC	on ground/max depth	60° 59.87' S	65° 21.64' W	2789
PS97/046-4	03.03.16	23:23	PC	on ground/max depth	60° 59.83' S	65° 21.37' W	2775.3
PS97/046-5	04.03.16	01:38	MUC	on ground/max depth	60° 59.83' S	65° 21.49' W	2776.4
PS97/046-6	04.03.16	03:13	MUC	on ground/max depth	60° 59.74' S	65° 21.40' W	2802.7
PS97/046-7	04.03.16	05:05	CTD/RO	on ground/max depth	60° 59.79' S	65° 21.23' W	2794.7
PS97/047-1	04.03.16	10:39	CTD/RO	on ground/max depth	61° 27.20' S	64° 52.45' W	3477.7
PS97/048-1	04.03.16	13:03	MUC	on ground/max depth	61° 26.40' S	64° 53.27' W	3455.2
PS97/048-2	04.03.16	15:34	PC	on ground/max depth	61° 26.39' S	64° 53.22' W	3448.1
PS97/049-1	04.03.16	20:50	PC	on ground/max depth	61° 40.28' S	64° 57.76' W	3757.5
PS97/049-2	04.03.16	23:29	MUC	on ground/max depth	61° 40.28' S	64° 57.74' W	3752.2
PS97/050-1	05.03.16	01:55	GoFlo	on ground/max depth	61° 44.71' S	65° 1.97' W	4243.6
PS97/050-2	05.03.16	03:44	CTD/RO	on ground/max depth	61° 44.72' S	65° 1.93' W	4242.4
PS97/051-1	05.03.16	08:40	CTD/RO	on ground/max depth	62° 11.97' S	64° 47.23' W	2714.3
PS97/052-1	05.03.16	13:56	CTD/RO	on ground/max depth	62° 29.95' S	64° 17.48' W	2889.9
PS97/052-2	05.03.16	15:19	GoFlo	on ground/max depth	62° 29.92' S	64° 17.65' W	2890.2
PS97/052-3	05.03.16	16:17	MUC	on ground/max depth	62° 29.93' S	64° 17.63' W	2889.8
PS97/052-4	05.03.16	17:50	GC	on ground/max depth	62° 29.94' S	64° 17.62' W	2890.4
PS97/053-1	05.03.16	23:54	MUC	on ground/max depth	62° 39.79' S	63° 5.68' W	2021.4
PS97/053-2	06.03.16	00:57	GC	on ground/max depth	62° 39.77' S	63° 5.61' W	2016.1
PS97/053-3	06.03.16	02:28	CTD/RO	on ground/max depth	62° 39.60' S	63° 6.20' W	2041.1
PS97/054-1	06.03.16	10:11	MUC	on ground/max depth	63° 13.99' S	61° 20.62' W	1283.1
PS97/054-2	06.03.16	11:13	MUC	on ground/max depth	63° 13.99' S	61° 20.63' W	1283.2
PS97/054-3	06.03.16	12:46	GC	on ground/max depth	63° 13.98' S	61° 20.61' W	1279.3
PS97/055-1	06.03.16	17:03	GC	on ground/max depth	63° 32.09' S	60° 40.36' W	722.6
PS97/055-2	06.03.16	17:54	MUC	on ground/max depth	63° 32.07' S	60° 40.38' W	725.7
PS97/056-1	06.03.16	21:05	MUC+SVP	on ground/max depth	63° 45.42' S	60° 26.51' W	633.4
PS97/056-2	06.03.16	21:50	GC	on ground/max depth	63° 45.45' S	60° 26.42' W	634.5
PS97/057-1	07.03.16	15:26	GoFlo	on ground/max depth	62° 35.03' S	59° 41.30' W	524.9
PS97/058-1	07.03.16	19:37	GoFlo	on ground/max depth	62° 26.59' S	59° 12.18' W	475
PS97/059-1	08.03.16	01:41	GC	on ground/max depth	62° 26.24' S	59° 39.50' W	353.8
PS97/059-2	08.03.16	02:25	GKG	on ground/max depth	62° 26.25' S	59° 39.49' W	353.9
PS97/060-1	08.03.16	04:29	GKG	on ground/max depth	62° 34.99' S	59° 38.70' W	462.4
PS97/061-1	08.03.16	05:37	GKG	on ground/max depth	62° 33.53' S	59° 48.00' W	466.6
PS97/062-1	08.03.16	06:28	GKG	on ground/max depth	62° 34.19' S	59° 50.82' W	477.4
PS97/062-2	08.03.16	07:14	GC	on ground/max depth	62° 34.19' S	59° 50.86' W	477.5
PS97/063-1	08.03.16	08:31	GC	on ground/max depth	62° 33.58' S	59° 47.84' W	468.5
PS97/064-1	08.03.16	09:42	GC	on ground/max depth	62° 35.00' S	59° 38.73' W	462.8
PS97/065-1	08.03.16	12:38	GC	on ground/max depth	62° 29.22' S	59° 20.86' W	480.7
PS97/065-2	08.03.16	13:32	GKG	on ground/max depth	62° 29.22' S	59° 20.84' W	480.1
PS97/066-1	08.03.16	16:47	GC	on ground/max depth	62° 34.16' S	59° 50.91' W	493
PS97/067-1	08.03.16	19:46	GC	on ground/max depth	62° 25.01' S	59° 8.60' W	550.3
PS97/067-2	08.03.16	20:20	GKG	on ground/max depth	62° 25.01' S	59° 8.59' W	793
PS97/068-1	09.03.16	03:46	GC	on ground/max depth	63° 10.08' S	59° 18.22' W	793
PS97/068-2	09.03.16	04:37	MUC	on ground/max depth	63° 10.05' S	59° 18.12' W	793.6
PS97/069-1	09.03.16	09:02	MUC	on ground/max depth	62° 35.36' S	58° 32.56' W	1641.8
PS97/069-2	09.03.16	10:12	GC	on ground/max depth	62° 35.37' S	58° 32.53' W	1635.4
PS97/070-1	09.03.16	12:14	GoFlo	on ground/max depth	62° 25.28' S	58° 29.18' W	1209.3
PS97/071-1	09.03.16	14:34	PC	on ground/max depth	62° 15.51' S	58° 46.32' W	442.4
PS97/071-2	09.03.16	15:33	MUC	on ground/max depth	62° 15.52' S	58° 46.31' W	441
PS97/071-3	09.03.16	15:59	PLA	on ground/max depth	62° 15.50' S	58° 46.27' W	427.1
PS97/072-1	10.03.16	04:13	PC	on ground/max depth	62° 0.39' S	56° 3.86' W	1992.9

PS97/072-2	10.03.16	06:05	MUC	on ground/max depth	62° 0.39' S	56° 3.88' W	1991.7
PS97/073-1	10.03.16	10:38	MUC	on ground/max depth	61° 49.73' S	55° 38.79' W	2682.9
PS97/073-2	10.03.16	12:13	MUC	on ground/max depth	61° 49.72' S	55° 38.82' W	2623.5
PS97/073-3	10.03.16	14:09	MUC	on ground/max depth	61° 49.75' S	55° 38.75' W	2627.9
PS97/073-4	10.03.16	15:37	GC	on ground/max depth	61° 49.73' S	55° 38.73' W	2624.1
PS97/073-5	10.03.16	16:55	GoFlo	on ground/max depth	61° 49.52' S	55° 38.92' W	2619.2
PS97/074-1	12.03.16	03:56	MUC	on ground/max depth	60° 52.11' S	56° 20.49' W	1831.4
PS97/075-1	12.03.16	22:19	GC	on ground/max depth	60° 52.53' S	56° 20.48' W	1851.4
PS97/076-1	13.03.16	03:20	CTD/RO	on ground/max depth	60° 30.02' S	55° 30.01' W	3640.9
PS97/076-2	13.03.16	05:59	CTD/RO	on ground/max depth	60° 30.00' S	55° 29.99' W	3644.1
PS97/076-3	13.03.16	06:38	MP	on ground/max depth	60° 29.93' S	55° 29.56' W	3641.5
PS97/076-4	13.03.16	18:02	PLA	on ground/max depth	60° 30.31' S	55° 29.70' W	3636.8
PS97/077-1	13.03.16	20:40	MUC	on ground/max depth	60° 35.44' S	55° 42.19' W	3586.5
PS97/077-2	13.03.16	22:33	GC	on ground/max depth	60° 35.43' S	55° 42.21' W	3543
PS97/078-1	14.03.16	00:50	GC	on ground/max depth	60° 39.15' S	55° 50.38' W	3666.4
PS97/079-1	14.03.16	13:05	MUC	on ground/max depth	60° 8.55' S	58° 59.42' W	3539.3
PS97/079-2	14.03.16	14:58	GC	on ground/max depth	60° 8.54' S	58° 59.48' W	3541.3
PS97/080-1	14.03.16	22:19	GC	on ground/max depth	59° 40.48' S	59° 37.88' W	3105.9
PS97/080-2	15.03.16	00:07	MUC	on ground/max depth	59° 40.49' S	59° 37.86' W	3112.7
PS97/081-1	15.03.16	04:06	CTD/RO	on ground/max depth	59° 34.80' S	59° 57.07' W	3728.8
PS97/082-1	15.03.16	07:20	CTD/RO	on ground/max depth	59° 27.49' S	59° 47.74' W	2128.6
PS97/083-1	15.03.16	13.58	MUC	on ground/max depth	58° 59.65' S	60° 34.28' W	3756.3
PS97/083-2	15.03.16	16:32	PC	on ground/max depth	58° 59.66' S	60° 34.22' W	3762.3
PS97/084-1	15.03.16	21:47	PC	on ground/max depth	58° 52.14' S	60° 51.94' W	3557
PS97/084-2	16.03.16	00:24	MUC	on ground/max depth	58° 52.14' S	60° 51.91' W	3617.4
PS97/085-1	16.03.16	12:40	PC	on ground/max depth	58° 21.27' S	62° 10.05' W	3086.5
PS97/085-2	16.03.16	15:02	MUC+SVP	on ground/max depth	58° 21.28' S	62° 10.07' W	3090.7
PS97/085-3	16.03.16	17:45	PC	on ground/max depth	58° 21.27' S	62° 10.03' W	3090.8
PS97/086-1	16.03.16	22:41	PC	on ground/max depth	58° 38.65' S	61° 23.84' W	2968.8
PS97/086-2	17.03.16	00:46	MUC	on ground/max depth	58° 38.65' S	61° 23.82' W	2968.9
PS97/087-1	17.03.16	07:14	CTD/RO	on ground/max depth	58° 52.16' S	60° 51.98' W	3639.8
PS97/087-2	17.03.16	09:07	PLA	on ground/max depth	58° 52.18' S	60° 51.94' W	3640.4
PS97/087-3	17.03.16	10:31	CTD/RO	on ground/max depth	58° 52.16' S	60° 51.83' W	3640.8
PS97/087-4	17.03.16	11:16	MP	on ground/max depth	58° 52.16' S	60° 51.90' W	3639.3
PS97/087-5	18.03.16	11:32	PLA	on ground/max depth	58° 52.11' S	60° 51.91' W	3640.7
PS97/088-1	18.03.16	15:20	PC	on ground/max depth	58° 38.64' S	61° 23.82' W	2964.8
PS97/089-1	18.03.16	23:58	PC	on ground/max depth	58° 13.60' S	62° 43.59' W	3437.2
PS97/089-2	19.03.16	02:20	MUC	on ground/max depth	58° 13.60' S	62° 43.63' W	3431.9
PS97/090-1	19.03.16	13:13	PC	on ground/max depth	58° 1.60' S	64° 47.83' W	4178.9
PS97/091-1	19.03.16	18:39	GoFlo	on ground/max depth	58° 4.96' S	66° 2.90' W	3252.5
PS97/092-1	20.03.16	07:40	PC	on ground/max depth	57° 45.78' S	69° 52.73' W	3823.7
PS97/093-1	20.03.16	13:31	PC	on ground/max depth	57° 29.94' S	70° 16.56' W	3781.4
PS97/093-2	20.03.16	17:30	PC	on ground/max depth	57° 29.95' S	70° 16.48' W	3782.2
PS97/093-3	20.03.16	20:03	MUC	on ground/max depth	57° 29.92' S	70° 16.57' W	3782.2
PS97/094-1	21.03.16	02:41	MUC	on ground/max depth	57° 0.17' S	70° 58.32' W	3993.4
PS97/094-2	21.03.16	05:28	PC	on ground/max depth	57° 0.16' S	70° 58.29' W	3996.1
PS97/095-1	22.03.16	12:09	MUC	on ground/max depth	56° 14.68' S	66° 14.95' W	1652.1
PS97/095-2	22.03.16	13:57	PC	on ground/max depth	56° 14.69' S	66° 14.96' W	1644.7
PS97/095-3	22.03.16	15:26	GC	on ground/max depth	56° 14.68' S	66° 14.96' W	1647
PS97/096-1	22.03.16	18:09	MUC	on ground/max depth	56° 4.53' S	66° 8.96' W	1620.7
PS97/096-2	22.03.16	19:18	GC	on ground/max depth	56° 4.56' S	66° 9.02' W	1612.6
PS97/097-1	23.03.16	19:03	MUC	on ground/max depth	57° 3.27' S	67° 4.00' W	2318.6
PS97/097-2	23.03.16	20:52	PC as GC	on ground/max depth	57° 3.25' S	67° 4.09' W	2312
PS97/097-3	23.03.16	22:53	PC as GC	on ground/max depth	57° 3.28' S	67° 4.10' W	2310.4
PS97/098-1	24.03.16	05:51	CTD/RO	on ground/max depth	57° 32.72' S	68° 4.25' W	3817.5
PS97/099-1	24.03.16	08:59	CTD/RO	on ground/max depth	57° 27.96' S	68° 1.72' W	3865.8
PS97/100-1	24.03.16	11:12	CTD/RO	on ground/max depth	57° 23.34' S	67° 59.03' W	4119.5
PS97/101-1	24.03.16	13:58	CTD/RO	on ground/max depth	57° 18.66' S	67° 56.59' W	4415.2
PS97/102-1	24.03.16	17:08	CTD/RO	on ground/max depth	57° 13.92' S	67° 53.76' W	4393.5
PS97/103-1	24.03.16	19:28	CTD/RO	on ground/max depth	57° 9.14' S	67° 51.09' W	3357.6

PS97/104-1	24.03.16	22:14	CTD/RO	on ground/max depth	57° 5.40' S	67° 48.67' W	3884.9
PS97/105-1	25.03.16	01:42	CTD/RO	on ground/max depth	57° 1.48' S	67° 47.49' W	2507.7
PS97/106-1	25.03.16	14:28	CTD/RO	on ground/max depth	56° 3.71' S	67° 15.51' W	97.1
PS97/107-1	25.03.16	15:59	CTD/RO	on ground/max depth	56° 13.62' S	67° 20.83' W	107.3
PS97/108-1	25.03.16	17:31	CTD/RO	on ground/max depth	56° 23.16' S	67° 25.84' W	110.8
PS97/109-1	27.03.16	00:29	PC	on ground/max depth	55° 30.79' S	71° 38.22' W	2084
PS97/110-1	27.03.16	08:25	GC	on ground/max depth	55° 6.94' S	72° 40.14' W	1840.3
PS97/111-1	27.03.16	21:34	PC	on ground/max depth	54° 23.08' S	74° 36.39' W	2364
PS97/112-1	28.03.16	13:12	PC	on ground/max depth	54° 34.74' S	76° 38.94' W	3866.9
PS97/113-1	28.03.16	17:52	SEISREFL	Airgun	54° 38.30' S	76° 56.91' W	3902
PS97/113-1	28.03.16	18:32	SEISREFL	Profile start	54° 37.41' S	76° 52.45' W	3951.3
PS97/113-1	29.03.16	04:56	SEISREFL	Profile end	54° 44.13' S	76° 33.37' W	4015
PS97/114-1	29.03.16	08:18	MUC	on ground/max depth	54° 34.68' S	76° 38.85' W	3863
PS97/114-2	29.03.16	11:16	PC	on ground/max depth	54° 34.73' S	76° 38.82' W	3869.3
PS97/115-1	29.03.16	17:16	CTD/RO	on ground/max depth	54° 27.26' S	75° 52.38' W	4111.2
PS97/116-1	29.03.16	20:23	CTD/RO	on ground/max depth	54° 23.49' S	75° 42.57' W	4225.8
PS97/117-1	29.03.16	22:54	CTD/RO	on ground/max depth	54° 19.90' S	75° 32.29' W	4258.5
PS97/118-1	30.03.16	01:52	CTD/RO	on ground/max depth	54° 16.18' S	75° 22.45' W	4273.8
PS97/119-1	30.03.16	05:53	CTD/RO	on ground/max depth	54° 12.48' S	75° 12.44' W	2941.5
PS97/120-1	30.03.16	08:39	CTD/RO	on ground/max depth	54° 8.72' S	75° 2.55' W	2803.1
PS97/121-1	30.03.16	11:18	CTD/RO	on ground/max depth	54° 4.99' S	74° 52.67' W	2600.1
PS97/122-1	30.03.16	13:47	PC	on ground/max depth	54° 5.81' S	74° 54.90' W	2557.9
PS97/122-2	30.03.16	15:41	MUC	on ground/max depth	54° 5.85' S	74° 54.89' W	2560
PS97/123-1	30.03.16	18:52	CTD/RO	on ground/max depth	54° 1.29' S	74° 42.66' W	2742.9
PS97/124-1	30.03.16	21:47	CTD/RO	on ground/max depth	53° 57.44' S	74° 32.82' W	2802.5
PS97/125-1	31.03.16	00:37	CTD/RO	on ground/max depth	53° 53.76' S	74° 23.25' W	1839.9
PS97/126-1	31.03.16	02:36	CTD/RO	on ground/max depth	53° 50.12' S	74° 12.86' W	320
PS97/127-1	31.03.16	04:12	CTD/RO	on ground/max depth	53° 45.04' S	73° 58.98' W	89.5
PS97/128-1	31.03.16	19:35	MUC	on ground/max depth	53° 38.04' S	75° 32.71' W	2293.7
PS97/128-2	31.03.16	21:28	PC	on ground/max depth	53° 38.06' S	75° 32.75' W	2313.4
PS97/129-1	01.04.16	03:19	PC	on ground/max depth	53° 19.29' S	75° 12.81' W	1870.2
PS97/129-2	01.04.16	04:53	MUC	on ground/max depth	53° 19.28' S	75° 12.84' W	1879.4
PS97/130-1	01.04.16	14:04	GC	on ground/max depth	52° 55.77' S	75° 54.25' W	3239.2
PS97/131-1	02.04.16	11:26	MUC	on ground/max depth	52° 39.58' S	75° 33.97' W	1028.2
PS97/132-2	02.04.16	13:36	MUC	on ground/max depth	52° 37.01' S	75° 35.14' W	843
PS97/133-1	02.04.16	14:54	MUC	on ground/max depth	52° 39.59' S	75° 33.96' W	1027.5
PS97/134-1	02.04.16	16:09	MUC	on ground/max depth	52° 40.97' S	75° 34.85' W	1075.1
PS97/135-1	02.04.16	17:19	MUC	on ground/max depth	52° 41.96' S	75° 35.54' W	1093.9
PS97/136-1	02.04.16	18:58	PC	on ground/max depth	52° 40.97' S	75° 34.87' W	1063.1
PS97/137-1	02.04.16	21:09	PC	on ground/max depth	52° 39.57' S	75° 33.89' W	1027.6
PS97/138-1	02.04.16	23:18	PC as GC	on ground/max depth	52° 36.98' S	75° 35.17' W	839.8
PS97/139-1	03.04.16	01:48	PC as GC	on ground/max depth	52° 26.56' S	75° 42.42' W	640
PS97/139-2	03.04.16	02:42	MUC	on ground/max depth	52° 26.54' S	75° 42.41' W	638.9
PS97/140-1	03.04.16	04:19	SEISREFL	Airgun	52° 28.88' S	75° 37.43' W	3902
PS97/140-1	03.04.16	05:54	SEISREFL	Profile start	52° 29.68' S	75° 27.50' W	3951.3
PS97/140-1	03.04.16	18:50	SEISREFL	Profile end	52° 39.48' S	75° 52.17' W	4015
PS97/141-1	03.04.16	00:18	CTD/RO	on ground/max depth	52° 20.00' S	77° 9.99' W	3981.4
PS97/142-1	04.04.16	02:30	CTD/RO	on ground/max depth	52° 20.01' S	77° 0.01' W	4005.3
PS97/143-1	04.04.16	04:45	CTD/RO	on ground/max depth	52° 19.97' S	76° 50.03' W	4034.9
PS97/144-1	04.04.16	07:01	CTD/RO	on ground/max depth	52° 20.03' S	76° 39.90' W	4083.9
PS97/145-1	04.04.16	09:18	CTD/RO	on ground/max depth	52° 20.03' S	76° 29.93' W	4093.4
PS97/146-1	04.04.16	11:35	CTD/RO	on ground/max depth	52° 19.96' S	76° 19.99' W	4205.6
PS97/147-1	06.04.16	11:43	CTD/RO	on ground/max depth	52° 19.77' S	76° 4.79' W	2339
PS97/148-1	06.04.16	13:51	CTD/RO	on ground/max depth	52° 19.85' S	75° 49.94' W	884
PS97/149-1	06.04.16	16:18	CTD/RO	on ground/max depth	52° 21.72' S	75° 30.00' W	200.2
PS97/150-1	06.04.16	17:41	CTD/RO	on ground/max depth	52° 25.30' S	75° 15.06' W	91
PS97/151-1	06.04.16	19:06	CTD/RO	on ground/max depth	52° 29.64' S	74° 59.86' W	